~~RFP-3006/68186/3533/79/14-2~~
UC-60

[redacted]

DOE/DP/03533-T1 (Vol.2)

Development of an 8KW Wind Turbine Generator for Residential Type Applications

Phase I-Design & Analysis Volume II-Technical Report

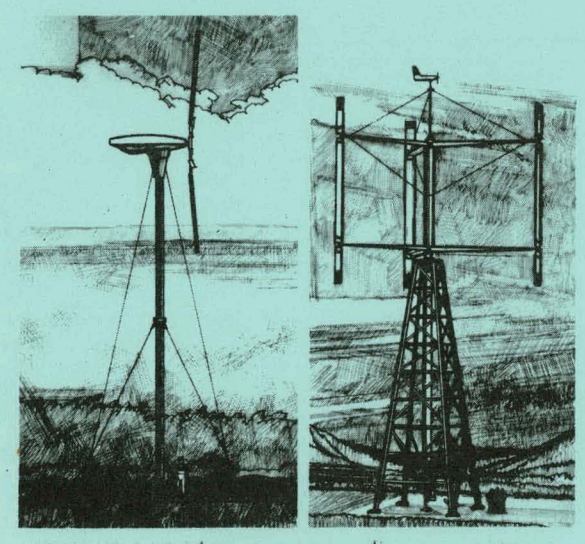

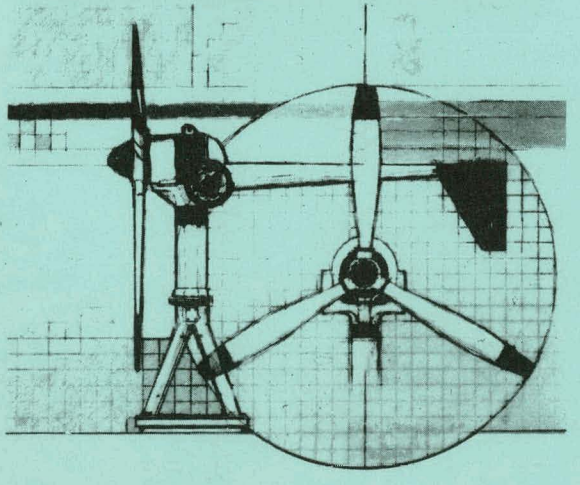

June 25, 1979

M. C. Cheney, et al

Prepared by
UNITED TECHNOLOGIES
RESEARCH CENTER
East Hartford, Ct. 06108

For
Rockwell International Corporation
Energy Systems Group
Rocky Flats Plant
Wind Systems Program
P. O. Box 464
Golden, Colorado 80401

Subcontract PF68186 F

As part of the
UNITED STATES DEPARTMENT OF ENERGY
DIVISION OF DISTRIBUTED SOLAR TECHNOLOGY
FEDERAL WIND ENERGY PROGRAM

Contract No. DE-ACO4-76DPO3533

DISCLAIMER

Printed in the United States of America
Available from
National Technical Information Service
United States Department of Commerce
5285 Port Royal Road
Springfield, Virginia 22151

Price: Printed Copy $____*; Microfiche $3.00

*Pages	NTIS Selling Price
001-025	$4.00
026-050	$4.50
051-075	$5.25
076-100	$6.00
101-125	$6.50
126-150	$7.25
151-175	$8.00
176-200	$9.00
201-225	$9.25
226-250	$9.50
251-275	$10.75
276-300	$11.00

~~RFP-3066/60186/3533/79/14-2~~
UC-60

DEVELOPMENT OF AN 8 KW WIND TURBINE GENERATOR FOR RESIDENTIAL TYPE APPLICATIONS

Phase I - Design and Analysis

Volume II - Technical Report

June 25, 1979

M.C. Cheney, et. al.

Prepared by

United Technologies Research Center
East Hartford, Connecticut 06108

For

Rockwell International Corporation
Energy Systems Group
Rocky Flats Plant
Wind Systems Program
P.O. Box 464
Golden, Colorado 80401

Subcontract No. PF68186 F

As part of the

UNITED STATES DEPARTMENT OF ENERGY
DIVISION OF DISTRIBUTED SOLAR TECHNOLOGY
FEDERAL WIND ENERGY PROGRAM

Contract No. DE-AC04-76DP03533

R78-914136-1

Development of an 8kW Wind Turbine Generator for Residential Type Applications

TABLE OF CONTENTS

TABLE OF CONTENTS (Cont'd)

ABSTRACT

This Phase I summary report contains a description of the 8 kW wind energy conversion system developed by the United Technologies Research Center (UTRC) for the Department of Energy. The wind turbine employs the UTRC Bearingless Rotor Concept in conjunction with a passive pendulum control system which controls blade pitch for start-up, efficient power generation, and high-speed survivability. The report contains a summary of the experimental and analytical programs in support of design efforts. These supporting programs include materials tests, a wind tunnel program, and aeroelastic analyses to evaluate system stability. An estimate is also made of the projected manufacturing cost of the system if produced in quantity.

ACKNOWLEDGEMENTS

The Program Manager gratefully acknowledges the assistance of the many staff members of the United Technologies Research Center and the Hamilton Standard Division who have contributed to this program. Without the benefit of their technical expertise, the wind turbine design reported on herein could not have been achieved.

The contributors to this program and the coauthors of this report are:

From UTRC,

R. K. Amiet	-	Noise prediction
R. L. Bielawa	-	Aeroelastic analysis
R. F. Dondero	-	Tower design
A. B. Caruolo	-	Blade joint design
B. W. Goepner	-	(Principal Investigator) Performance, wind tunnel tests
K. M. Prewo, J. R. Strife, R. D. Veltri	-	Composite materials experiments
R. H. Ross	-	Principal Designer
D. Scola	-	Self skinning foam development
R. B. Taylor	-	East Hartford site design

From Hamilton Standard

R. Gregoire	-	Product warranty
P. W. Ingle	-	Failure mode and safety analysis
J. Jennings, J. MacMillan	-	Production pricing

The Program Manager would like to thank the Wind Systems staff at Rocky Flats for their guidance, encouragement, and patience shown during the course of this design effort.

SUMMARY

This report contains a summary of the major results of Phase I of the United Technologies Research Center's (UTRC) contract to design, fabricate, and test an 8 kW Wind Turbine Generator (WTG) under the Department of Energy's small wind energy conversion system program. The UTRC system was conceived under an earlier DOE study, and the current contract, through Rockwell International, is to carry the WTG concept through hardware development and field evaluation at Rocky Flats, Colorado.

The final WTG design which has evolved from this study is a horizontal-axis two-bladed down-wind rotor having a diameter of 9.45 m (31 ft), an in-line double-step gear box producing 1840 rpm into a 15-kW induction generator, and a tower comprising two 0.27-m-diam steel pipe sections totaling 16.8-m in height and supported by guy wires. The rotor controls consist of hub-mounted centrifugally actuated pendula which adjust blade pitch from its start-up setting to its optimum operating position. The rotor/pylon assembly is free yawing and automatically adjusts for wind direction changes. Control in high winds is achieved by blade stall and the system is designed to survive wind gusts up to 74 m/s (165 mph).

The Phase I activity reported on herein consists of several experimental programs in support of the design, including composite material characterization tests, a 1/7-scale wind tunnel test, and an induction generator calibration experiment. Studies which are also included, in addition to a description of the complete design and performance characteristics, are a system safety analysis, product warranty considerations, a production cost estimate, and a loads and stability investigation. A complete set of detailed engineering drawings have been prepared for the prototype which will be built and tested during Phase II.

The final report for Phase II of the program will be written following the field evaluation at Rocky Flats. This report, not expected to be available until late 1980, will contain a summary of test results, any design modifications which may have been incorporated, and a final production cost estimate.

INTRODUCTION

The Composite Bearingless Rotor (CBR), after eight years of development for helicopter applications, was initially studied for wind turbine applications in 1975 under an ERDA contract resulting from a program solicitation from the National Science Foundation. The United Technologies Corporation (UTC) Composite Bearingless Rotor was proposed for use as a wind turbine in light of the considerable reduction in weight and maintenance this rotor system demonstrated as the tail rotor for the Sikorsky Blackhawk and S-76 helicopters. It was anticipated that the simplicity of this rotor design would have a favorable impact on reducing wind turbine costs which, of course, is vital to the success of the wind energy program. The initial ERDA contract (Refs. 1 and 2) explored several CBR wind turbine concepts in an effort to examine control concepts to simplify the design and reduce costs. One such design was achieved which was comprised of a centrifugally actuated hub-mounted pendulum which, through a connecting strap to the blade, automatically controlled blade pitch over the operating range from start-up through maximum wind speed. A small scale wind tunnel test was also conducted under that ERDA contract which demonstrated the operating characteristics of this control concept.

A second ERDA contract was received in 1976 to design a full-scale wind turbine incorporating the concepts developed during the feasibility study. A 12.2-m (40-ft)-diam rotor was selected which was considered adequate for home or farm use, and the results of this design are presented in Ref. 3.

The current contract with Rockwell International is to fabricate a prototype bearingless wind turbine with an output of at least 8 kW in a 9-m/s wind. This contract was initiated in October 1977 and continues into 1980 with the delivery and evaluation of the system at Rocky Flats, Colorado. The overall objectives of the contract are to design and fabricate a system in the 8 kW range which could be produced in quantities of 1000 units per year for not more than $750/kW (1977 dollars), have a useful life of at least 25 years, and withstand severe weather conditions including wind gusts up to 74 m/s.

The final report for this project will be presented in two volumes. This volume will report on Phase I of the program which encompasses the design effort and supporting experiments. Volume II will be published following the field evaluation of the system by Rockwell and will report on the fabrication and performance testing of the hardware. This second volume will also include the final production cost estimates.

CONCEPT DESCRIPTION

The composite bearingless wind turbine reported on herein was made possible by employing the specialized features of the Composite Bearingless Rotor (CBR), developed initially for helicopter applications to reduce the cost and complexity of rotor systems. An in-depth review of the concept is presented in the final contract report (Ref. 4) for the CBR feasibility study conducted at UTRC from 1971 to 1976 under NASA and Army sponsorship. A summary of the CBR concept and its application to the UTRC wind turbine is presented in this section.

The composite bearingless rotor evolved as a result of the unique application of fiber reinforced composite materials. The nonisotropic nature of unidirectional composites, generally considered an undesirable feature, yields a structure which is decidedly softer in torsion than in a direction which loads the fibers axially. By employing a finite length of this material at the blade root, torsional deflections can be achieved to satisfy the pitch angle change requirements of a wind turbine or helicopter rotor while providing sufficient stiffness in the in-plane and out-of-plane directions to satisfy hingeless rotor frequency requirements.

A general overview of the UTRC wind turbine is shown in Fig. 1 and a schematic of the basic components of the system are shown in Fig. 2. The rotor is comprised of two distinct parts. The blade, or aerodynamic portion, is fabricated from fiberglass hopefully using a pultrusion process. The inner portion of the rotor, called the flexbeam, is made up of unidirectional graphite epoxy. The dimensions of the flexbeam are dictated by the edgewise and flatwise frequency requirements, and the required torsional properties are determined from the pendulum control system. The free length of the flexbeam runs from the hub to approximately 20% of the radius where it is joined to the fiberglass blade. As shown in Fig. 2 the outer portion of the flexbeam is connected to the pendulum through a steel strap, called the flexstrap. The flexbeam is layed-up and cured in a preconed and pretwisted configuration, and extends through the hub and is connected to the opposite blade in a similar fashion. The flexbeam is pretwisted -16° (Positive blade pitch is defined, as in helicopter terminology, as the blade angle direction to produce positive, or normal, thrust on the rotor, i.e., leading edge away from the wind direction) to place the blade in a position for self-starting. In this static condition the pendula are coned into the tower approximately 45° by virtue of their connection to the flexbeam through the flexstraps. For optimum performance it has been shown that, with the rotor at operating speed, the blade pitch angle should operate in the vicinity of ±2°. This is achieved by virtue of the pendula acting under the influence of centrifugal force as rpm increases. The pendula begin to move towards the plane of rotation and, through the flexstrap connections to the flexbeam, provide a moment to the blades which twists the flexbeam, thereby increasing the blade pitch. The pendula, acting against the torsional spring of the flexbeam, are always in moment equilibrium with the flexbeam.

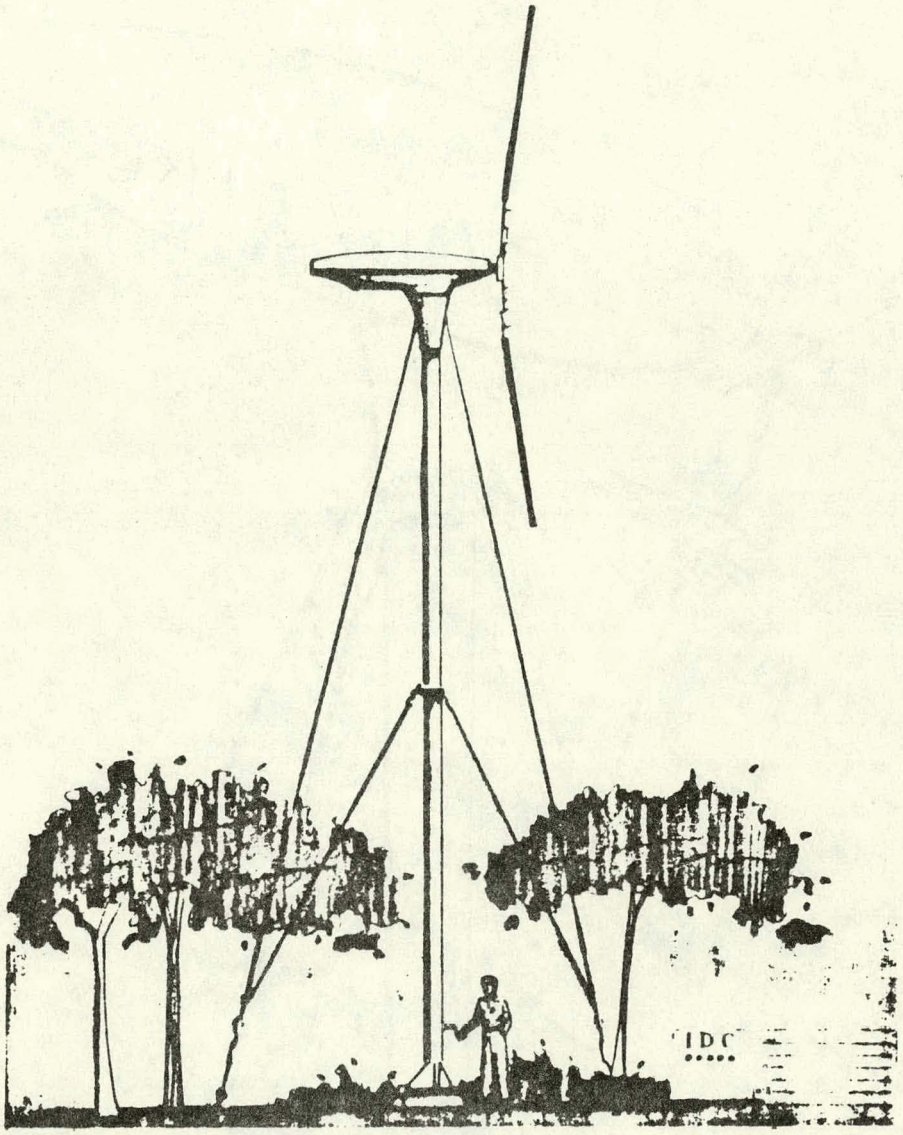

Fig. 1 UTRC Wind Turbine

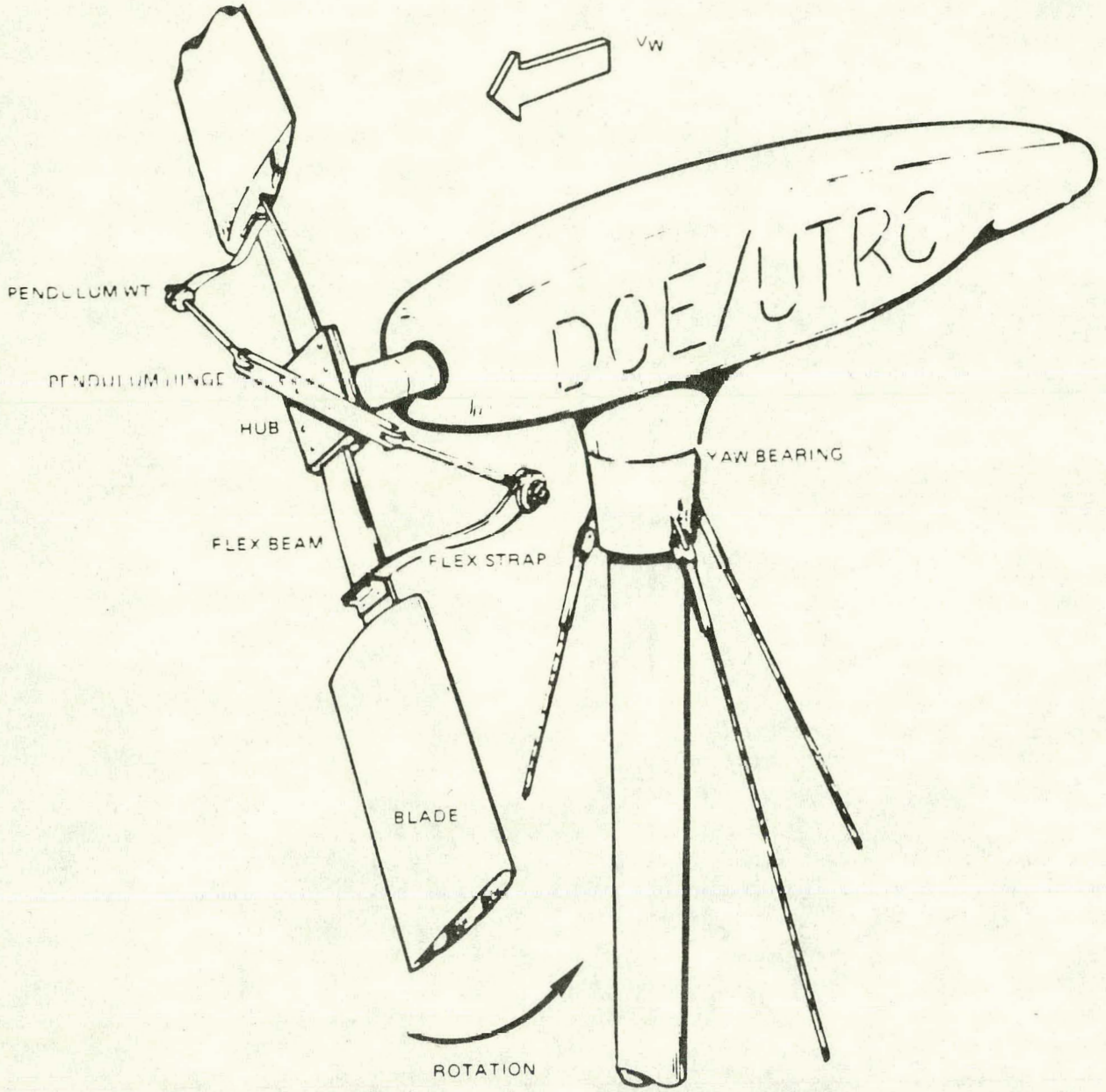

Fig. 2 Wind Turbine Components

79-05-34-2

The self-aligning feature of the CBR wind turbine results from the inherent dynamic response characteristics of low stiffness hingeless rotors. This arises from the phase lag of a simple spring-mass-damper system, wherein the mass experiences a finite lag between the time of excitation and the time of response. The duration of the lag is a function of the frequency and damping of the system. In the case of the wind turbine, which is yawed at an angle to the wind direction, the excitation results from the higher dynamic pressure of the blade rotating into the wind as compared to the blade moving away from the wind. These blades would be in their vertical positions when experiencing the greatest difference in lift. Their maximum flatwise deflection would occur at some position during the next quarter of a revolution. This in turn would produce a moment at the blade root which feeds directly into the hub. The turbine would respond to this moment and yaw in a direction to eliminate the differential lifts on the advancing and retreating blades. The motion would end when the blades are at equal lift which occurs generally when the turbine axis is aligned with the wind. In a free yawing system, such as that used for the CBR wind turbine, any wind direction change would create advancing and retreating blades and therefore the turbine would continuously self-align.

Under high wind speed conditions the wind turbine rotational speed would increase in proportion to wind speed if the pitch angle were left at its optimum value of $\pm 2°$. This would result in excessive tip speeds and thrust levels which could potentially lead to a blade failure. Also, as rpm increases it will approach the blade edgewise frequency which would result in a coalescence with the one-per-rev (1P) gravity excitation creating a potential instability. The problem of overspeeding has been solved by producing stall on the rotor blades at a specific combination of wind speed and rpm. At a tip speed of approximately 122 m/s (400 ft/s) which is approximately double the design rpm, the pendula will be essentially in the plane of rotation and produce a pitch angle on the blades of approximately 5°. This angle, in combination with the aerodynamic angle produced by the wind speed, is sufficient to stall the blades. At this point the rotor tip speed is reduced and adjusts itself to a lower equilibrium which is approximately 90 m/s (300 ft/s). The centrifugal force remains sufficiently high at this rpm to assist the blade in counteracting the root moment caused by blade thrust. The rotor will remain stalled until the wind speed drops below the stall point which is estimated to occur at approximately 22 m/s (50 mph). The question of the coupled performance of the wind turbine rotor and the power generator under various operating modes is discussed in the performance section of this report.

DEVELOPMENT EXPERIMENTS

Background

In support of the rotor design effort, several experimental programs were identified to characterize the various blade materials. The initial blade design consisted of a graphite/epoxy spar with the remaining portions of the blade made up from various formulations of polyurethane. The airfoil shape was to be formed by an injection molding process, wherein the center of the blade would be a closed cell foam material with a tough outer skin formed in the foaming process. The leading edge would consist of a solid polyurethane material which would balance the blade at the quarter chord and also serve as an abrasive strip. This blade concept has the potential for very low production cost by virtue of the high speed of injection molding. Discussions were held with people from the Olin Chemical Corporation, and it was determined that to injection mold a blade of this size would require a period of time to develop the process. It was felt that due to the uncertainty of the time and cost to complete such development, another blade design should be considered. Eventually, a design using fiberglass and employing a pultrusion process was selected. However, prior to considering the fiberglass design, supporting experiments for the molded blade concept were conducted. Although this work provided useful results relative to the properties of polyurethanes, it is not expected to impact the final wind turbine design; and thus, the results will be presented only as an appendix to this report (see Appendix A).

Material characterization tests were also conducted on graphite/epoxy, which is the material used for the flexbeam. Although extensive material tests have been conducted by other researchers (for example, Ref. 5 and 6) it was felt that additional experiments should be conducted due to the unique application of the material for this wind turbine. These tests were conducted principally to measure the effects of temperature extremes on the ultimate strength of graphite/epoxy and to measure the torsional fatigue characteristics under high steady loading. Ultimate strength tests were also conducted on the joint design which connects the flexbeam to the blade.

A small-scale wind tunnel test was conducted during this phase of the contract to evaluate the stability and blade stress characteristics of the rotor system under high speed stall conditions. It was determined analytically that the rotor could withstand high wind speeds up to 74 m/s if operated under totally stalled conditions with the rotor maintaining a tip speed of approximately 90 m/s. The blade and test equipment used for this wind tunnel experiment were obtained from an earlier DOE contract reported in Ref. 1. The test was conducted in the Pilot Tunnel at UTRC which has a forward speed capability in the wind turbine test section of only 27 m/s. This was, of course, not sufficient to test the operating characteristics at 74 m/s; however, it did demonstrate the important transition phenomena from unstalled to stalled flow

as wind speed is increased and, conversely, the transition from stalled flow to unstalled flow as wind speed is decreased.

The final developmental experiment conducted in support of the design phase was related to the power generation design. In this test a small induction motor was operated as a generator to determine its efficiency when running in this mode. It was felt that if adequate efficiency could be demonstrated, then this would represent the most cost effective approach to power generation, since induction motors are readily available at nominal cost.

Composite Materials Experiments

The materials evaluation of the composite components for this program consisted of two parts. The first part consisted of material property verification for composite materials that were to be incorporated in the wind turbine generator. The second part of the materials evaluation program involved experiments which were performed on specimens modeled after a particular incorporated design for which handbook property data were not available or could not easily be applied.

Graphite/Epoxy Tests

Hercules continuous type AS graphite filaments in a Hercules 1908 epoxy resin matrix was chosen as the source of graphite prepreg tape for use in this program for the flexbeam material. The Hercules prepreg tape AS4-1908 contains a 120°C curable epoxy and is recommended for structural applications where high strength and high modulus are required. Enough prepreg tape was purchased to prepare composite panels of various thicknesses and fiber orientation. From these panels test specimens were cut. Tensile modulus, ultimate tensile strength and strain-to-failure were measured via strain gaged specimens for both 0° and $\pm$45° orientation. The results of these tests are listed in Table 1.

The bending modulus and flex strength were measured on specimens which had a span-to-depth ratio of greater than 32:1 for both the 0° and $\pm$45° fiber orientation. Data could not be obtained for the $\pm$45° specimens from this three-point bend test due to excessive deflection. The results of the flexure tests of the 0° fiber orientated graphite epoxy specimens are given in Table 2.

To determine the behavior of this composite at temperature extremes, specimens were prepared from composite panels containing unidirectional reinforced filaments. Flexural properties were then measured at temperatures of -50°C, room temperature, and +60°C of specimens with a span-to-depth ratio of

TABLE 1

GRAPHITE/EPOXY TENSILE TEST RESULTS

Fiber Orientation	UTS MPa	UTS (Kpsi)	E GPa	E (10^6psi)	Strain to Failure %
0^o	876	(127)	130	(18.9)	0.65
	965	(140)	139	(20.1)	0.75
	1103	(160)	127	(18.4)	0.83
Average	979	(142)	132	(19.1)	0.74
$\pm 45^o$	239	(34.7)	35.9	(5.2)	>10
	228	(33.0)	31.7	(4.6)	>10
	248	(36.0)	17.2	(2.5)	>10
Average	239	(34.7)	28.3	(4.1)	>10

Tensile Test Parameters: 51-mm gage length
Strain gaged
No doublers used, all 0^o specimens failed at grip edges

TABLE 2

UNIDIRECTIONAL GRAPHITE/EPOXY FLEX STRENGTH RESULTS

Sample Number	Flexure Strength		Modulus E	
	MPa	(Kpsi)	GPa	(10^6 psi)
1	1696	(246)	132	(19.1)
2	1786	(259)	114	(16.5)
3	1606	(233)	115	(16.7)
4	1820	(264)	125	(18.2)
5	1868	(271)	128	(18.5)
6	1827	(265)	120	(17.4)
Average	1765	(256)	122	(17.7)

Flexure Test Paramenters: Three point bend test

Span-to-Depth 32:1

Deflectometer used for deflection

32:1. These results are given in Table 3. The shear strengths at these temperatures were also determined using the short beam shear test (span-to-depth 4:1). The shear strength results are listed in Table 4.

All the test results obtained were within the values quoted by the manufacturer and those used for design purposes.

Fatigue Test

The flexbeam at a stall condition of 20° steady twist and an oscillation of ±5°, was calculated to experience a shear stress of 34.5 ± 8.3 MPa (5000 ± 1200 psi). A test specimen of the unidirectional fiber reinforcement, 152-mm long, with a free length of 97 mm, 18-mm wide, and 1.8-mm thick was tested in the UTRC torsion fatigue machine with this steady and oscillatory stress level. Due to slight geometric scaling differences the test specimen in the fatigue machine experienced a shear stress of 39.9 ± 10 MPa (5780 ± 1450 psi). The test specimen was removed periodically from the fatigue tester and the static shear modulus was measured. Approximately nine interruptions in the fatigue test were made to monitor shear modulus. The results of this modulus measurement with cumulative cycles are listed in Table 5.

A second specimen was fatigue tested to 10×10^6 cycles to model a flexbeam design condition of 16° of pretwist with a ± 5° oscillation. The test specimen geometry was such that for this case the flexbeam would experience a calculated shear stress of 25 ± 7.8 MPa (3621 ± 1131 psi). These results are also given in Table 5. In both of these fatigue tests, no appreciable change in shear modulus was observed after 10×10^6 cycles. However, both test specimens developed longitudinal cracks under the gripping pads between 8.4 to 10×10^6 cycles. A depression near the side of the specimens under the edge of the gripping pad indicates that excessive and nonuniform gripping pressure in the test fixture probably initiated the observed cracks in both specimens. It was also noted that a permanent set of approximately 2-3° was observed in the fatigued specimen.

In an attempt to alleviate the gripping problem, a third specimen was tested with fiberglass doublers bonded to the grip sections. The test section geometry and test conditions were identical to those of the previously tested specimens. In addition to determining the static shear modulus as a function of test cycles, the degree of permanent set observed in the specimen was also recorded. These data are listed in Table 6. No significant decrease in shear modulus was observed after 1×10^6 cycles. Examination of the test specimen revealed that the longitudinal splitting associated with the grip section had been eliminated through the use of doublers. The measurement of permanent set demonstrated that a twist of approximately 1.4° had been induced in the sample after 1×10^6 cycles. This would reduce the maximum shear stress the sample was exposed to by approximately 8%. After 10×10^6 cycles, a permanent set of approximately 3° was measured which corresponds to a decrease in maximum cyclic shear stress of 16%.

TABLE 3

GRAPHITE/EPOXY THREE POINT FLEXURE BENDING TEST RESULTS

Test Temperature	Bending Strength MPa	(Kpsi)	Average E GPa	(10^6psi)
-50°C	1887	(273)	124	(18.0)
	1648	(239)		
	1931	(280)		
	2130	(309)		
	2124	(308)		
	2096	(304)		
Average	1965	(285)		
Room Temperature	1696	(246)	122	(17.7)
	1786	(259)		
	1606	(233)		
	1820	(264)		
	1868	(271)		
	1827	(265)		
	1593	(231)		
	1496	(217)		
	1413	(205)		
Average	1675	(243)		
+60°C	1620	(235)	119	(17.2)
	1469	(213)		
	1482	(215)		
	1641	(238)		
	1620	(235)		
	1544	(224)		
Average	1565	(227)		

TABLE 4

GRAPHITE/EPOXY SHORT BEAM SHEAR TEST RESULTS

Test Temperature	Shear Strength MPa	(Kpsi)	Average MPa	(Kpsi)
-50°C	86.2	(12.5)		
	97.9	(14.2)	94.5	(13.7)
	98.6	(14.3)		
	100.0	(14.5)		
	88.3	(12.8)		
	95.1	(13.8)		
Room Temperature	75.8	(11.0)		
	75.8	(11.0)	75.8	(11.0)
	77.9	(11.3)		
	77.2	(11.2)		
	71.0	(10.3)		
	76.5	(11.1)		
+60°C	60.0	(8.7)		
	60.7	(8.8)	57.2	(8.3)
	57.2	(8.3)		
	56.5	(8.2)		
	55.2	(8.0)		
	53.1	(7.7)		

TABLE 5

FATIGUE TEST RESULTS

Test at $\theta = 20^{\circ} \pm 5^{\circ}$

Time Hours	Cumulative Cycles	Shear Modulus GPa	Shear Modulus (10^6 psi)
-	-	5.2	(.756)
1	$2.09 \cdot 10^5$	5.2	(.751)
4	$8.38 \cdot 10^5$	5.2	(.751)
6.6	$1.38 \cdot 10^6$	5.0	(.727)
9.7	$2.04 \cdot 10^6$	5.0	(.724)
16.0	$3.35 \cdot 10^6$	5.0	(.724)
24.0	$5.03 \cdot 10^6$	5.0	(.724)
32.0	$6.70 \cdot 10^6$	5.0	(.724)
40.0	$8.37 \cdot 10^6$	5.4	(.778)
48.0	$1.01 \cdot 10^7$	5.0	(.720)
	Test at $\theta = 16^{\circ} \pm 5^{\circ}$		
16	$3.35 \cdot 10^6$	5.0	(.730)
24	$5.03 \cdot 10^6$	5.9	(.849)
32	$6.70 \cdot 10^6$	5.1	(.735)
40	$8.37 \cdot 10^6$	4.9	(.707)
48	$1.01 \cdot 10^7$	5.3	(.762)

TABLE 6

FATIGUE RESULTS - DOUBLER REINFORCED GRIP SECTIONS

$\theta = 16 \pm 5^{o}$

Cumulative Fatigue Cycles (10^6)	Shear Modulus Ratio (G/Go)	Permanent Set
0	-	0^{o}
1	1.00	1.4^{o}
2	1.00	1.55^{o}
5	0.97	--
6.70	1.00	2.0^{o}
8.38	0.99	2.25^{o}
10.05	0.98	3.0^{o}

The torsional creep phenomenon may require an adjustment to be made to the selected pretwist of the full-scale flexbeam following field testing of the system. These material tests indicate a creep of 2-3° under high twist conditions. However, the peak twist angle reached was 25° which is significantly greater than the angle of the design operating condition. For the design condition, the blade operates at a pitch angle of -2° which requires a flexbeam elastic twist of only 14°. This level of twist should result in a much lower creep rate due to the reduced stress level. It may be found, following full scale experience, that a permanent set of 1-2° could be allowed without effecting the starting capability, i.e. a -14 or -15° pitch angle may be adequate for start-up rather than the -16° now planned.

Cantilever Tests

It was of design interest to determine what maximum load a unidirectional reinforced graphite epoxy bar could withstand when clamped in a cantilever condition and loaded on the extreme free end. A test specimen 152-mm long, 12.7-mm wide, was clamped such that a 76-mm free length was available to load. The edges of the clamps were rounded to avoid a stress concentration area during specimen deflection. In Fig. 3 are shown photographs of the cantilevered specimen at various stages of applied load. It can be seen in this figure that the magnitude of the tip deflection is so great that the strength equations from beam theory would not be valid at the fracture load. The maximum bending stress therefore can only be approximated under these extreme conditions by the equation

$$\sigma = \frac{Mc}{I} = \frac{6PL}{bh^2}$$

For the two tests made, results of 1103 and 1186 MPa (160 and 172 kpsi) were calculated. Modulus values 87.6 and 93.1 GPa (12.7 and 13.5 10^6 psi) obtained from the load deflection curves indicate that a significant fraction of the beam deflection was due to shear.

Simulated Flexbeam Joint

A flat-plate, two bolt clamp design was suggested for the flexbeam joint. Reinforcing the unidirectional flexbeam with $\pm 45°$ fiber orientation in the vicinity of the clamping area was needed to prevent bolt pull-out. At the completion of the design a simulated joint member was prepared in which bearing load pull-out measurements could be made. These specimens had a cross section composed of 11 layers of $\pm 45°$, 22 layers of 0°, and 11 layers of $\pm 45°$. The

START OF TEST

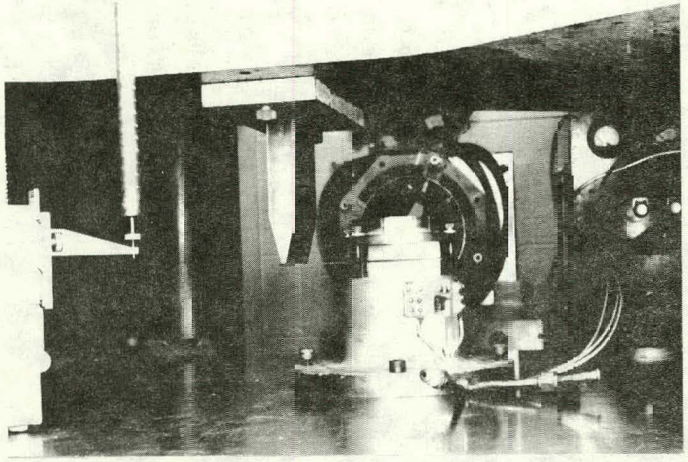

20% OF MAXIMUM LOAD

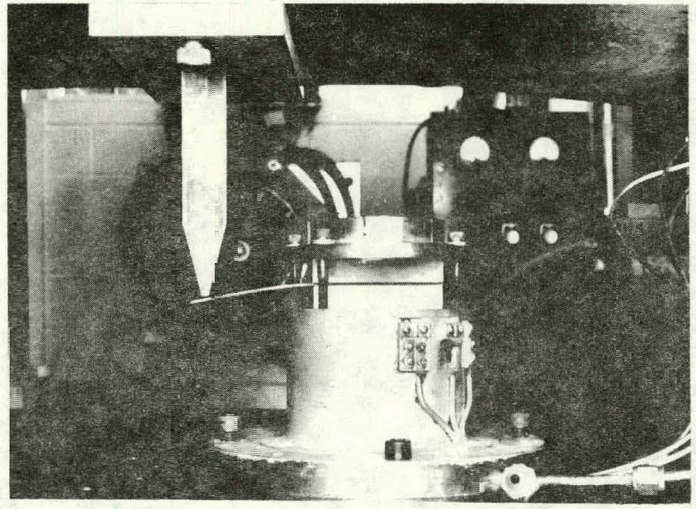

75% OF MAXIMUM LOAD

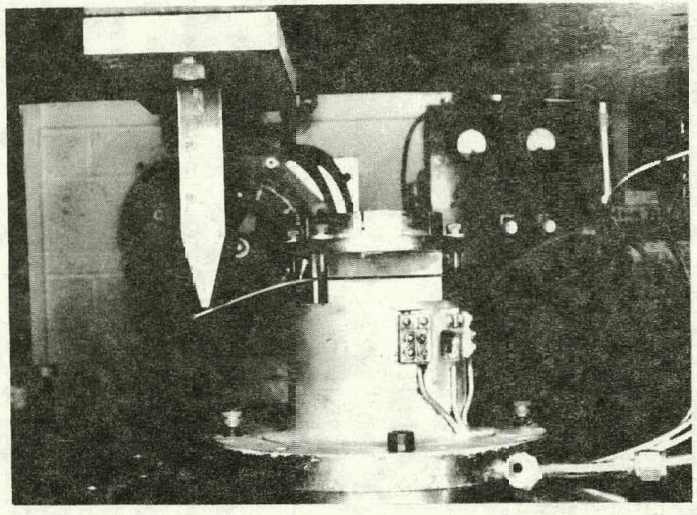

MAXIMUM LOAD JUST PRIOR TO FAILURE

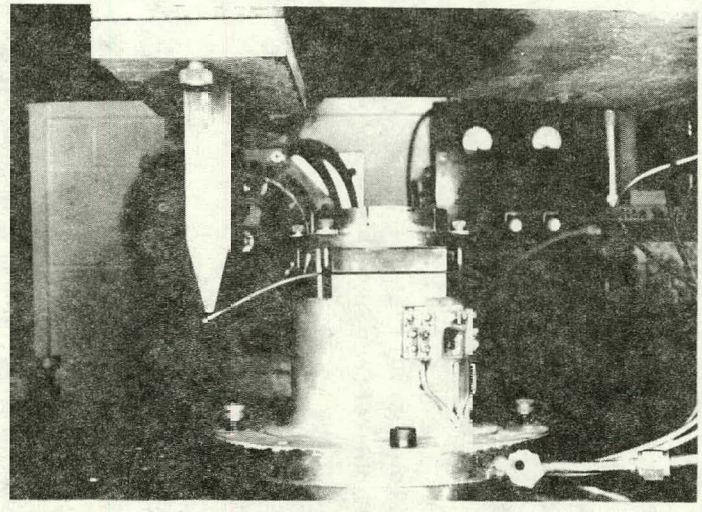

Fig. 3 Cantilever Beam Under Load

final thickness was 6.6 mm, width of 36.3 mm, and length of 152 mm. For each specimen, two holes were placed at each end. The four holes were located, drilled, filled with bushings, and provided with precision fit pins. A photograph of the simulated joint with load pins in position is shown in Fig. 4a.

The first test was made with the joint clamped at one end and a yoke loading device used to apply the load to the two pins at the other joint end. A second test was made in which two yokes were used so that all four bolt holes were loaded at one time. A photograph of the second test specimen after being loaded in the test machine is shown in Fig. 4b. For both tests, the 4.76-mm-diam loading pins exhibited permanent deflection and had to be removed with an arbor press before the specimens could be examined.

In the first bearing load test, both holes failed at the same time. The cold bonded steel bushing elongated. The $\pm 45°$ layers delaminated in the vicinity of the hole. This can be seen in Fig. 5a. The 0° core of the composite, in the vicinity of the hole, pushed up and out of the entire composite approximately 1.6 mm. The delamination of the $\pm 45°$ layers was only about one bolt hole diameter wide and propagated to the outer edges of both sides of the joint. The load at each bolt hole was measured to be 16,690N (3750 lb) at failure.

In the second test, the sample joint was mounted with a double yoke arrangement (as was shown in Fig. 4b) so that all four bolt holes were loaded simultaneously. The test was terminated when one hole failed at a measured load of 13,540N (3042 lb). The failure mode was very similar to that of the previous two holes except that the individual plys of $\pm 45°$ did not delaminate outward to the edges but the bond between the $\pm 45°$ layers and the 0° core separated in this region. The entire 0° core of the composite perpendicular to the hole in the direction of loading again pushed outward as is shown in Fig. 5b. Thus, for six bolt holes tested, the minimum bearing load was 13,540N (3042 lb), which results in a safety factor of greater than four for the maximum full-scale load.

Fiberglass Tests

To obtain information on the properties of the proposed fiberglass blade skin a composite panel was fabricated containing the design fiber orientation of this skin. The material used was available "S" glass type SP-250-52 prepreg tape which contained a high strength moldable epoxy with Owens Corning S2-463 glass and could be cured at 120°C. The orientation of the glass type layers within this composite panel were as follows: 0°, +45°, -45°, 0°, 90°, -45°, +45°, 0°.

Six tensile specimens 12.7-mm wide by 152.4-mm long were cut from the composite panel and 51-mm doublers were bonded to each end. Three of the six

a) BEFORE TEST WITH LOADING PINS IN POSITION

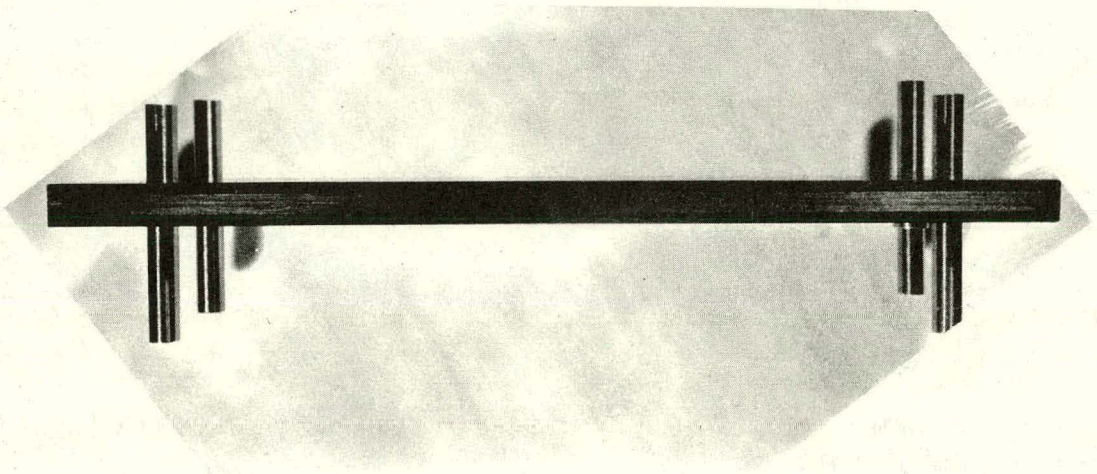

b) AFTER TEST OF ALL FOUR BOLT HOLES

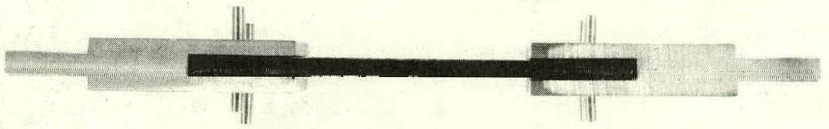

Fig. 4 Simulated Joint

78-09-56-2

a) NOTE DELAMINATION IN $\pm 45^{o}$ LAYERS

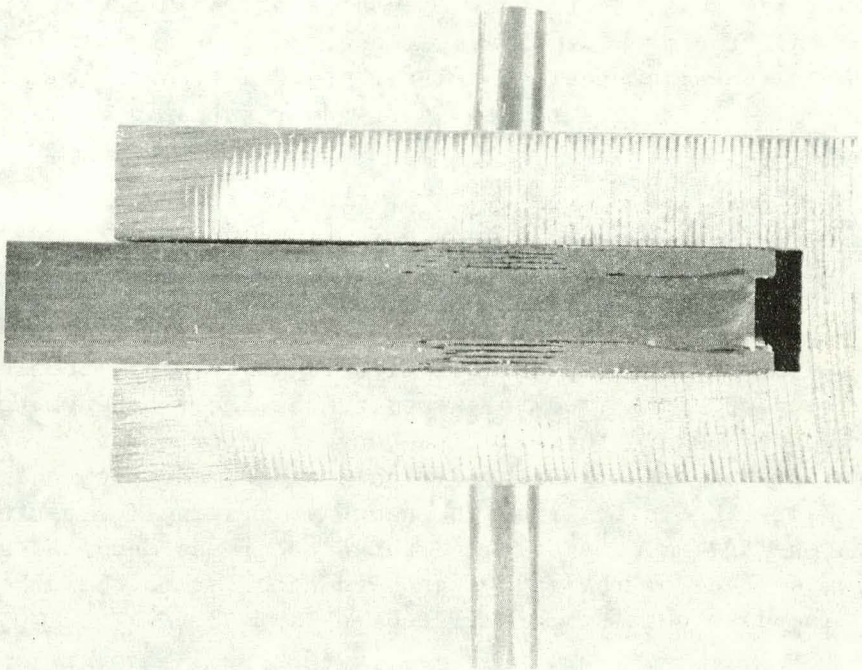

b) NOTE 0^{o} CORE POP–OUT IN VICINITY OF HOLE

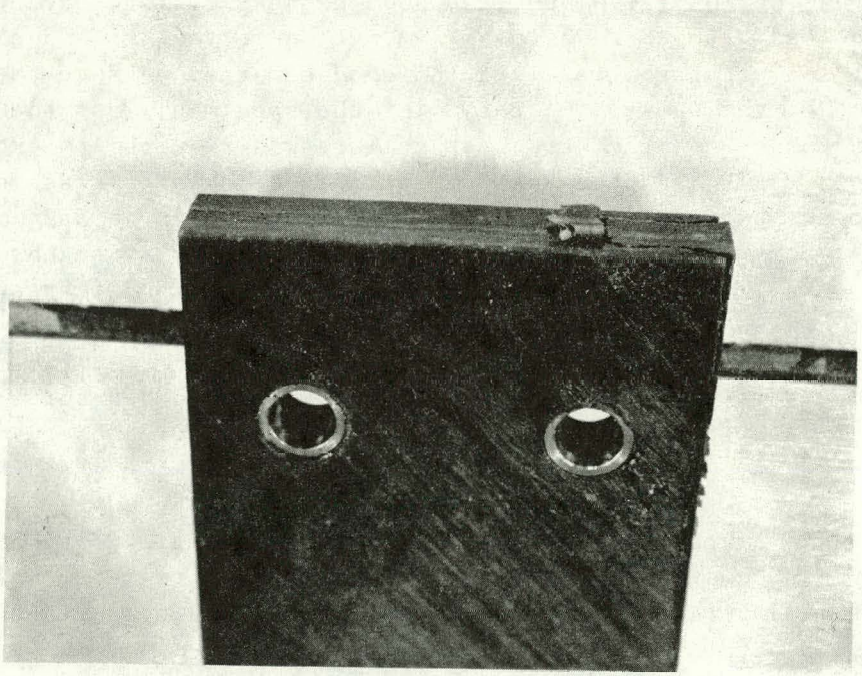

Fig. 5 Bearing Load Pull Out Test

78–09–56–1

specimens did not break during the test due to slippage of the doublers during load application. The results of three specimens which all failed within the gage length are given in Table 7. The average value of ultimate tensile strength obtained for this eight layer composite of 765 MPa (111 kpsi) was slightly higher than the predicted value extracted from the manufacturer's data for 0°, 45°, 0°/90° tensile specimens. From previously available comparisons of S-glass and E-glass, it is estimated that the results in Table 7 would be 15% less for E-glass.

Aluminum - Epoxy Bond Tests

It was envisioned that a potential solution for attaching the flexbeam to the spar could involve an intermediate aluminum bar which would be joined to the spar using a molded epoxy joint. With regard to this problem, some preliminary testing was performed to determine the shear strength of an aluminum-epoxy bond. Toward this end, rectangular aluminum bars of cross section 25 mm x 12.5 mm were pretreated with a dichromate etch and embedded in epoxy (Epon 828 with Sonite 41 curing agent). Testing was performed in a tensile mode on one specimen as-cast and three specimens machined such that the load bearing surface of the epoxy was perpendicular to the embedded aluminum bar. The data obtained are listed in Table 8.

The as-cast specimen exhibited a catastrophic failure at a load level of only 3560N (800 lb) yielding a calculated shear strength of 1.54 MPa (224 psi). Reassembly of the shattered epoxy around the aluminum bar indicated that off-axial loading had resulted in brittle failure of the epoxy. In contrast, the behaviour exhibited in machined specimens #1 and #2 was characterized by increasing load level until a sudden shear failure occurred, at which point the load dropped to zero. Examination of the test specimen showed that a shear offset of approximately 1.5 mm had occurred between the bar and machined surface of the epoxy. On reloading the specimen, less than 10% of the maximum load observed prior to shear failure was required to extract the bar from the epoxy. It is noted that in specimen #1 a large crack emanated from the bar to the exterior surface of the epoxy, whereas in specimen #2, no cracking of the epoxy was observed. The calculated shear strengths for specimens #1 and #2 were 12.9 MPa (1867 psi) and 11.2 MPa (1625 psi) respectively, a significant increase over that observed for the as-cast specimen.

Specimen #3 was a bar embedded in 38 mm of epoxy and had sustained a load of 21,350N (4800 lb) when yielding of the aluminum was observed so the test was terminated.

Although these tests were preliminary in nature, the reality of brittle failure of the epoxy due to off-axial loading was demonstrated. Only in the case of careful load alignment via machined surfaces could substantial bond shear strengths be obtained.

TABLE 7

EIGHT LAYER FIBERGLASS TEST RESULTS

Specimen	UTS		E	
	MPa	(Kpsi)	GPa	(10^6 psi)
A	758	(110)	18.2	(2.64)
B	779	(113)	17.4	(2.53)
C	765	(111)	17.9	(2.60)
average	765	(111)	17.9	(2.59)

TABLE 8

SHEAR STRENGTH OF ALUMINUM-EPOXY BOND

Specimen	Embedded Depth		Failure Load		Surface Area Embedded		Shear Strength	
	mm	(in.)	N	(lb)	mm^2	(in^2)	MPa	(Psi)
As-cast	30.5	(1.20)	3560	(800)	2310	(3.578)	1.54	(224)
1	12.4	(0.490)	16300	(3660)	1260	(1.960)	12.87*	(1867)
2	25.7	(1.012)	21800	(4900)	1950	(3.018)	11.20	(1625)

*Note: The bar end was embedded in #1 whereas it was exposed for the other specimens.

1/7-Scaled Model Wind Tunnel Test

The UTRC wind turbine will utilize rotor blade stall as a means of limiting rotor tip speed in high winds. Rotor tip speed must be limited to prevent excessive centrifugal loads or a coalescence of the rotational frequency (P) with the edgewise natural frequency. However, some rotation is desirable to add centrifugal flatwise stiffening to the flexbeam to counteract the high lift loads produced at high wind speeds. A test program to demonstrate the concept of rotor blade stall as a means of limiting rotor speed, was conducted in the UTRC Pilot Wind Tunnel.

Test Apparatus

The model wind turbine was similar to the unit used in the demonstrator tests documented in Ref. 1. However, different rotor blades were used during the subject program. These blades were constructed of plastic foam covered with several layers of fiberglass, and had a larger chord and smaller diameter than those used during the earlier demonstrator program. The physical characteristics of the demonstrator model are summarized in Table 9.

The rotor was two-bladed with a swept diameter of 1.07m. The flexbeam and pendulum were identical to those used during the earlier demonstrator program and are similar to the full-scale hardware. The flexbeam was constructed of hand laid-up carbon epoxy and was 1.8-mm thick by 17-mm wide. It had, however, no pretwist as will be incorporated into the full-scale flexbeam. The pendulum network consisted of a pendulum pitch arm, weight, and flexstrap. The flexbeam was instrumented with flatwise, edgewise, and torsional strain gages. The output of these three strain gages, along with a yaw potentiometer and a rotor one-per-rev signal were displayed on a Honeywell 1108B Visicorder. The turbine installation is shown in Fig. 6, and the model characteristics are summarized in Table 9. The instrumentation is summarized in Table 10.

Test Conditions

The model was tested in the diffuser section of the UTRC Pilot Wind Tunnel to the tunnel's maximum velocity of 29.5 m/s. Test conditions simulating high wind and generator cutout were conducted by allowing the rotor to operate at no-load at wind speeds from 0 to 29.5 m/s. These tests, in essence, were conducted at a constant velocity ratio. Parametric variations to blade pitch and the pendula mass and static flap angle were made to determine their effect on rotor stall. Operational limits were established for the model which included: peak flatwise stress not to exceed 1040 MPa (150,000 psi) peak rotor speed limited to 1800 rpm (100-m/s tip speed) due to a rotor speed/edgewise natural frequency coalescence at 2100 rpm. Flexbeam stresses were monitored continuously and data records were taken at each data point. A data point is defined as a new wind speed setting.

TABLE 9

MODEL DEMONSTRATOR PARAMETERS

Airfoil Series	0012
Rotor Diameter	1.07 m
Blade Chord	0.05 m
Blade Twist	3^{o}
Initial Blade Pitch	20^{o}
Static Pendulum Angle	50^{o}
Pendulum Weight	21 g
Pendulum CG Location	0.053 m

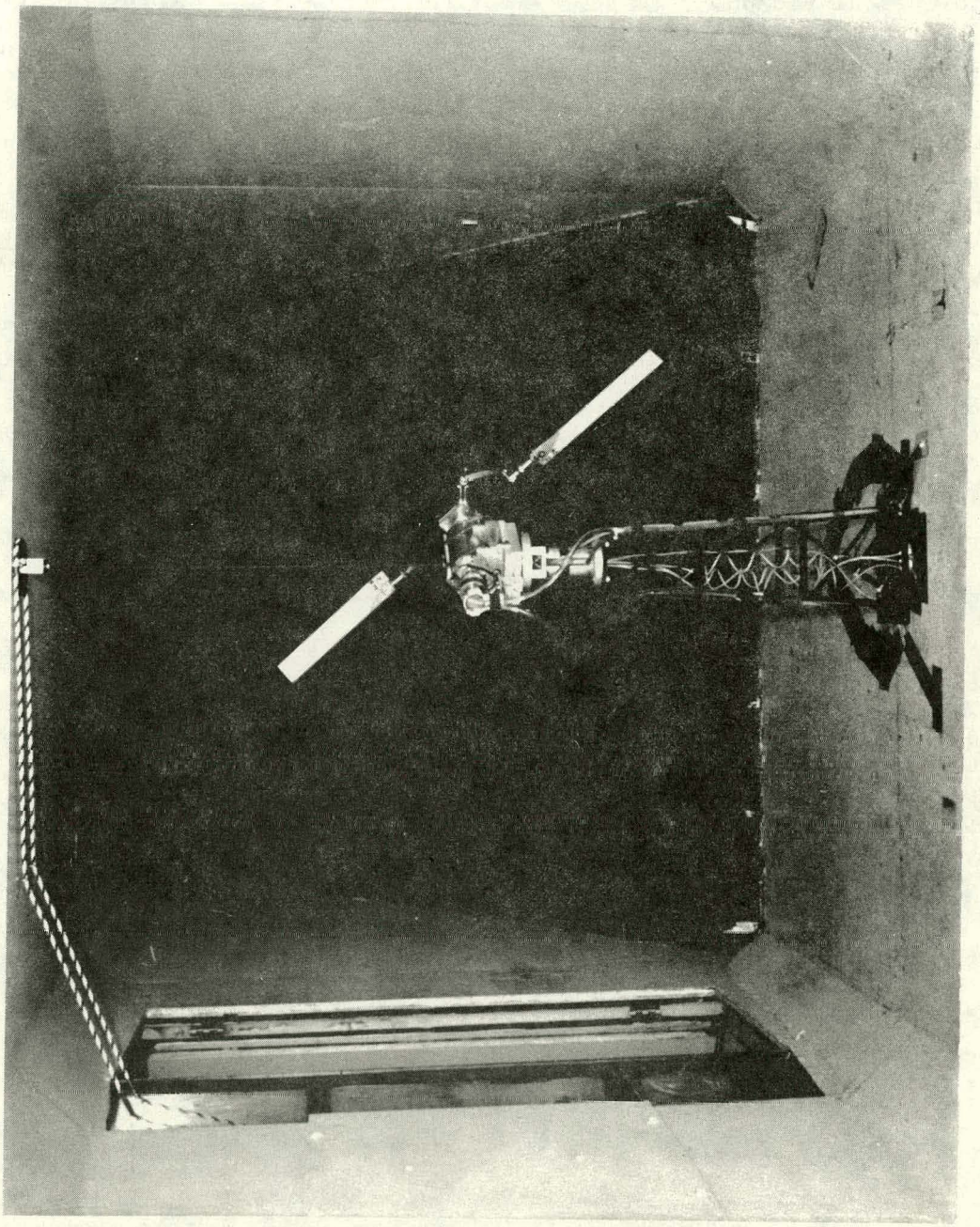

Fig. 6 3.5—ft Diameter Wind Tunnel Model

TABLE 10

MODEL DEMONSTRATOR INSTRUMENTATION

Rotor Speed, RPM	
Photo-Optical Pickup	EPUT Counter
Rotor Azimuth Reference, 1/Rev	
Photo-optical Pickup	Visicorder
Tunnel Speed	
Pitot Probe	Micro-Manometer
Drive System Yaw Angle	
Potentiometer	Visicorder
Flexbeam Stresses	
Flatwise-Edgewise-Torsion	
MM Strain Gages (0-10 V)	Visicorder
Blade Pitch Angle	
Clinometer & Torsion Strain Gage	Visicorder

The possibility of using rotor pitch-up as a method of increasing the blade-to-tower clearance was investigated by pitching the rotor drive shaft and generator 5° from the horizontal. The effect of lateral offset was also tested to determine the feasibility of this method as a means to counteract potential steady yaw bias angles due to wind shear or tower wake. The condition tested amounted to a lateral displacement of the rotor axis relative to the yaw axis by 0.6% of the diameter.

In addition, tests were conducted on a stopped rotor at tunnel speeds up to 23 m/s, to demonstrate a second possible high wind shutdown system, and also to simulate a possible failure mode, where either the drive shaft bearings, gearbox, or generator have seized-up causing the rotor to stop.

Results

The rotor could be made to stall by adjusting the initial blade pitch angle and/or pendula geometry. Stall occurred at a geometric angle of approximately +4° at a velocity ratio of 9.4 (the ratio of rotor tip speed/wind speed).

At stall the rotor decelerated to a new velocity ratio of 5.8. The stall phenomena was benign, causing no "hunting" on rpm and no large blade stresses. Increasing wind speed beyond rotor stall, resulted in small increases in rotor speed, however, at ever decreasing velocity ratios. At the maximum tunnel speed of 29.5 m/s, the velocity ratio had dropped to 2.16 and the blade angle was approximately +3.5°, indicating that the rotor was in deep stall. Rotor response to wind speed is shown in Fig. 7.

Rotor stall, being a function of blade pitch, could be brought about at various tip speeds by adjusting the initial blade pitch angle, as shown in Fig. 8. Similarly, the point of rotor stall could be moved up or down the wind speed curve by adjusting the pendulum pitch schedule. For example, by adding pendulum mass, stall would occur at a lower tip speed (hence lower wind speed). Increasing the pendulum mass cg location from the axis of rotation produced similar results.

Stopped Blade Results

When the stopped rotor was subjected to winds up to 23 m/s the flatwise stress at the root of the flexbeam increased as the square of the velocity, as shown in Fig. 9, to a maximum of 207 MPa (30,000 psi). The system's response was stable, the blades remaining downstream of the tower with very little vibratory stress, either edgewise or flatwise. Shown also on Fig. 9 are the flatwise stress results from the rotating test, Fig. 7. It can be seen that the stress variation with the benefit of centrifugal relief increases linearly with speed as opposed to the stopped blade stress which increases parabolically.

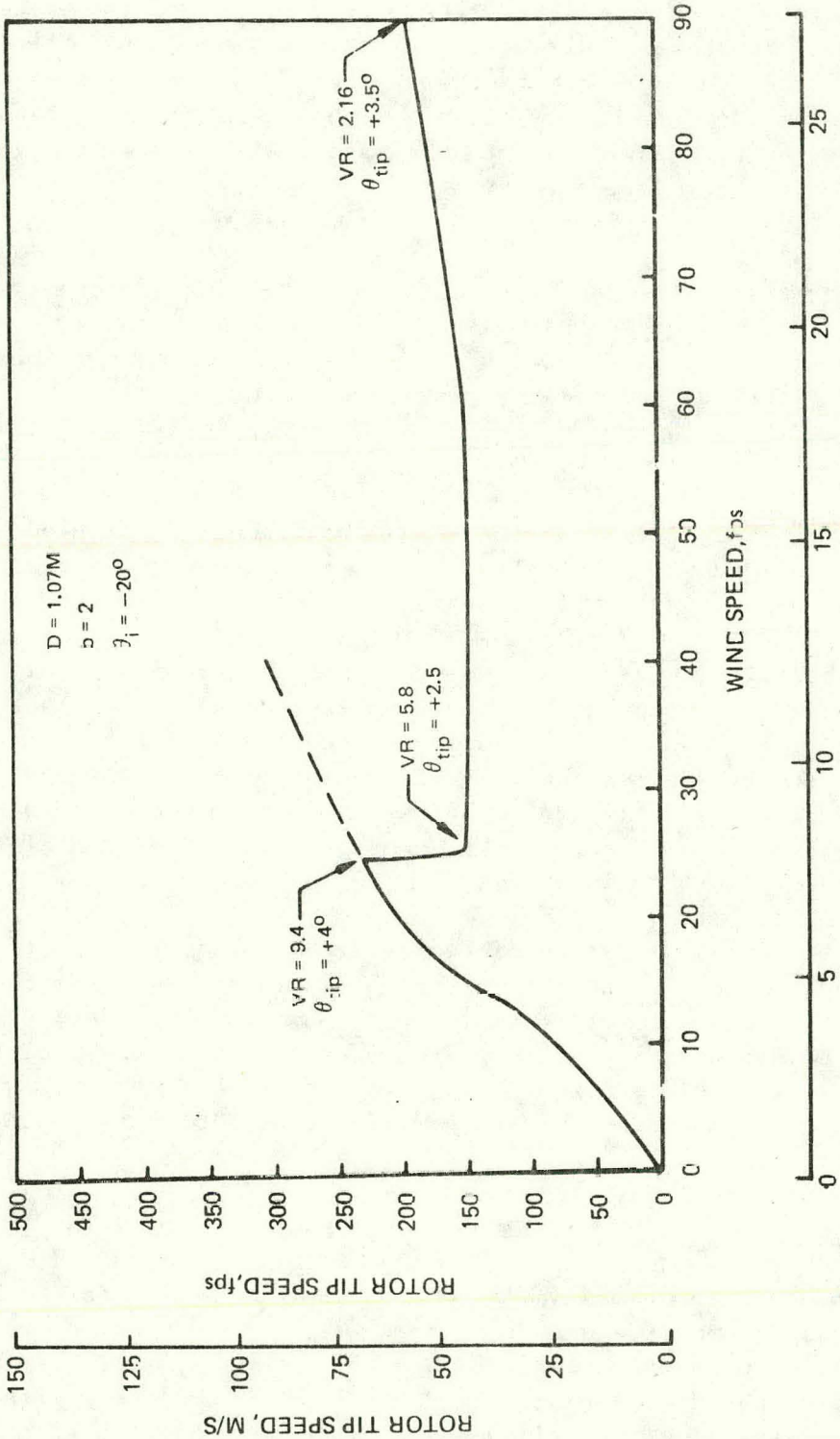

Fig. 7 Model Demonstration — Rotor Stall

78-09-184-3

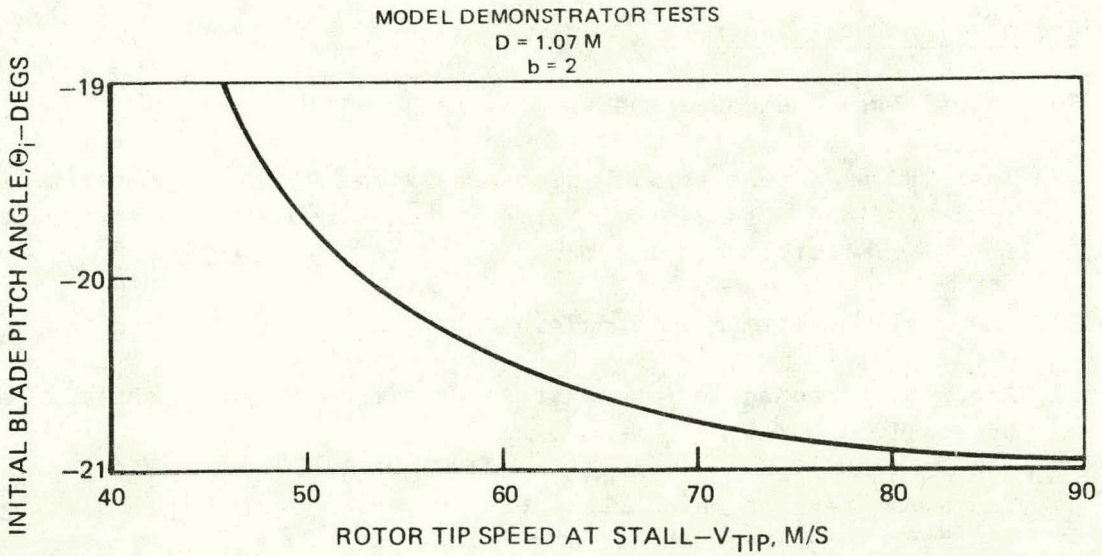

Fig. 8 Rotor Stall Speed vs. Initial Blade Pitch

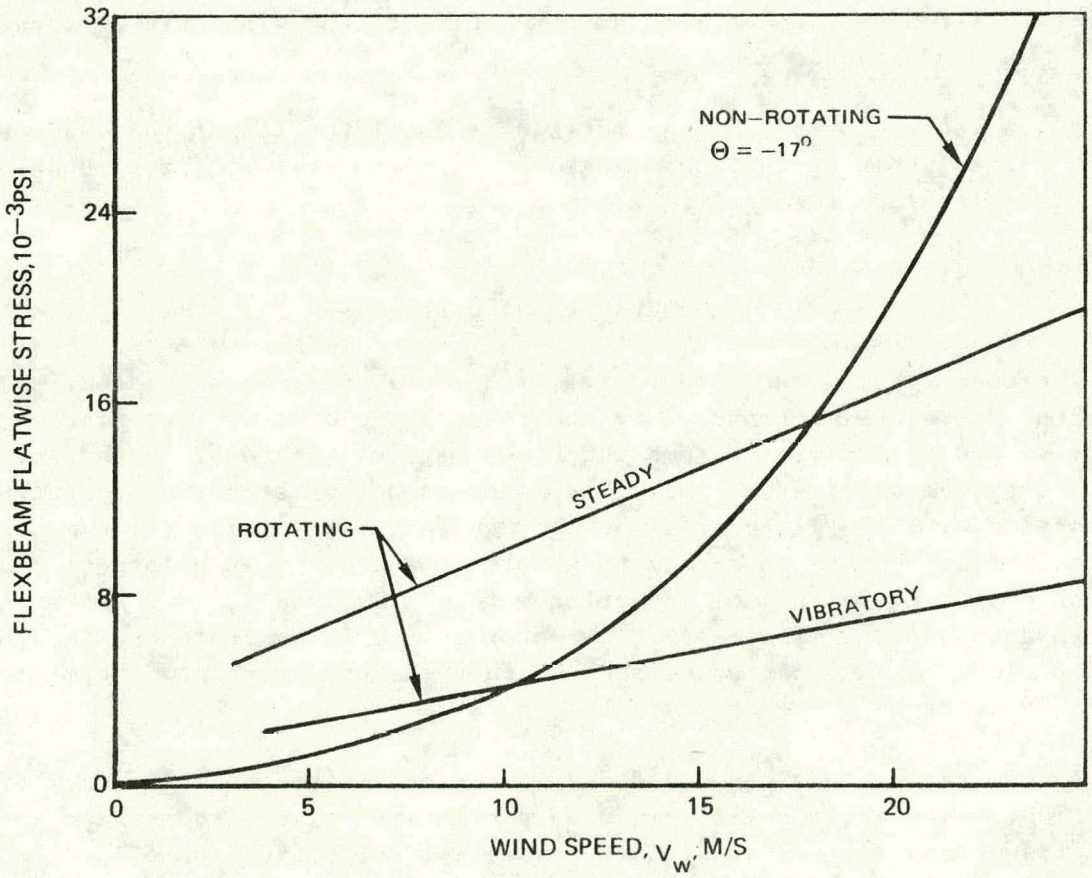

Fig. 9 Flexbeam Stresses Under Stalled Conditions

78-09-184-2

Conclusions from Model Tests

The model tests indicated that:

a) The UTRC wind turbine with self-regulating blade pitch can be stalled in its unloaded condition, typically at a geometric blade angle, for the untwisted blade, of approximately +4°.

b) The stall phenomena is stable and benign.

c) Rotor flatwise and edgewise stresses are not significantly affected by stall.

d) The wind speed at which stall occurs can be varied by adjusting the pendulum pitch schedule.

e) Stopped rotor flatwise stresses vary as the square of the wind speed and are therefore predictable. No dynamic stress problems exist with the stopped rotor.

f) A pitch-up of the rotor axis relative to the wind axis produces no undesirable dynamic effects.

g) A lateral offset of the rotor axis equal to 0.6% of the diameter results in a steady yaw angle of 17°, and does not cause undesirable blade responses.

Generator Calibration

The electrical power output of a wind energy conversion system is dependent on the power produced by the rotor as well as by the efficiency of the drive and electrical systems which are part of the total conversion system. The UTRC system utilizes an induction motor as a generator when operating in conjunction with a utility or M/G set. Manufacturers of induction motors, as well as the literature on such motors were consulted in an effort to determine the conversion efficiency of induction motors. Typically, data are available only to document the efficiency of a motor in a driving state and then only at rated power. No information existed which documented part-power efficiencies nor for a motor in a driven state (generator state).

A test program was conducted at UTRC to determine the efficiency of induction motors while being driven as generators. The test program was conducted on small (fractional horsepower) motors, as they were readily available. The following motors were tested:

a. 3/4 hp three-phase G.E. induction motor

b. 3/4 hp single-phase Dayton motor

The three-phase motor was tested: a) wired for three-phase power; b) wired for single-phase power; and c) wired for single phase with the remaining two phases connected to resistor loads (incandescent lights). The 3-phase motor was tested in the wired-for-single-phase power mode because the buyer of the wind turbine could be located in an area where 3-phase power is not available. It was, therefore, necessary to determine if the buyer could then wire his 3-phase motor into existing single phase power lines and proceed to efficiently and cheaply generate a-c power.

Test Apparatus

The two induction motors under investigation were driven by a variable frequency 90-hp induction motor through a BLH torque shaft. A typical installation is shown in Fig. 10. The motors were wired to an existing 208 Vac power line as shown in Fig. 11. A precision laboratory-type watt meter was used to measure power output and a volt and ammeter were used, in conjunction with the watt meter, to determine the rotor's power factor. Input torque was measured by the BLH torque shaft.

Results

Test results indicating motor efficiency, when driven as a generator, are presented as a function of power output/rated power in Fig. 12. Results indicate that the 3-phase generator has a peak efficiency of approximately 85% over the range of 60-140% rated power when wired as a 3-phase motor. Generator efficiency is reduced to approximately 78% when only one phase of the 3-phase motor is hooked up. The 85% efficiency is regained when the remaining two phases are connected to a resistor load bank. The single-phase motor proved to be least efficient with a peak of only approximately 72%. It would, therefore, seem to be wiser to use a 3-phase motor wired for single phase operation, with the other two phases hooked up to resistance loads, when faced with the availability of single phase power, only, rather than utilizing a single-phase motor.

The 3-phase motor was driven to three times the rated power, and although conversion efficiency decreased, when driven above rated power, there was no evidence of motor "break-out" nor unusual heating within the rotor. The power factor of the 3-phase motor, defined as $\cos\left[\tan^{-1}\sqrt{3}\,\frac{W_1 - W_2}{W_1 + W_2}\right]$ was 0.84 at rated power.

Since, typically, motor efficiency increases with motor size; these tests increase confidence that a 15-kW motor, when driven above synchronous

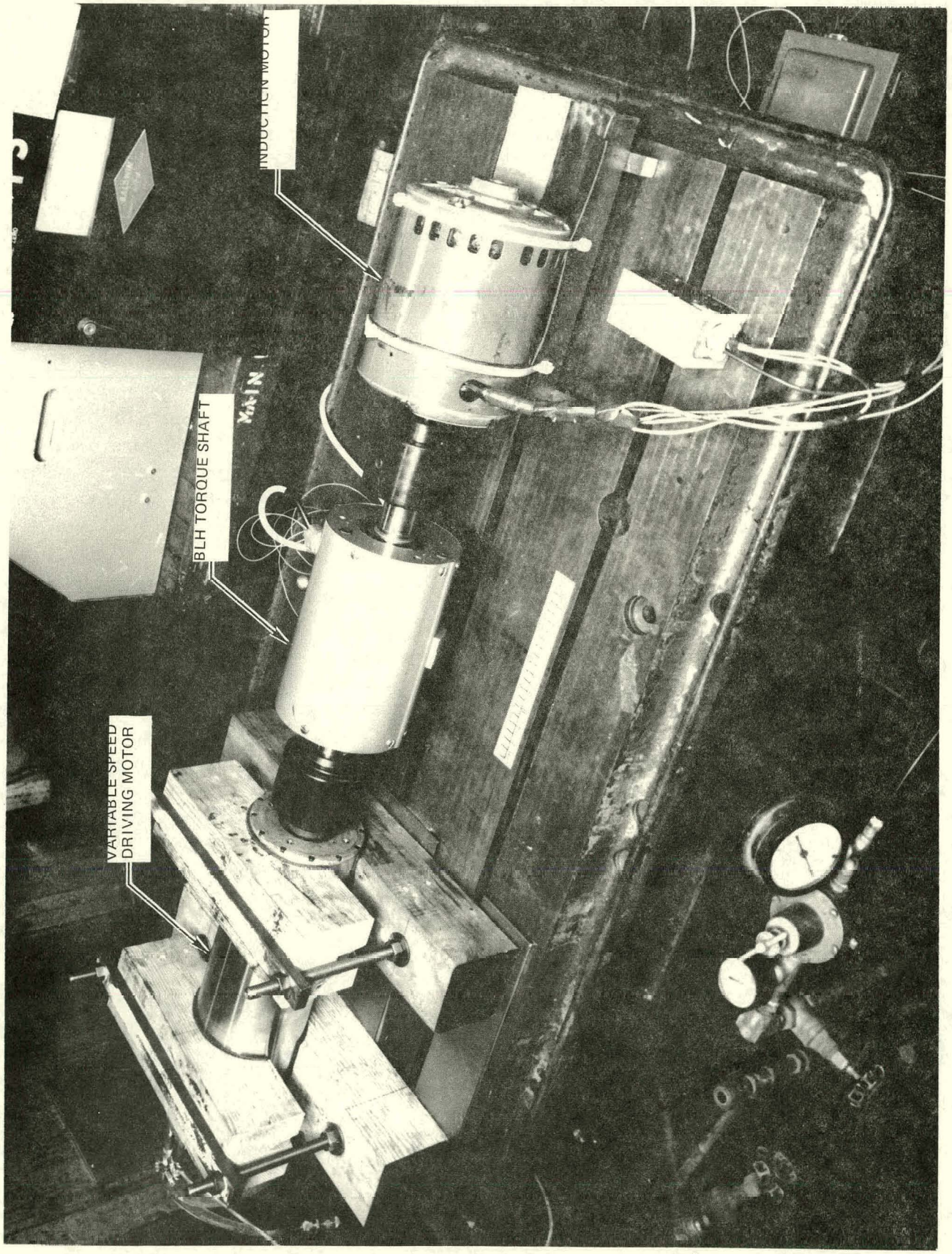

FIG. 10 Induction Motor Calibration Test Set–Up

78–09–193–4

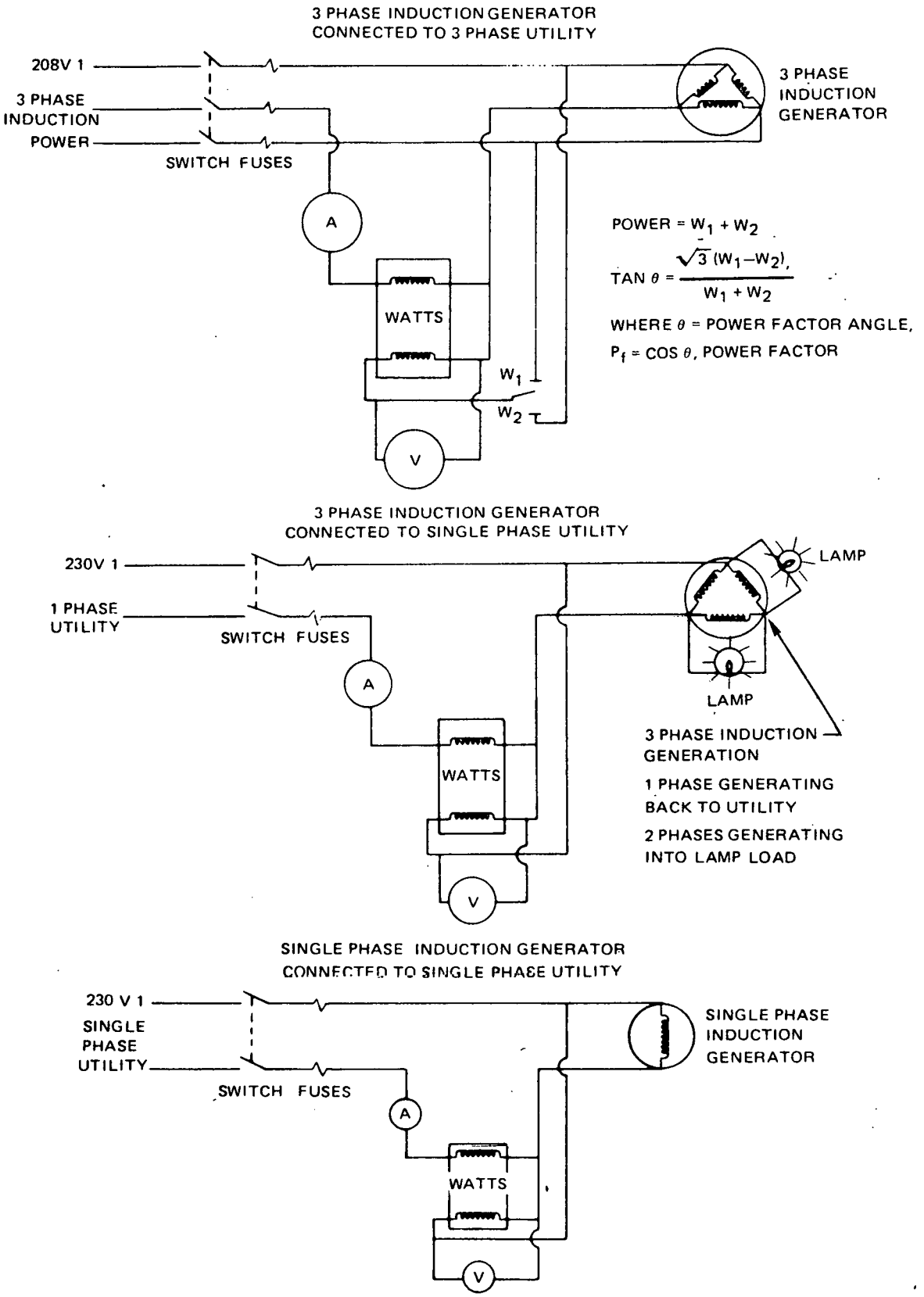

Fig. 11 Induction Motor Calibrations, Electrical Hook-Up

78-09-206-1

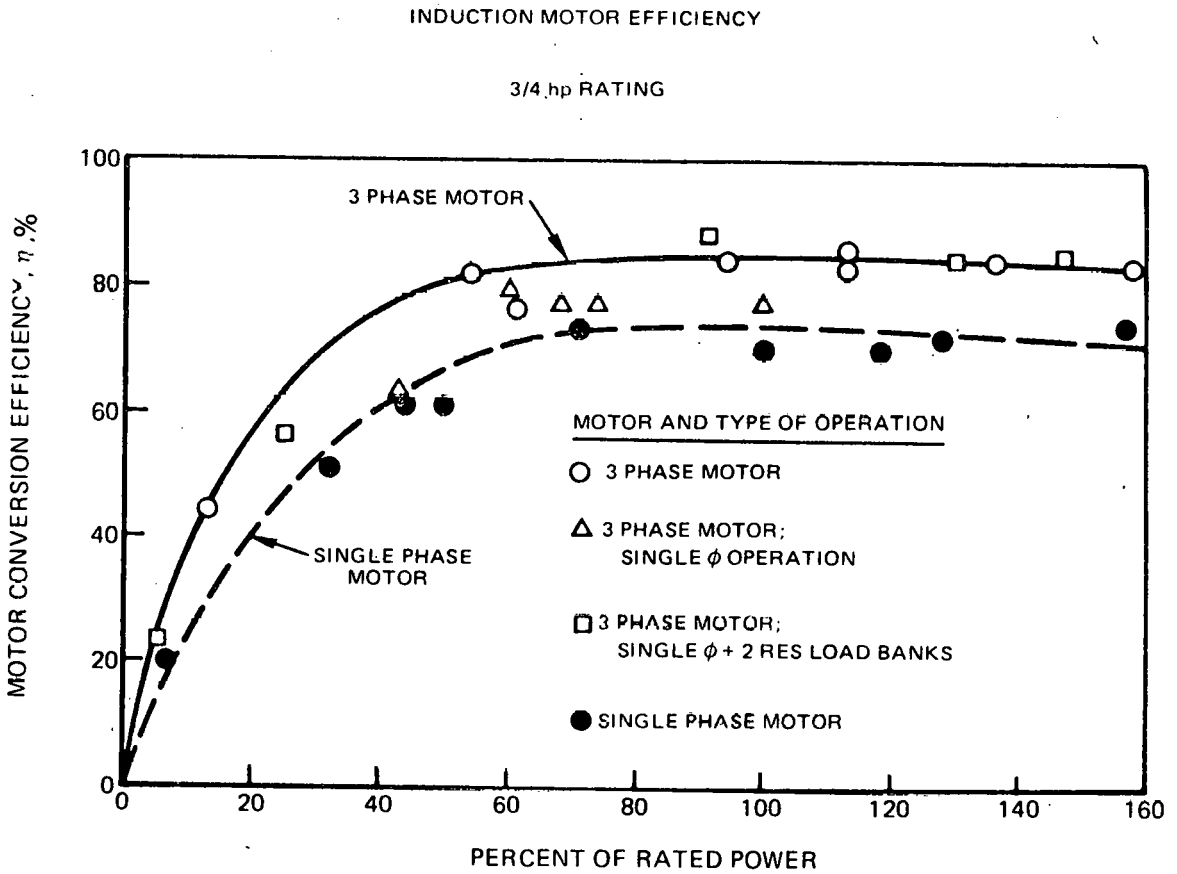

Fig. 12 Motor/Generator Calibration

78-09-193-3

speed as a generator, will result in peak conversion efficiencies of at least 85% and that this larger motor could momentarily absorb up to three times rated power without any adverse effects. It is apparent, however, that when operating in an area where public utilities require a system power factor of 0.9, capacitors will be required to increase the power factor of a 3-phase motor.

PERFORMANCE

This section describes the approach taken to size the rotor, and it summarizes the performance characteristics of both the rotor and the overall system. The three operating modes specified in the Work Statement are reviewed, and in support of operating in conjunction with a utility (Mode I), discussions were held with Northeast Utilities, Inc., and the results of those discussions are also included. Finally, the estimated noise level of the wind turbine rotor, calculated using an existing UTRC computer code, is presented for three operating conditions.

Control System

The basic control features of the UTRC system were defined in the CONCEPT DESCRIPTION section. The advantages of the pendulum control system lie in its passive simplicity in serving three important functions. First, it provides an adequate static pitch angle to create accelerating torques at low wind speeds, to bring the generator rpm up to operating speed quickly. Second, it places the blade at an aerodynamically efficient pitch angle for optimum performance, and finally, the same mechanism provides speed control, through stall, in the event of a power failure or if the generator break-out torque is exceeded. The blade angles which correspond to these three pendulum operating conditions are: -17° (leading edge into the wind) for accelerating torques, 0° for optimum performance at synchronous speed, and +5° for speed control.

Rotor Sizing

The major rotor design parameters were determined during the design study conducted under the DOE contract reported in Ref. 3. Trade-off studies were performed to evaluate the effect of rotor diameter, number of blades, twist, and taper. It was shown in that study that the benefits of optimizing blade aerodynamic parameters could improve performance from 5-10%, however the higher blade manufacturing cost associated with these parameters would tend to reduce overall cost effectiveness. The approach taken in that study, and continued in the current design was to use a blade that was simple to manufacture, which is a blade having a constant cross section without twist or taper. The 12.2-m (40-ft) rotor design of Ref. 3 was slightly larger than that required for the 8 kW system, however, it was decided to maintain the same chord dimension of 0.38 m (15 in.) to benefit from the earlier design effort. The chord dimension is generally dictated by the edgewise stiffness requirement that the first mode frequency be greater than the maximum rotor rotational speed to avoid the one-per-rev (1P) coalescence with the 1P gravity and wind shear excitations. By

maintaining the same chord, while reducing the blade length to accommodate the lower power requirement, the design would be somewhat more conservative and one in which higher rotor speeds would be permitted.

The initial rotor diameter was selected to provide 8 kW output power at the design wind speed of 9 m/s (20 mph). Using the following expression for power,

$$P = C_p \; 1/2 \; \rho A V^3 \eta$$

and assuming the system efficiency, η, to be 80%, and the power coefficient, C_p, to be 0.4, the rotor diameter to produce 8 kW in a 9-m/s wind is 8.5 m (28 ft). The power output for this size rotor was substantiated using the UTRC F456 performance program (Ref. 7), and these results are discussed later in this section. Performance calculations were made for the 8.5-m rotor, and it was found that, when operating at low-to-moderate wind sites, such as the Hartford, Connecticut area, only about 1 kW of power could be generated at 6.2 m/s (14 mph) if the rotor rpm was selected to give 8 kW at 9 m/s. Also, the cut-in speed did not occur until about 5.4 m/s (12 mph) which is considered inadequate for most wind sites. Thus it was decided to increase the rotor diameter so that at least 2 kW could be produced at 5.4 m/s and that the cut-in speed could be reduced to about 4.5 m/s (10 mph). The freedom to nominally increase rotor diameter could be taken without jeopardizing structural integrity since the original rotor diameter for the 0.38-m (15-in.)-chord design was 12.2 m (40 ft) as described in Ref. 3. It was determined that only a minimal negative cost impact would be felt if the rotor diameter was increased 10% to 9.5 m (31 ft). The edgewise frequency was still safely above 1P and the remaining components would not be compromised by this slight increase in diameter. The resulting power output at 9 m/s increased to 11 kW compared to the requirement of 8 kW. Details of the performance characteristics are presented below.

Rotor Performance Method

A rotor performance prediction program utilizing the Prescribed Rotor Wake analysis (code F456) was developed at UTRC to determine helicopter rotor performance. This program was modified for wind turbine rotor performance under the subject contract. The program assumes a classical, undistorted wake with variable inflow to compute local induced axial velocities. These local induced velocities, along with rotational speed, wind velocity, and two-dimensional airfoil data, are then used in calculating local, spanwise forces which are integrated over the rotor span, resulting in overall rotor performance for one combination of geometric and aerodynamic condition. To generate a performance map the program must be re-run for each new combination of parameters. Input variables in the program include: rotor tip speed,

number of rotor blades, rotor radius, blade twist angle, blade collective pitch, blade coning angle, blade chord, rotor solidity, wind speed, and two-dimensional airfoil data. Output data include: spanwise circulation, spanwise angles-of-attack, spanwise induced velocities, rotor torque, rotor thrust, rotor power, velocity ratio, power coefficient, thrust coefficient, and mean induced velocity.

Utilizing the UTRC rotor performance code F456, a set of general performance data was generated which covers a wide range of geometric blade pitch angles and velocity ratios. These results are presented as power coefficient and thrust ratio as a function of velocity ratio in Figs. 13 and 14, respectively. At any given blade angle, these three parameters describe the aerodynamic performance of the rotor system, at any combination of rotor tip and wind speed.

Wind turbines, in general, may be operated in two modes; at constant rotor speed or at optimum velocity ratio. A rotor system operating at constant speed will experience a velocity ratio variation with wind speed as shown in Fig. 15 and, therefore, a variation in power coefficient. The typical wind turbine, with active pitch control or fixed pitch will be operating at a constant velocity ratio when it is in the optimum velocity ratio mode of operation. This results in a variation of rotor speed with wind speed as shown in Fig. 16. The UTRC wind turbine, which has a passive pitch control system which is solely a function of rotor speed (Fig. 17), when operating in this mode will operate at varying blade pitch angles as rotor speed is varied. Since the power coefficient is a function of both the velocity ratio and the blade pitch angle, the maximum power can be realized at only one combination of velocity ratio and the blade pitch angle and hence, with a passive pitch control system, the rotor performance will be optimized at only one rotor speed and will therefore result in off-design operation at other speeds. The parameters resulting in power optimization require a blade pitch angle of 0° at a velocity ratio of 7.5.

Modes I & II Performance

The electrical power output of the WTG, when operating in parallel with an established source of 60 Hz a-c power such as the utility (Mode I) or a motor-generator set (Mode II), must be constant voltage and frequency. Several rotor/generator configurations can be devised to meet these requirements. Possible candidates are listed in Table 11.

A rotor operating at optimum velocity ratio, and therefore varying speed, will, if connected to the generator through a fixed ratio transmission, produce variable frequency a-c power. For this system to produce constant frequency a-c power requires a variable speed gearbox or a variable speed generator.

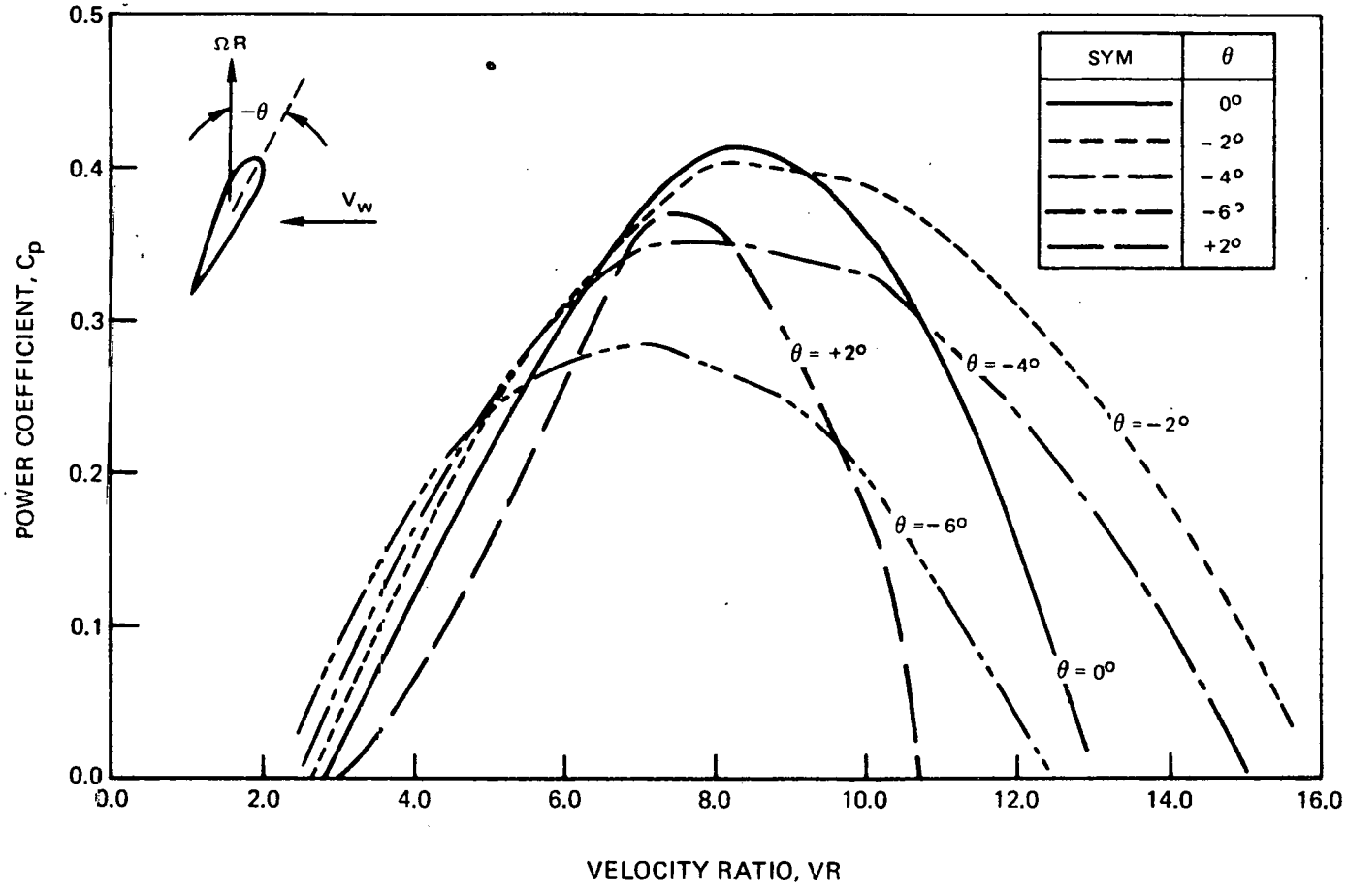

Fig. 13 Rotor Power Coefficient as a Function of Velocity Ratio and Blade Pitch, θ

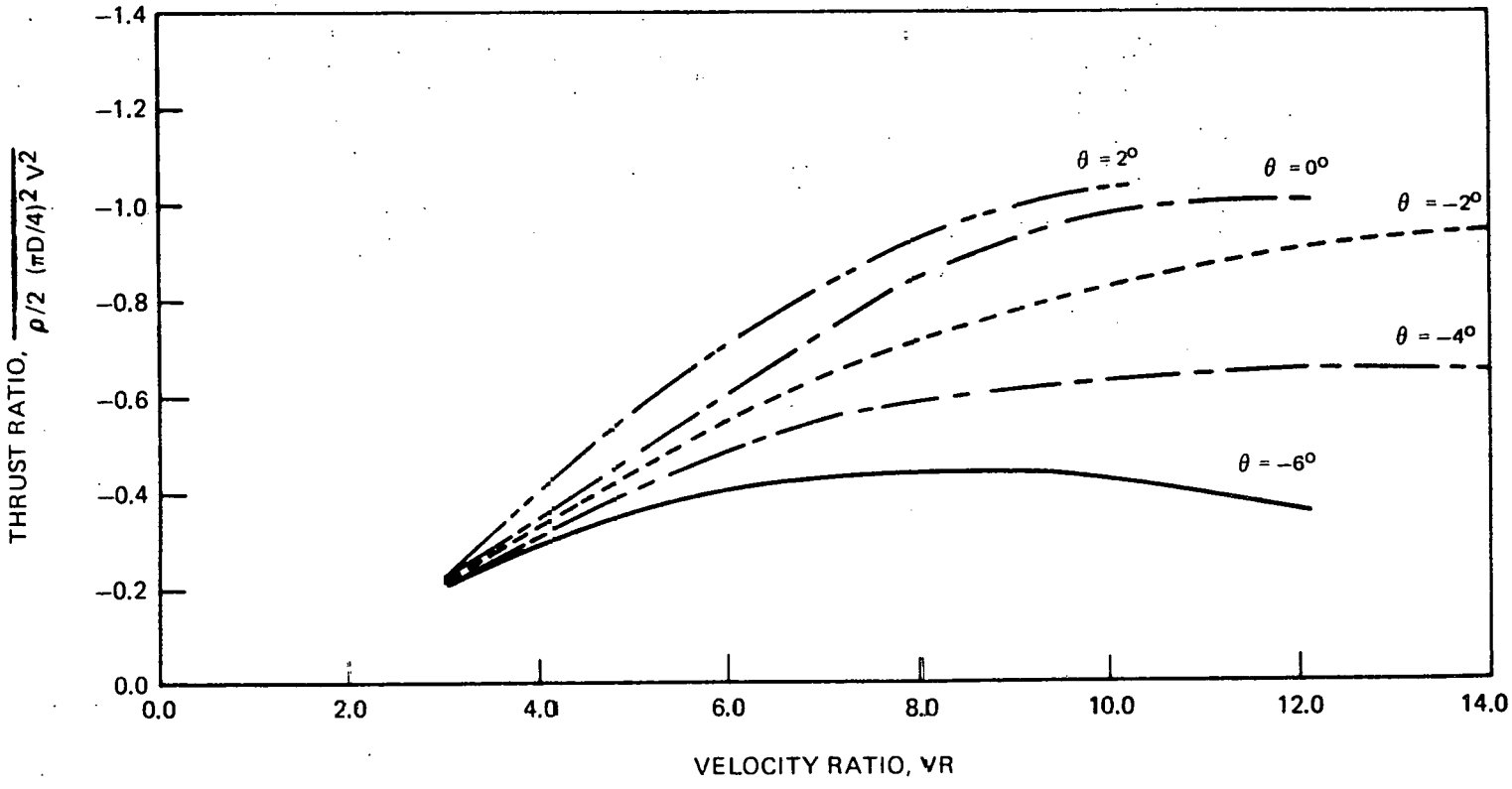

Fig. 14 Thrust Ratio As A Function Of Velocity Ratio And Blade Pitch Angle, θ

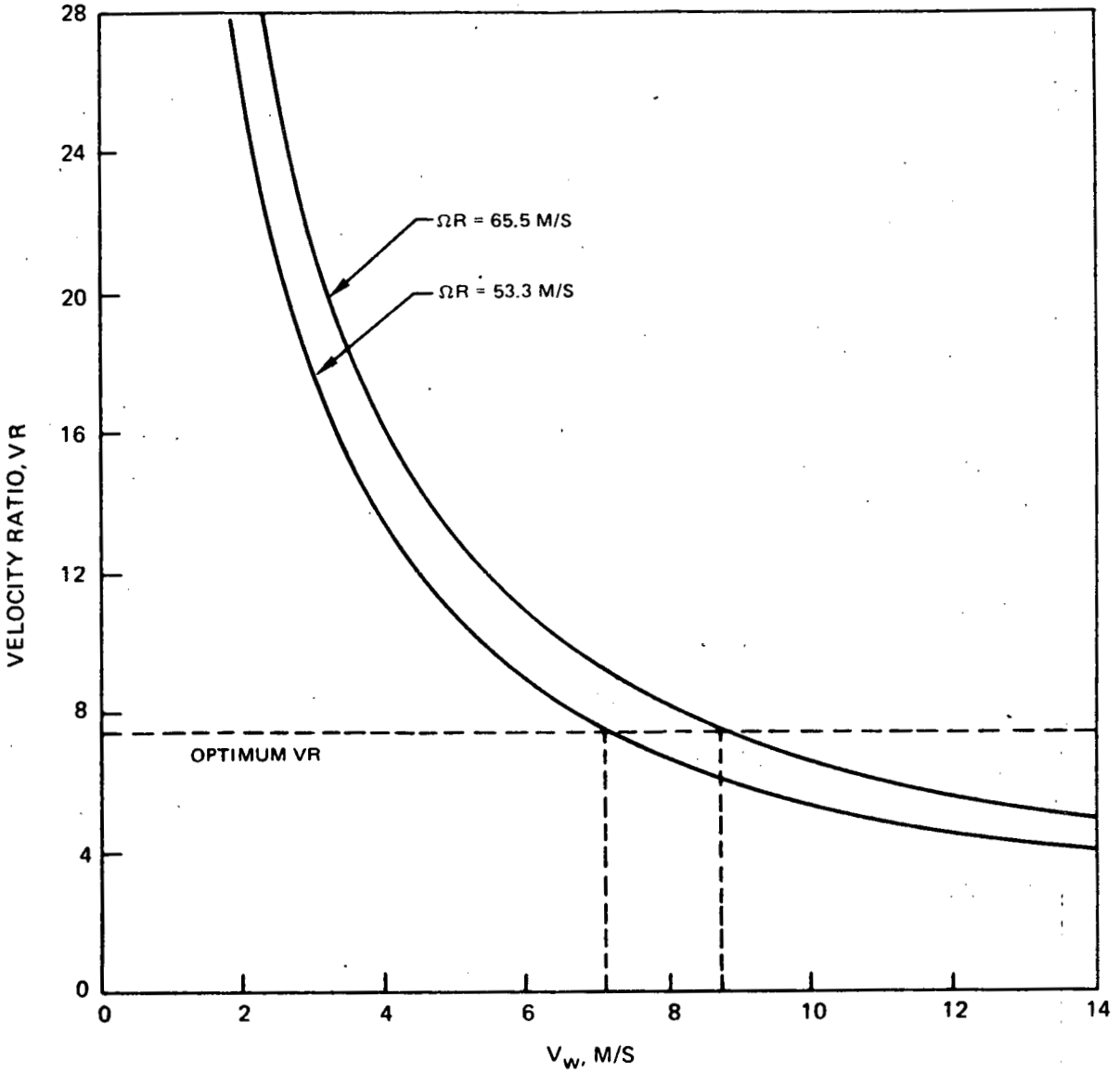

Fig. 15 Effect of Wind Speed on Velocity Ratio (VR) - Constant RPM System

78-09-219-4

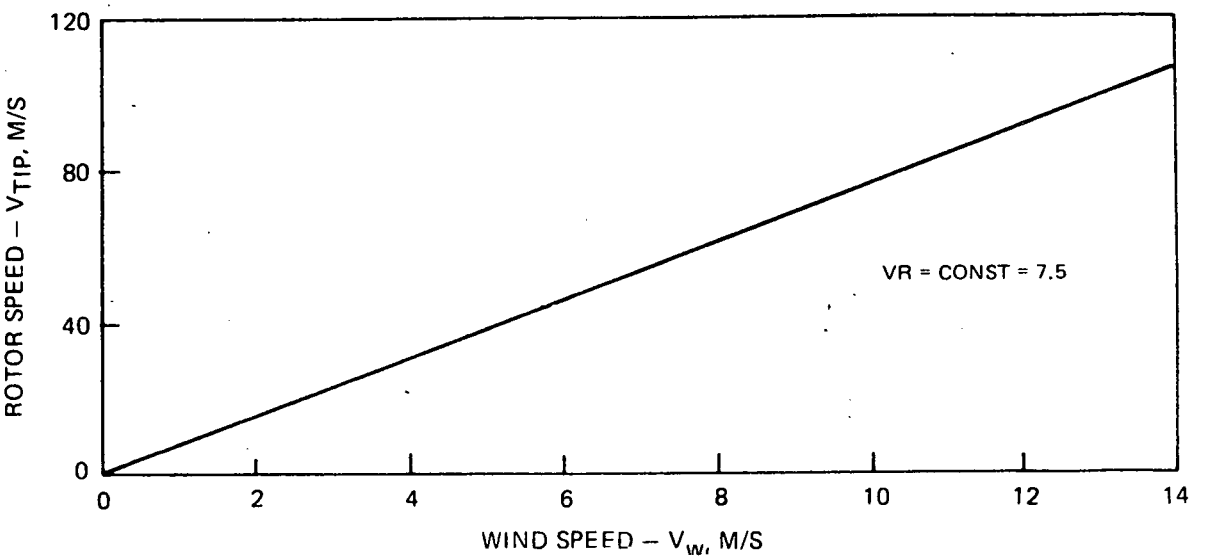

Fig. 16 Tip Speed vs. Wind Speed at Constant Velocity Ratio

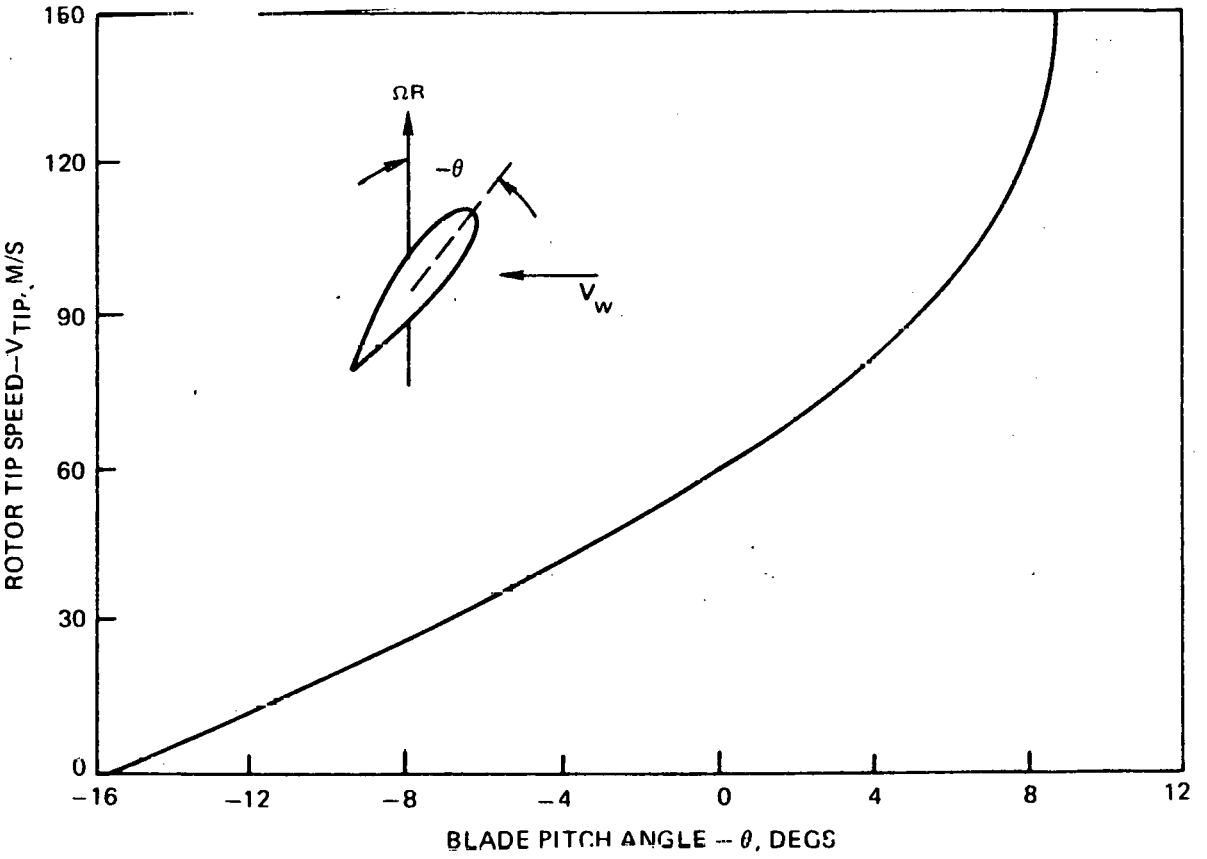

Fig. 17 Blade Pitch Schedule

78-09-219-3

TABLE 11

ROTOR/GENERATOR OPERATING MODES

		Rotor Operating Mode	Power Regulation	Transmission	Generator
Constant RPM Rotor	1a	Fixed Pitch	External	Fixed Ratio	Constant RPM
	1b	Variable Pitch	Blade Pitch	Fixed Ratio	Constant RPM
Optimum Velocity Ratio Rotor	2a	Fixed Pitch	None	Variable Speed	Constant RPM
				Fixed Ratio	Variable Speed
	2b	Variable Pitch	Blade Pitch	Variable Speed	Constant RPM
				Fixed Ratio	Variable Speed

Both solutions require custom and, therefore, expensive equipment. A third solution would be a fixed ratio transmission driving a variable speed generator producing variable frequency a-c power which could then be rectified and the resulting d-c power inverted to produce constant frequency a-c power. But, as will be shown later, this system would be expensive and therefore undesirable.

A rotor operating at constant rpm, when mated to a fixed ratio transmission and a constant speed generator, will produce constant frequency a-c power. Two methods exist to maintain a fixed rotor speed. The first utilizes variable blade pitch to maintain speed. However, as was stated earlier; the simple, passive blade pitch mechanism of the UTRC design does not permit a blade pitch variation independent of the rotor speed. Therefore, if the blade pitch is to be varied, the rotor speed must first be changed. Hence operation in configuration 1b (Table 11) is impossible. Therefore, to operate at constant rotor speed an external governing device must be connected to the rotor. An induction generator is such a device. Its rotational speed is determined by the power line frequency to which it is connected, and is constant from no load to rated power within 10%. Configuration 1a, therefore, is a viable candidate for efficient power generation. This scheme of operation is highly desirable for several reasons. First, the generator output frequency and voltage is that of the power lines. All the power produced by the rotor can be converted by the generator; there is no high power cutout required and the generator can be sized for peak power at fairly low wind speeds since the power coefficient decreases at high wind speeds due to off-design operation. The efficiency of the electrical conversion hardware is high and the cost is low, resulting in an optimization of $/kW.

Therefore, when the UTRC wind turbine generator is operated in parallel with an existing source of 60 Hz a-c power, the rotor will be operating in a constant rpm, constant blade pitch, varying velocity ratio mode. For the user to efficiently convert wind to electrical energy it is desirable to optimize the velocity ratio for the user's annual mean wind velocity. From Fig. 13 it can be seen that the maximum C_p occurs at a velocity ratio of about 7.5.

The rotor's velocity ratio is a function of rotor tip speed and wind speed: $VR = \Omega R/V_W$. The wind speed, V_w, is a function of the turbine site only, and the rotor tip speed is a function of rotor diameter (D); speed increaser gear ratio (GR); and the rated speed of the generator (Ng) as follows:

$$\Omega R = \frac{Ng}{60} \times \frac{1}{GR} \times D/2. \quad \text{Therefore, } VR = \frac{Ng \quad D/2}{60 \ GR \ V_W}$$

Since the rotor diameter is fixed at 9.45 m, and the wind speed is a given value dependent on the wind site only, the rotor's velocity becomes a function of generator speed and gear ratios. Generators are available which are rated at 900, 1200, 1800, and 3600 rpm. However, due to mass production and generator availability, the 1800-rpm generator is considerably cheaper and was, therefore selected for power generation. This leaves velocity ratio as a function of gear ratio, only. The rotor's velocity ratio and consequently the power coefficient will vary with gear ratio as shown in Fig. 18a and 18b at wind sites of 7 m/s and 9 m/s, respectively. As shown, the peak power coefficient at the low wind site is produced at a gear ratio of approximately 1:17, while, at the high speed site (18b) a gear ratio of approximately 1:14 produces peak power. It is evident that each discrete wind site with its own velocity duration curve would require a speed increaser with ratios selected for that site, to optimize power output. This would result in a wind turbine system which is custom designed for each wind site and would require the purchase of different speed increasers to meet the needs of the individual user. Since the cost of a single unit decreases with the number of similar units purchased, the purchase of large numbers of differing units would not be cost effective. It is, therefore, recommended that only two basic wind turbine generators be offered for parallel operation with an existing source of 60 Hz a-c power. The low wind site unit would incorporate a 1:17 speed increaser and would operate at optimum velocity ratio at a mean wind speed of about 5 m/s. The high wind site unit would come with a 1:14 increaser, and it would be optimized at a mean wind speed of about 9 m/s.

Rotor power output as a function of wind speed is presented in Fig. 19 for both the high and low wind units. The high wind unit (65.5-m/s tip speed) produces more power at a higher wind speed than the low speed unit (53.3 m/s), although at the expense of reduced power at the lower wind speeds. This is reflected in the annual energy output of the units at low mean wind velocities

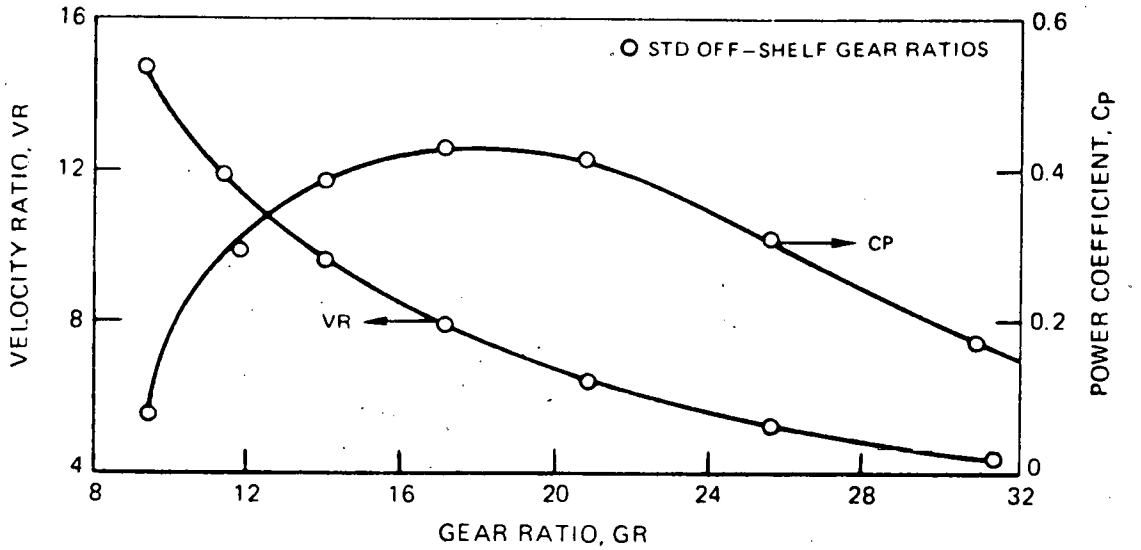

Fig. 18a Effect of Gear Ratio on Velocity Ratio and Power Coefficient
V_W = 7 M/S

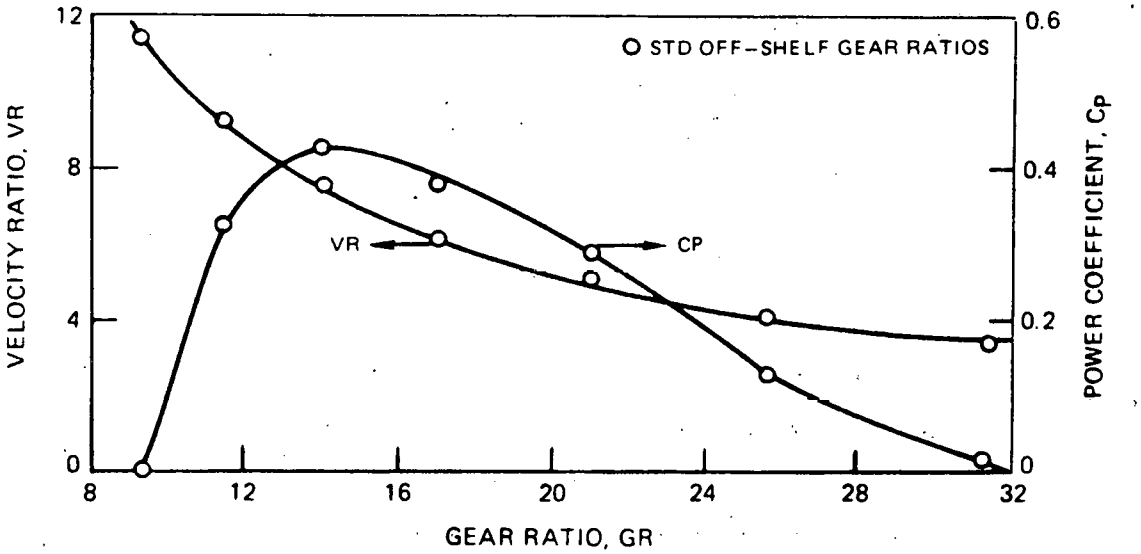

Fig. 18b Effect of Gear Ratio on Velocity Ratio and Power Coefficient
V_W = 9 M/S

78-09-206-2

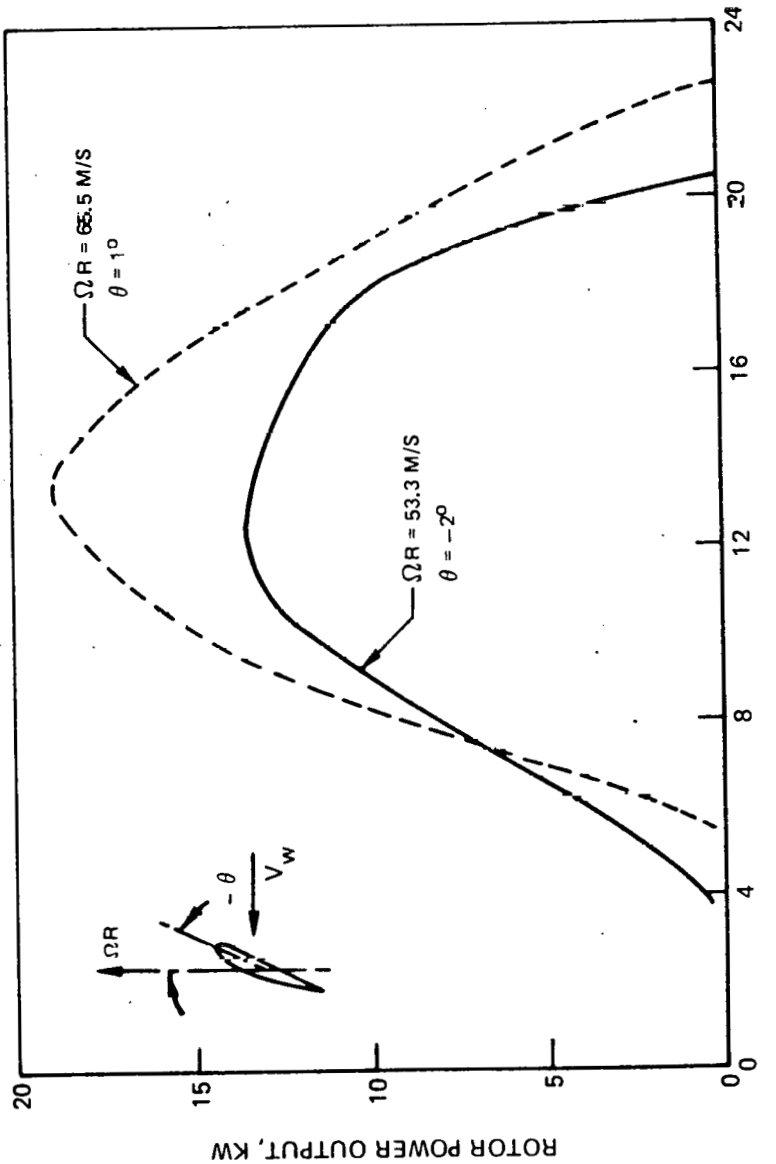

Fig. 19 Constant rpm Mode of Operation

78-09-193-1

(Fig. 20) where the low speed unit shows a higher power output and less down-time (Fig. 21) than the high speed unit. This is due primarily to the lower cut-in speed of the low speed unit, which cuts in at a wind speed of 3.4 m/s. The high speed unit cuts in at a wind speed of 5 m/s. This advantage of the low speed unit, which is optimized for a low wind site and therefore can extract the lower energy content of lower wind speeds more efficiently, quickly disappears with increasing mean wind speed. This is due to the fact that the high speed unit can more efficiently convert the high energy content of higher wind speeds even though the time duration at high speeds may be relatively short.

Mode III Performance

The stand-alone system (Mode III) has no external source of 60 Hz a-c power. Therefore, it cannot operate with an induction motor which, as was shown earlier, acted as a rotor speed governor. Also, since the inherent design of the UTRC wind turbine generator includes a passive pitch mechanism, where blade pitch cannot be varied independently of rpm, this system cannot operate at a fixed rotor speed. In this stand-alone mode, the system operates at more nearly a constant velocity ratio. In this operating mode; as the wind speed varies so does the rotor speed; and since the blade pitch angle is a function of rotor speed, so does the blade pitch angle vary with rpm. As was discussed earlier, rotor power output is maximized at only one combination of velocity ratio (7.5) and blade pitch angle (0°). The power output for this mode of operation is shown in Fig. 22. The actual operating points would represent the envelope of the various curves shown. The annual power output of the stand-alone system, as a function of mean wind speed, is shown in Fig. 23 and the system downtime is presented in Fig. 24.

Summaries of the performance characteristics in both the Mode I and II and Mode III operating conditions are given in Table 12.

Electrical Design

Since Modes I and II are similar, in that the turbine is operated in parallel with an established source of 60 Hz a-c power, the resulting design can be the same for both. The design for Mode I and II operation uses a 3-phase induction motor, driven above synchronous speed by the rotor. The power generation scheme for the Mode III, stand alone system, is a d-c generator for charging of lead acid batteries or other d-c load.

To arrive at an optimum solution for power generation in any of the three modes of operation several factors such as cost, efficiency, complexity, and reliability had to be carefully weighed. In addition, for Mode I generation, additional restrictions imposed by public utilities on power co-generation systems had to be met.

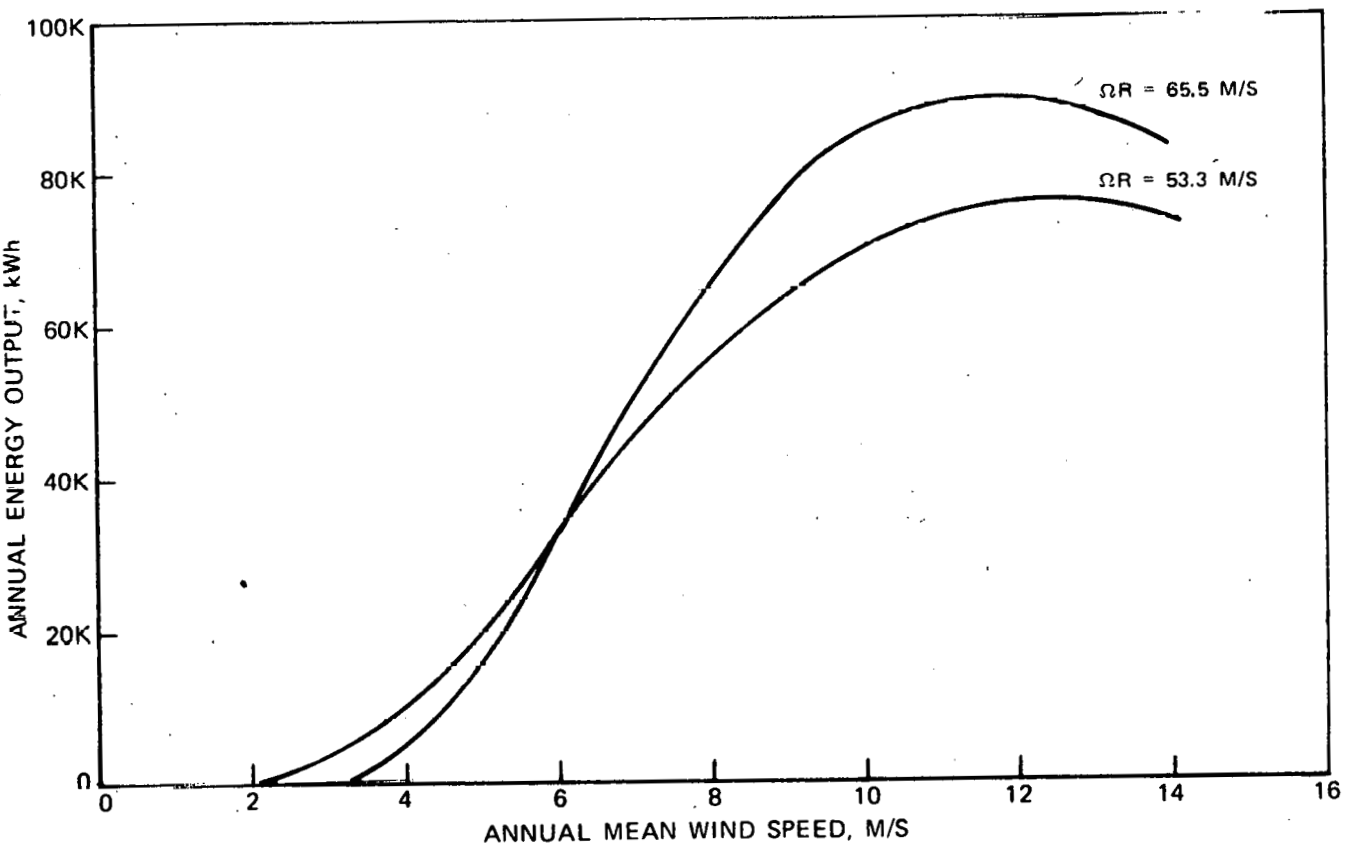

Fig. 20 Annual Energy Output, Modes I & II

78-11-53-1

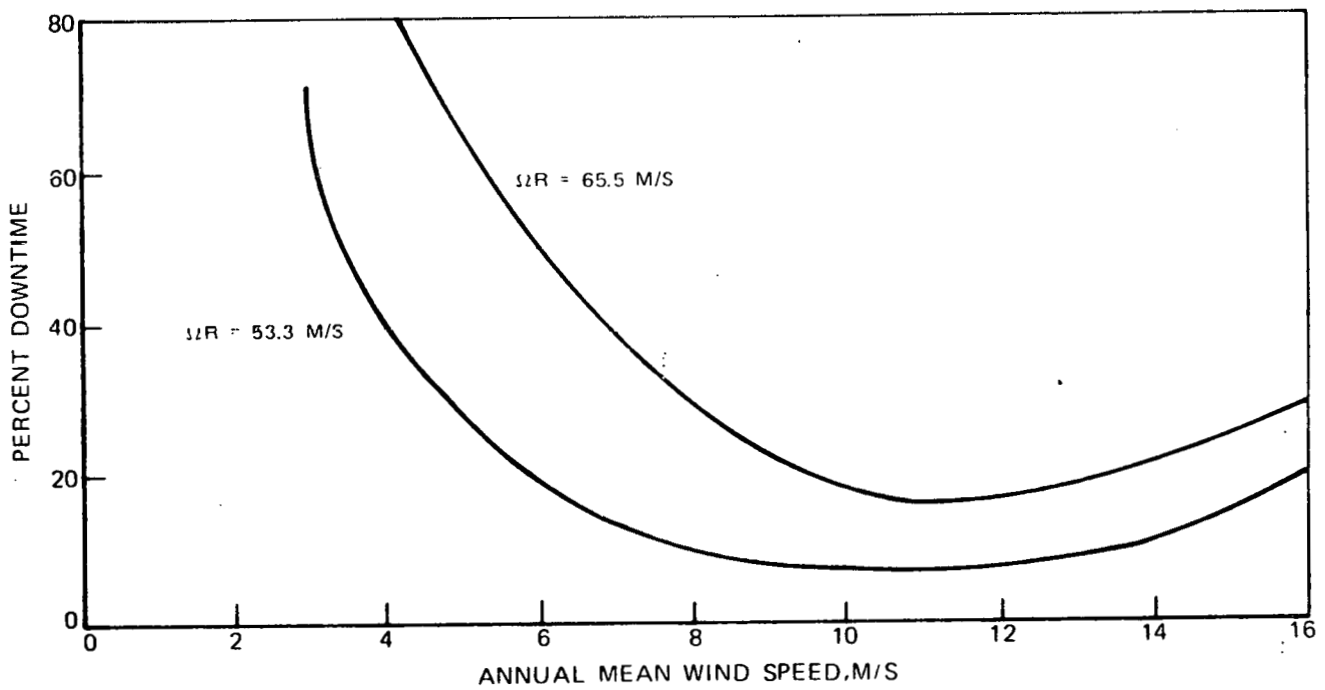

Fig. 21 Annual Percent Downtime, Modes I & II

78-11-53-2

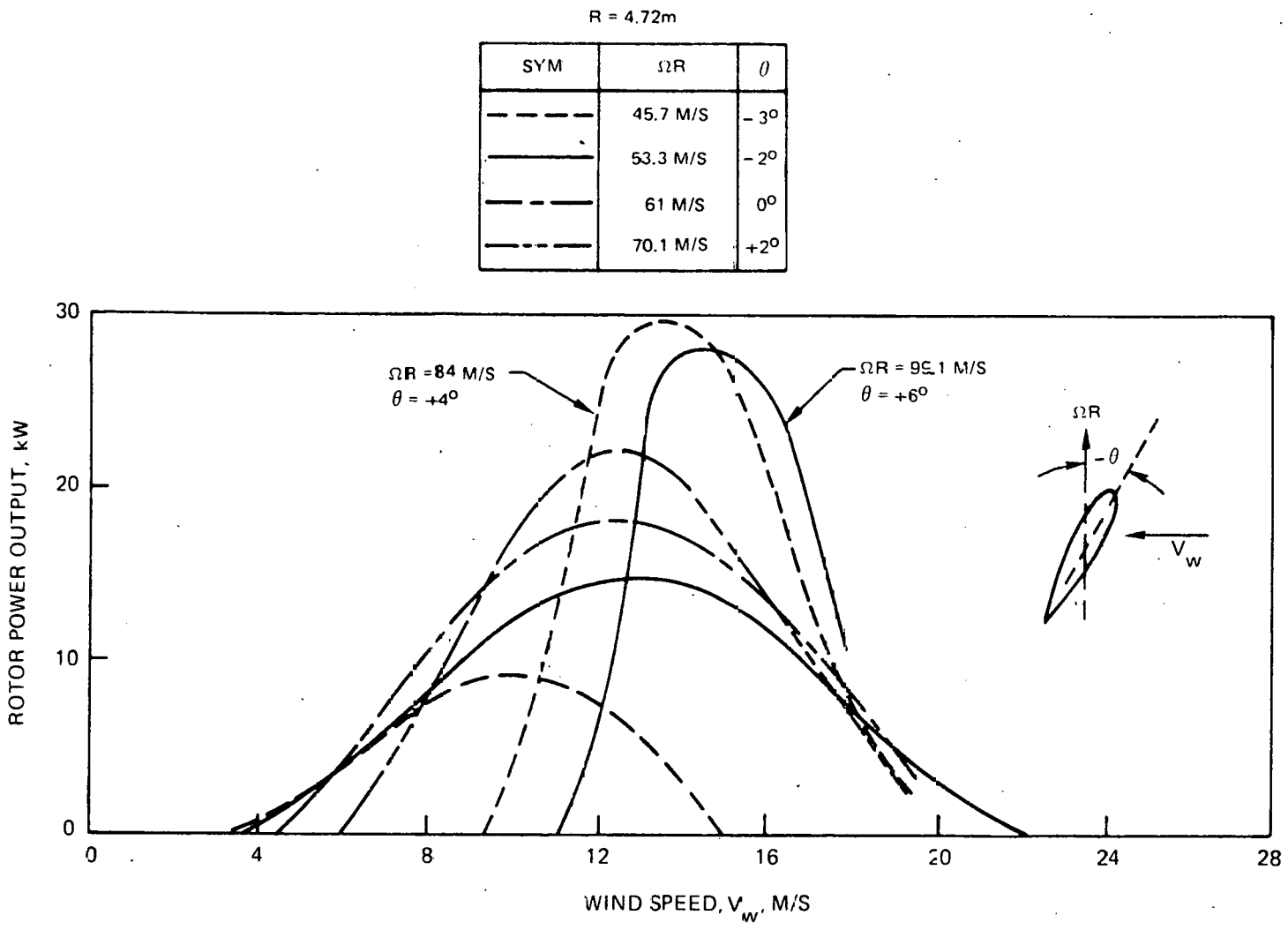

Fig. 22 Rotor Power Output, Mode III

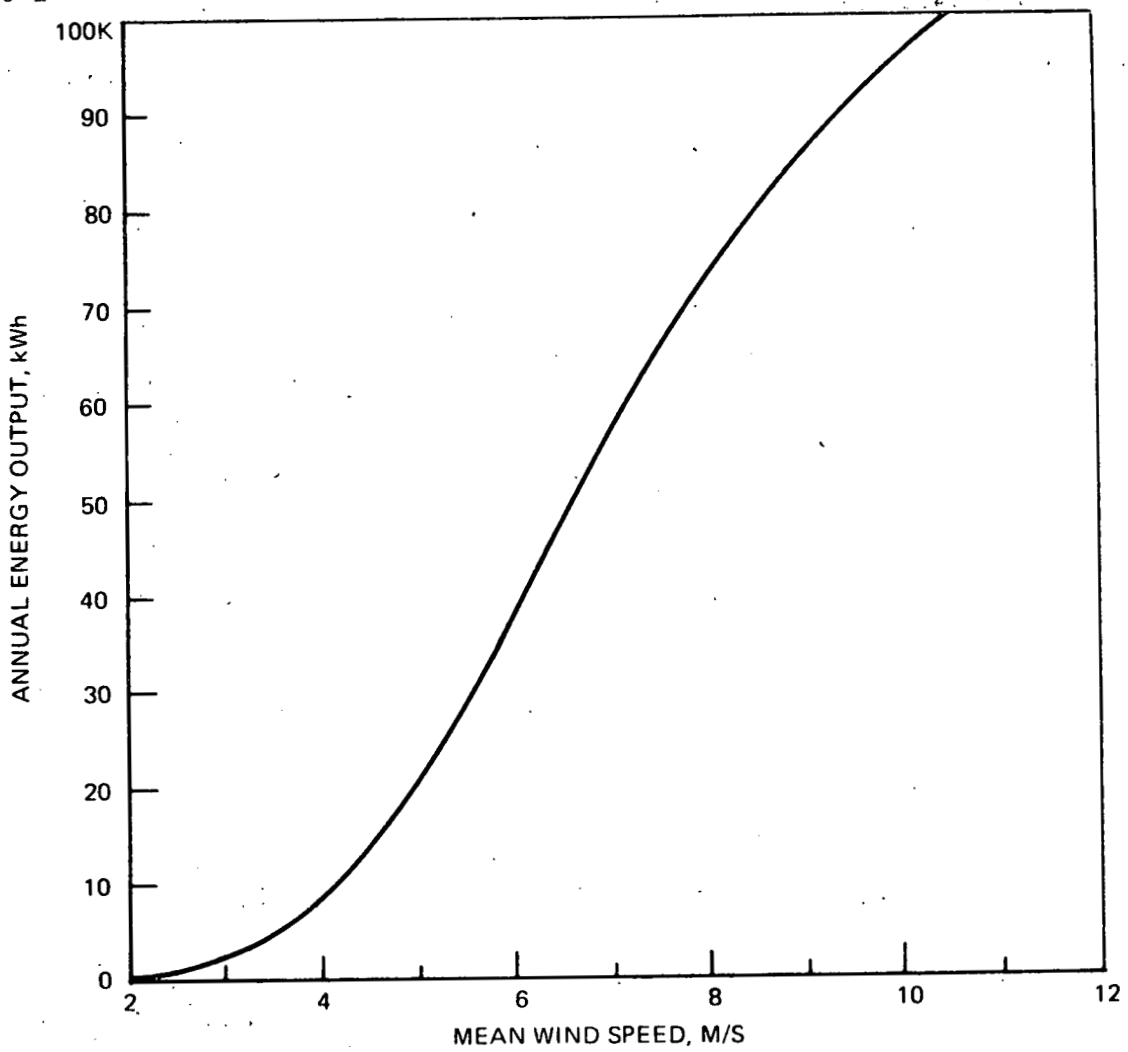

Fig. 23 Annual Energy Output, Mode III

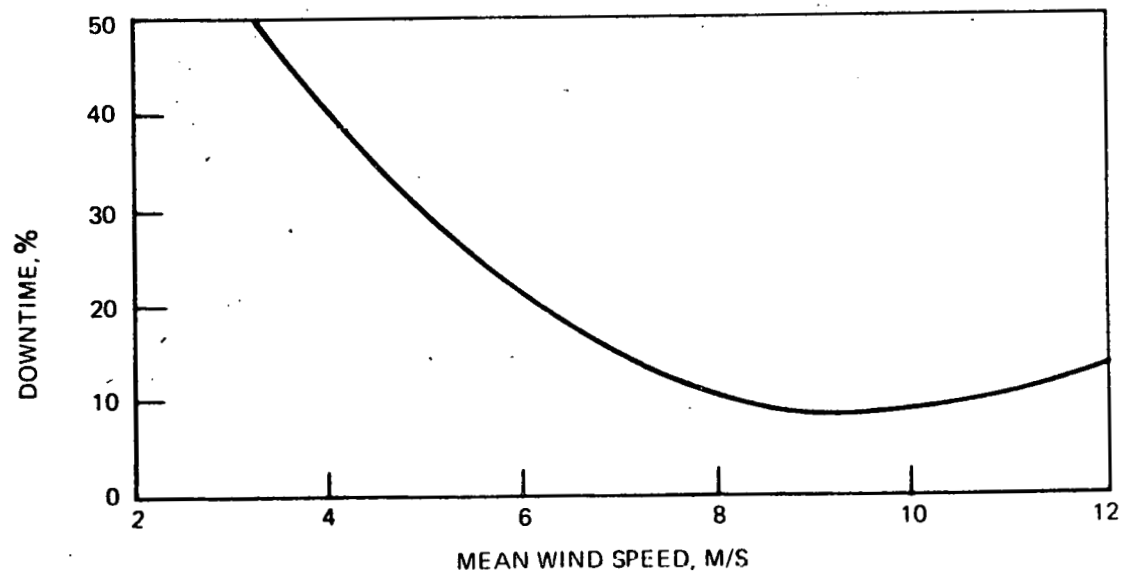

Fig. 24 Annual Percent Downtime, Mode III

78-10-301-1

TABLE 12

PERFORMANCE SUMMARY

	Modes I and II Low Speed Unit/ High Speed Unit	Mode III
No. of Blades	2	2
Blade Chord	0.381 m	0.381 m
Airfoil Series	23112	23112
Pre-Cone	8^{o}	8^{o}
Solidity	0.0568	0.0568
Static Blade Pitch	-16^{o}	-16^{o}
Rotor Diameter	9.45 m	9.45 m
Rated Wind Speed	8.93 m/s	8.93 m/s
Rotor Tip Speed at V_{RATED}	53.3/65.5 m/s	53.3 m/s
Blade Pitch at V_{RATED}	$-2/+1^{o}$	0^{o}
Rotor Power Output at V_{RATED}	11.1/13.6 kW	13.0 kW
Generator Power Output at V_{RATED}	9.5/11.7 kW	12.2 kW
Cut-In Wind Speed	3.36/6 m/s	3.0 m/s
Cut-Out Wind Speed	22.9/21 m/s	22.9 m/s
Annual Electrical Power Output at V_{MEAN} = 5 m/s	20,000/16,500 kWh	20,000 kWh

Modes I & II

Three power generating schemes were investigated to determine the optimum method of converting wind energy to electrical energy when used in parallel with an existing source of 60 Hz a-c power. The three schemes include: a) a d-c generator, b) a synchronous a-c generator, and c) an a-c induction generator. The characteristics of the three generators are summarized in Table 13. The d-c generator and the synchronous a-c generator are completely adequate for general purposes, but when used to change wind energy to electrical energy to supplement power from a public utility these two have inherent complications not experienced by the induction generator. The output of the d-c generator must be converted from variable voltage d-c to constant voltage, constant frequency a-c. This can be done by a voltage regulator and an electrical inverter. The resultant a-c voltage wave shape may not be the ideal sinusoidal shape required by the utility. To provide low wave-form distortion requires high quality, and hence, high cost inverters.

The synchronous a-c generator, when driven by a varying speed wind turbine with passive pitch control, will be producing variable frequency a-c power which must be rectified to d-c and then inverted to constant frequency a-c. In addition, both the d-c generator and the synchronous a-c generator require an automatic shutdown system which senses a power grid failure and immediately disconnects the generator from the grid. These two schemes, therefore, require additional conversion hardware which serves to decrease system reliability and efficiency while increasing the overall system cost.

None of the above mentioned unfavorable characteristics exist for the induction generator. If the voltage of the power lines became zero, the voltage of the induction generator would instantly become zero. It is therefore self (and instantaneously) clearing from the power grid in the event of a grid fault. The speed of the induction generator can vary slightly with changing wind speed, but the frequency of its output remains that of the power lines to which it is connected. No conversion circuits are required. The only external equipment required by the wind-driven induction generator would be a speed switch to connect the generator to the grid when its speed is greater than its synchronous speed and to disconnect it when the turbine decelerates to synchronous speed. This switch is not a safety or operational requirement of the utilities but is required to optimize the overall efficiency of the system, by preventing the generator from driving the rotor. Thus, to meet the requirements of system simplicity, reliability, efficiency, and low cost, an induction generator was selected to provide electrical energy in Modes I & II.

The wind turbine rotor's aerodynamic power curve in Modes I & II was presented in Fig. 19. Peak rotor power output is expected to be 15 kW at a rotor tip speed of 53.5 m/s (175 ft/s). This corresponds to a shaft speed of

TABLE 13

ELECTRICAL GENERATING SCHEMES

Modes I and II

Generator	Full Load Efficiency	Turbine Operation	Voltage Output	Frequency	Price	Required Electrical Hardware
d-c	80%	Variable Speed	Variable	0	$3900	Voltage regulator, inverter, self-clearing network
Synchronous a-c (G.E. SJ324)	85%	Variable speed	Variable	Variable	$3470	Voltage regulator, rectifier inverter, self-clearing netw
Induction a-c (Baldor)	88%	Constant speed	Constant	60 Hz	$ 470	Speed switch

108 rpm. The induction motor (called generator from now on) must therefore be capable of absorbing up to 15 kW of wind power and converting this efficiently to electrical energy. A 20-hp (15-kW)-Baldor three-phase induction motor was selected as the generator for Modes I & II. Based on small motor (3/4 hp) calibration tests, reported earlier, and manufacturers' literature, an overall conversion efficiency for this generator should be approximately 88% at rated power. The generator will be driven above synchronous speed (1760 rpm) through an FMC inline gearbox with a numerical ratio of 1:17.1. The quoted gearbox efficiency is 98% according to the manufacturer. The total conversion efficiency of the drive system is, therefore, expected to be approximately 86%. An electrical schematic showing the hookup of the induction generator to public utility lines, in addition to all electrical hardware, is presented in Fig. 25.

Initially, since the speed switch has not detected any generator speed, the generator is disconnected from the utility grid due to switch S1 being open. As the wind speed increases, the rotor speed will increase under no-load conditions until the generator is turning at least 1780 rpm. This corresponds to a rotor tip speed of 51.5 m/s (169 ft/s). At this point the speed switch contacts close, causing the magnetic switch S1 to be energized and closed, thereby connecting the generator to the utility grid. The generator is now producing power which is being absorbed by the grid. As the wind speed builds, the rotor will try to accelerate. The generator, however, retards the rotor allowing rotor speed to only build slowly. The aerodynamic power available dictates the amount of rotor speed increase. The generator will absorb rated power (15 kW) at a slip of 10% above rated. This means that when the generator is at full power its shaft speed will be 1.1 x 1760 rpm or 1936 rpm, which corresponds to a rotor shaft speed of 113 rpm or 56-m/s (184-ft/s) tip speed. This condition would occur at wind speeds between 11.2-13 m/s (25-29 mph). As the wind speed increases above 13 m/s (29 mph), the rotor's power output due to rotor stall would begin to decrease, causing a decrease in the generator slip resulting in a deceleration of the rotor. There are two possible scenarios which would occur as wind speed increases. Rotor torque could drop below the level to sustain synchronous rpm, and the speed switch S1 would decouple the grid, or power source. The rotor rpm would continue to drop until the pendulum control reduced blade pitch until accelerating torque was again generated, at which point the rpm and pitch would increase and stabilize in a stalled condition. A more likely scenario is the case in which rpm does not drop below synchronous speed and the system continues to generate power. As wind speed increases, power output increases until line current exceeds the fuse rating at which point the power source is decoupled. The rotor rpm will then increase until the pendulum control produces stall and a stable condition is reached. This latter case was demonstrated in a wind tunnel test conducted subsequent to this design study.

The manufacturers of the various electrical components, along with prices, are presented in Table 14.

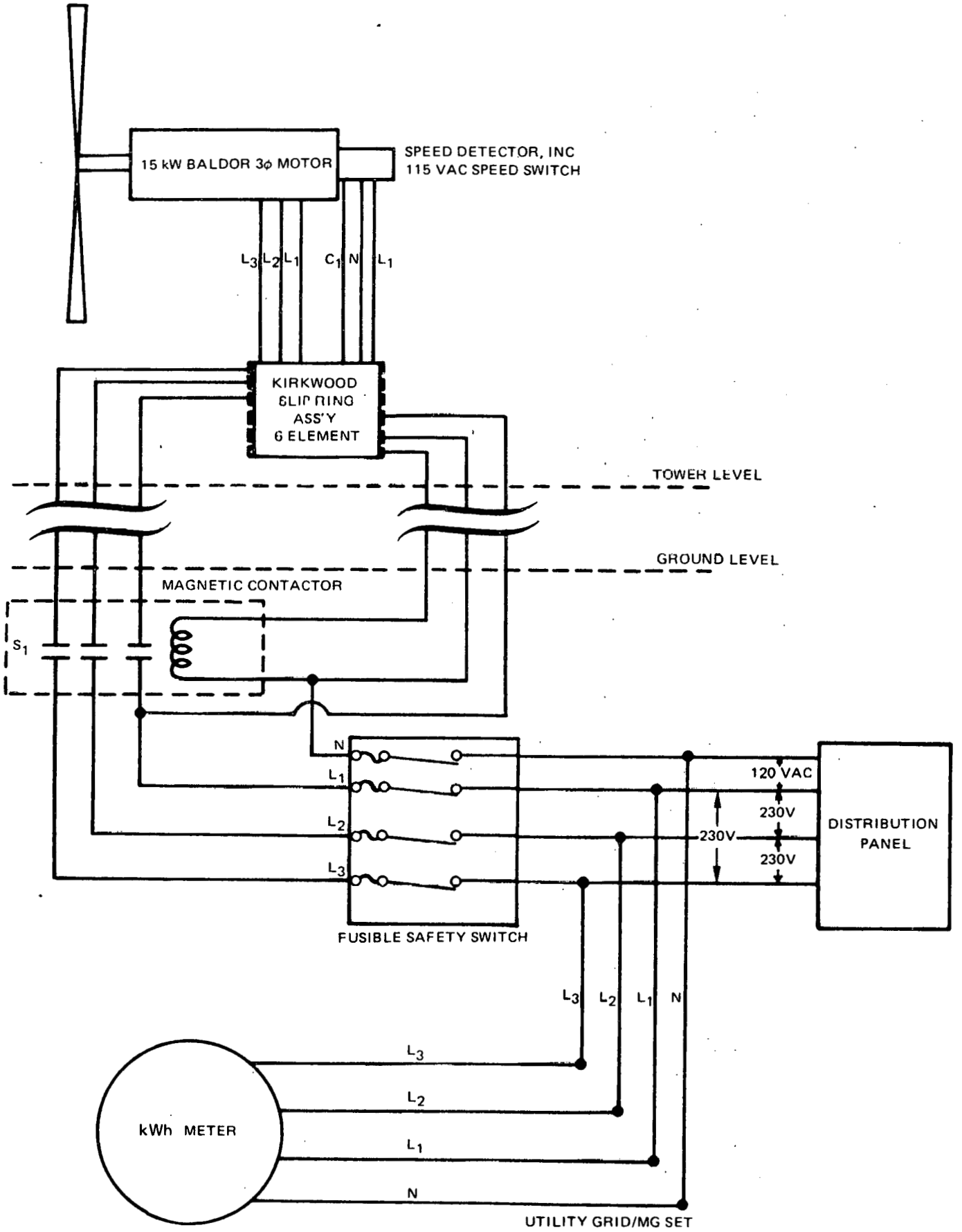

Fig. 25 Electrical Schematic Modes I and II

78-09-193-5

TABLE 14

ELECTRICAL HARDWARE

Modes I & II

Generator

3-phase Baldor Induction Motor
Model 256TC
20 hp - 1800 rpm - 208 Vac
Overspeed Capability - 3450 rpm
Estimated Conversion Efficiency 88%
Cost $405

Magnetic Contactor
Square D Model SEG2
3-phase 230 Vac 90 A
Cost $240

Power Slip Rings
Kirkwood Industries
90 A 6 rings
Cost $150

Tachometer Switch

Speed Detectors, Inc.
Model ESS-1
115 Vac
Variable cut-in speed to 5000 rpm
Cost $138

Fusible Safety Switch
Square D Model H363 RB
100 A
Cost $221

Mode III

Generator
30 hp d-c Generator
1800 rpm
Estimated Conversion Efficiency 80%
Cost $4980

Power Slip Rings
Kirkwood Industries
105 A 2 rings
Cost $138

Fusible Safety Switch
Square D Model H363RB
100 A
Cost $221

Mode III

The requirements for power generation, in the stand-alone wind turbine system, are:

a. the generator shall produce constant voltage d-c power, or
b. the generator shall produce 60 Hz constant voltage a-c

D-c power can be generated in two ways. A d-c generator with a voltage regulator will generate constant voltage d-c power for battery charging or for resistance loads at the user's site, such as heaters, incandescent lights and d-c motors. An a-c alternator with voltage regulation and rectification will also produce d-c power in a manner similar to a d-c generator.

The generation of 60 Hz constant voltage a-c power, in the stand-alone system, becomes slightly more complicated. The alternator, although producing a-c, does so at varying frequencies due to the speed variation of the prime mover inherent in this rotor design. This is an unacceptable power source for a-c motors which require 60 Hz voltage. By rectifying the regulated power, d-c is obtained which can be used to charge a bank of storage batteries, in effect creating a large electric filter where the output power is not greatly affected by small variations in the rotor power output. Similarly, a d-c generator could be used to charge batteries. Once a supply of d-c power is established, an inverter can be introduced into the system to provide 60 Hz a-c power which can now be consumed by electric motors. A schematic of the Mode III electrical system is shown in Fig. 26.

The nature of the stand-alone system, i.e., absence of 60 Hz power, precludes the use of line-commutated synchronous inverters. The inverter must be self-commutating and capable of generating high quality a-c at the lowest possible cost. The Pratt & Whitney division of United Technologies has produced self-commutated prototype and production inverters, coupled to fuel cells, of varying power capacities from 8 kW to 4.8 MW. The cost of a power inverter is directly proportional to the number of phases and its rated power, and is inversely proportional to the number of units built. For an approximation of inverter costs see Table 15.

The size of the inverter is dictated by the user's demand for 60 Hz a-c power and not by the size of the generator or storage system. In the stand-alone system, the user can elect to dissipate all or part of his generated power as d-c, through resistance loads with the inverter being sized to provide a-c for the maximum number of a-c motors expected to be in operation at any one time, allowing for start-up overloads. Since it is the user's demand for a-c, and not the capacity of the wind turbine generator, that determines the size of the inverter, the inverter should be an option. Some users may require no a-c

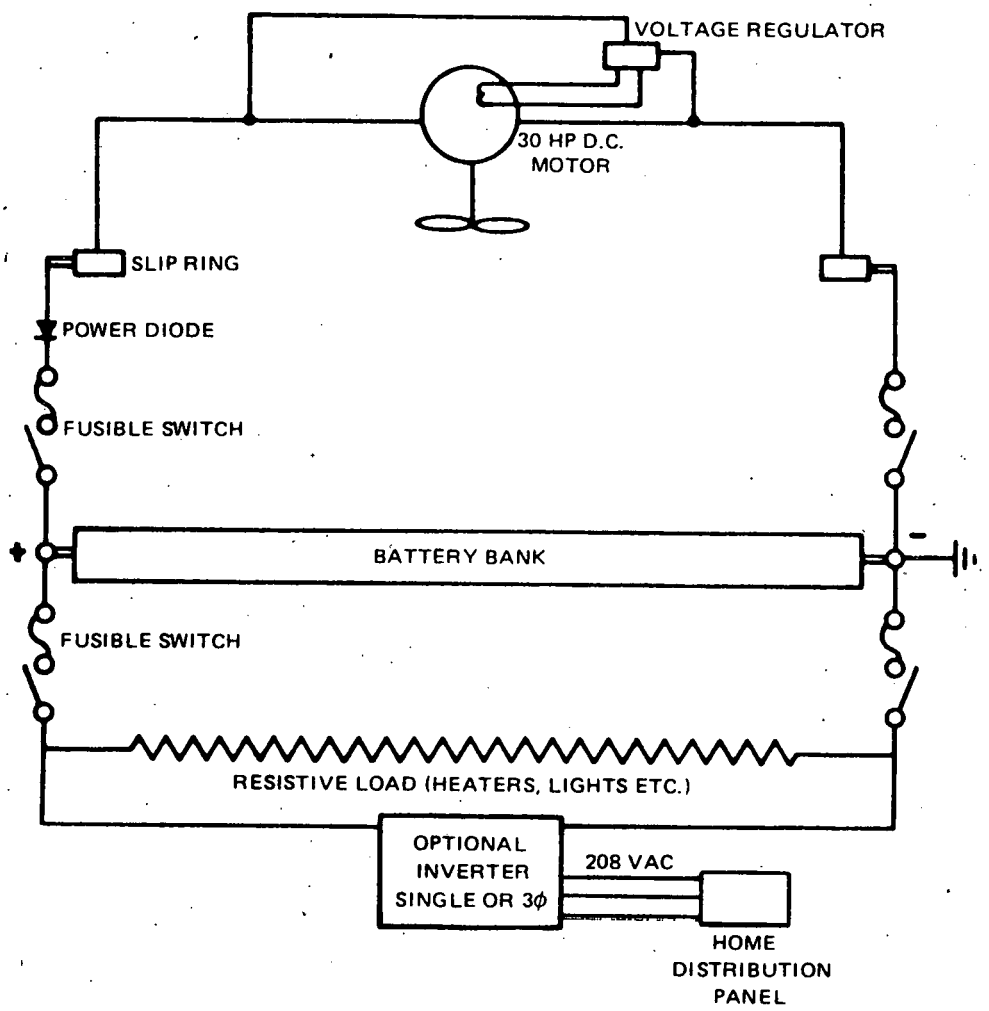

Fig. 26 Electrical Schematic Mode III

78-09-193-2

TABLE 15

INVERTERS FOR STAND ALONE SYSTEM.

Unit	Type	Size	Cost	$/kW	Efficiency*	Remarks
Gemini	Line-Commutator	20 kW	$5808	$290	98%	Not capable of stand-alone operation
UTC	Self-Commutator	40 kW	$2000**	$ 50**	90%	SCR Controlled
Advanced Conversion Device Co.	Self-Commutator	15 kW	$17,031	$1135	80%	Power transistor controlled

* Manufacturer's quote

** Estimate of cost to produce in quantities of 10,000/yr. (Not selling price).

R78-914136-1

power; some may require very little to drive fractional horsepower motors, while others may require most or all of the generated power be available in a-c form. The user's dependence on a-c power would, therfore, dictate his total wind energy conversion system cost.

Co-Generation

Public Utilities were contacted to determine what requirements existed for power co-generation. Many utilities had no guidelines, several had no response, but some companies have given thought to the possibility of co-generation and have detailed their requirements in writing. One utility, which has firm guidelines for co-generation be it solar, wind, hydro-electric, etc., is Northeast Utilities, a New England power company covering Connecticut and Western Massachusetts. They have indicated that they will cooperate fully and positively with any persons or firms in co-generation or the production of electricity by alternate methods, regardless of system size or capacity. The company will, if requested, purchase any excess electricity, regardless of quantity, provided that such energy can be purchased at less than the cost of the company's alternative energy supply. The ground rules for co-generation have been tentatively established as:

1. Power generation of single phase is limited to 15 kW

2. No power limit exists for 3-phase generators

3. The co-generator must provide an automatic-synchronizing relay package to match line frequency

4. The co-generation system must clear itself, automatically, from the company's system in the event of a power fault

5. Generator power factors, at load, should exceed 0.9

6. Co-generator will require a special contract

7. The approximate price of electric energy purchased by the company from the co-generator will be the company's average displaced fuel cost less 20%.

Once the co-generator has satisfied the utility that his energy conversion system meets these requirements and is connected to the power grid, Northeast Utilities will, under special contract with the co-generator, buy surplus power from the co-generator at a rate based on the actual cost of the fuel saved minus a service charge of 20%. For a co-generator in the New England area, based on present electrical rates, this would result in a rebate of approximately $.01/kWh. In addition, of course, the co-generator would save approximately $.04/kWh when generating power for his own consumption.

Rotor Noise Prediction

The noise produced by the wind turbine rotor was calculated using a method developed at UTRC. This method assumes that the noise is due to interaction of the blade with inflow turbulence which produces unsteady forces on the rotor blades. The von Karman spectrum formula, which assumes isotropic turbulence, was used to model the turbulence. The only inputs needed for the von Karman model are the turbulence integral scale and the turbulence intensity. Using spectral analysis this turbulence model is combined with an airfoil response function to yield the prediction scheme used here. This prediction scheme is detailed more fully in Refs. 8, 9, and associated references.

The method has been experimentally verified for the case of an airfoil moving rectilinearly through turbulence, and initial experiments for the extension to the case of rotational motion of a propeller through turbulence show excellent agreement with theory. This agreement between theory and experiment is especially remarkable since the theory gives an absolute level prediction; i.e., there are no adjustable constants which can be used after the fact to improve agreement between theory and experiment.

The theory does include the effect of blade-to-blade correlations which are important when any eddy is chopped more than once by a blade. This is evident from the predictions shown in Fig. 27 where at the lower frequencies the spectrum becomes peaked around harmonics of the blade passage frequency. At the higher frequencies (smaller eddy sizes) a given eddy is chopped by only one blade and the noise is broad band.

The overall noise level, dbA, is also shown on Fig. 27 for the three operating conditions. For operation at normal wind conditions (V_w = 12 mph) the overall level is 45.1 dbA which is equivalent to the noise level of a quiet automobile. At the high-wind and tip-speed conditions, the dbA reaches 70.6 which may be related to the noise level of a busy street. It should be noted, however, that this tip speed corresponds to an overspeed condition and would only be experienced in a power failure or at extreme wind speeds.

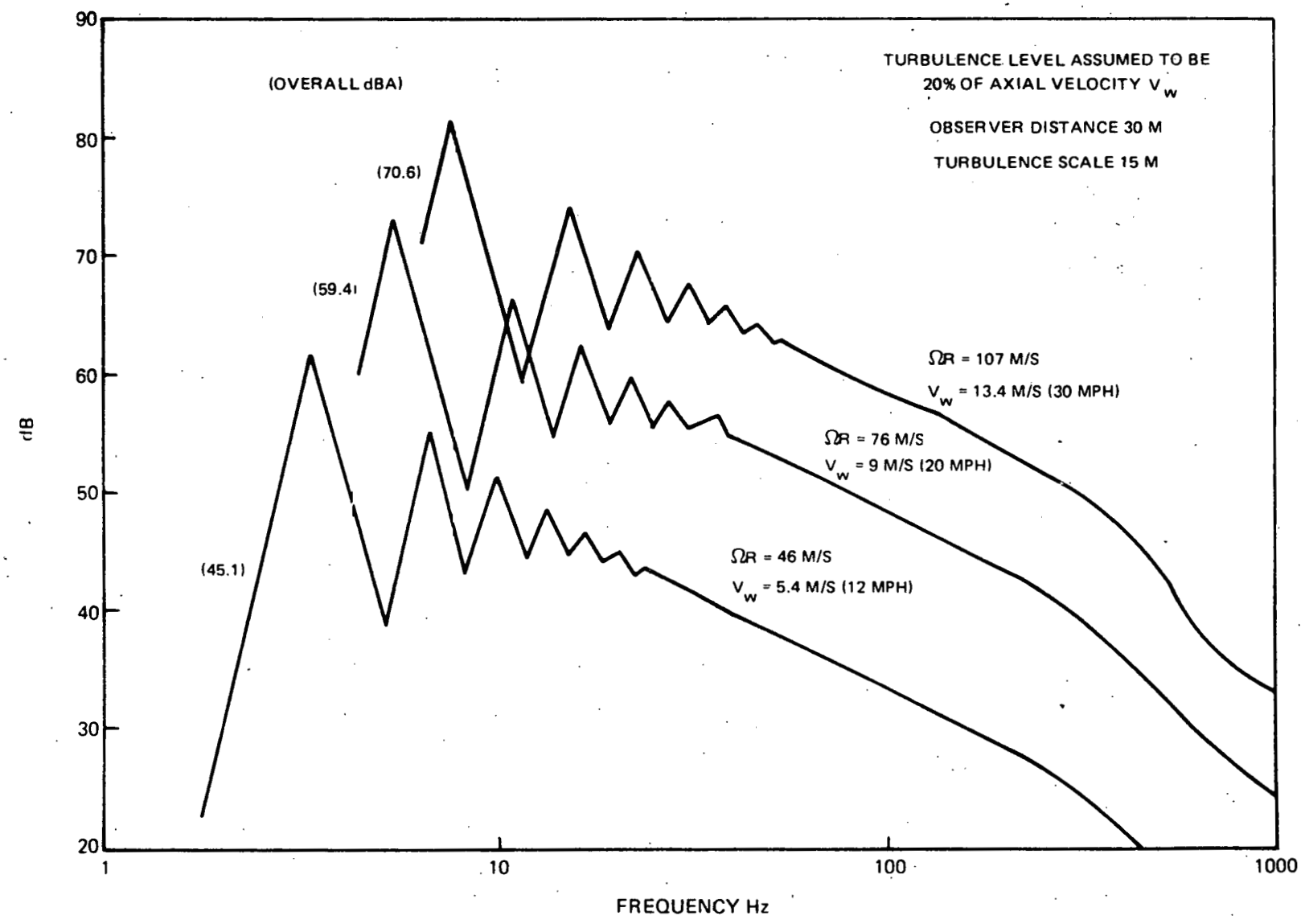

Fig. 27 Predicted Noise Level

SYSTEM DESIGN

Descriptions of the major components of the wind turbine are presented in this section. The system is broken down into five design areas which were separately studied during this design phase. These consist of 1) blade, 2) blade/flexbeam joint, 3) control pendulum, 4) head components, and 5) tower. As indicated earlier, the basic design pursued in this program was initiated during an earlier ERDA contract (Ref. 3), and the modifications made to this basic design resulted from experience gained during the wind tunnel test conducted during this contract and the additional research trade-offs performed to produce a more cost effective system.

Each subsystem identified above was modified to some extent to accommodate the specific requirement set forth in the work statement of this contract (Ref. 10). There were three major criteria which governed the design: first, the system must produce at least 8 kW of power in a 9-m/s (20-mph) wind; second, the rotor center be located 16.8 m (55 ft) above the ground; and third, that the production sell price of the system be targeted at $750/kW. Although maximum rotor size was not specified in the work statement, it was felt that the minimum diameter to produce 8 kW would be the best approach from the standpoint of the individual user. This resulted in an 8.8-m (28-ft)-diam rotor, as discussed earlier in the performance section; however, to improve low speed performance, the diameter was increased to 9.5 m (31 ft). During the design of the overall system, other design decisions were necessary that required trade-off studies to evaluate their impact on system cost and reliability. A qualitative measure of the major design decisions made is presented in Table 16 where the impact of each decision on several cost items is shown as a cost factor relative to the original design. An attempt to weigh their overall impact was made by assigning a weighting factor (W.F.) to each cost area, taking the product of this factor and the cost factor, summing, and dividing by the sum of the weighting factors (3). This provides a qualitative measure of the cost impact of each decision and is shown in the last column in Table 16. It can be seen that in two instances, increasing rotor diameter and selecting a gear step-up over the belt drive, that the costs escalated slightly; however, on the average, the major design decisions resulted in lower costs.

A general layout of the complete system is shown schematically in Fig. 28. For each of the subsections that follow, the considerations that went into the decisions of Table 16, and others, will be discussed in greater detail. It should be noted that throughout the design activity there were decisions made which favored the prototype over the final production system. In other words, the design or purchase of a specific component was motivated primarily by the success probability of the prototype and secondarily by the cost effectiveness of the production system. There were instances where the design reduced the

TABLE 16

IMPACT OF DESIGN DECISIONS ON COST

Design Decision	Cost Factor* Purchase Price WF = 1.0	Labor to Fabricate 1.0	Maintenance and Replacement 0.5	Operation Cost 0.2	Erection Cost 0.2	Packaging and Shipping 0.1	Summary
Increase Diameter to 9.5 m (31 ft)	1.14	1.03	1.0	1.0	1.0	1.02	1.06
Foam to F/G Blade	0.3	0.2	1.0	1.0	1.0	1.0	0.5
ac-Alternator to Induction Motor	0.3	1.0	0.9	0.1	1.0	1.0	0.7
Belt Step-Up to Gear Box	1.8	0.7	0.5	1.0	1.0	0.9	1.08
3 Section Tower to 2 Sections	0.9	0.8	1.0	1.0	1.0	1.1	0.9

* These cost factors represent a qualitative judgment as to the impact of design decisions on cost compared to the cost before the change was made. The summary column reflects the use of weighting factors (WF) to downgrade the less costly considerations (such as packaging and shipping). The summary indicates where design decisions increased the cost (above 1.0) or decreased the cost (below 1.0).

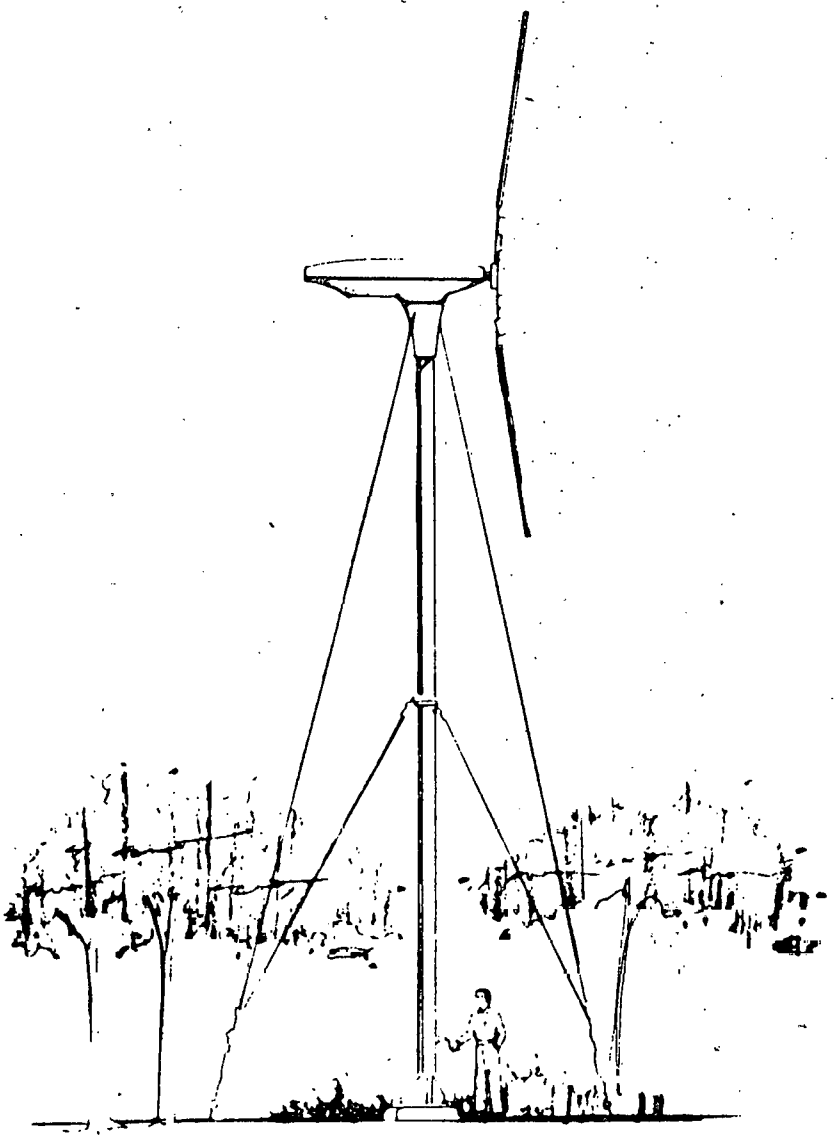

Fig. 28 UTRC Wind Turbine

risk of the prototype operation but may have been too conservative for a high volume production system. For example, the primary yaw motion may be achieved by a simple low-cost bushing; however, it was felt that its friction characteristics could not be calculated with sufficient accuracy to insure that this would not pose a problem during field testing of the prototype. Similar dilemmas were faced in other aspects of the design; and in most cases, the design selection was made to improve the probability of success of the prototype. Such decisions are generally all revokable in the event that the prototype demonstrates overconservatism. A discussion of some of the potential production cost savings compared to the prototype will be presented in the cost study section of this report.

Blade Design

The basic blade dimensions were determined under an earlier ERDA contract (Ref. 3) where design parameters were varied to establish their influence on performance and aerolastic stability. In summary, it has been shown (Ref. 11) that peak performance is not significantly influenced by blade area, within realistic limits; therefore, the chord and number of blades selected should be based on other considerations. The principal consideration for a hingeless wind turbine blade is that the fundamental edgewise frequency (1E) be located above the rotational speed for all operating speeds to avoid amplification due to the 1 per rev (1P) gravity and wind shear excitations. The radius and chord dimensions are the principal parameters which govern edgewise frequency, and for the Ref. 3 design, which had a 12.2-m (40-ft.)-diam rotor, the flexbeam chord was 78 mm (7 in.) and the blade chord was 380 mm (15 in.). Since the fundamental edgewise frequency is approximately proportional to the ratio of the flexbeam chord to blade length, the flexbeam was scaled down by the ratio of the original Ref. 3 diameter 12.2 m, to the current diameter, 9.5 m (31 ft.). This resulted in a flexbeam cross-sectional dimension of 140 x 14 mm (5.5 x 0.55 in.) compared to the earlier design of 178 x 17.8 mm (7.0 x 0.7 in.), but resulted in approximately the same edgewise frequency. The flexbeam free length is determined by the maximum allowable torsional stress due to the blade pitch change from the start-up position of -16° to the overspeed stall condition of +6°. This produces a total flexbeam twist of 22°. The experiments of Ref. 4 indicated an allowable fatigue limit stress of approximately 104 MPa (15,000 psi), and assuming a safety factor of 3 for this critical structural component, an allowable torsional stress limit of 34.5 MPa (5,000 psi) was used. The torsional stress in a rectangular uniform beam is:

$$\sigma = \frac{Gt\theta}{\ell}$$

Using values of σ = 34.5 MPa (5,000 psi), G = 5.17 GPa (0.75 x 10^6 psi), t = 14 mm (0.55 in.), θ = 0.384 rad, and solving for the free length, ℓ, yields a flexbeam length of about 0.8 m (31 in.) which was used for the final design. This is equal to 16.7% of the rotor radius. The major portion of blade curvature due to aerodynamic and dynamic loading occurs in the flexbeam region. The flexbeam must also resist the blade centrifugal load which is 10,300 N (2,300 lb) at a tip speed of 53.4 m/s (175 ft/s) and grows to 30,250 N (6,800 lb) at 91.5 m/s (300 ft/s) and 54,000 N (12,150 lb) at 130 m/s (425 ft/s). However, the tensile stress due to centrifugal loading is low, having a value of only 26.9 MPa (3,900 psi) at 130-m/s (425-ft/s) tip speed. The outer portion of the blade remains relatively straight as a result of the centrifugal field producing high stiffness over this region. The motions the flexbeam experiences are depicted in Fig. 29. The flexbeam is cured in a pretwisted position so that during normal operation it will be relatively untwisted, thereby maintaining high edgewise stiffness. Pretwisting also facilitates the attachment of the flexbeam to the blade, since it is then not necessary to pitch the blade relative to the flexbeam to achieve the correct static angle for start-up (-16°). Graphite/epoxy was selected for the material for the flexbeam; however, fiberglass and Kevlar 49 were also considered. Fiberglass was desirable from the standpoint of cost, however, the modulus is only 40% that of graphite/ epoxy, which would result in a flexbeam chord of about 25% greater to provide the equivalent EI. Such a configuration would produce a significant increase in the hub dimension and would create a more difficult task to join the flexbeam to the blade. Kevlar 49 was eliminated due to the poor fatigue properties of this material. Experimental data have shown that the strength of Kevlar 49 is only 50% that of graphite/epoxy. The current high cost of graphite/epoxy ($50/lb) is the major negative aspect of this material; however, projections have been made that prices of about $20/lb may be achieved in the near future and even lower prices are anticipated if greater applications are found in major consumer industries.

The flexbeam is preconed in order to minimize the steady stress level under high-thrust condition and also to improve the turbines downwind stability during start-up. Initially, an angle of 10° was selected to reduce the stress level at the 75-m/s wind condition; however, a subsequent wind tunnel test of a dynamically scaled model revealed that the rotor rpm under high wind conditions was greater than predicted and resulted in a natural cone angle of less than 10°. A compromise value of 8° was thus selected for the full-scale design.

The initial design of the outboard portion of the blade incorporated a rectangular graphite spar with a self skinning foam forming the airfoil shape. A molded solid polyurethane leading edge provided mass balance as well as resistance to abrasion and hail. Using the pultrusion process for the graphite spar and an injection molding process for the remainder of the blade, held promise for very low fabrication costs. The final production cost would depend

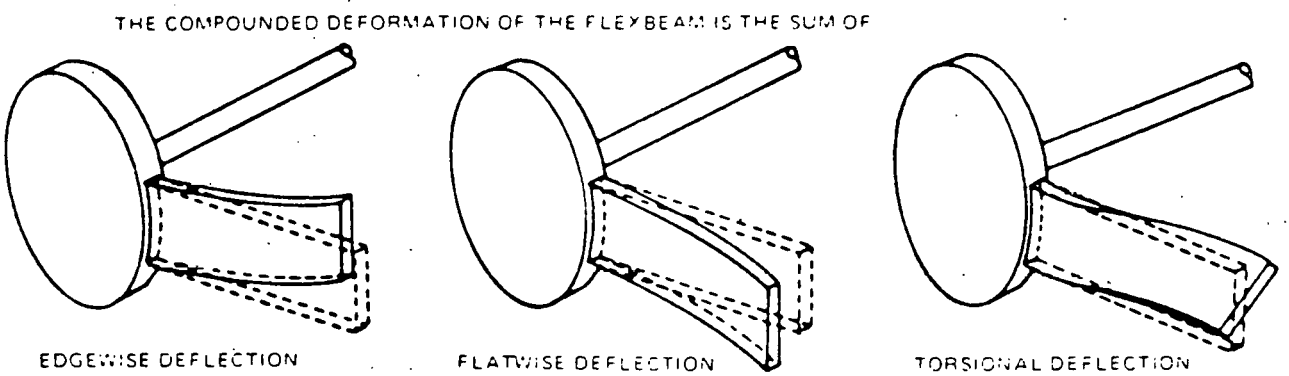

Fig. 29 Schematic of Primary Functions of Flexbeam

to a great extent on the cost of graphite, and this was still an unknown. Significant progress was made in developing a self skinning foam during this contract, and these results were presented earlier. However, the implementation of this technique in full-scale dimensions remained a sizeable development task in itself. Discussions were held with experts in the field and plans were formulated to foam a full-scale sample blade. However, before an investment was made to fabricate a mold for this process, the concept of using a totally pultruded fiberglass blade was introduced. The potential for a very significant cost saving for a production system using the pultrusion process, and the established technology in this field led to the decision to switch to this design.

There were several constraints which dictated the general design of the fiberglass blade cross section. These were: that the blade be relatively mass balanced (c.g. close to quarter chord) to minimize the chance of classical flutter, that the leading edge be solid to withstand hailstone collisions, that the wall thickness be greater than 1.5 mm (0.060 in.) as prescribed by the manufacturer of the pultrusion machine (Goldsworthy Engineering, Inc.), that the outer and inner plies be unidirectional as prescribed by Goldsworthy, and that the ply layup be symmetrical to avoid distortions during curing. This resulted in the cross section shown in Fig. 30. The wall configuration which provided a symmetrical layup is also shown in this figure. The principal loads which must be resisted by the blade, other than centrifugal, are those which produce torsion. The major bending moments are resisted by the flexbeam, as discussed earlier; however, torsional moments are experienced along the entire span, and, unlike the flatwise and edgewise modes, the centrifugal force field has little influence in resisting torsional deflections. Thus, a significant percentage of the wall plies are laid up in a $\pm$ 45° arrangement, thereby providing a high modulus about the torsional axis. The thicknesswise shear webs are provided to maintain the airfoil contour under pressure and suction loads. Within the outer skin of the leading edge region, and extending rearward 63 mm (2 1/2 in.), solid unidirectional fiberglass is used. This portion of the blade not only contributes to the stiffness but also provides a forward mass to balance the blade at approximately the quarter chord and a solid structure to resist leading edge/ foreign object impacts.

The airfoil shape itself was selected to provide good start-up characteristics, i.e., high C_l max, and perform with little or no pitching moment during normal operating conditions. The NACA 23112 airfoil (Ref. 12) satisfied these requirements and had been successfully tested on model rotors at UTRC in 1971 (Ref. 13).

E-glass was selected over S-glass as the blade material due to its lower cost, approximately $0.50/lb as compared to $2.50/lb. E-glass has modulus and strength properties about 15% below those of S-glass; however, a modest increase

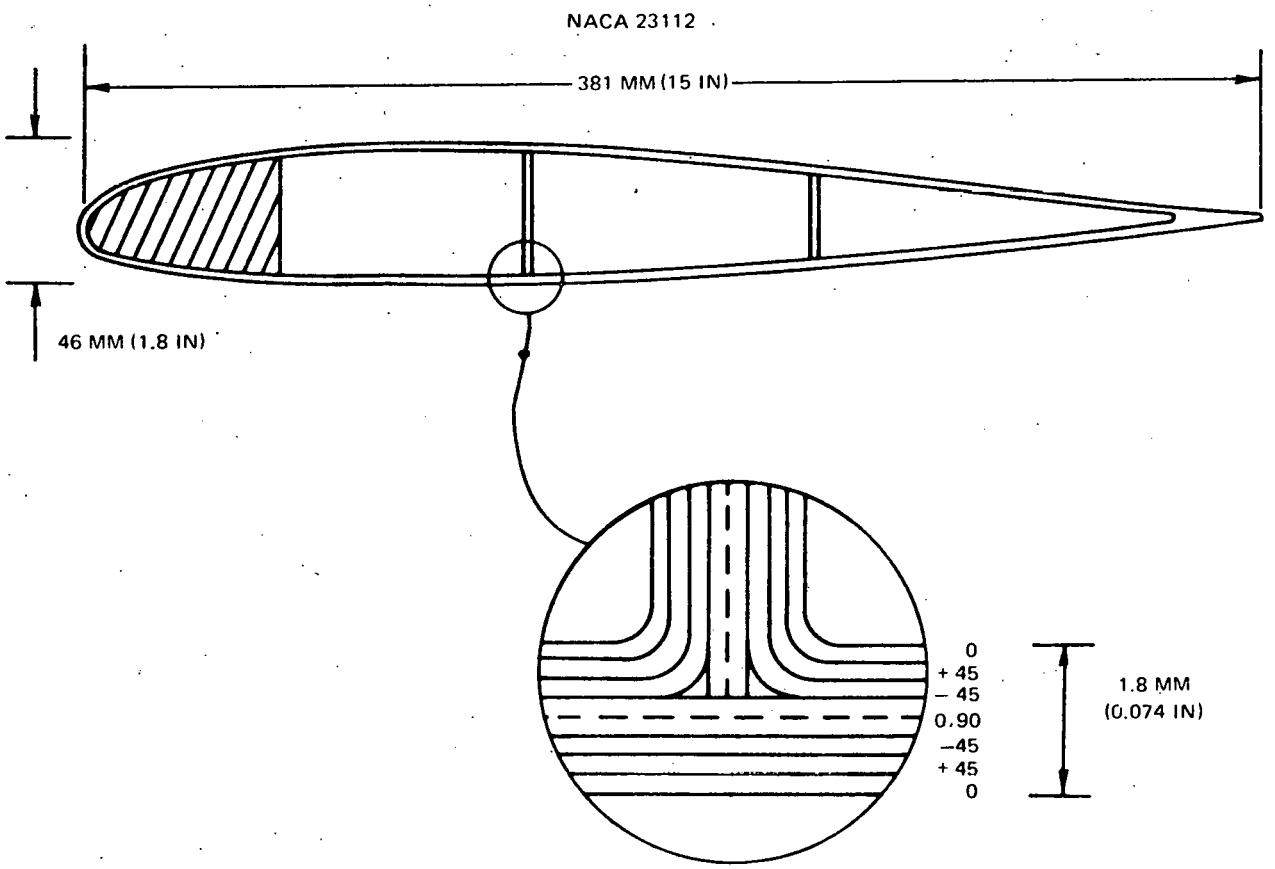

Fig. 30 Airfoil Section - Pultruded Blade

78-11-17-14

in wall thickness offsets this reduction in properties. The blade tip cap is formed by potting in resin to approximately 127 mm (5 in.) which serves as a sealer and a tip weight. It was found during the loads analysis that a significant reduction in the flexbeam steady flatwise stress in high speed stall can be achieved with the addition of a 5-lb tip weight. Increasing tip weight lowers the blade edgewise frequency; however, a weight of 5 lb would lower this frequency only a small percentage. The general material properties of E-glass used in the pultruded blade design were obtained by averaging data obtained from various sources. These sources included a compendium of data assembled by the Sikorsky engineering department (Ref. 14) and data provided by Goldsworthy which were generated by Narmco Materials, Inc. A summary of the results is presented in Table 17. The graphite/epoxy properties were presented earlier in the Composite Material Experiments Section (Tables 1 to 4).

The blade properties are presented in Figs. 31 to 36, where weight, stiffness, inertia, and blade axes locations are shown as a function of blade

TABLE 17

E-GLASS/EPOXY PROPERTIES
DENSITY = 1.94 g/cc (0.07 lb/in^3)

Layup	Tensile Modulus, GPa	Tensile Strength, MPa	Shear Modulus, GPa	Shear Strength, MPa
0°	37.9	1103	3.24	62
0°, 90°	25.5	517	3.24	62
±45°	11.7	159	10.34	241

radius. The total radius is comprised of four distinct regions: 1) hub (0.2 m), 2) flexbeam (0.8 m), 3) joint (0.5 m), and 4) blade (3.2 m).

It can be seen in Fig. 36 that the flexbeam axes (cg, ea, and na) are located at 38% of the blade chord and not at the quarter chord (25% c) as would be expected. The blade was positioned forward of the flexbeam centerline in order to minimize the high nose-down pitching moment which occurs during stall when the chordwise center of pressure moves from the quarter chord rearward. This resulted in a nose-down pitch deflection which tended to unstall the blade, thus delaying the desired stall condition which is necessary to prevent overspeeding. This problem was resolved by placing the blade attachment point closer to the center of pressure in the stalled condition, which varies from 30-50% depending on the extent of stall.

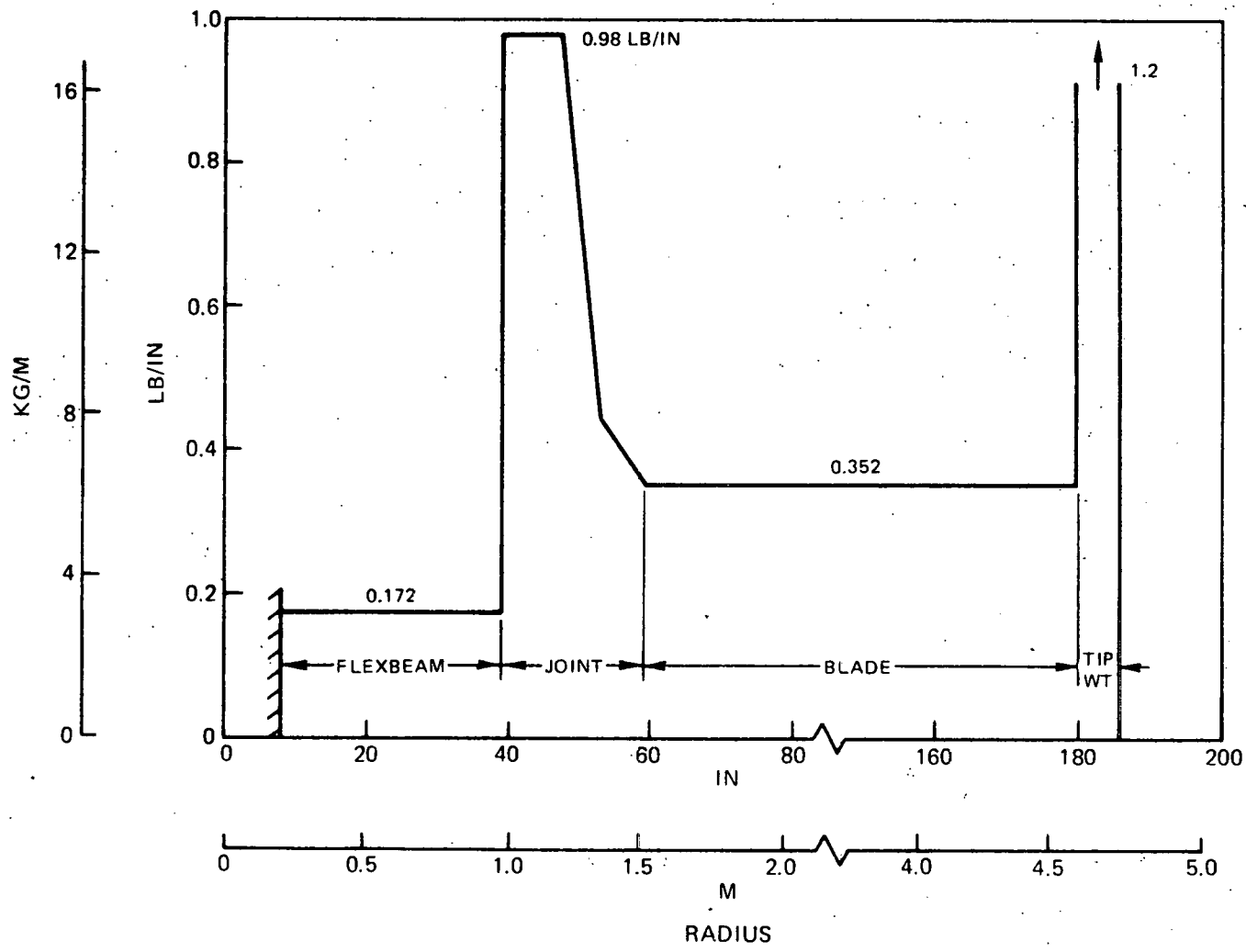

Fig. 31 Blade Weight

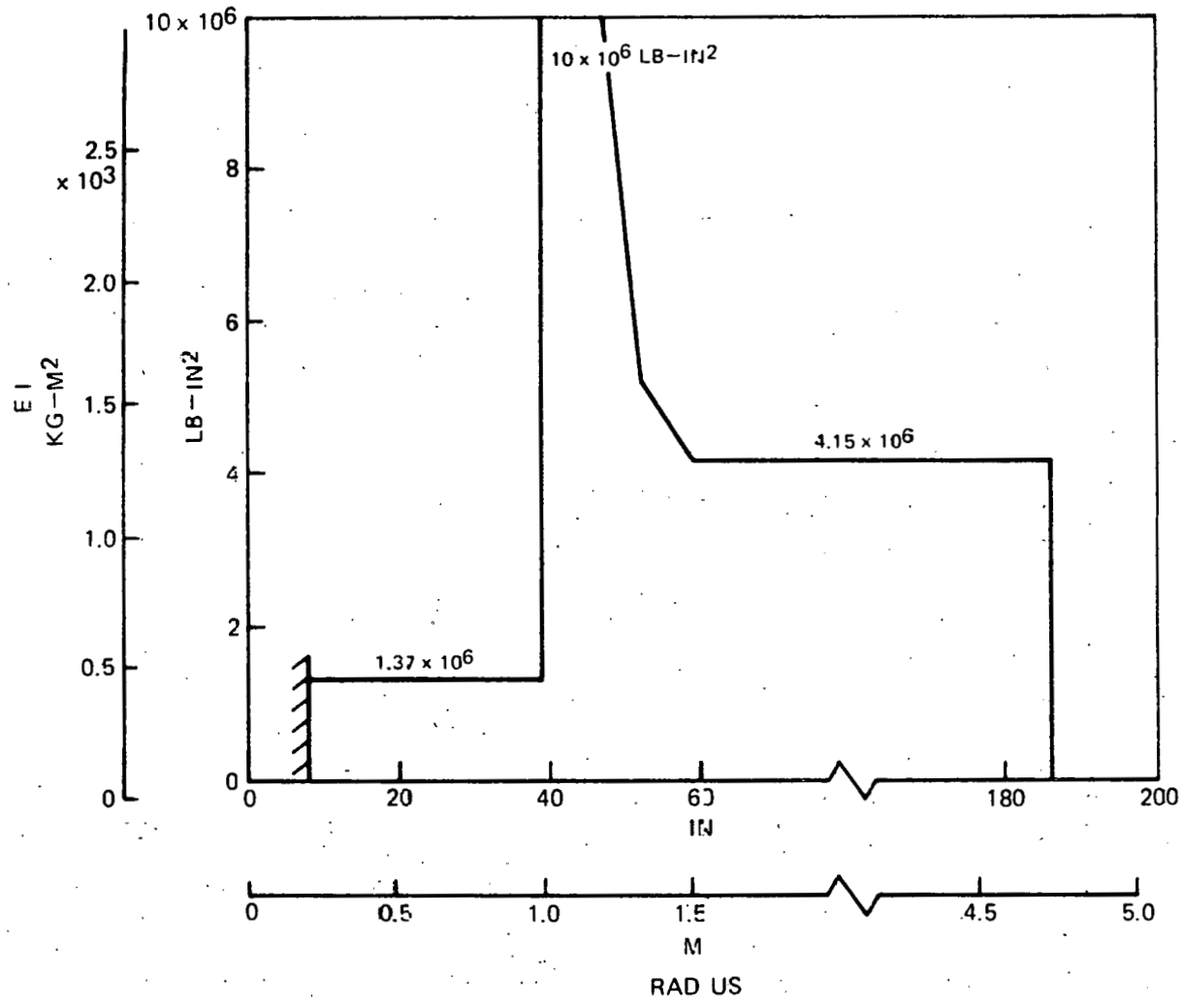

Fig. 32 Flatwise Stiffness

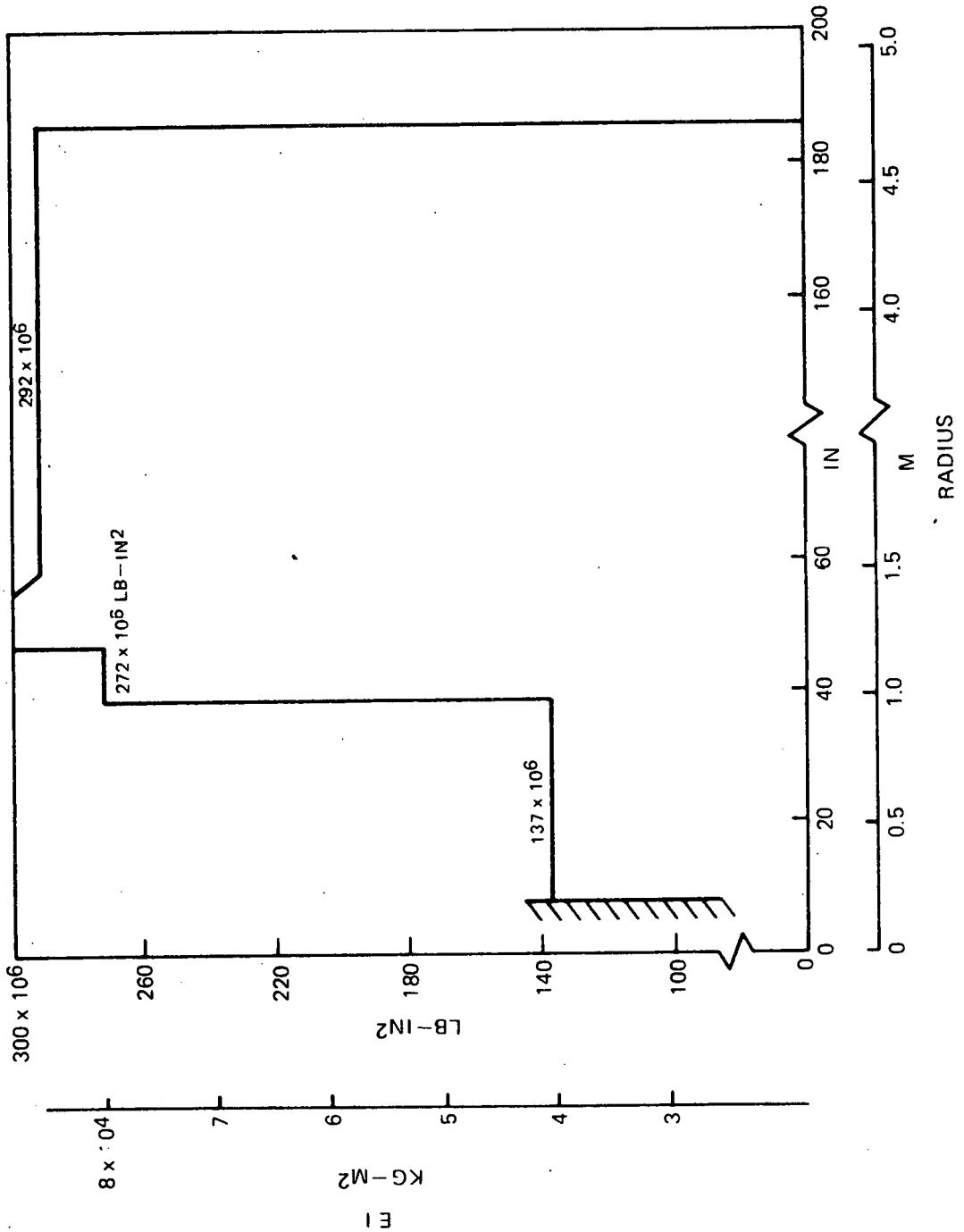

Fig. 33 Edgewise Stiffness

78-11-17-9

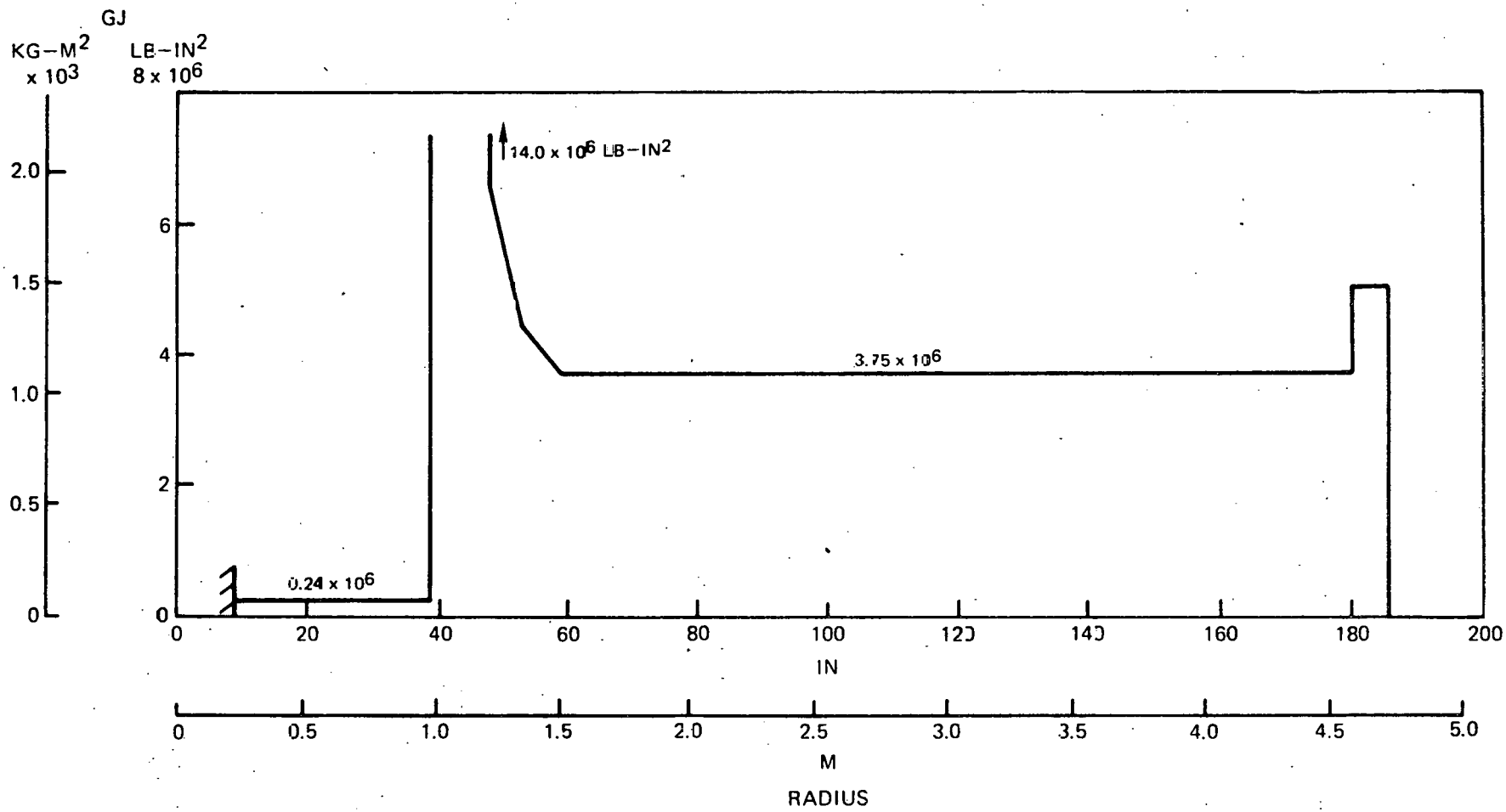

Fig. 34 Torsional Stiffness

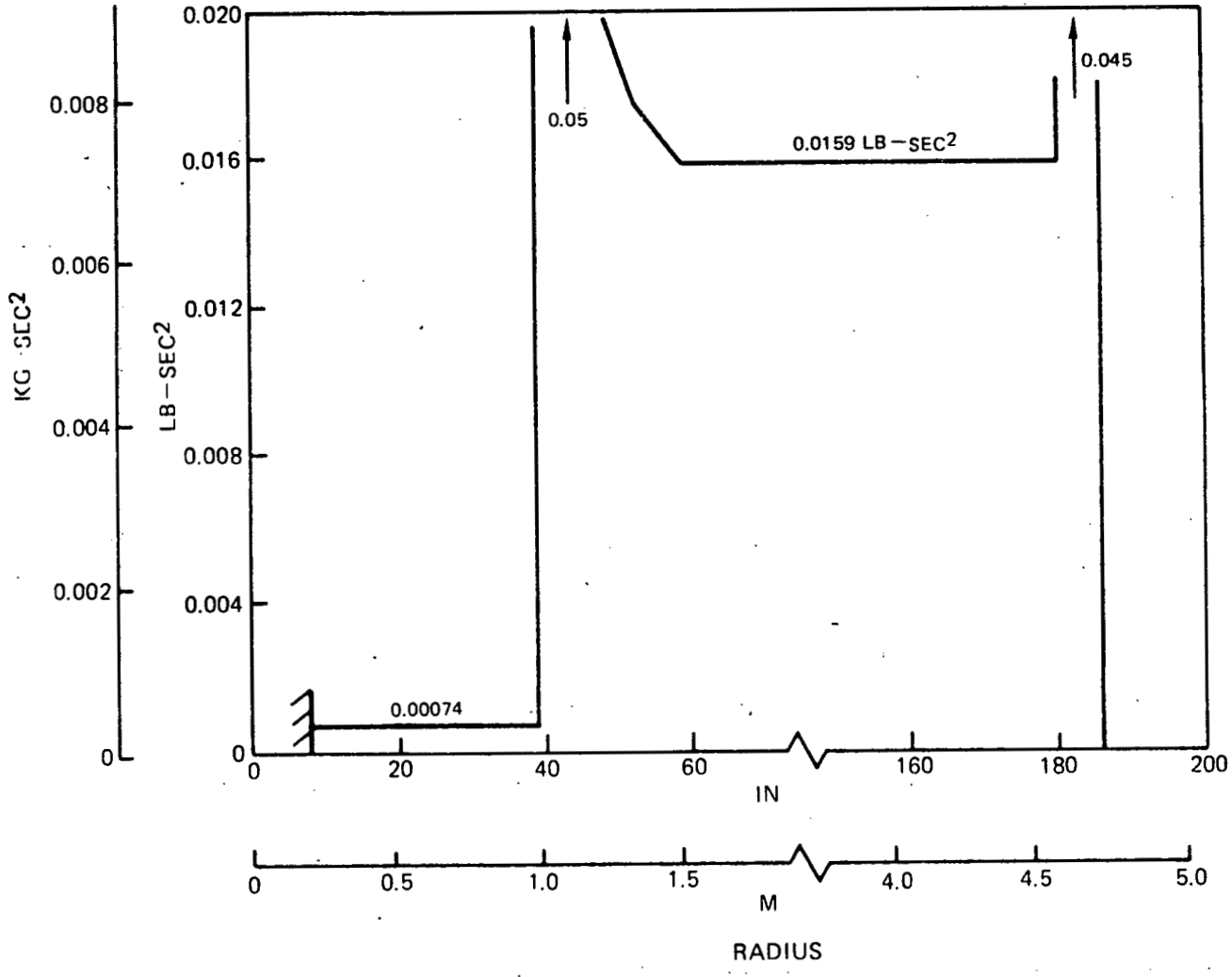

Fig. 35 Moment of Inertia

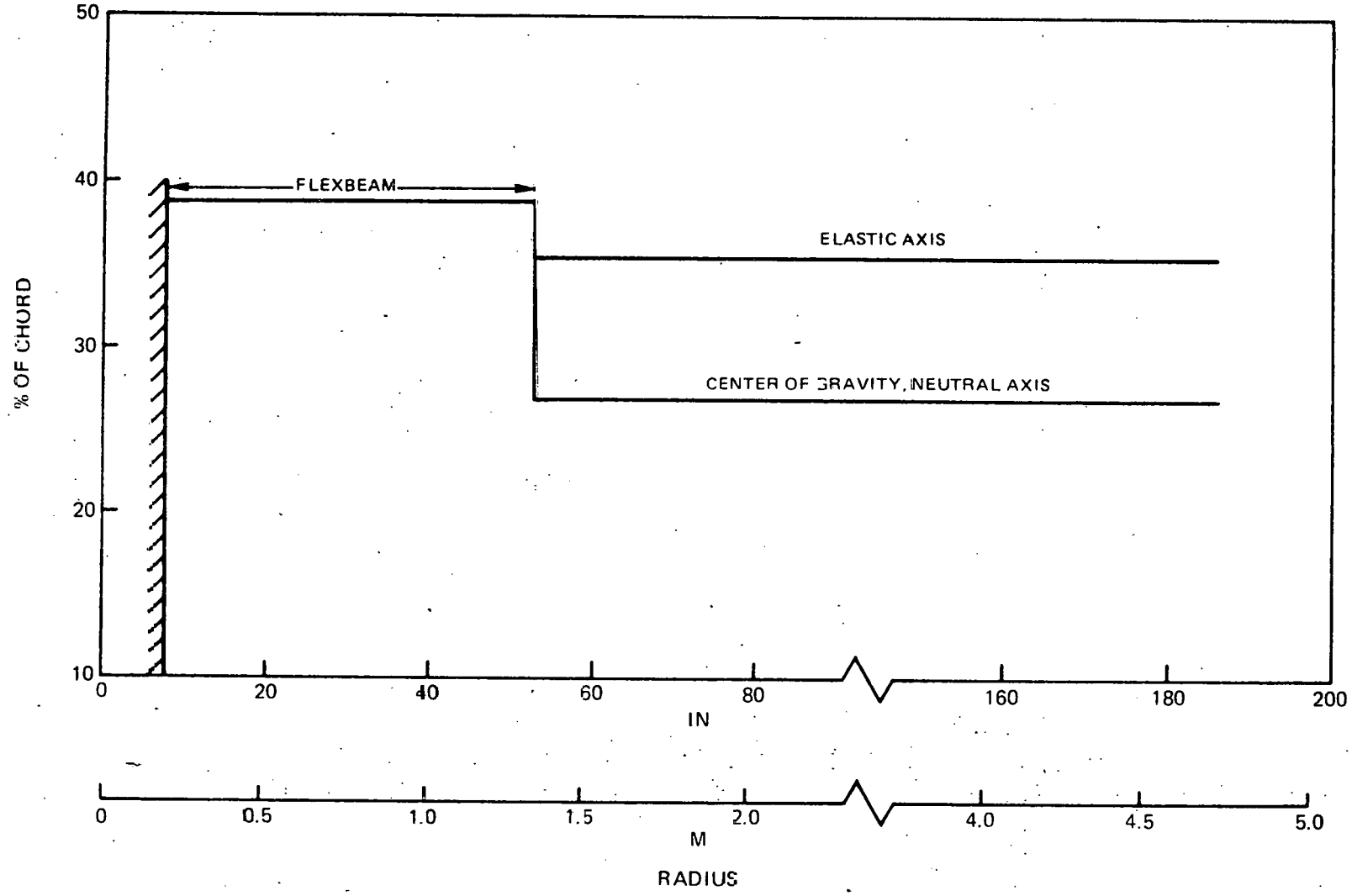

Fig. 36 Blade Axis

The structural properties of the blades were used in a mode shape/frequency computer program (UTRC code E159), and the frequency diagram resulting from this analysis is shown in Fig. 37. It can be seen that the blade first flatwise mode (1F) is relatively "soft" as indicated by the proximity of this frequency to the 1P line. This is typical of hingeless rotor helicopters. It can also be seen that there is an intersection of the first edgewise mode (1E) with 2P at a tip speed of about 110 m/s. This condition has been tested during wind tunnel experiments and a slight 2P amplification of the edgewise response was measured, however, due to the low level of 2P excitation the stress levels were insignificant. It should be noted that the first torsion mode (1T) shown on Fig. 37 is the unrestrained mode, that is, without the flexstrap-to-pendulum attachment. It is shown as such since this is the mode that is inputted into the aeroelastic analysis (code F762BR, to be described later), which is then analytically joined to the flexstrap. The normalized mode shapes of the more significant, lower frequency modes, are presented in Fig. 38. A summary of all major blade parameters is presented in Table 18.

Blade/Flexbeam Joint

The initial considerations in selecting a blade joint design were low cost and simplicity. Additional requirements were that the blade could be disconnected from the flexbeam, and that bending moments be uniformly distributed from the flexbeam to the blade. A simple spar inserted into the

TABLE 18

ROTOR DESIGN PARAMETERS

Diameter	9.45 m (31 ft)
No. of blades	2
Blade chord	380 mm (15 in.)
Twist & taper	0
Airfoil	NACA 23112
Blade material	E-glass/epoxy
Flexbeam size	11.4 x 140 x 787 mm
Flexbeam material	Graphite/epoxy
Flexbeam pretwist	-16°
Hub offset	203 mm (8 in.)
Design Tip Speed	53.4 m/s (175 ft/s)
Pre-Cone	8°

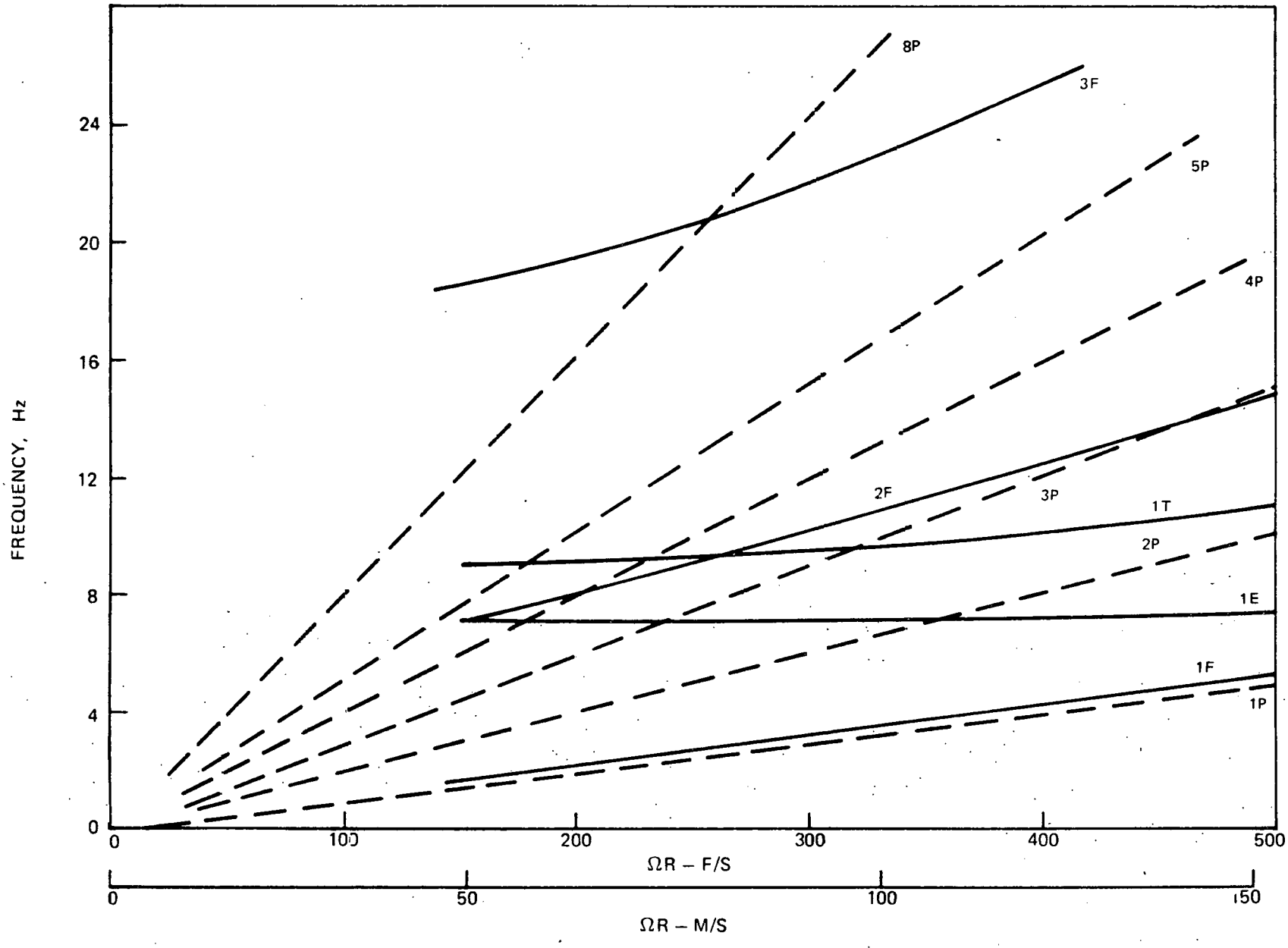

Fig. 37 Frequency Diagram Fiberglass Blade

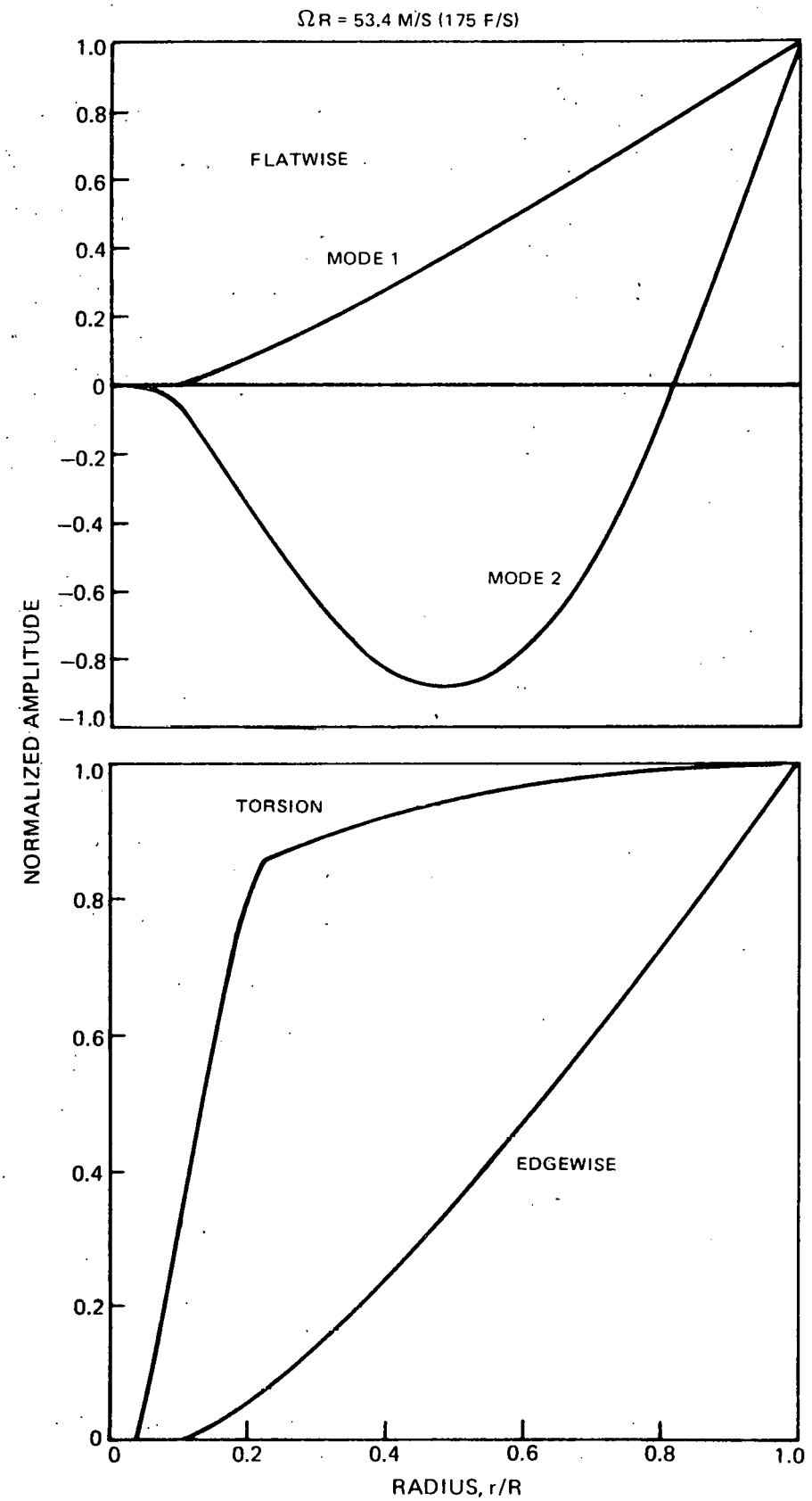

Fig. 38 Blade Mode Shapes

78-11-17-13

hollow blade end and potted in place with epoxy would be considerably less expensive than a contoured spar but the strength of a large amount of epoxy was questionable. Shear tests were run which incorporated a rectangular spar inserted into a hollow shell with a clearance space to be filled with various epoxy resins. The results of these tests, reported in an earlier section, proved the approach to be unacceptable due to criticalness of alignment between the center line of the applied load and the epoxy-to-spar interface. A close fit between spar and blade with a thin epoxy interface would be the most reliable design.

An airfoil-shaped spar which would closely match the internal shape of the blade could be cast in aluminum at relatively low cost. Consideration was given toward making the spar out of titanium for a reduction in size and weight, but the idea was dropped due to excessive material and fabrication cost. The thin epoxy interface would provide a uniform load distribution between parts; but to further insure against a possible failure, three shear sleeves were added to the joint. The sleeves have a total load capacity greater than the maximum shear load. The design is shown in Fig. 39. In order to reduce the stress concentration where the perimeter of the spar bears on the thin blade wall, additional layers of fiberglass were applied to the outside surface of the blade to locally increase its stiffness. The fiberglass layers are also tapered around their perimeter to gradually distribute stresses between components. The additional reinforcing layers also provide increased bearing area where the shear sleeves penetrate the blade. A yoke configuration on the flexbeam end of the spar was selected to keep the axial loads symmetrical and eliminate any additional bending stresses.

The flexbeam itself was reinforced with multi-aligned plies of graphite/epoxy to distribute the concentrated loads at the bolts. Tests were conducted of the pull-out strength of such a design and were reported earlier. The maximum loads of the blade/flexbeam joint occurred for the maximum gust condition examined during the loads calculations discussed in a later section of this report. This condition is referred to as Gust II and involves a gust of 54 m/s (120 mph), occurring while operating at a steady condition of 9 m/s (20 mph). This represents a gust factor of 6:1 which is an extreme condition and not expected to be experienced. These loads were greater at the joint than those produced for the steady 74 m/s (165 mph) condition, and therefore were used in the joint design. The various flatwise, edgewise, torsion, and centrifugal loads were applied simultaneously to the blade joint design, and the stresses at various points in the structure were calculated. These are shown in Table 19 along with safety factors based on yield strengths of the materials. Yield strengths and safety factors are shown for both the aluminum machined part (6061-T6) which would probably be used in the prototype, and for an aluminum casting (355-T61) which would be used in production.

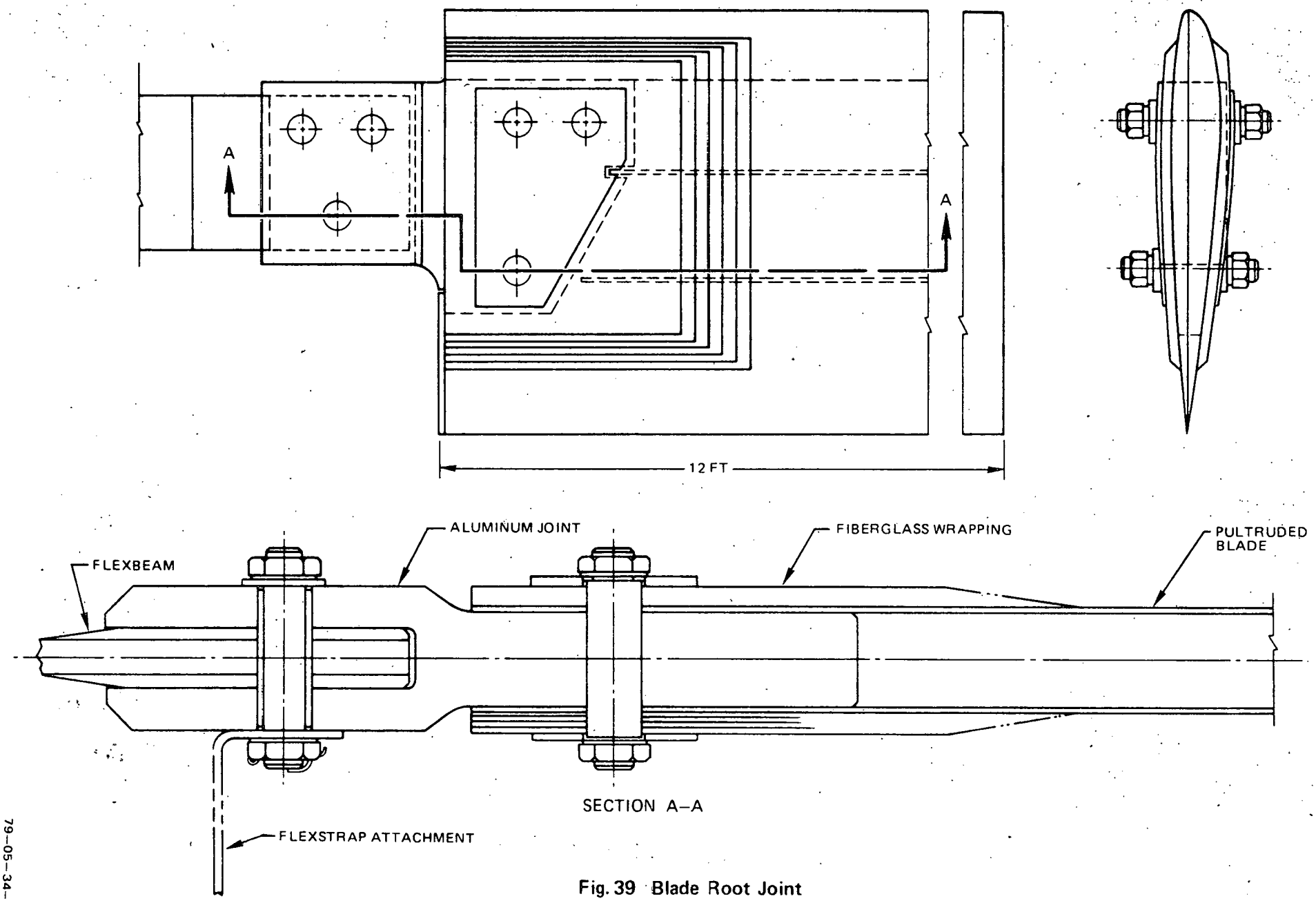

Fig. 39 Blade Root Joint

TABLE 19

BLADE JOINT STRESS CHARACTERISTICS

Location	Maximum Stress, MPa	Yield Stress, MPa	Min S.F.	Design Stress, MPa	Design S.F.	Fatigue S. F. (Design)
Max σ_T at root of Alum yoke	σ_T = 91.4	241-6061-T6 207-C355-T61	2.64 2.26	11.4	21.1 18.1	6.3 2.7
σ_s in 3165 S Sleeves at fiberglass	σ_s = 70.2	σ_s = 331	4.7	8.8	37.6	
σ_s in 3165 S sleeves at flexbeam	σ_s = 82.4	σ_s = 331	4.0	10.3	32	
σ_B in fiberglass from pins	σ_B = 105.9	σ_c = 241	2.26	13.4	18.1	
σ_B in alum yoke from pins	σ_B = 50.3	386-6061-T6 207-C355-T61	7.6 4.1	6.3	61 32.8	
Shear stress in alum yoke	σ_S = 16.8	138-6061-T6 179-C355-T61	8.2 10.7	2.1	65.6 85.6	
σ_T at yoke three flexbeam pins	σ_T = 80.7	241-6061 207-C355-T6	3.0 12.0	10.0	24 20.8	7.2 3.1
σ_S in adhesive between f.g. & alum.	σ_S = 2.3	σ_S = 20.7	8.9	0.3	71.2	
σ_T in alum yoke thru pin sect (fiberglass end)	σ_T = 111.5	241-6-61 207-C355-T61	2.16 1.35	13.9	17.3 14.8	5.2 2.2
tigue Strength -- 10^6 cycles		72.4-6061-T6 31-C355-T61				

Rotor Hub

The rotor hub is comprised of two simple steel plates separated by spacers to accommodate the flexbeam and are bolted together to provide a tight assembly. A thin ply of 1.6-mm (1/16-in.) polyurethane is inserted between the flexbeam and hub plates and spacers to minimize stress concentrations and fretting. The hub is then attached to the main shaft by means of two Ringfeders®. Two dowel pins provide the driving lugs between the hub and plates. In stressing the dowel pins, it was assumed that they transmitted the full torque plus all of the lift force plus the weight of the rotor assembly. The safety factor for anl combined stresses for the 75-m/s (165-mph) wind condition in this circumstance is 7. Similar analysis of the bolts with all combined loads acting simultaneously gives a stress value of 158 MPa (23,000 psi). Using bolts of low cost 1020 untreated steel, the safety factor is 1.6. Two of the hub plate bolts also secure the pendulum support bar to the outer hub plate. The support bar is made from cold rolled steel and contains bushings at either end to support the pendula. The configuration is shown in Fig. 40.

Pendulum Design

The control functions which the pendula must perform were described in the concert description section of this report. In summary, the pendula must provide a schedule of blade pitch versus rpm so as to position the blade pitch at an angle for optimum performance at a selected wind speed. The pendula must also place the blade at its stall angle when rotor overspeed occurs due to high wind speeds. The motion of the pendulum and the corresponding deflections of the flexstrap and flexbeam are difficult to simulate accuratelv in an analysis. The design of pendulum geometry and mass was arrived at by scaling up the experimentally determined values of these parameters obtained during the 1/7-scale model tests reported earlier. Scaling laws for dynamically similar rotor blades show that dimensions are scaled directly with the scale factor (linearlv), loads are scaled by the square of the scale factor, and moments and masses by the cube of the scale factor. Adjustments were made to important parameters of the model to achieve a system which was self-starting, operated at a proper pitch angle at the design condition, and produced blade stall at high wind conditions. In scaling up the model dimensions to full scale, the flexbeam thickness ratio was used since this is the most sensitive parameter in determining the flexbeam torsional spring, and thus the moment which the pendulum must balance. This ratio is 0.55/0.072 = 7.64. The centrifugal spring of the pendulum was selected to have the same ratio to the torsional spring of the flexbeam as that of the model. The model pendulum spring is:

® Ringfeder Corp., Westwood, N. J.

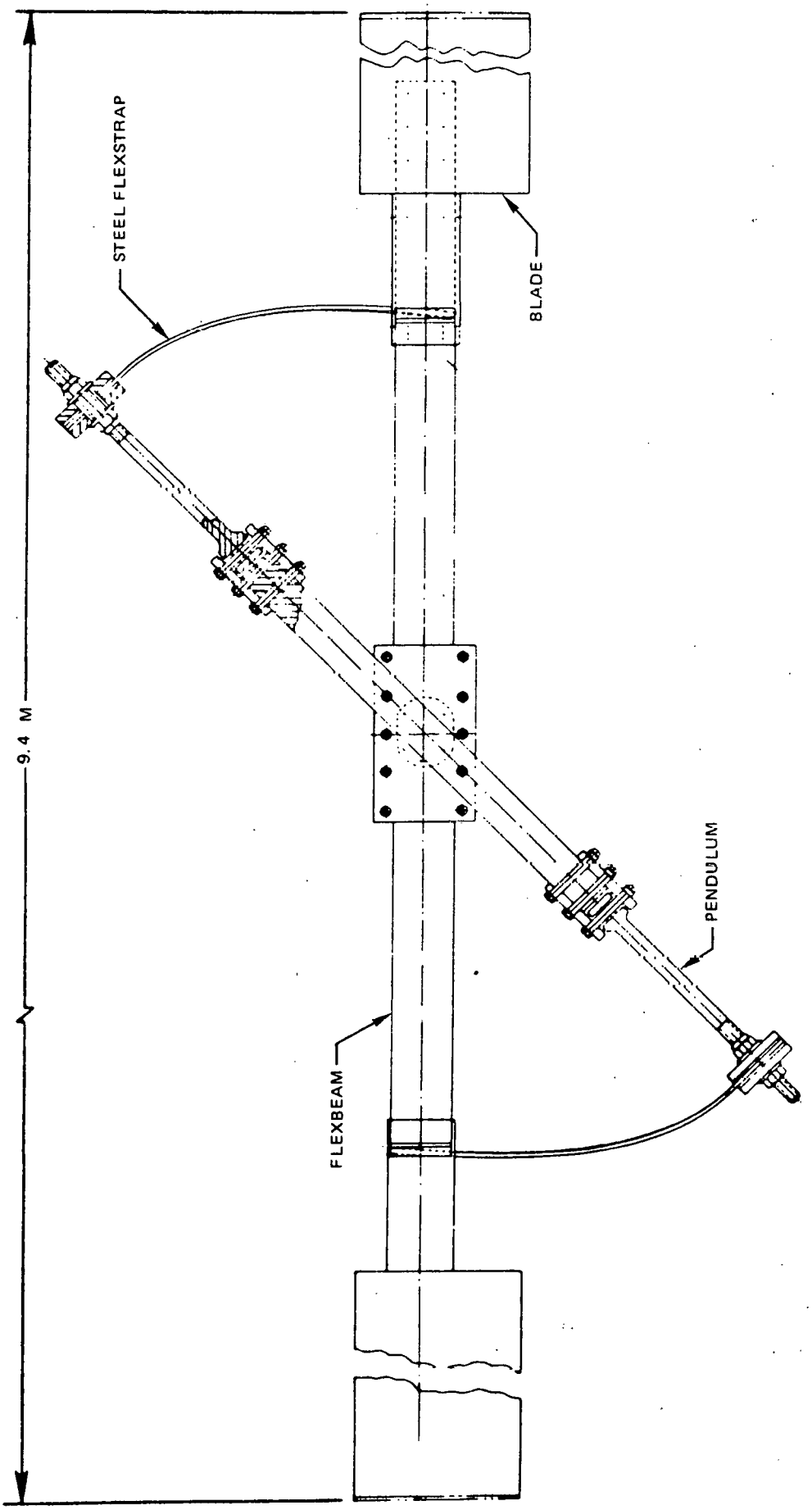

Fig. 40 Hub and Pendulum Assembly

79-05-34-10

$$K_{P_M} = mrl\Omega_m^2$$

$$= 0.021(0.131)(0.053)\Omega_m^2 = 1.458 \times 10^{-4}\Omega_m^2 \quad \text{(SI units)}$$

$$= 0.00012(5.17)(2.1)\Omega_m^2 = 0.0013\Omega_m^2 \quad \text{(English units)}$$

where m is the pendulum mass, r the cg of the pendulum from the center of rotation, and l the pendulum cg from the hinge point. The model flexbeam spring is:

$$K_{F_M} = \frac{GJ}{l_F}$$

$$= (5.17 \times 10^9)(3.01 \times 10^{-11})/0.1 = 1.558 \quad \text{N·m}$$

$$= (0.75 \times 10^6)(7.24 \times 10^{-5})/3.95 = 13.8 \text{ in.-lb}$$

The ratio of the model pendulum spring to flexbeam spring is $\frac{1.458 \times 10^{-4}\ \Omega_m^2}{1.558}$ $= 9.4 \times 10^{-5}\ \Omega_m^2$.

The full-scale flexbeam spring is:

$$K_{F_F} = (5.17 \times 10^9)(1.19 \times 10^{-7})/0.79 = 779 \quad \text{N·m}$$

$$= (0.75 \times 10^6)(0.286)/31 = 6{,}919 \text{ in.-lb}$$

Therefore the pendulum spring is:

$$K_{P_F} = (781)(9.4 \times 10^{-5})\Omega_m^2 = 0.0734\Omega_m^2 \quad \text{(SI)}$$

$$= (6{,}919)(9.4 \times 10^{-5}\ \Omega_m^2) = 0.650\ \Omega_m^2 \quad \text{(English)}$$

The full scale hinge location and center of gravity are determined by ratioing up the model by the scale factor, 7.64. Thus, the full scale pendulum mass is:

$$
\left.
\begin{aligned}
m_F &= K_{P_F}/r_F l_F \Omega_F^2 \\
&= 0.0734 \Omega_m^2/(0.131 \times 7.64)(0.053 \times 7.64)\Omega_f^2 \\
&= 0.181(\Omega_m/\Omega_f)^2
\end{aligned}
\right\} \quad \text{(SI)}
$$

$$
\left.
\begin{aligned}
&= 0.653 \Omega_m^2/(5.17 \times 7.64)(2.1 \times 7.64)\Omega_F^2 \\
&= 0.00103(\Omega_m/\Omega_F)^2
\end{aligned}
\right\} \quad \text{(English)}
$$

Also, for the same tip speed, or advance ratio, Ω_m/Ω_F = scale factor = 7.64.

Therefore,

$$m_F = 0.181(7.64)^2 = 10.57 \text{ kg } (23 \text{ lb})$$

The distance of the mass center from the hinge is determined by scaling the model moment arm.

$$\ell = 0.053 \times 7.64 = 0.405 \text{ m } (16 \text{ in.})$$

The hinge location from the center of rotation for the model was 78 mm (3.07 in.). The full scale hinge location is:

$$h = 78 \times 7.64 = 596 \text{ mm } (23.5 \text{ in.})$$

The model values of the pendulum nonrotating droop angle and the flexstrap attachment angle to the flexbeam are maintained for the full-scale rotor. A summary of all the pendulum dimensions is shown in Fig. 41. The variations of the pendulum angle and blade pitch angle with rotor speed are shown in Fig. 42. These curves are presented assuming no gravity, aerodynamic feedback, or pitch-flap coupling effects. During normal operation, the flapping position of the blade and the aerodynamic pitching moment produce deflections in the system which are not shown on the idealized results of Fig. 42. Also, during start-up, where centrifugal forces are low, the pendula flap cyclically under the action of gravity. These angles vary from $\pm$ 5 to $\pm$ 15° when the tip speed is below 30 m/s (100 ft/s) but have little effect on blade responses due to the low dynamic pressure. The cyclic flapping of the pendula was treated in greater depth in Ref. 3.

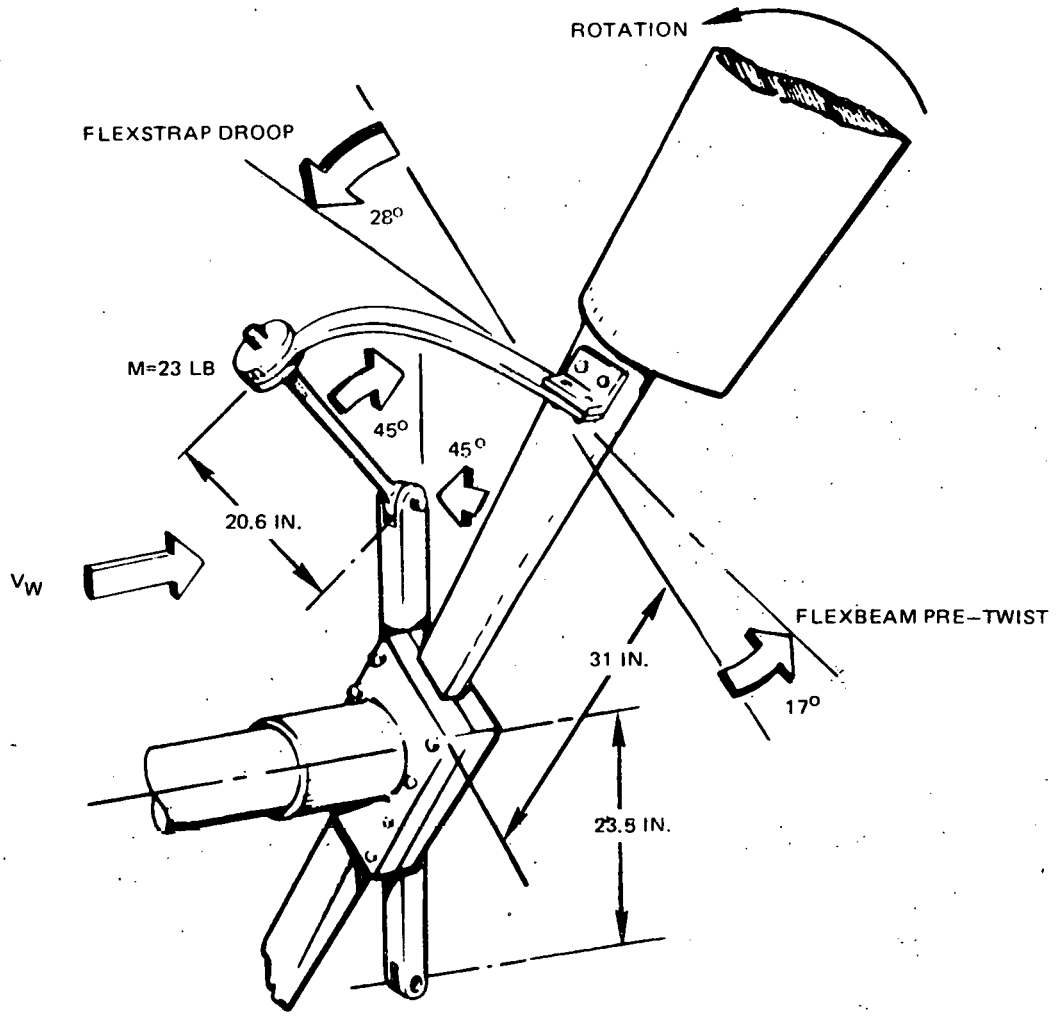

Fig. 41 Pendulum and Flexbeam Dimensions

79-05-34-11

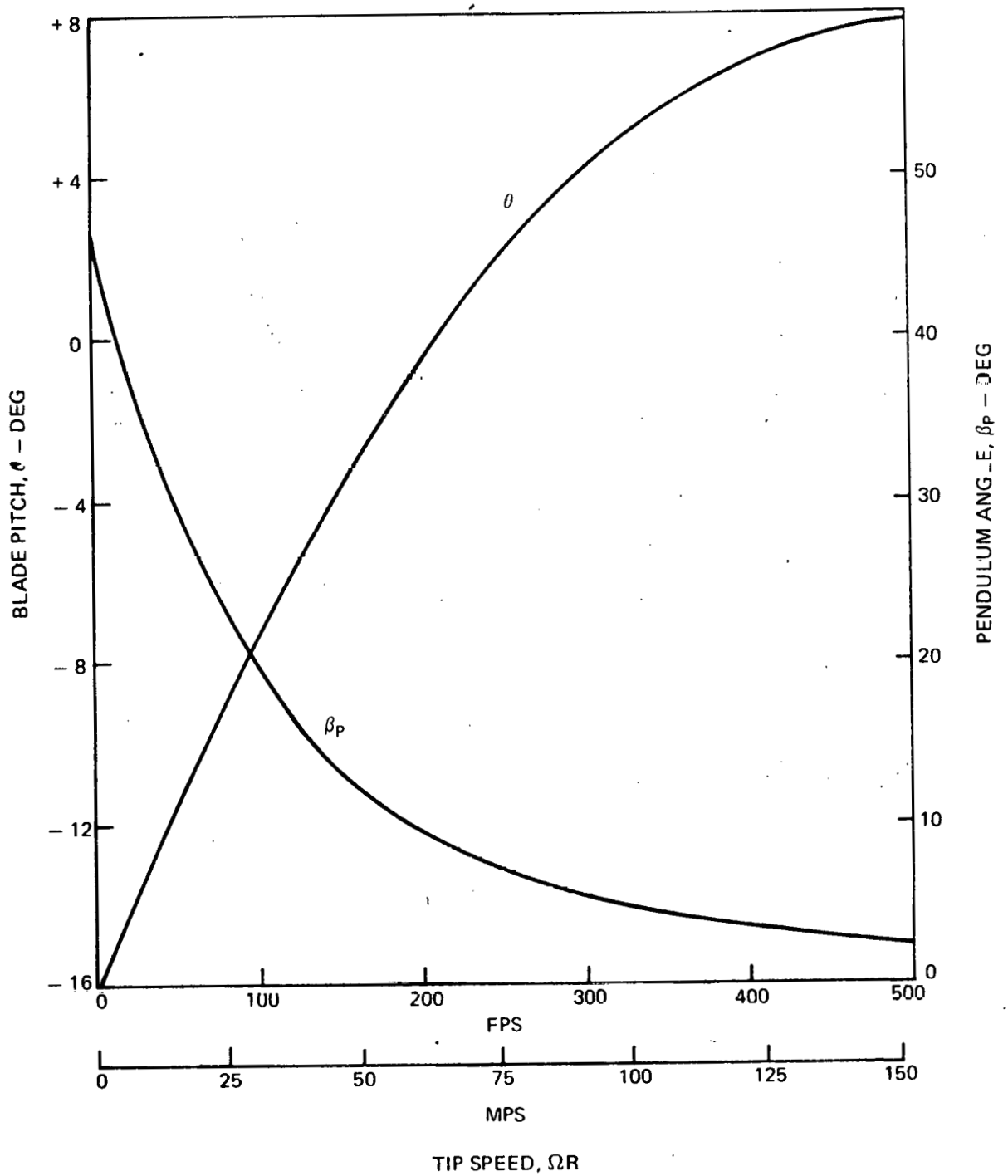

Fig. 42 Control Angles vs. Tip Speed

78-11-17-12

Nacelle Components

The nacelle components shown in Fig. 43, consist of the rotor drive shaft, supported at either end by self-aligning spherical roller bearings, a flexible coupling connecting the shaft to the 1:17 gearbox, and a face-mounted 15 kW induction generator. The components are mounted on a steel weldment, mechanically connected to a steel yaw shaft which in turn is held in the tower cavity by spherical roller bearings. The entire assembly is enclosed in a molded fiberglass shell which is sectional and designed for easy removability. An automotive disk brake is included for the prototype system but it is expected not to be required for a production system. The main chassis is constructed of hot rolled steel and for the prototype it will be totally hand welded. It is envisioned that, on a production basis, the weldment will be replaced by a casting.

The yaw shaft is attached to a center bulkhead by means of two U-bolts. Bolting was chosen after conceptual designs, which incorporated a welded yaw shaft, made it apparent that the post welding normalizing and machining of such a large weldment would be more costly. The U-bolts are made of 4130 steel. The yaw shaft is made of 114-mm-o.d. x 51-mm-i.d. 4130 heat treated tubing, and the shaft is supported by self-aligning spherical roller type bearings with tapered i.d. shaft mounts. These bearings were selected primarily for their high load capacity, and the self aligning and taper mount features reduce the precision to which the bearing housings must be machined. The upper bearing is the most highly loaded of the two as it takes out the load due to head weight in the form of bearing thrust in addition to the radial load. The lower bearing is loaded radially only. The yaw bearings, as well as the rotor shaft bearings, were sized and selected on the basis of a 25 year operating life. Design studies which incorporated a smaller lower bearing showed an increase in machining costs which offset the less costly bearing. Because of this and the difficulty in replacing yaw bearings, it was decided to use identical parts.

The rotor shaft is fabricated from 4130 heat treated steel bar and is supported at each end by spherical roller bearings, which again permit less precision machining on the weldment due to their self aligning feature. The rotor-end bearing carries both the radial and rotor thrust components while the gearbox-end bearing carries radial load only. The gearbox-end bearing is overdesigned for this application; however, it is the lightest duty available for the required shaft size. A summary of the bearing safety factors and other information is presented in Table 20.

The blade hub is attached to the rotor shaft by two standard Ringfeder® couplings. These units permit easy assembly and disassembly of the hub to the shaft and do not deform the shaft when installed. Other means of attaching the hub

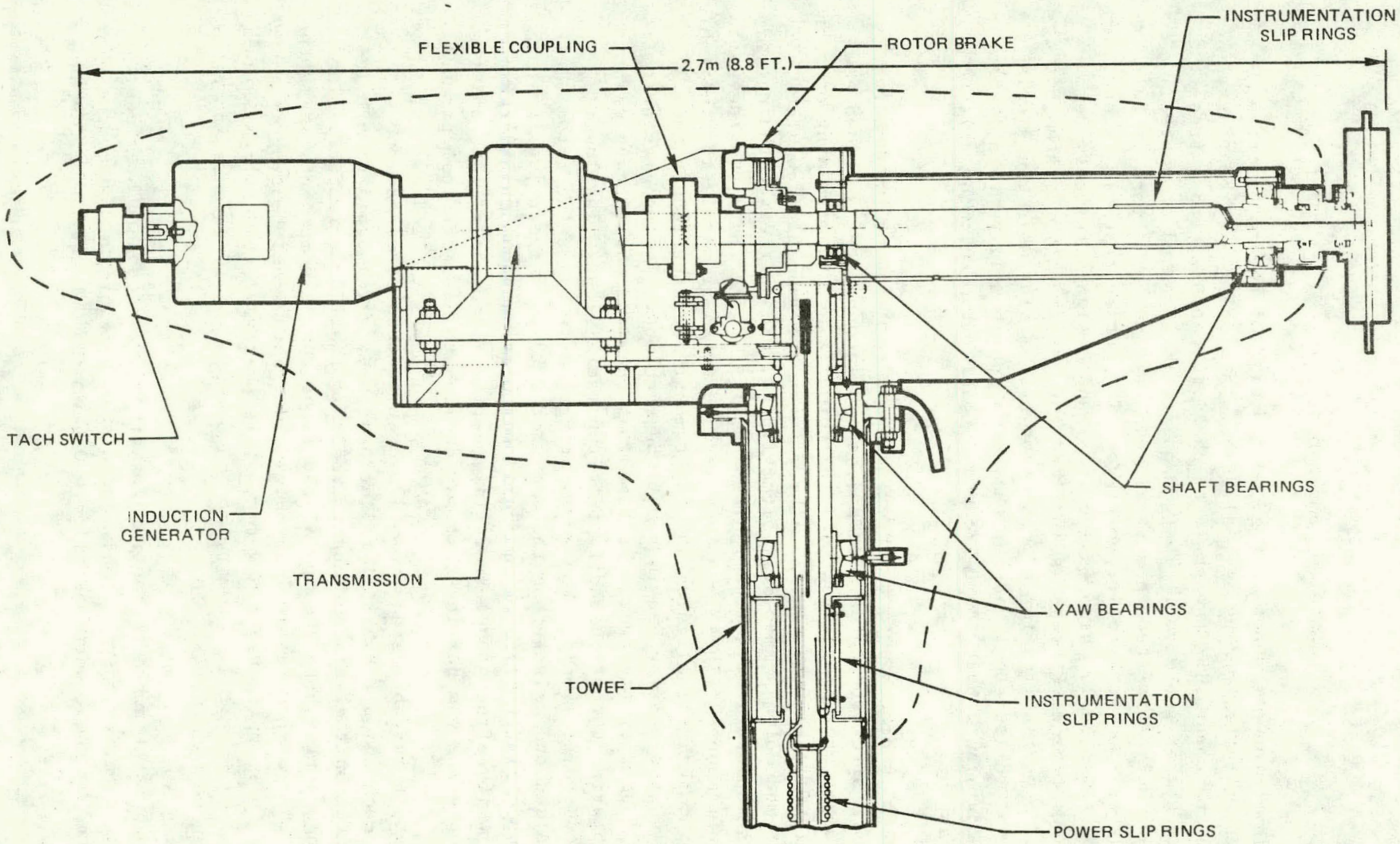

Fig. 43 Nacelle Components

TABLE 20

BEARING SELECTION SUMMARY

Bearing overdesign ratings (25 yrs)

Wind Condition m/s	Blade-end rotor brng.	Gearbox-end Rotor brng.	Upper yaw bearing	Lower yaw bearing
74 w/gust	2.45 for 500 hr	2.02	4.42 for 500 hr	1.35
74	2.50 for 500 hr		4.98 for 500 hr	
54 w/gust			1.09	
120			1.30	
9 w/gust			1.21	
9	2.5		2.33	
FMC brg no.	22317 lbk	22214 lbk	23224 lbk	23224 lbk
Price	$71.78 + 15.70	27.53	134.86 + 31.56	134.86 + 31.56
Mission	Radial Component + thrust	Radial Component	Radial Component + thrust	Radial Component

in position such as cross bolts and keys were designed but were traded off due to cost or operational deficiencies. The Ringfeders® in combination exceed the torque and axial load requirements by several times. The opposite end of the rotor shaft is mated with the generator gearbox by means of an FMC model XR-2-1/2 double engagement geared flexible coupling. This coupling allows for 1-1/2° of angular misalignment and 1.45 mm (0.057 in.) of direct offset. These parameters exceed the maximum shaft deflection to a degree which allows a concentricity tolerance of ± 0.4 mm (1/64 in.) when aligning the gearbox with the shaft at assembly.

The gearbox is aligned by means of adjustable locking nuts which are above and below the mounting base of the casting feet. This, together with the radial clearance between the mounting feet and studs encompass the required adjustment envelope. It is felt that final adjustment may be made by merely feeling the radial match of both sides of the coupling while the coupling tie bolts are loosened. The generator is face mounted to the gearbox and presents the most compact design possible. A complete design of a belt-driven generator was originally laid out for evaluation; however, studies of the setup made it apparent that, from the standpoint of weight, compactness, reliability, efficiency, and life cycle costs, the face mounted gearbox design was superior.

A hydraulic disc brake assembly is located between the gearbox-end rotor shaft bearing and the coupling. The rotor is a 292-mm (11-1/2-in.)-diam automotive product and is attached to the rotor shaft with a Ringfeder®, the same size as those used to attach the shaft to the rotor hub. A previous design incorporated the same brake design located upstream of the rotor hub between it and the rotor-end shaft bearing. However, this design had the shortcoming of requiring a larger diameter rotor shaft and bearings because of the longer unsupported length of the rotor shaft that was required. It is anticipated that a rotor brake will not be required for a production system.

The entire head package attaches to the tower by means of a bolted flange which is welded to the yaw bearing support tube. This method has the advantage of not requiring precision machining operations to be performed on the tower.

The rotor loads which the head components must react were calculated using the UTRC F762BR aeroelastic analysis, and a description of this analysis and a discussion of the loads are presented in the Loads and Stability Characteristics section. The stresses and load factors resulting from the loads for three wind conditions are presented in Table 21 for the major structural components.

The instrumentation slip rings shown on Fig. 43 are required to transmit blade stress data for the prototype testing. These would not be present on a production unit.

TABLE 21

NACELLE COMPONENT SAFETY FACTORS

Generator Head Component
Stresses and safety factors*

Item	165 MPH Stress (MPa)	S.F.	120 MPH Stress (MPa)	S.F.	Design Stress (MPa)	S.F.
Yaw shaft "U" bolts	254	1.55	174	2.25	100	3.93
Yaw shaft	328	2.52	223	3.71	83	9.99
Ringfeder® dowels (Torque loading)	89	7.00	89	7.0	89	7.0
Ringfeder® bolts	159	3.0	144	3.5	127	4.0
Ringfeder® adapter (Bending)	169	2.66	155	2.89	138	3.26
Overhung rotor shaft	227	3.64	212	3.90	195	4.23
Front bearing connection bolts	50	5.00	31	8.26	7	37.0
Yaw bearing housing flange	127	1.99	85	2.96	29	8.65
Rotor bearing housing (Bending)	81	3.10	62	4.08	46	5.53

*with gust moment of 4180 N.m included

Tower and Erection Device

Tower

The tower is composed of two flanged sections of Schedule ten 394-mm (10-in.)-diam steel pipe, each approximately 7.9-m (26-ft) long. This is a low cost scheme both from the standpoint of fabrication time and material cost. Three cables of improved 25-mm (1-in.)-diam plow steel, with simple thimbles and clamps, are attached to the upper flange. A similar guy system of 19-mm (3/4-in.)-diam cable is attached at the mid-station. The guys are attached to the ground anchors by means of turnbuckles, one for each wire, which are located above the ground level at a point where it is convenient for manual adjustment. A pivot at the base of the tower is composed of a 102-mm (4-in.)-diam bar welded to the base and tangent to the pipe. The assembly is shown schematically in Fig. 44. Pretension in the upper guys is set at 44,500 N (10,000 lb) and in the lower guys at 22,250 N (5,000 lb). A discussion of the tower loads and dynamic characteristics is presented in a later section.

Tower Erection

As shown in Fig. 45, it is assumed that erection of the tower by means of the winch will begin with the centerline of the head assembly approximately 2.9 m (9 1/2 ft) above the pivot centerline. This is necessary for two reasons. First, the safety factor on combined stresses in the tower goes below 1.5 when jacking from a lower elevation. Second, the required winch capacity rises above 4535 kg (5 tons).

The jib boom used for erection is primarily composed of a piece of 127-mm (5-in.)-diam standard weight carbon steel pipe 7.6-m (25-ft) long. Various schemes for raising the boom were explored before deciding on the method shown in Fig. 45. The worst case stress condition for the boom is at the beginning of the erection cycle. The safety factor on combined stresses at this point is 3.0.

The sequence of events that occur during the erection procedure are shown schematically in Fig. 45. Figure 45(1) shows the side view and the plan view of the wind turbine assembly in the near horizontal position and prepared to be rotated to the upright position. Two of the lower guy wires are attached to the permanent anchors and are shown slack. The third lower guy wire, to be connected to the anchor nearest the winch, is shown unattached from the anchor and lying on the ground. The upper guy wire that attaches to that same anchor is shown attached to the end of the erection boom. This guy wire is shown slack until the erection boom is raised to a vertical position. The guy wire then becomes taut and capable of transferring the moment-producing force to rotate the tower. The other two upper guy wires are shown attached to temporary anchors. These temporary anchors are located along the axis of rotation of the tower pin and they hold the upper guy wires taut with constant tension

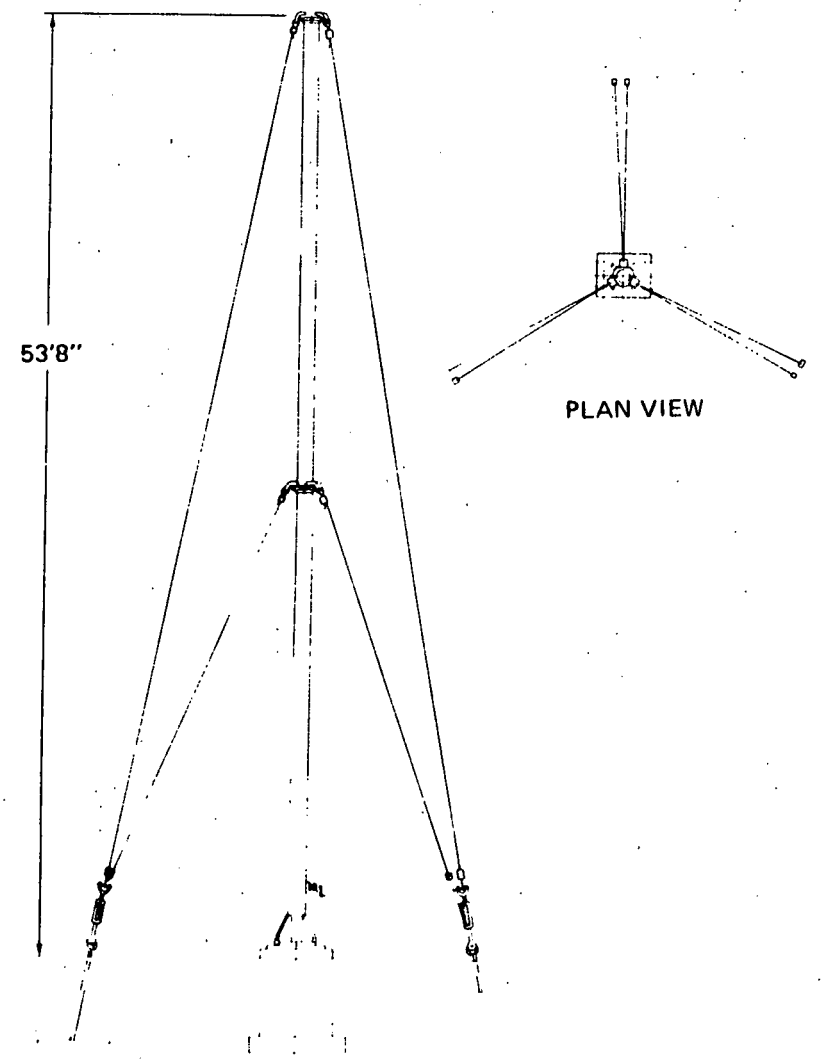

Fig. 44 Tower Assembly

78-10-04-3

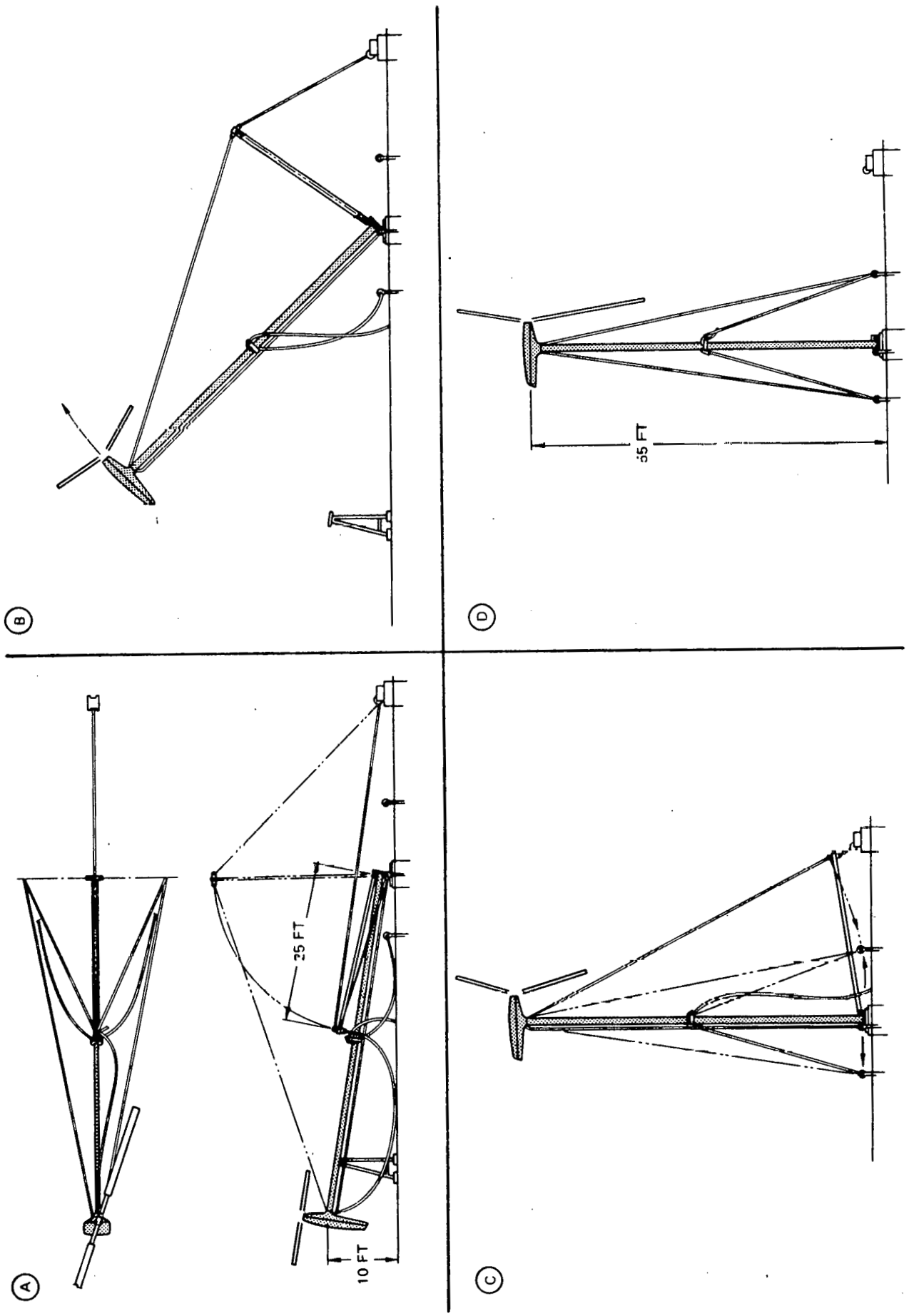

Fig. 45 Erection Procedure

79-05-34-14

throughout the erection procedure. The purpose of this temporary arrangement of the upper guy wires is to stabilize the tower during the erection operation and prevent any lateral movement. This will prevent the tower base from having to react a transverse moment. The erection boom is also stabilized to prevent lateral movement by temporary guy wires extending from the boom tip to each of the temporary anchors.

Continuing with the erection procedure, once the boom and all guy wires are in place, the winch cable attached to the erection boom tip is drawn up and the boom moves to the vertical position as in Fig. 45①. The winch cable is then drawn farther and the tower starts to rotate about the base pin. This is the point during the erection procedure at which the maximum tower foundation loads occur for the erection condition. The column load in the erection boom produces a vertical compressive force on the foundation of 36,000 N (8,100 lb) and the column load in the tower produces a shear force on the foundation of 28,000 N (6,300 lb). The winch cable is drawn further as in Fig. 45②, and the tower continues to be rotated to the vertical position. As the tower reaches the near vertical position (Fig. 45③), the two lower guy wires that were attached to the permanent anchors become taut, and the other loose lower guy wire is then attached to the third permanent anchor. The tower is then stabilized in the vertical position by the three lower guy wires. The two upper guy wires can be removed from the temporary anchors and attached to the permanent anchors, and the erection boom can be removed and the remaining upper guy wire attached to its permanent anchor. Proper tensioning of all guy wires is then performed to complete the erection operation (Fig. 45④). The turnbuckles would then be locked in position to prevent vandalism.

Wind Turbine Site Design, East Hartford, Ct.

Operation of the wind turbine in East Hartford, Connecticut, prior to delivery to Rocky Flats, required a design study to be conducted to prepare an adequate site for testing. The site design must satisfy erection requirements as well as high-wind conditions which might occur.

The wind turbine site hardware is composed of two major items; the tower base foundation and three guywire anchors. The tower base is simply a concrete block 1.5-m (5-ft) square and 1.2-m (4-ft) deep. The concrete block is steel reinforced to carry column loading and bending, where standard concrete is used (average strength) and the reinforcing is accomplished using low cost steel bars. The guy wire anchors are common steel boiler plate 1.2-m (4-ft) square and 32-mm (1.25-in.) thick. Two eyebolts are attached to the center of the plate and normal to it. When buried in the ground with the eyebolt shanks parallel to the upper and lower guy wires, the anchors will engage a pyramidal volume of soil through the soil shearing action. The total excavation requirement is 20 m^3 (27 yd^3), including a 50 % surcharge, and the total steel used is 1225 kg (2,700 lb).

Design Loads for Site

There are two conditions to be considered in calculating the design loads acting on the wind turbine site (foundation and anchors). The first, Case 1, is the erection of the system using the method described earlier; and the second, Case 2, is the high-wind condition which might be expected to occur in East Hartford, Connecticut.

The loads produced during erection were reported earlier, and a schematic of this condition is shown in Sketch 1. The second design condition is the high-wind condition, where it was assumed the maximum wind which might occur at this location was 45 m/s (100 mph). The maximum thrust that would be generated at this speed is 8900 N (2,000 lb). This force, which must be reacted by the guy wires, in combination with the guy wire pretension forces, forms the vertical design loads for the foundation and anchors. These are depicted in Sketch 2. The horizontal design loads are determined by the erection forces.

Table 22 summarizes the site design loads for both the erection condition (Case 1) and the high-speed condition (Case 2). A factor of safety of 1.5 has been used for stress calculations in the site design.

TABLE 22

FOUNDATION AND ANCHOR DESIGN LOADS FOR EAST HARTFORD SITE

			1.5 Factor of Safety	
	Case 1 Erection	Case 2 High Wind	Case 1 Erection	Case 2 High Wind
Foundation				
Vertical compressive	36,000 N	222,500 N	54,000 N	333,800 N
Horizontal shear	28,000 N	0	42,000 N	0
Anchor				
Vertical tension	0	111,300 N	0	166,900 N
Horizontal tension	0	4,500 N	0	6,700 N

Because both the foundation and anchor system interact with the soil, two assumptions had to be made concerning the soil characteristics: a) Safe bearing capacity of soil. Marks Engineering Handbook, Page 12-20, shows that the bearing capacity of soil can vary from 1 ton/ft^2 for soft clay to 100 ton/ft^2 for ledge rock. A conservative value of 2.5 ton/ft^2 was chosen which corresponds to a medium soft clay. b) Soil coefficient of internal friction.

SKETCH 1

INITIAL ERECTION LOADS

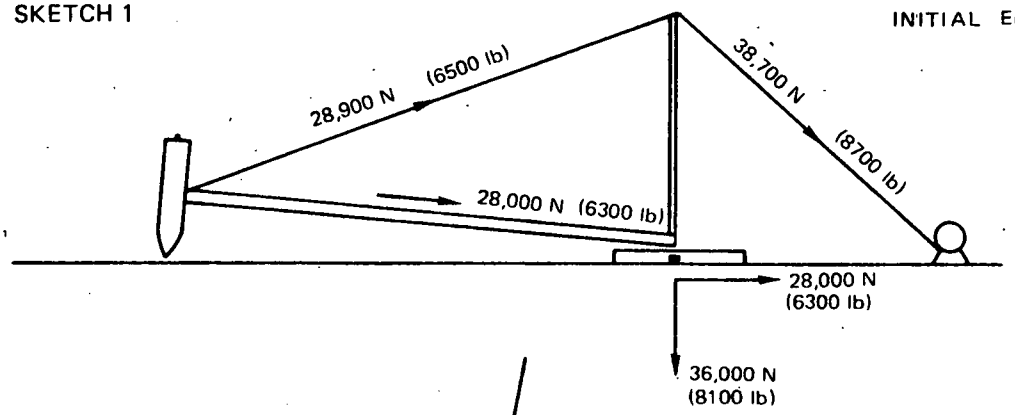

SKETCH 2

HIGH WIND OPERATION,
V_w = 45 M/S (100 mph)

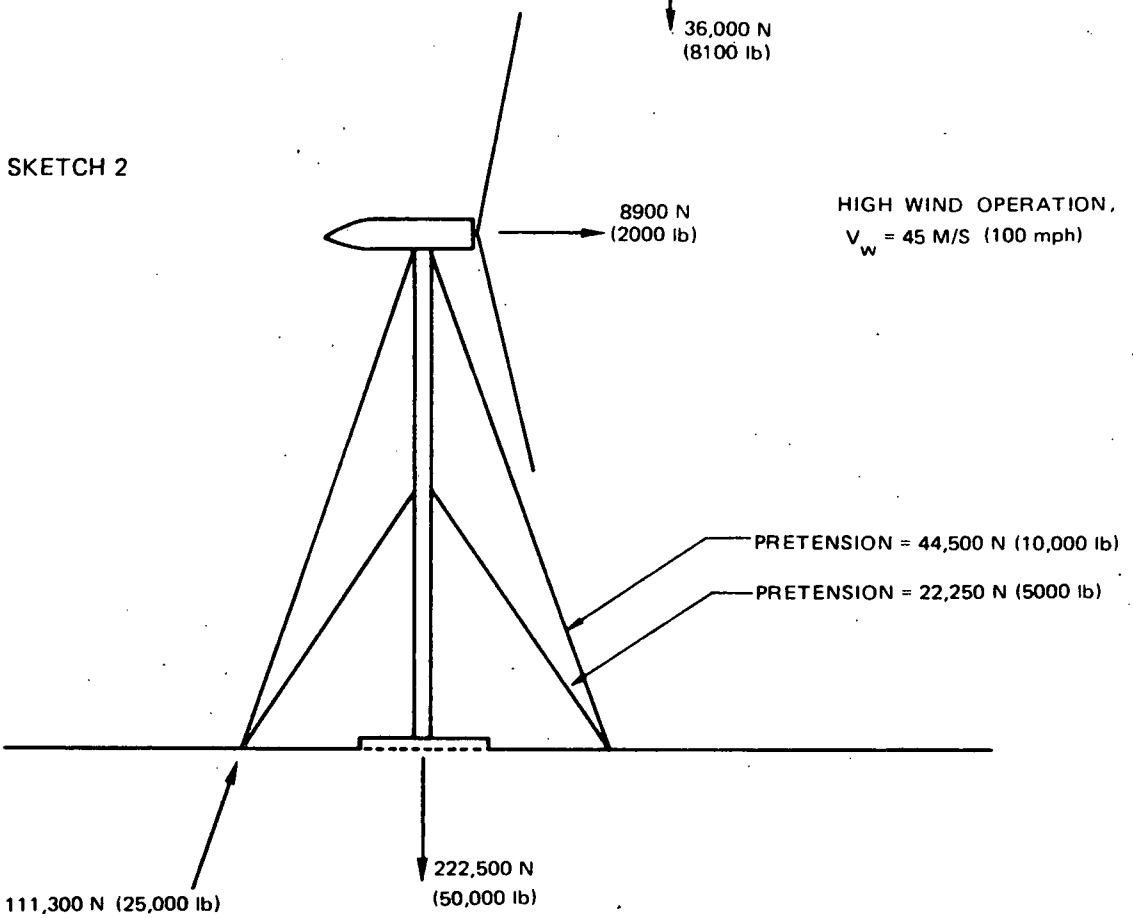

78-11-17-5

This soil characteristic is important in calculating the area requirements for the guy wire anchors and is an indicator of the soil shearing capability. Uquharts Handbook of Civil Engineering, Page 7-175, gives two values for earth as determined by two experimentors: 48° and 37°. These values are the equivalent soil friction angles. The more conservative value (48°) was chosen for the anchor area calculation. A soil test will be performed at the site prior to excavation to verify the soil safe bearing capacity and the coefficient of internal friction.

Foundation Design

The tower foundation is a steel-reinforced concrete block 1.5 x 1.5 x 1.2-m deep. The foundation is steel-reinforced horizontally in both axis directions near the bottom of the foundation to help react shears and moments. The foundation also has vertical steel reinforcement on a 0.4-m square in the center of the foundation top that extends vertically to the horizontal steel bars. These vertical bars react the column loading of the tower. A schematic of the foundation is shown in Fig. 46. Four 38-mm (1.5-in.)-diam anchor bolts are cast in the foundation top to secure the tower base.

Anchor Design

The three guy wire anchors all have the same design and are simply a 1.2 x 1.2-m sheet of boiler plate steel 32-mm thick. Two 38-mm-diam holes are cut in the center of the plate (203 mm from center to center) to accommodate the 38-mm-diam eyebolts to the upper and lower guy wires. A 25-mm-thick, two-hole steel washer 406-mm square is placed below the plate to help transfer the tension loads from the eyebolts to the anchor plate. The holes in both the washer and the anchor plate are slightly oversized to allow some angular freedom of the eyebolts. Steel discs 25-mm thick and 76-mm-diam are welded to the bottom of the eyebolts to secure the two eyebolts to the anchor plate washer assembly. Figure 47 shows a schematic of the anchor. The material requirements for both the anchors and foundation are listed in Table 23.

Temporary Anchors

It was previously mentioned during discussion of the erection procedure that two temporary anchors were required to stabilize the tower and the erection boom during the erection procedure. These temporary anchors will be premade concrete blocks with built-in steel eyebolts. The concrete blocks are 0.4-m square by 1.2-m long and weigh on the order of 454 kg. They are off-the-shelf available items that are reusable and cost about $50 retail. Since their only function is to remove slack from the upper guy wires and the erection boom cables during erection, and provide a low pretension, their dead weight size is more than adequate.

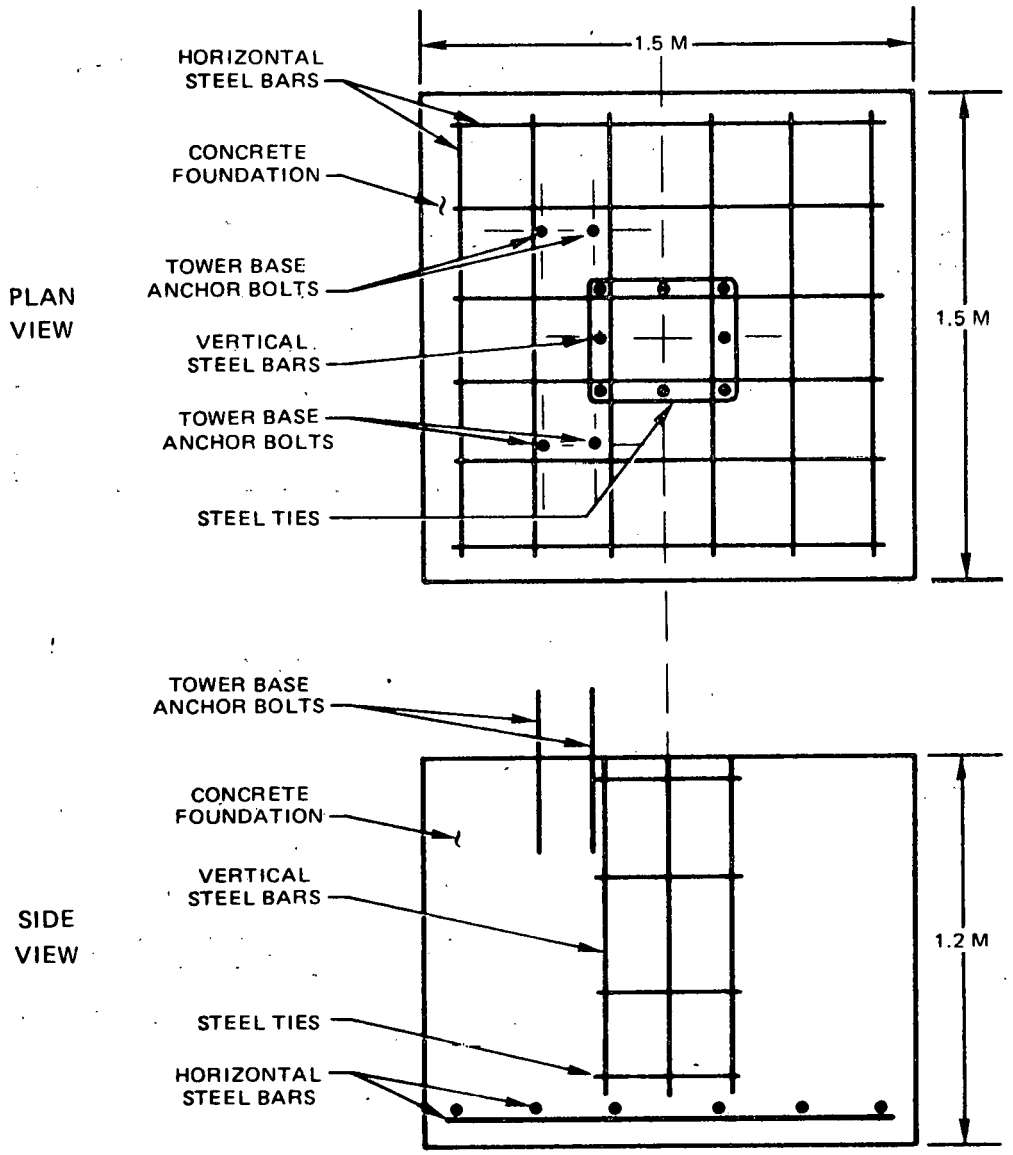

Fig. 46 Schematic of Typical Tower Foundation (Requirements May Vary According to Specific Site Conditions and Local Code Requirements).

79-05-34-15

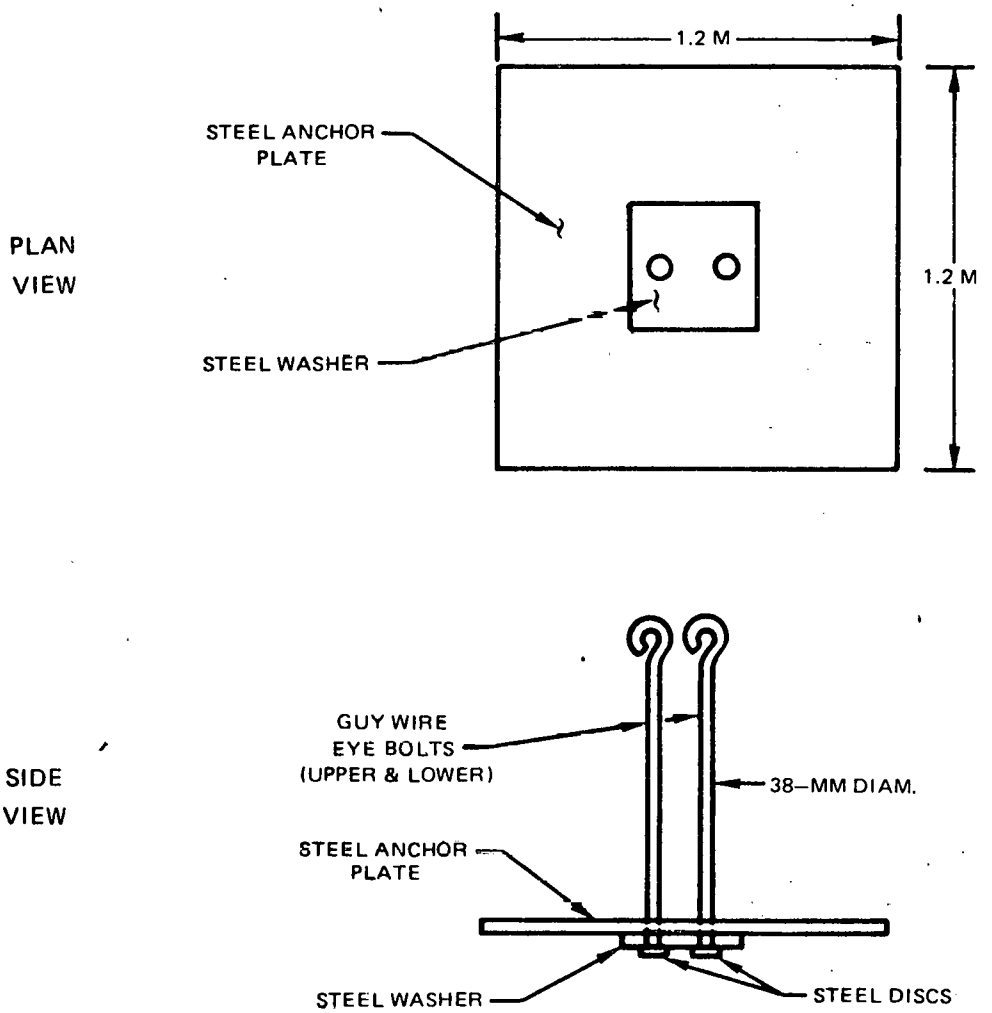

Fig. 47 Schematic of Typical Guy Wire Anchor

79-05-34-16

TABLE 23

TYPICAL FOUNDATION AND ANCHOR MATERIAL REQUIREMENTS*

Foundation

Concrete (17.2 MPa):	2.83 m^3
Horizontal Steel Bar:	12 No. 6 Bar 1.37-m long each
Vertical Steel Bar:	8 No. 9 Bar 1.09-m long each
Steel Tie Bar:	4 No. 2 Bar 1.78-m long each
Anchor Bolts:	4 38-mm diam 0.51-m long each

Anchors

Steel Boiler Plate	1.2 m x 1.2 m x 32 mm	1 per Anchor	3 Total
Steel Washer:	406 x 406 x 25 mm	1 per Anchor	3 Total
Eye Bolts:	38-mm diam x 2.75 m	2 per Anchor	6 Total
Steel Discs: (Welded to bottom of eye bolts)	76-mm diam x 25-mm thick	2 per Anchor	6 Total

* Actual requirements may vary according to specific site conditions and local code requirements.

Weight, Balance, and Material Specifications

The individual weights of all components and their horizontal distances from the yaw axis are listed in Table 24. Their resultant weight moments and the cg location of the total system is also calculated. The cg is calculated to be 57 mm forward (towards generator) of the yaw axis. This is desirable from the standpoint of erection since the rotor will swing up and away from the slack guy wires during erection. The major weight item is the tower and cables which total 1110 kg and the total system weight is estimated at 1920 kg.

The purchased parts and the raw materials required for the complete system, not including the foundation and ground anchors, are listed in Tables 25 and 26.

Appearance Studies

A study was conducted to determine the effect that various nacelle shapes and color schemes had on the overall appearance of the wind turbine. Since the system aesthetics is an important factor in public acceptance of WECS, it was felt that personnel trained in this area should be involved. Therefore, an industrial design firm, Industrial Design Consultants (IDC) of Farmington, Connecticut was employed to study this problem.

IDC has supplied a variety of enclosure concepts which led to the construction of several small-scale mock-ups which are currently under evaluation. Photographs of three models are shown in Fig. 48. Color concepts are also being evaluated; however, this activity will not be completed until Phase II of the program. It is anticipated that the selected design will be fabricated from blown fiberglass with colored resin.

TABLE 24

WEIGHT AND BALANCE SUMMARY

Item	Weight (kg)	Dist. From Yaw Axis (mm)	Moment (kg-mm)
-Moments			
Generator	134	1213	162542
Gen Adapter	10	841	8410
Gear Box	165	617	101805
Coupling	26	262	6812
Housing Gussets	44	187	8228
Lower Housing Pl.	21	183	3843
Brake Act.	7	152	1064
Caliper, Ears, Cyl.	16	133	2128
Brake Disc	10	86	860
Brake Coupling	9	6	54
TOTAL	442		-295746
+Moments			
Rear Rotor Brg. Assy.	14	57	798
Housing/Tube Pl.	20	89	1780
Housing/Tube Gussets	20	219	4380
Rotor Shaft	52	464	24128
Chassis Tube	36	526	18936
Chassis Tube Flange	5	968	4840
Blade End Bearing	4	1003	4012
Blade End Housing	10	1003	10030
Ringfeder^{R} Housing	7	1118	7826
Pend. Assy.	29	1143	33147
Inbd. Blade Hub	9	1197	10773
Blades	68	1219	82892
Outbd. Blade Hub	9	1245	11205
Pend. Sys. Bar	27	1289	34803
TOTAL	310		249550

WEIGHT@CENTER:

Yaw Shaft	46	Tower	807
Bearings	12	Cables	303
TOTAL	58		1110

TOTAL WEIGHT OF HEAD ASSEMBLY 810 kg COMPLETE SYSTEM WT = 1920 kg

ΔMOMENT = -46196 kg-mm

C G - $\frac{46196}{810}$ = 57 mm from yaw axis on gen. side

TABLE 25

PURCHASED PARTS LIST

No. Req.	Title
1	Motor (Baldor 256 TC)
1	Gear Red. (Link Belt DDI)
1	Tach. Switch (Speed Det ESS1)
2	Slip Ring (Inst)
1	Slip Ring (Power)
1	Hyd. Cyl. (Ford)
1	Disc Brake (11½ Dia Ford)
1	Coupling (Link Belt #XR-7)
2	Yaw Brg. (FMC #23224 LBK)
1	Upstream Rotor Brg. (FMC #22214)
1	Downstream Rotor Brg. (FMC #22317)
3	Ringfeder^{R} (#7012)
4	3/4 - 10 Locknut
6	Dowel 1/2 Dia 1" LG
6	Hex Hd Bolt (NYLOCK) 1/2 - 13 1/4
6	Hex Hd Bolt (NYLOCK) 1/2 20 x 3 1/4
6	Hex Hd Bolt (NYLOCK) 1/2 20 x 2 1/2
16	Soc. Hd Cap SCR (NYLOCK) #5 40 x 1/2
2	Hex Hd Bolt (NYLOCK) 3/8 16 x 1"
5	Hex Hd Bolt (NYLOCK) 1/2 13 x 1"
4	Hex Hd Bolt (NYLOCK) 1/2 13 x 1 1/2
1	Cup P_T Set SCR (NYLOCK) 1/4 20 x 3/8
2	Cup P_T Set SCR (NYLOCK) 5/16 18 x 3/8
4	Stud 7/8 14 x 6"
8	Locknut 7/8 14 x 6"
4	Grease Fitting 1/8 NPT
1	Pipe Coupling 1/8 Pipe
1	Pipe Nipple 1/8 Pipe x 2"
1	Snap Ring PIC
1	Clevis Pin 3/8 Dia x 1"
1	Cotter Pin 1/8 Dia x 1/2
1	Cable Terminal (Safelock # SA160)
1	Cable Fork (Safelock # SC8C)

TABLE 26

RAW MATERIALS

Head Assembly

DWG. No.	No. Req.	Title	Material
1740-3	1	Head Assy	
-91635	1	Frame	See DWG. STL
-94291	1	Cover	See DWG. STL
-94288	1	Retainer	See DWG. STL
-94296	1	Lever	See DWG. STL
-94290	1	Sleeve	STL
-91636	1	Cylinder	See DWG.
-91638	1	Support	See DWG. STL.
-91639	1	Housing	See DWG. STL.
-94292	1	Shaft	STL 4130
-94297	1	Yaw Shaft	STL 4130
-94298	1	Clevis	STL
-94295	1	Pin	STL
-94293	1	Retainer	STL
-94285	1	Cover	STL
-94287-1	1	Upper Block	STL
-2	1	Lower	STL
-91637	1	Tube	STL
-94286	2	'U' Bolt	STL 4130
-94294	1	CAP	STL 4130
-94289	1	Flange	STL 4130
-00110	1	Shaft Extension	STL 4130
-00846		Slip Ring	Pur. Part
-00843	2	Slip Ring	Pur. Part
-96735	1	Housing	STL
-96736	1	Housing	STL
-96737	1	Speed Indicator	Pur. Part
-96738	1	Adapter	STL
-00111	4	Stand-Off	STL
-00839	1	Motor Cover	STL
-00112	1	Motor Alteration	Pur. Part

TABLE 26 (Cont'd)

RAW MATERIALS

Rotor Assembly

DWG. No.	No. Req.	Title	Material
1704-4		Rotor Assy	See Below
-00161	2	Backing Plate	STL
-00629	1	Hub	CRS
-00158	2	Spacer	CRS
-00160	1	Hub	CRS
-00163	1	Flexbeam	Graphite/Epoxy
-00630	2	Arm	STL
-00159	4	Plate	STL
-00157-1	4	Weight	STL
-2	4	Washer	TEFLON
00631	1	Arm	STL
-00164	2	Strap	See DWG (STL)
-00162	2	Bracket	CRS
-94973	2	Blade	Fiberglass/Epoxy

Tower Assembly

1740-5	1	Tower Assy	See Below
-36371-1	3	Tang	E-4130 STL
-96371-2	3	Tang	E-4130 STL
-00626	1	Extension	Welded Assy STL
-00144	2	Retainer	HRS
-96372	1	Base	Welded Assy STL
-00146	1	Plate	HRS

Erection Device

1740-6	1	Device	See DWG
-92066	1	Boom	See DWG-STL

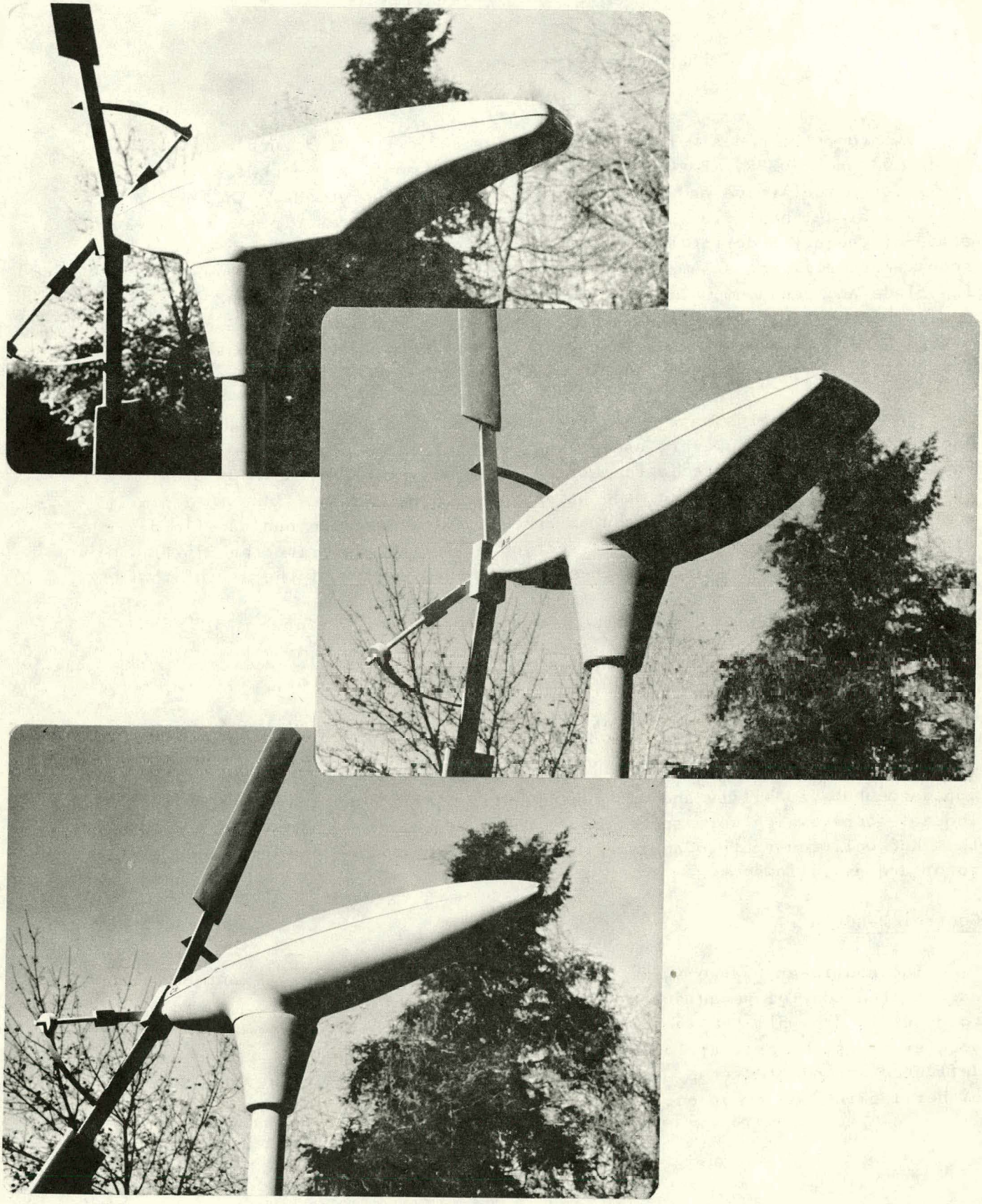

Fig. 48 Nacelle Enclosure Concepts

LOADS & STABILITY CHARACTERISTICS

Two computer codes were used in the design of the wind turbine: G400 (Ref. 15) and F762BR. Both of these codes use a modal approach for simulating the rotor aeroelastics and obtain time-history type solutions. The former is a single-blade, hub-fixed analysis whose blade dynamic description uses recent state-of-the-art modeling techniques. The use of this analysis, however, required simplifying assumptions to be made with regard to the interaction of the blade and pendulum. This analysis was the primary tool for the preliminary design of the rotor blade from a stress standpoint, and provided a check on the F762BR blade stress characteristics. Agreement between the two analyses was demonstrated, and thus only F762BR results will be presented in this report.

The F762BR analysis is a comprehensive, multi-blade, finite impedance hub analysis which, however, uses a less sophisticated blade dynamic description. Following the demonstrated agreement of this analysis with the G400 program all subsequent calculations were made using this F762BR analysis, due to its more complete description of the pendulum control system and the hub/nacelle degrees-of-freedom. The remainder of this section will first describe the F762BR analysis in greater detail, and then present the results of the use of that analysis.

Description of the F762BR Analysis

This analysis is a variant of an analysis originally developed under Sikorsky Division funding for the ABC (Advancing Blade Concept) helicopter development program. This earlier analysis already had multi-blade, finite impedance hub capability and was subsequently modified to analyze wind turbines. Those features which were specifically incorporated into the computer code under this Rockwell contract to analyze the pendulum controlled composite bearingless rotor are as follows:

Control Pendula

The nonlinear (large swing angle) differential equations of motion for each of the control pendula were derived and coded. The pendula were assumed to be excited by all the inertia loads associated with rotor speed and hub/nacelle accelerations, by gravity loads, and by the elastic loads generated by the deflected curved flexstrap. Additional (optional) provision was made for either locking out the pendula motions or for ganging them together.

Elastic Flexstraps

The general computational approach in the F762BR computer program is to calculate mass accelerating forces from known system deflections and/or displacements, in order to calculate accelerations. From the accelerations the time-history solutions are obtained by numerical integration to obtain new deflections to complete the solution loop in a step-by-step fashion. Consequently, the appropriate dynamic description required for the flexstraps is a stiffness matrix giving the complement of 6 loads (3 forces and 3 moments) at each end of the flexstrap due to as many relative deflections at the ends of the flexstrap. To this end, it was assumed that the flexstrap is a circularly curved beam and possesses two modes of deflection: bending in the radial direction (about the minimum bending modulus axis), and torsion about the circular arc elastic axis. These two modes were, furthermore, assumed to be uncoupled. Although the flexstrap was assumed to be rigid in the direction normal to the radii (the maximum bending moduli), nevertheless deflections in this direction are allowed due to effects of a twisted, curved elastic axis. The stiffness matrices were then obtained by inverting the appropriate influence coefficient matrices.

The influence coefficient matrix for radial deflections was obtained from a standard compendium of beam bending formulae (Ref. 16). The influence coefficient matrix for deflections due to torsion was derived from first principles using a differential equation for torsion which included both St. Venant and plate bending effects (see Ref. 15) and assumed a nominally circular arc torsion axis.

Vortex Ring State Modification to Time Variable Inflow

Wind turbines are designed to operate at blade lift coefficients far in excess of those typically encountered by helicopter rotors. As such, they are capable of operating in the "vortex ring state" (see Ref. 17). In such a state the usual momentum balance relationships used to obtain (uniform) inflow distributions break down. The time variable inflow description originally developed for this analysis, however, was derived using a differential equation version of the statement of momentum balance. Consequently, this differential equation had to be modified to incorporate an empirical relationship between inflow and induced velocity appropriate to the vortex ring state as given in Ref. 17.

In addition to these specific features, several others had already been made to the original "helicopter" program to enable the analysis of more conventional wind turbine systems. These basic wind turbine modifications were already part of the analysis capability of UTRC at the inception of this study, and a detailed discussion of them is beyond the scope and intention of this report.

Dynamic Data Required for Analysis

Since the F762BR aeroelastic analysis models the features of this wind turbine system with more rigor than the G400 analysis used in the preliminary design, some of the input data for the former will be somewhat different, both in scope and value, from that for the latter. This subsection briefly describes the pertinent dynamic data required as input for the F762BR program.

Blade Torsion Mode

The explicit dynamic description of the control pendula relaxes the need for approximating the equivalent root torsion spring due to pendulum impedance. Consequently, the appropriate torsion modeling required to calculate the torsion frequency and mode shape requires that the flexstrap be completely disconnected and the blade stiffened in torsion only by the rotor blade flexbeam. For the nominal wind condition of 5.4 m/s (12 mph) and tip speed of 53.3 m/s (175 fps) this torsion mode was calculated to have a frequency of 9.07 Hz (5.05 P). This increased to 10.4 Hz (2.38 P) at a tip speed of 130 m/s (425 fps). The remaining blade mode natural frequency variations with tip speed used in this stability study are essentially those shown in Fig. 37.

Flexstrap and Pendulum Geometry

The derivation of the torsion-dependent flexstrap influence coefficients was made making the assumption of a nominally circular arc elastic axis. From the design details of the flexstrap selected and discussed earlier in this study, the following table presents the simplified geometric and mechanical data used in the stability analysis.

Flexstrap and pendulum Data

Pendulum radial hinge location	0.60 m (23.7 in.)
Pendulum axial hinge location	0.07 m (2.8 in.)
Forward sweep angle of pendulum	45°
Flexstrap-pendulum attachment point from hinge	0.48 m (18.8 in.)
Flexstrap radius of curvature	1.12 m (44.1 in.)
Flexstrap-blade attachment pitch angle	-28°

Tower-Nacelle Dynamic Description

In order to analyze the nacelle stability in yaw, as well as the effects of side gusts, the inherent zero frequency yaw mode due to the free yaw bearing had to be included in the tower dynamic description. The adopted method for including finite impedance characteristics of the rotor hub in the F762BR program is to input inertia, damping and stiffness matrices for a "movable

hub". All of these matrices are 6 x 6 to account for the 6 degrees-of-freedom of the hub. The inertia and stiffness matrices used in the calculations which closely simulate the first elastic bending modes of the tower, as well as the zero frequency yaw mode, are shown in Table 27. Note that since zero hub damping was assumed, the damping matrix was omitted. The six elements in each row and column correspond, in order, to vertical (downward) deflection, lateral (starboard) deflection, clockwise (viewed from above) yaw rotation, nacelle (nose up) pitching rotation, axial (downwind) deflection, and rotation about an axis coincident with the rotor shaft.

Variable Inflow Due to Wind Shear

The F762BR computer program has the capability of inputting a discrete inflow distribution over the rotor disk which varies both radially and azimuthally. Consequently, for each wind speed an appropriate inflow distribution is calculated so that the inputted wind speed and variable inflow distribution combine to simulate the earth wind shear distribution. The wind shear model so selected is the typical power curve,

$$\frac{V}{V_o} = \left(\frac{h}{h_o}\right)^{0.2}$$

where V_o is the velocity at the reference height, h_o, and V is the speed at any height, h.

Rotor Loads

The blade structural characteristics described in the Blade Design Section, along with the pendulum and tower information, were used in the F762BR analysis to calculate blade and component loads for use in the overall design described in the System Design Section. The computer output has been modified for graphical display so that all important parameters are presented graphically in time history format. The conditions which were selected for calculating loads are presented in Table 28. These were selected to give a broad range of operating conditions; the low speed normal operating conditions which give the loads for the major portion of the system's life, as well as those which were expected to produce high stresses which would not occur with high frequency, but would certainly have to be survived for a finite number of occurances during the life of the system. The extreme gusts shown in Table 28 are not likely to occur in actual practice; however, they were used for conservatism and to demonstrate the load capability of the low stiffness rotor used in this system.

TABLE 27

DYNAMIC MATRICES USED TO SIMULATE FLEXIBLE TOWER WITH FREE YAW BEARING

Inertia Matrix

$$M = 10^3 \begin{bmatrix} 175.13 & & & & & & \text{kg} \\ & 1.0247 & 1.4971 & & & & \text{kg} \\ & 1.4971 & 2.9052 & & & & \text{kg-m} \\ & & & 225.97 & & & \text{kg-m} \\ & & & & 175.13 & & \text{kg} \\ & & & & & 112.99 & \text{kg-m} \\ & & \text{m} & \text{m} & & \text{m} & \end{bmatrix}$$

Stiffness Matrix

$$K = 10^6 \begin{bmatrix} 175.13 & & & & & & \text{N} \\ & 1.751 & 2.669 & & & & \text{N} \\ & 2.669 & 4.0675 & & & & \text{N-m} \\ & & & 1581.8 & & & \text{N-m} \\ & & & & 175.13 & & \text{N} \\ & & & & & 790.89 & \text{N-m} \\ /\text{m} & /\text{m} & /\text{rad} & /\text{rad} & /\text{m} & /\text{rad} & \end{bmatrix}$$

The F762BR program was run with wind shear effects using the standard shear distribution described earlier. Blades were simulated with two flatwise bending modes, one edgewise mode and one torsion mode, which included the pendulum, and the blade was segmented aerodynamically into 15 sections. The yaw and tower dynamics were incorporated by means of the inertia and stiffness matrices presented in Table 27. For the cases presented it was assumed that the gearbox/generator system was of infinite impedance and fixed rpm. It is recognized that the drive system torsional characteristics would be effected to some degree by the stiffness, inertia, and damping of the load, however these parameters were not simulated in F762BR during its use for this study. Earlier model tests, under this contract and those reported in Ref. 1, did not reveal unstable or lowly damped responses in the drive system torsional modes, although this cannot be conclusive since perfect scaling of the 31-ft system was not achieved. It is believed that only through properly scaled model testing or through full-scale field testing will the drive system torsional characteristics be accurately quantified.

TABLE 28

ROTOR LOAD CONDITIONS STUDIED

WIND CONDITION	VELOCITY
Steady	V_W = 9, 18, 36, 54, 74 m/s (= 20, 40, 80, 120, 165 mph)
Axial gust	V_W = 9 + 27 = 36 m/s (= 20 + 60 = 80 mph) (severe gust) V_W = 9 + 45 = 54 m/s (= 20 + 100 = 120 mph) (extreme gust)
Lateral gust	V_W = 9 m/s (20 mph) wind direction = + 40 deg @ t = 0 wind direction = - 40 deg @ t = 0

The detailed time histories of the conditions listed in Table 28 are presented in Appendix B. The parameters which are displayed in these figures are defined in Table 29. All individual blade values are for blade number 1 which is positioned downward at time = 0.

TABLE 29

NOMENCLATURE FOR APPENDIX B

Wind Speed:	The undisturbed wind speed measured at the rotor center. Variations over the disk are used according to the wind shear profile.
Theta X:	The yaw position of the rotor axis relative to the undisturbed wind direction, positive clockwise viewed from above. Degrees
Delta Z:	The deflection of the tower along the rotor axis non-dimensionalized by the rotor radius, positive downstream.
Torque:	Percent of rotor torque relative to torque at time = 0.
MX5:	The blade pitching moment of the attachment point to the flexbeam, positive leading edge downstream, ft-lb.
QT1:	Deflection of the first torsion mode which is essentially the elastic twist of the flexbeam, positive leading edge downstream, deg.
Flatwise Stress:	Stress on graphite/epoxy flexbeam at 5.1%R (Station 1) and on fiberglass blade at 23%R (Station 2), positive when blade deflects downstream, psi.
Edgewise Stress:	Same locations as flatwise stress, positive in direction of rotation.
Blade Tip Deflection:	Tip deflection relative to undeformed blade, positive downstream, in.
Beta pendulum:	Pendulum angle relative to plane of rotation, positive downstream, deg.

A summary of the pertinent steady and vibratory blade stresses obtained from the Appendix B time histories is presented in Figs. 49-51. The predicted

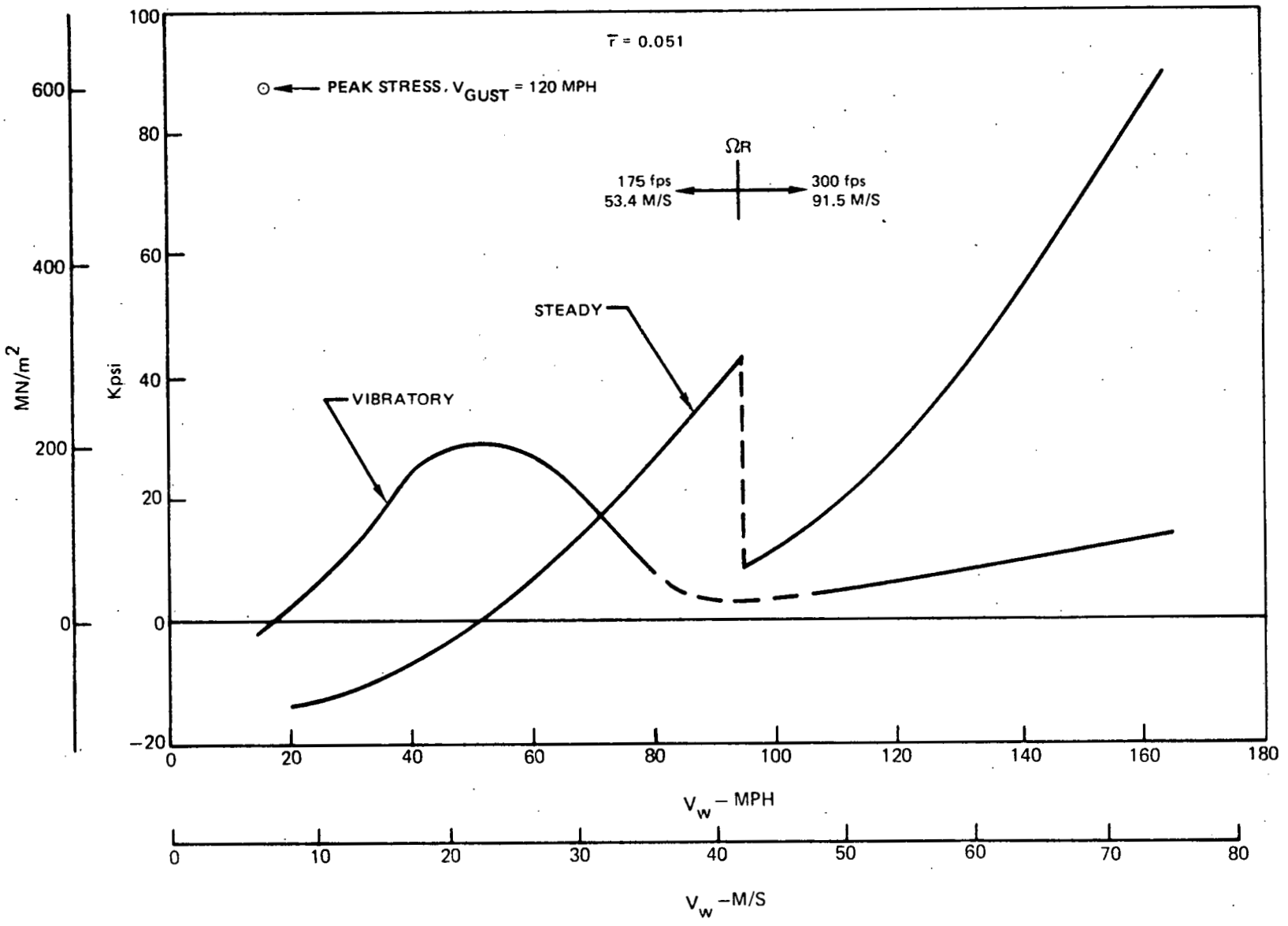

Fig. 49 Flexbeam Flatwise Stress Characteristics

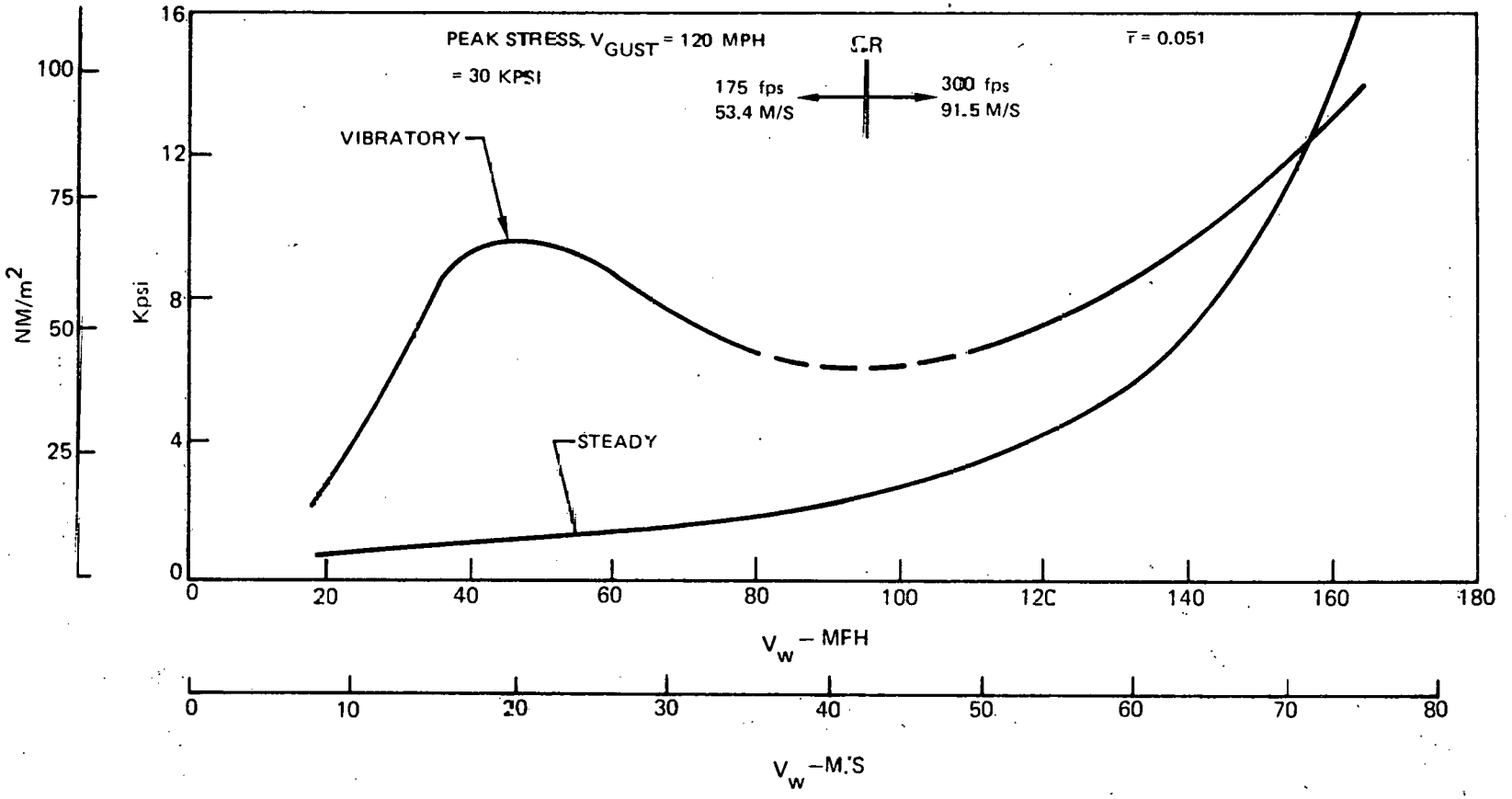

Fig. 50 Flexbeam Edgewise Stress Characteristics

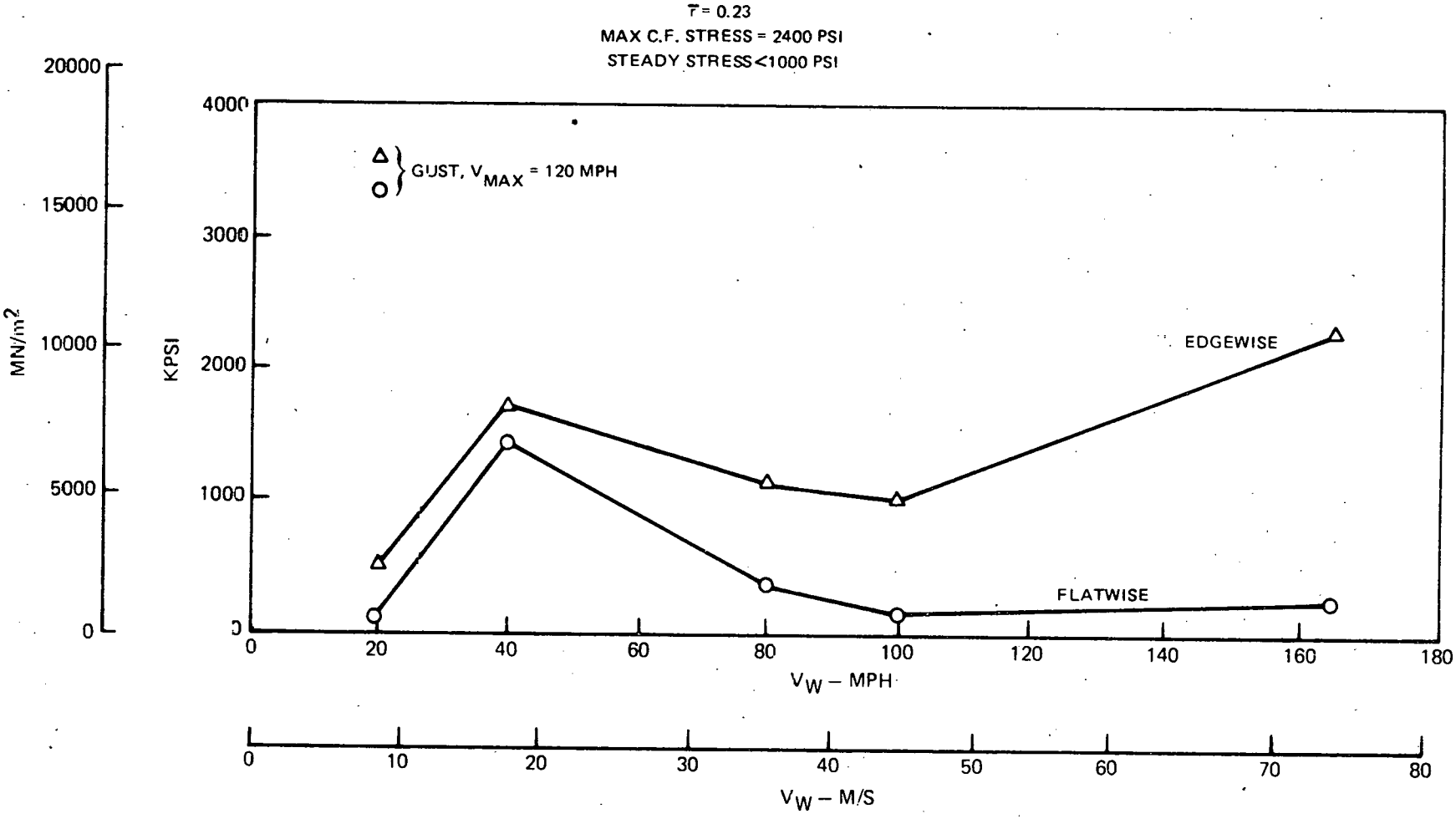

Fig. 51 Fiberglass Blade Stress Characteristics

increase in vibratory stresses at 17.9 m/s (40 mph) is caused by the onset of blade stall where sections of the blade are experiencing aerodynamic angles of attack above and below the stall angle in a periodic manner. The blades tend to momentarily exhibit negative damping which amplifies the response as shown in the figures at 17.9 m/s. Above this speed, where deeper and eventually full stall is experienced, the unsteady behavior is not present. The predicted change in the steady flatwise stress at approximately 45 m/s (100 mph) is a result of the change in tip speed from the design value of 53.3 m/s to the fully stalled unloaded condition of 91.5 m/s. This transition will actually be gradual; however, for the loads study it was assumed to occur at 45 m/s. The reduction in steady flatwise stress at this speed is caused by the increase in centrifugal bending moment, offsetting the aerodynamic moment.

The two-per-rev (2P) vibratory torque moments are shown on Fig. 52 where, as with the blade stresses, the large increase in load is shown at 18 m/s. It should be noted again, however, that the load which the rotor acts against is assumed to have infinite impedance and constant rpm. The peak 2P vibratory torque of 2700 N.m occurred with a sharp-edged gust of 54 m/s (120 mph), but would be expected to be attenuated before reaching this level with finite values of the load stiffness and inertia. The rotor thrust variation with wind speed is shown in Fig. 53. This curve was calculated assuming steady wind conditions at each speed. Gusts would naturally alter the thrust levels shown; however, it was assumed that under no gust condition would the thrust exceed that which is produced at the fully stalled, 74 m/s (165 mph) condition (T = 23140 N).

Also shown on Fig. 53 is the total tower drag which was calculated assuming a drag coefficient of 0.3, which represents the value for a circular cylinder above the critical Reynold's number of 300,000. The Reynold's number of the tower cross section exceeds this level at wind speeds above 13.4 m/s (30 mph).

The wind conditions which produced the maximum loads at the blade/flexbeam joint (Fig. 39) was the gust of 54 m/s from a steady wind of 9 m/s. A summary of these loads are given in Table 30. For conservatism, the centrifugal force shown is that produced in the maximum overspeed condition of 130 m/s tip speed.

TABLE 30

MAXIMUM LOADS AT BLADE JOINT FOR 54 M/S GUST CONDITION

Centrifugal Force	54070 N
Flatwise Moment	586 N.m
Edgewise Moment	4610 N.m
Torsion Moment	209 N.m

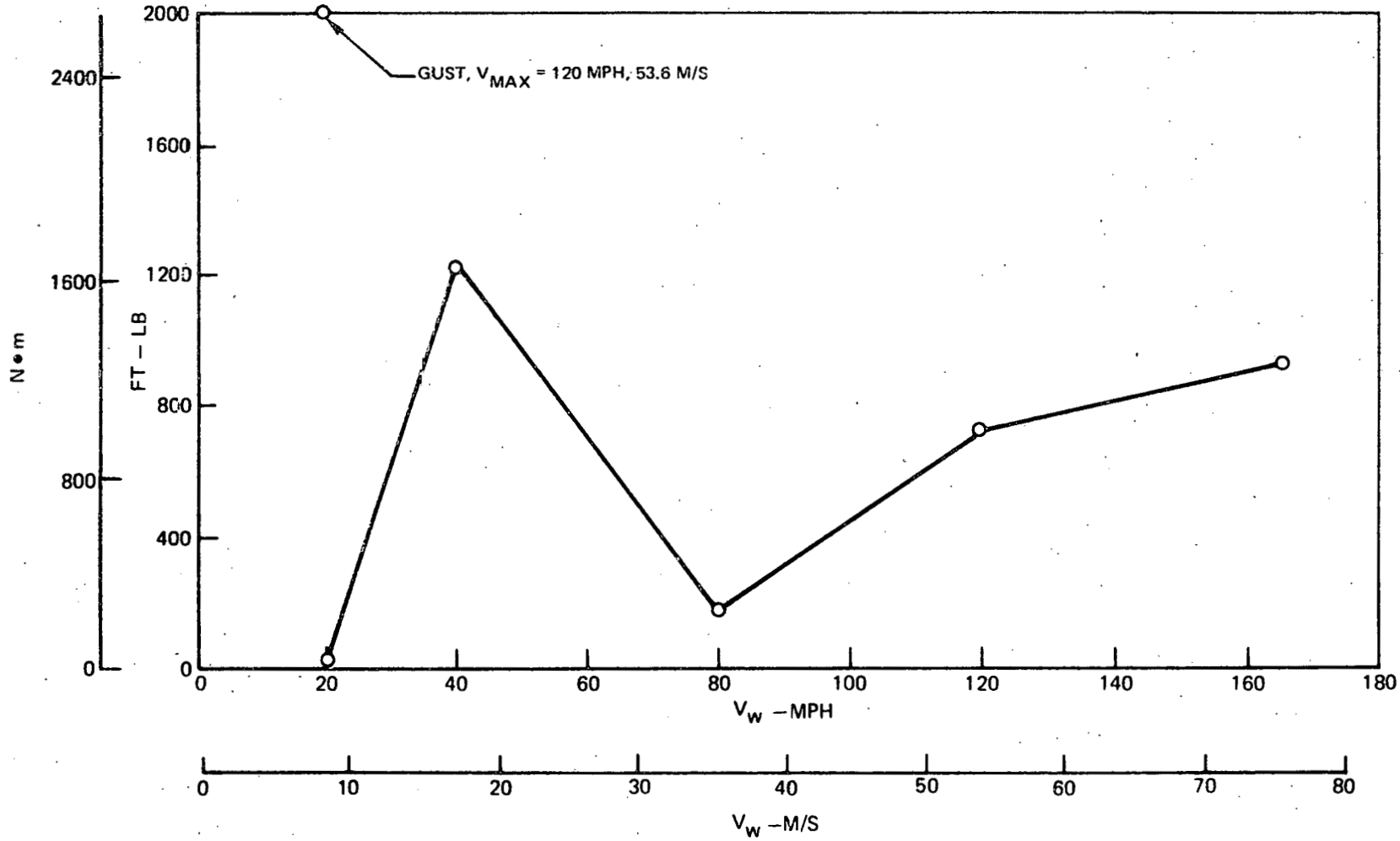

Fig. 52 Two-Per-Rev Vibratory Torque vs Speed

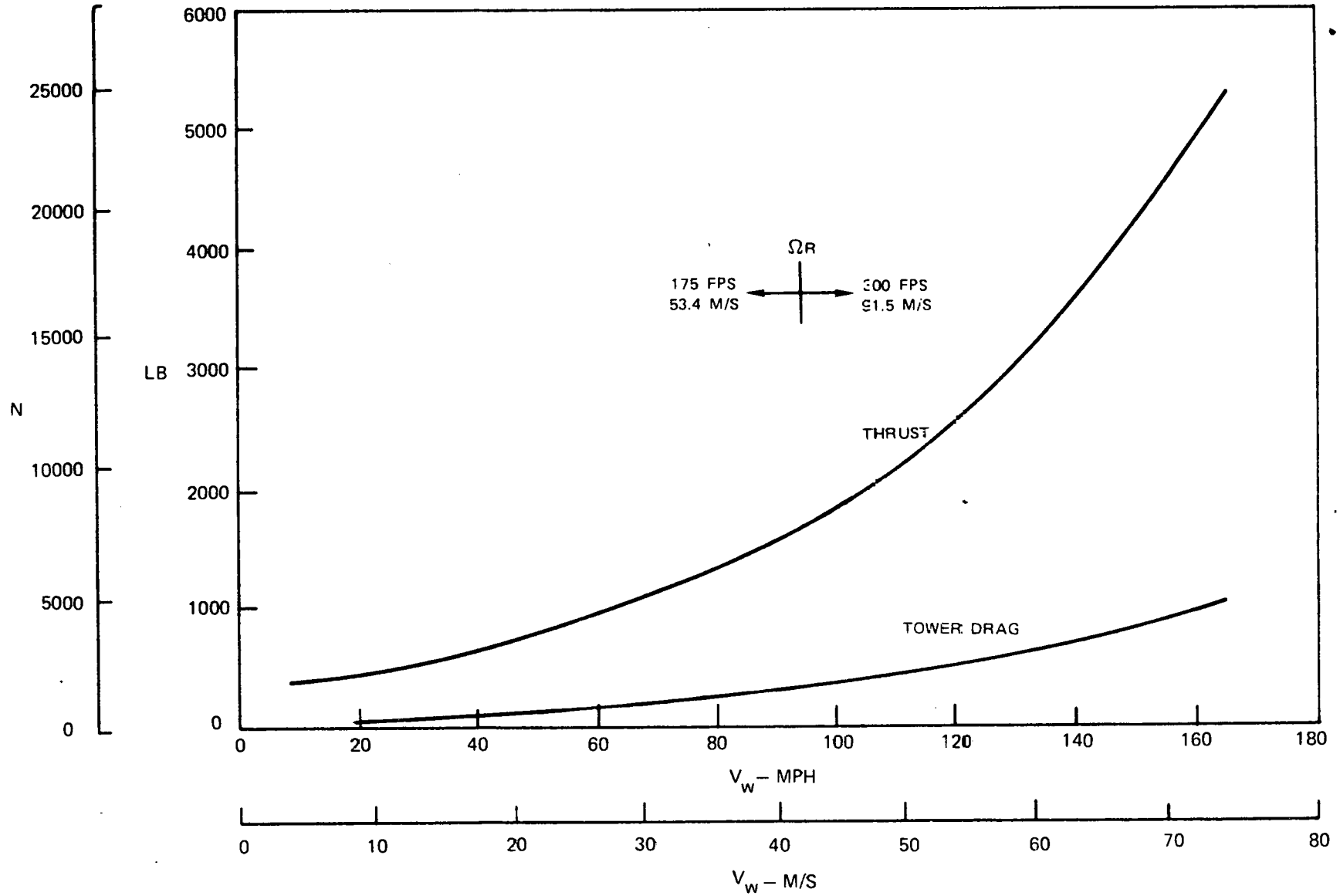

Fig. 53 Rotor Thrust and Tower Drag vs Wind Speed

These loads were used in the joint design discussed in the System Design Section and were used in determining the stresses and safety factors in Table 19.

Nacelle Loads

A relatively conservative approach was taken to determine the maximum loads to which the nacelle components would be designed. The hub loads which are calculated in the F762BR analyses, used for the blade stresses, showed relatively modest levels, except for thrust and torque, for the conditions examined. These conditions included severe gust conditions but did not indicate high nacelle loads. The maximum pitching moment, for example, was calculated to be only 790 N.m. This is a result of the types of gusts which could be applied in the analysis, and the fact that the nacelle is free in yaw. The gust conditions studied were streamwise gusts and lateral gusts. Streamwise gusts act along the rotor axis and do not exceed the maximum steady load shown at 74 m/s on Fig. 53. The lateral gusts produce moments tending to yaw the system, and since the yaw bearing eliminates these moments, the system experiences very low moments. Instead, it was assumed that a gust could be produced in a positive direction over the right half of the disk and in a negative direction over the left half. This type of loading would result in a pitching moment on the rotor which would be fed directly into the supporting structure. Another condition which could load the system in this manner is a case where the yaw shaft became locked and the rotor experienced a lateral gust. The condition selected to produce the maximum load was a combined positive-negative gust sufficient to deflect the rotor tip path plane to the extent that the blade tips just intersected a guy wire. It was believed such a condition could conceivably be reached and that the structure should support the resulting loads and moments with adequate safety factors. The tip path plane deflection to cause contact with the guy wire is approximately 11°. To produce this deflection would require a gust of 13.4 m/s acting in opposite directions on either side of the rotor disc, in a circular, or tornado-like fashion. This produces a maximum of 4180 N.m in the rotor shaft which must be reacted by the nacelle structure. Accompanying this moment is a vertical shear force which is caused by the tilting of the thrust vector in the same direction as the tip path plane tilt. For the maximum thrust condition of 23140 N at 74 m/s, the vertical force amounts to 4400 N and added to the rotor gravity loads comes to 5800 N. These loads, coupled with the maximum 2P vibratory torque were used to size the structural components. It was decided to design for a safety factor greater than 2.0 for all wind conditions up to 54 m/s, and for a safety factor greater than 1.0 for speeds above 54 m/s, including the maximum unsymmetrical gust condition producing the 4180 N.m pitching moment. A summary of the loading conditions for the high wind conditions of 54 m/s and 74 m/s and the design speed of 9 m/s is presented in Table 31.

TABLE 31

DESIGN LOADS AT HUB

Wind Velocity, V	74 m/s (165 mph)	54 m/s (120 mph)	9 m/s (20 mph)
Thrust, N	23140	14240	2050
Vertical force, N	5800	4130	1800
Pitching moment, N.m	4180	4180	4180
Shaft torque, N.m	2710	2710	1240

These loads were used in the calculation of the component safety factors presented earlier in Tables 20 and 21.

Tower Loads

The tower loads arise principally from the vertical compression loads produced by the pretension in the guy wires. The guy wire diameter selection is based on two criteria. The first is that the maximum load produced by the rotor and the tower aerodynamic drag should not exceed the wire strength, assuming a single wire reacts the load. The second is that the frequencies of the tower bending modes should be placed so as not to coalesce with critical rotor frequencies. For a given guy wire configuration the primary factor influencing tower frequency is wire diameter, and this subject is treated in the following section. The initial wire diameters selected for the prototype wind turbine are 25.4 mm for the upper guys and 19 mm for the lower guys. The pretension is selected so that during normal operation one or more wires do not go slack, creating a situation for shock loading due to "snapping". It is also advisable to avoid sudden losses in tower stiffness creating potential problems related to tower frequency changes. On the other hand, excessive pretension is undesirable from the standpoint of possible wire failure or tower buckling and the requirement for large costly ground anchors. A pretension of 44,500 N (10,000 lb) was selected for the upper guy wires and 22,250 N (5000 lb) for the lower guys. With the nacelle weight and rotor loads included, this results in a compressive load of approximately 146,850 N (33,000 lb) in the upper column and 218,050 N (49,000 lb) in the lower column. The critical buckling load for the lower column, using the buckling load formula, $P_{ER} = \pi^2 EI/L^2$, is calculated to be 1.424×10^6 N (320,000 lb). This is based on a steel tower with a diameter of 273 mm (10.75 in.) and a wall thickness of 6.4 mm (0.25 in.). This results in a safety factor, from buckling considerations, of 6.5. If a failure occurred in a lower guy wire the critical buckling load drops to 356,890 N (80,200 lb), however, the safety factor is still greater than 1.0.

The maximum wire tension is experienced at 74 m/s where a rotor thrust of 23140 N (5200 lb) must be resisted. This produces a tension in the cable of 120,150 N (27,000 lb) which, when added to the pretension, results in a maximum load of 164,650 N (37,000 lb). The allowable load for 25.4-mm cable is 356,000 N, which yields a safety factor of 2.2. At the design condition the cable tension is 57850 N, yielding a safety factor of 6.2.

Loads Due to Ice Encrustation

Ice encrustation can potentially cause damaging loads in two ways: First, with sufficient build-up, the added blade weight could potentially cause ultimate static bending loads in a shutdown (nonrotating) mode of operation. Second, if sufficient ice adhered to the blade in a rotating mode of operation the blade frequencies could be so modified as to precipitate an unstable condition. The results of analyzing the blade design for these two potential failure modes are given in the following paragraphs.

Static Blade Root Stresses Due to Ice Build-up

A Myklestad bending analysis was made of the blade situated in three static azimuthal positions: pointing straight down from the hub ($\psi = 0$), pointing horizontally ($\psi = 90°$) and straight up ($\psi = 180°$). Due to a precone angle of 8°, flatwise bending stresses are developed at the 0° and 180° azimuthal positions. Table 32 presents static stress results typical of the selected blade design for zero and two thicknesses of ice encrustation up to a maximum uniform thickness of 63.5 mm, and at each of the three selected blade positions. The results show the horizontal position to produce the greatest root stresses, but which are still quite below the assumed ultimate stress for the graphite/epoxy flexbeam material of 1034 MPa.

Effects of Icing Conditions on Blade Natural Frequencies

Because of the inherently smooth skin of both the flexbeam and the aerodynamic portion of the blade (outboard of the juncture) it was assumed that the rotor would easily shed any ice encrustation over these portions when it was rotating. The potential does exist, however, for ice to accumulate and remain locked to the juncture portion of the blade even when the rotor is turning. As such, an ice accumulation at that point would consist, dynamically, of a concentrated mass. Accordingly, the effects of icing on blade natural frequencies was calculated by adding a concentrated mass corresponding to a sphere representing 63.5 mm ice build-up at the juncture. Figure 54 shows typical results of this concentrated mass on the blade natural frequency characteristics. The most important blade frequency change would be a lowering of the

TABLE 32

STATIC BLADE ROOT STRESSES DUE TO ICE BUILD-UP

	FLATWISE, MPa		EDGEWISE, MPa
	$\psi = 0$	$\psi = 180$	$\psi = 90$
ICE FREE	31.3	31.9	19.2
31.8 mm BUILD-UP	90.9	93.5	77.9
63.5 mm BUILD-UP	130.2	132	143.7

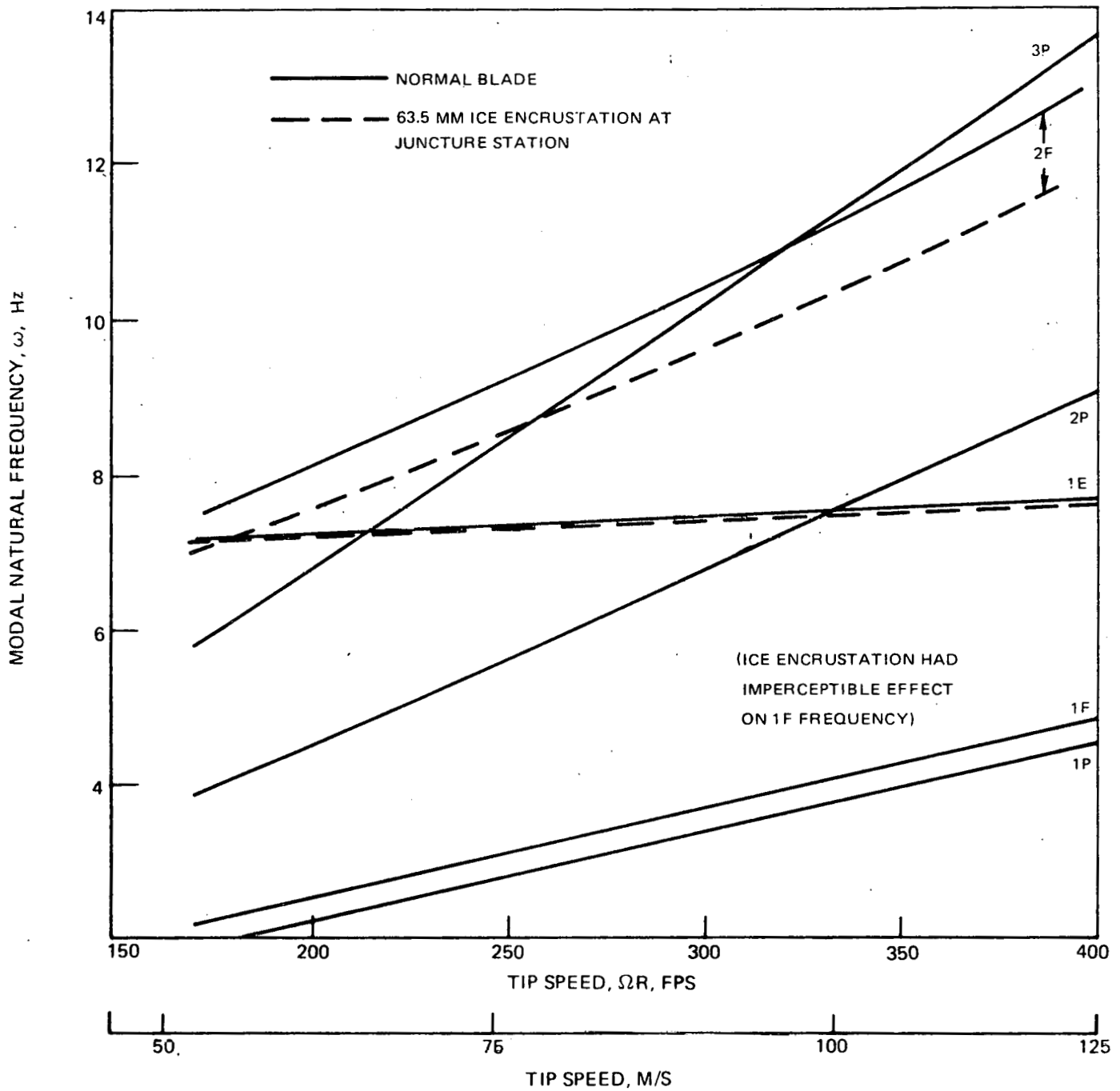

Fig. 54 Effects of Icing Conditions on Blade Natural Frequencies

78-11-17-11

first edgewise frequency close to the one per rev (1P) line within the operational rotor speed range. The figure clearly shows, however, that the effect of icing on this frequency is negligible. Although the second flatwise frequency (2F) did drop to intercept the 3P line at a lower rotor speed, this is not expected to cause any adverse effect as the 3P excitation is negligible and the mode is, moreover, well damped.

Study of Tower Dynamics

Two aspects of the tower-nacelle dynamics were considered in this study. First, as was described above, a set of dynamic matrices for input to the F762BR program had to be calculated to simulate the inherent zero frequency yaw mode accruing from the free yaw bearing. Second, the tower-rotor-nacelle had to be analyzed as an elastic system to insure the avoidance of any 2P resonances within all modes of operation.

The first calculation was a relatively simple mathematical chore involving rigid body inertias and geometry of the nacelle wherein the assumption is made that the design is free of any 2P resonances. The adopted method for including finite impedance characteristics of the rotor hub in the F762BR program is to input inertia, damping, and stiffness matrices for a "movable hub".

The second set of calculations, those required to determine elastic system resonances, were performed using NASTRAN. Using Figure 44 as a guide, the finite element break-up was selected as follows: The pipe was divided into ten equal segment lengths using 11 grid points. Three additional grid points were used for the guy wire attachment points at the ground. Three additional points were used to define the nacelle; one point was taken as the hub (rotor mass) point, one point coincident with the pipe upper terminal grid point, and one, the upstream end of the nacelle. Thus, in all, 17 grid points were used for the finite element break-up of the combined elastic system. Elastic bar elements were used to model the pipe sections of the tower and the guy cables, and a rigid bar element, multi-point constrained at the yaw bearing point, for the nacelle. The nominal design had a combined nacelle and rotor weight of 822 kg, a steel inner pipe (273-mm o.d., 6.4-mm wall thickness), upper guy wires of 25.4-mm-diam 6 x 19 (fiber core) wire rope, and lower guy wires of 19-mm-diam (similar) wire rope.

The frequency characteristics of the pertinent modes for the nominal design as well as design alternates are shown in Table 33. For mode III operation, the rotor speed can vary from a nominal design value of 1.80 Hz (107.8 rpm) to a maximum of 4.36 Hz (261.8 rpm) which corresponds to a 2P excitation frequency range of 3.59 Hz to 8.73 Hz. As the table shows, the

TABLE 33

RESULTS OF NASTRAN CALCULATION FOR VARIOUS TOWER-NACELLE-ROTOR CONFIGURATIONS

Design	Description	Frequencies (Hz) Long./Lateral Cantilever	Long./Lateral Pipe Bending
I.	Nominal	1.43/1.51	4.84/5.10
II.a	25 mm diam solid rod, lower guying	1.52/1.61	8.91/11.37
II.b	38 mm diam solid rod, lower guying	1.46/1.54	9.08/11.30
II.c	25 mm diam solid rod, lower & outer guying	3.02/3.18	8.85/11.29
III.	19 mm diam wire rope, lower guying, 0.46 m diam fiberglass pipe	1.43/1.51	7.12/8.30
IV.	25 mm diam solid rod lower guying, 0.46 m diam fiberglass pipe	1.49/1.58	10.19/14.11

nominal design has a fundamental or cantilever type mode with a frequency of approximately 1.5 Hz and second pipe bending type mode at approximately 5.0 Hz. The first mode is capable of 2P resonant excitation during run-up to the nominal condition, and the second is capable of excitation at a rotor speed of approximately 150 rpm, well within the operational rotor speed range. The basic result of these NASTRAN calculations is that the nominal design is too soft. Much of this softness is attributable to the inherent softness of the lower 19-mm-diam wire rope guying.

In an attempt to achieve a satisfactory design for the tower without requiring major changes, two basic parametric variations were made; First, the lower and upper guy ropes were changed to solid (steel) rods of varying diameters. Second, the use of pultruded fiberglass was considered for the center pipe sections in place of the heavier steel piping. The results of these parametric variations are also given in Table 33.

The first significant result of the parametric variation is that the first cantilever mode frequency is controlled by the stiffness of the upper guying, but cannot easily be raised above the 2P excitation frequency range with simple design changes. That the tower will pass through a 2P excitation point during run-up is not considered a critical dynamic characteristic, however. In fact, the lower cantilever mode frequency resulting from the wire rope guying is to be preferred as the 2P excitation point will then occur at a lower rotor speed, and hence lower rotational energy level. Furthermore, it is expected that the rotor will not loiter at the lower 2P excitation rotor speed during run-up.

The second significant result of the parametric variation is that the next higher critical mode (pipe bending) can be controlled to values above the maximum assumed 2P excitation frequency by combinations of solid rod lower guying and either the nominal steel, or a fiberglass pipe inner portion of the tower. The use of fiberglass is seen to offer the most margin and would be the preferred design.

The nominal design shall be examined for frequencies, mode shapes, and damping during full scale testing. If it is found that potentially undesirable frequency crossovers exist, then modifications such as those discussed above will be made. It is felt that modifications relative to the guy supports can be made quickly and at low cost, and that this type of development effort is most cost effectively performed with full-scale hardware.

WTG SYSTEM SAFETY ANALYSIS AND FAILURE MODE AND EFFECTS ANALYSIS

The Hamilton Standard Division of United Technologies has conducted both a System Safety Analysis and a Failure Mode and Effects Analysis (FMEA) of the Phase I design. The results are presented in this section of the report.

The 8 kW WTG has been designed to operate safely and with a minimum of maintenance over a long time period. Failures which could result in severe injury or major system damage have been minimized by a design which provides high margins of safety in the materials and/or processes to be employed in the construction of the WTG.

System Safety Analysis

Hazard Classification Analysis

a. Have you reviewed the FMEA for this item to determine that no single failure will result in a Class I hazard and to determine what Class II hazards exist? Yes X No _____

b. Were any Class I hazards found? Yes X No _____

c. If yes, list the part name associated with the hazard and define the nature of the hazard.

Numerous - see Failure Mode and Effects Analysis

d. What steps were taken to eliminate the hazard or reduce its classification?

Designed for high margins of safety.

e. Were any Class II hazards found? Yes _____ No X

f. If yes, list the part name associated with the hazard and define the nature of the hazard.

g. What steps were taken to eliminate the hazard or reduce its classification?

Maintenance and Overhaul Hazard Analysis

a. Have you reviewed the drawings for this part in the light of the anticipated maintenance and overhaul requirements and methods to determine if any maintenance or overhaul hazards exist? Yes X No _____

b. Were any significant maintenance or overhaul hazards found?
Yes X No _____

c. If yes, list the part name associated with the hazard and define the nature of the hazard.

Maintenance, such as annual inspection of the wind turbine generator hardware for wear, damage, and integrity as well as bearing lubrication requires that the entire assembly be lowered to the ground. Should any worn or damaged part fail during this process, serious injury could result.

d. What steps were taken to eliminate the hazard or reduce the probability of its occurrence?

The lowering/erection associated hardware is designed with high margins of safety to reduce the probability of failure occurrence.

Noxious Materials Hazard Analysis

a. Have you reviewed the drawings for this item to determine if the design contains any materials that have noxious effects or can decompose into materials that have noxious effects? Yes X No _____

b. Were any such materials found? Yes _____ No X

c. If yes, list the part name, the material, and its effect.

d. What steps were taken to eliminate these materials or reduce the probability of noxious effects?

Protective Function Analysis

a. Does this item have any protective functions? Yes _____ No X

b. If yes, are they "fail safe" or checked during some phase of the normal system operating cycle? Yes _____ No _____

c. If no to "b", would a failure of such a function result in a hazardous condition if another failure occurred? Yes _____ No _____

d. If yes to "c", list the part name having the protective function and define the nature of the hazard.

e. What steps were taken to eliminate the hazard or reduce the probability of its occurrence?

Human Reactions Analysis

a. Have you reviewed the FMEA for this item to determine if the hazard caused by any failure would be aggravated by normal human reactions to the indication of same? Yes X No _____

b. Were any such situations uncovered? Yes _____ No X

c. If yes, list the part name associated with the hazard and describe the situation.

d. What steps were taken to eliminate the situation or reduce the probability of its occurrence?

Recommended Procedures or Precautions

Give any recommended procedures or precautions that the user of the system should follow with regard to each of these hazards if they have not been eliminated by the actions taken above.

Hazard/warning notices will be highlighted in owner/maintenance manuals.

Failure Mode and Effect Analysis

Introduction

The opinions contained in this FMEA represent best estimates based upon information presently known to Hamilton Standard, and the current development of the proposed equipment. Hamilton Standard reserves the right to revise such estimates as additional information becomes available. This report shall not be construed as a warranty or guarantee of the equipment described, nor constitute the basis of liability to Hamilton Standard either in contract or otherwise.

Fundamentals of the Analysis

Certain fundamental criteria and definitions have been established and consistently applied in the preparation of this FMEA. They are as follows:

1. Hazard severity

Hazard severity categories are defined to provide a qualitative measure of the worst potential consequences resulting from personnel error, environmental conditions, design inadequacies, procedural deficiencies, system, subsystem, or component failure or malfunction as follows:

a. Category I - Catastrophic. May cause death or system loss.

b. Category II - Critical. May cause severe injury, severe occupational illness, or major system damage.

c. Category III - Marginal. May cause minor injury, minor occupational illness, or minor system damage.

d. Category IV - Negligible. Will not result in injury, occupational illness, or system damage.

2. Hazard probability

The probability that a hazard will occur during the planned life expectancy of the system is described in potential occurrences for each item. Assigning a quantitative hazard probability to a potential design or procedural hazard is generally not possible early in the design process. The qualitative hazard probability ranking is defined in Table 34.

3. Only single failure cases will be considered in the analysis.

TABLE 34

HAZARD PROBABILITY

Descriptive Word	Level *	Specific Individual Item
Frequent	A	Likely to occur frequently
Reasonably Probable	B	Will occur several times in life of an item
Occasional	C	Likely to occur sometime in life of an item
Remote	D	So unlikely, it can be assumed that this hazard will not be experienced
Extremely Improbable	E	Probability of occurrence cannot be distinguished from zero
Impossible	F	Physically impossible to occur

*Note: The assigned probability of hazard occurrence (as designated by alphabetic level) will be listed adjacent to the Hazard Severity Category in the FMEA.

TABLE 35

FAILURE MODE & EFFECT ANALYSIS

SYSTEM: 8 kw WIND TURBINE GENERATOR

COMPONENT: ROTOR ASSEMBLY

VENDOR:

ENGINE MODEL:

LAYOUT OR DWG. NO:

PREPARED BY: P.W. Ingle

DATE REVISION: 9/27/78

APPROVAL:

ITEM NO. AND COMPONENT OR PART DESCRIPTION & FUNCTION (a)	ASSUMED FAILURE MODE (b)	PROBABLE FAILURE CAUSE (c)	FAILURE EFFECT AND CONSEQUENCE ON SUBSYSTEM AND SYSTEM (d)	DESIGN PHILOSOPHY OR INHERENT COMPENSATING PROVISIONS (e)	DESIGN CRITERIA OR DESIGN MARGINS (f)	METHOD OF DETECTION (g)	HAZARD CATEGORY	REMARKS (i)
ROTOR ASSEMBLY Blade Assembly								
Blade Shell: The blades are formed from unidirectional layers of fiberglass cloth bonded with epoxy resin. The layers of cloth are initially laid over a male die which is configured to form the inside shape of the blade. The laid-up cloth is then impregnated with epoxy resin and the inner die with the impregnated cloth is drawn through a heated female die configured to the outside airfoil shape of the blade. The end result is a blade of constant cross-section over the entire length, which has controlled thickness and integral stiffeners.	1. Shell fractures across its width.	Inherent defect in shell structure or damage by foreign object.	Loss of blade with resulting rotor unbalance. Resulting unbalance loads will cause opposite blade to break free as well.	Three way layup of glass cloth in the laminated shell provides a redundant type of structure which will resist fracture and/or propagation thereof. Also, integral fiberglass stiffening members will aid in fracture resistance and/or propagation.	Designed for safety factors as shown based on stress analyses Design Cond. S.F. V = 20 mph >5 High Speed V = 120 mph >5 V = 165 mph >2	Visual	ID	Extensive blade fatigue tests and basic foreign object damage (FOD) development tests will be conducted to show that blade fracture from fatigue or FOD has an extremely low probability.
	2. Radial delamination of shell.	Inherent defect in shell lamination. e.g., Poor impregnation of epoxy resin into cloth layers.	Same as above.	Same as above.	Same as above.	Visual	ID	a. Depending on degree of delamination, the blade may hold together until annual inspection at which time appropriate corrective action can be taken. b. Manufacturing processes and inspection techniques will be employed to reduce this type of malfunction to an extremely low probability.
Blade Yoke:	Fractures	Fatigue	Same as above.	Prime structure, designed to not fail.	Same as above.	Visual	ID	

TABLE 35 (Continued)
FAILURE MODE & EFFECT ANALYSIS

SYSTEM 8 kw WIND TURBINE GENERATOR
PREPARED BY P.W. Ingle
COMPONENT ROTOR ASSEMBLY
ENGINE MODEL
DATE/REVISION 9/27/78
VENDOR
LAYOUT OR DWG NO
APPROVAL
SHEET 2 OF 6

ITEM NO. AND COMPONENT OR PART DESCRIPTION & FUNCTION (a)	ASSUMED FAILURE MODE (b)	PROBABLE FAILURE CAUSE (c)	FAILURE EFFECT AND CONSEQUENCE ON SUBSYSTEM AND SYSTEM (d)	DESIGN PHILOSOPHY OR INHERENT COMPENSATING PROVISIONS (e)	DESIGN CRITERIA OR DESIGN MARGINS (f)	METHOD OF DETECTION (g)	CRITICALITY (h)	REMARKS (i)
Hub Assembly								
Hub Flange:	Fracture	Fatigue or corrosion	Loss of rotor.		Same as for blade assembly.	Visual	ID	
Ring Feder Coupling:	Slips or fails.	Insufficient torque on attach bolts.	Loss of rotor.	Proven-off the shelf equipment.	Same as for blade assembly.	Visual	IC	Specified torque values for fasteners must be strictly adhered to by installer/owner.
Rub Strip (s): (Nylon)	Worn	Relative motion of parts due to improper torque or loss of torque.	Flexbeam becomes loose between front and rear hub plates and works against retaining bolts.	Bolt torque requirements for clamping are specified at assembly.		Visual	IIIC	

TABLE 35 (Continued)

FAILURE MODE & EFFECT ANALYSIS

SYSTEM: 8 kw WIND TURBINE GENERATOR | PREPARED BY: P. W. Ingle

COMPONENT: ROTOR ASSEMBLY | ENGINE MODEL: | DATE REVISION: 9/27/78

VENDOR: | LAYOUT OR DWG. NO: UTRC/1740-4 | APPROVAL:

SHEET 3 OF 6

ITEM NO. AND COMPONENT OR PART DESCRIPTION & FUNCTION (a)	ASSUMED FAILURE MODE (b)	PROBABLE FAILURE CAUSE (c)	FAILURE EFFECT AND CONSEQUENCE ON SUBSYSTEM AND SYSTEM (d)	DESIGN PHILOSOPHY OR INHERENT COMPENSATING PROVISIONS (e)	DESIGN CRITERIA OR DESIGN MARGINS (f)	METHOD OF DETECTION (g)	HAZARD CATEGORY	REMARKS (i)
ROTOR ASSEMBLY (CONT)					Designed for safety factors as shown based on stress analyses			
Flexbeam: The flexbeam is made up from unidirectional graphite/epoxy and is a simple rectangular cross section running from one blade through the hub out to the other blade. It is cured in a preconed configuration to minimize steady flatwise stresses.	1. Flexbeam fractures across its width.	Fatigue	Loss of blade with resulting rotor unbalance, and loss of opposite blade.	Material layup inherently precludes crack propegation.	Design Cond. S.F. V = 20 mph >5 High Speed V = 120 mph >3 V = 165 mph >1	Visual	ID	See appropriate remark for blade shell.
	2. Radial delamination of flexbeam.	Inherent defect in lamination.	Chafing of fibers will occur leading to fiber fracture and loss of blade with resulting rotor unbalance, and loss of opposite blade. Flexstrap will restrain blade from flying free. Rotational energy will dissipate.	Structural strength of the graphite fibers is sufficient to prevent loss of blade even if the epoxy binder should detericrate.	Same as above.	Visual	ID	See appropriate remark for blade shell.
Pitch Change Assy								
Pendulum Support Arm: (Steel bar stock)	Fractures	Fatigue	Blade pitch control will be lost to one or both blades. Blade(s) will go to preset non-rotating -16 degree blade angle.		Same as above.	Visual	IIID	
Pendulum Arm: (Steel)	Fractures	Fatigue	Same as above except that only one blade will go to the preset angle.		Same as above.	Visual	IIIC	
Pendulum Weights: (Steel)	Fly-off	Loss of retention nut.	Same as for pendulum arm.		Same as above.	Visual	IIIC	
Flexstrap: (Spring steel)	Fractures	Fatigue	Same as for pendulum arm.		Same as above.	Visual	IIIC	

SYSTEM 6 kw WIND TURBINE GENERATOR

TABLE 35 (Continued)
FAILURE MODE & EFFECT ANALYSIS

PREPARED BY P. W. In

COMPONENT HEAD ASSEMBLY

ENGINE MODEL

DATE REVISION 9/27/78

VENDOR

LAYOUT OR DWG NO UTRC/1740-3

APPROVAL

SHEET 4 OF 6

ITEM NO. AND COMPONENT OR PART DESCRIPTION & FUNCTION (a)	ASSUMED FAILURE MODE (b)	PROBABLE FAILURE CAUSE (c)	FAILURE EFFECT AND CONSEQUENCE ON SUBSYSTEM AND SYSTEM (d)	DESIGN PHILOSOPHY OR INHERENT COMPENSATING PROVISIONS (e)	DESIGN CRITERIA OR DESIGN MARGINS (f)	METHOD OF DETECTION (g)	HAZARD CATEGORY	REMARKS (i)
HEAD ASSEMBLY					Designed for safety factors as shown based on stress analyses			
Generator Drive Assy					Design Cond. S.F. V = 20 mph >5 High Speed V = 120 mph >2 V = 165 mph >1			
Rotor Shaft: (Steel)	Shears	Fatigue	Rotor assembly may fly free. Blades may strike tower guy wires.			Visual	ID	
Rotor Bearings:	Disintegrate	Bearings seize initially due to fatigue or from lack of lubrication.	Loss of proper support for rotor shaft. Shaft will wobble loosely within bearing support tube, resulting in shearing of the rotor shaft/gearbox input drive coupling. Rotor shaft may eventually wear through and rotor assembly will fly free.		Same as above.	Visual	IC	
Bearing Support Tube: (Steel)	Does not provide support for rotor shaft bearings.	Failure of weld at either bearing end of tube.	Same as for rotor bearings above.	Low loads are imparted into the support tube because of the self-aligning rotor bearings.	Same as above.	Visual	ID	
Reduction Gearbox:	Disintegrates	Bearings seize initially due to fatigue or from lack of lubrication.	No power output.	Off the shelf, proven, parallel shaft, single step unit.		Visual	IVC	Shear coupling is provided in the load path from rotor shaft to gearbox.
Yaw Assembly								
Yaw Shaft: (Steel)	Fractures	Fatigue	Possible loss of head assembly.		Same as above.	Visual	ID	

TABLE 35 (Continued)
FAILURE MODE & EFFECT ANALYSIS

SYSTEM 8 kw WIND TURBINE GENERATOR
COMPONENT HEAD ASSEMBLY
VENDOR
ENGINE MODEL
LAYOUT OR DWG NO UTRC/1740-3
PREPARED BY P. W. Ingle
DATE REVISION 9/27/78
APPROVAL
SHEET 5 OF 6

ITEM NO AND COMPONENT OR PART DESCRIPTION & FUNCTION (a)	ASSUMED FAILURE MODE (b)	PROBABLE FAILURE CAUSE (c)	FAILURE EFFECT AND CONSEQUENCE ON SUBSYSTEM AND SYSTEM (d)	DESIGN PHILOSOPHY OR INHERENT COMPENSATING PROVISIONS (e)	DESIGN CRITERIA OR DESIGN MARGINS (f)	METHOD OF DETECTION (g)	HAZARD CATEGORY (h)	REMARKS (i)
HEAD ASSEMBLY (CONT)								
Yaw Bearings:	Disinte-grate.	Bearings seize initially due to fatigue or lack of lubrica-tion.	Loss of support for head assembly. Head assembly will grind around in top of tower. Head rotation will be slug-gish and rotor performance will decrease.		Same as for previous page.	Visual/ audible	IIIC	
Generator	Fails to operate.	Bearings seize initially due to fatigue or lack of lubrica-tion.	No power output.	Off the shelf proven hardware.		Visual	IVC	
	Short/open circuit.	Improper maintenance, inherent defect, or lightning strike.	Generator will burn out. No power output. Possible fire.	Grounding is provided to reduce damaging effect of electrical shorts or lightning strike.		Visual	IIIB	
Support Structure (Steel)	Weld joint fractures.	Fatigue, corrosion.	Major component such as generator may break loose and drop to the ground.	Prime structure, designed to low stress levels.		Visual	ID	
Nacelle Assembly (fiberglass)	Failure of attachment fastener(s) or of one or more panels of the nacelle assembly.	Improper maintenance.	Portion or all of the nacelle assembly may tear loose and blow away. Blades may be damaged in the process.	Design will be adequate for specified conditions with redundancy pro-vided by numerous fasteners.		Visual	IC	

TABLE 35 (Concluded)

FAILURE MODE & EFFECT ANALYSIS

SYSTEM: 8 kw WIND TUREINE GENERATOR

COMPONENT: TOWER ASSEMBLY

VENDOR:

ENGINE MODEL:

LAYOUT OR DWG NO: UTRC/1740-5

PREPARED BY: P. W. In

DATE REVISION: 9/27/78

APPROVAL:

SHEET 6 OF 6

ITEM NO. AND COMPONENT OR PART DESCRIPTION & FUNCTION (a)	ASSUMED FAILURE MODE (b)	PROBABLE FAILURE CAUSE (c)	FAILURE EFFECT AND CONSEQUENCE ON SUBSYSTEM AND SYSTEM (d)	DESIGN PHILOSOPHY OR INHERENT COMPENSATING PROVISIONS (e)	DESIGN CRITERIA OR DESIGN MARGINS (f)	METHOD OF DETECTION (g)	HAZARD CATEGORY	REMARKS (i)
TOWER ASSEMBLY								
Base Assembly								
Pivot Pin (AISI 1018 Steel)	Shears during tower erection or lowering.	Corrosion or fatigue.	Complete WTG assembly will fall to ground. Total loss of WTG.	Prime structure. Designed to low stress levels.		Visual	ID	
Pivot Bracket(s) (Hot Rolled Steel)	Weld joint fractures during tower erection or lowering.	Corrosion or fatigue.	Same as above.	Same as above.		Visual	ID	
Pipe Assembly					Designed for safety factors as shown based on stress analyses Design Cond. S.F. V = 20 mph >6 High Speed V = 120 mph >2 V = 165 mph >2			
Pipe Section (ASTM A-53 Steel Pipe)	Buckles during erection or while lowering.	Corrosion or fatigue.	Same as above.	Pipe sections have 0.5 x 10^6 lb buckling resistance.		Visual	ID	
Flange(s) (ASTM A-181 Steel)	Fracture at weld joint.	Improper weld or corrosion.	Same as above.	Prime structure. Designed to not fail.		Visual	ID	
Guy Wire Assembly								
Wire Rope (Improved Plow Steel)	Fractures	Fatigue or corrosion	Complete WTG assembly will fall to ground. Probably total loss.	Redundancy is provided by upper and lower wire ropes.	Same as above.	Visual	ID	
Tang (AISI E-4130 Steel)	Fractures	Fatigue or corrosion.	Same as above.	Redundancy is provided by upper & lower tangs.	Same as above.	Visual	ID	
Turnbuckle (Forged Steel)	Fractures	Fatigue or corrosion.	Same as above.	Off the shelf proven hardware.	Same as above.	Visual	ID	

PRODUCT WARRANTY

A warranty can be viewed as a mechanism for allocating the risks of product imperfection between purchasers and sellers. At the extremes, the seller could provide an unlimited, unconditional lifetime warranty, or the purchaser could buy the product in the absence of any stated or implied promise of quality or performance. There is a product price associated with each of these extremes and with any point within these limits. The primary questions related to any given product are: What is the risk of imperfection, and how should the risk be distributed between the buyer and the seller?

The answer, when dealing with existing products or reasonable facsimiles, is fairly straightforward. Usually, there is sufficient generic historical data to reasonably project product performance/durability over time versus acceptable norms for like products in like markets. In these instances, the cost associated with various levels of protection afforded to the consumer can be estimated and decisions made as to the market acceptance of various warranty policies. In the final analysis, the selection of a specific warranty policy will be determined to a great extent by competitive pressures.

In the "new-product, new-market" arena, wherein small wind turbines can be categorized, the situation is entirely different. The major problem here is assessing the degree of imperfection in the product, the variable service conditions, the peculiarities of the customers, and, finally, the idiosyncrasies of maintenance personnel. The problem can be approached by way of theoretical engineering analysis. However, this method is not fully developed, tends to be cumbersome, is extremely time consuming, and is generally unable to predict specific problems and failure patterns. Certainly, theoretical analysis provides a point of departure; however, it cannot be relied upon to accurately forecast the cost of various warranty policies. It is clear that specific field experience under real-world conditions is required for the establishment of viable warranty alternatives.

There are several types of product warranties, ranging from the normal parts-and-labor warranty to service contracts, including selective parts-and-labor and pro-rata arrangement based on time in service. Each of these would have to be carefully evaluated in terms of customer acceptance and cost. As indicated earlier in this discussion, the final selection will be dictated to a great extent by market pressures.

Implicit in this discussion is the assumption that the product has, in fact, been designed for its intended use. This further implies that the designer/seller understands the nature of wind energy systems and possesses the mathematical tools to analyze the system in terms of structural loads, performance, etc. It is further assumed that the designer has conducted failure mode

and effect analysis to assure that the design is inherently sound. Similarly, it is assumed that the manufacturer/seller will establish and utilize firm material and process specifications for the manufacture and assembly of the wind turbine.

It is clear that, without a clear understanding of the engineering fundamentals and without high standards of product acceptance, there can be no realistic warranty policy.

MANUFACTURING COST ESTIMATE

Manufacturing costs were estimated with an assumed production rate of 1000 units per year in a year when both the product and the manufacturing process and techniques are fully developed, thus achieving maximum efficiency. In deriving realistic estimates, cost avoidance procedures are as significant a consideration as the accurate calculation and summing of machining times for the system's component details. This analysis presumes that cost avoidance will be a basic operating policy. Lot sizes for purchased goods and material will be optimized. Inventories of finished manufactured details must be minimized to avoid local inventory taxes. The manufacturing process must be controlled to the extent that the patterns for cutting sheet and plate stock are arranged to leave a minimum of waste trim.

The results of this estimating effort are shown in terms of sell price, rather than cost to the manufacturer. Prices are based on: labor charges at $12 per hour, an assumption of 1977 economy for purchased items, a 10% charge for handling purchased items, and a 30% mark-up to cover G&A & Fee bringing the total mark-up to 40%. No provisions have been made for the expense of providing warranty or liability protection nor are shipping expenses considered.

Blades

The blades have a uniform cross section without twist or taper. As such, they are eminently suited to high production manufacturing techniques such as composite fiberglass/epoxy pultrusions. The raw pultrusions are cut to length and finished with the installation of a tip plug, retention reinforcements, lightning conductive tapes, and erosion resistant paint, and finally an individual balance operation. The blade cost estimate includes the aluminum adapter which joins the blade to the flexbeam.

Costs of the blade and joint system were based on estimates for production manufacture from Goldsworthy Engineering, who will provide the prototype blade pultrusions, making a short summary of operations for finishing the blade and manufacturing the joint and estimating the time and materials associated with each step of the operations. The price of a set of blades with the aluminum joint installed is $733.

Flexbeam and Hub

The flexbeam is match die molded with 0° fiber orientation. To establish its cost, the volume of graphite fiber was calculated and its cost established.

An operation summary was prepared and labor and material charges for each step was determined. For the hub, each detail of the drawing was itemized, and the price of standard items such as nuts, bolts, and washers was obtained from manufacturer's catalogue price lists. Manufactured components have a material expense calculated on the basis of the weight of raw material and a basic steel price. A summary of operations required to manufacture the part was determined and machining, setup, and inspection time assigned. The material and labor charges were combined to yield the total price. Finally, time was included for assembly and finishing. The price of the hub and flexbeam sub-assembly totals $1135.

Rotor Head Assembly

The rotor head assembly consists of the pylon structure, the gearbox and coupling, and the induction motor. Prices for the gearbox, coupling, and induction motor-generator reflect quotations for production quantities received during procurement of the prototype units. The pylon structure was analyzed in the same manner as described for the hub. The estimated selling price of the production system totals $5405 with $3536 for the pylon structure and fairing, $1338 for the gearbox and coupling, and $531 for the motor-generator.

Tower

The tower is a guyed mast which is fabricated in two sections for ease of transportation. The price of the tower was determined by obtaining the cost of the raw material and standard items such as cable and fittings and estimating the time required for welding and machining to fabricate the tower sections and for assembling the fittings on the guy wires. The price of this assembly totals $2614.

Functional Tests

Functional tests, required to insure that delivered systems have proven reliability, were defined and their expense determined. The tests include calibration of the flexbeam torque vs angular displacement relationship and balance of the rotor hub and the flexbeam and pendulum system. In addition, after the whole system of the tower head is assembled, it must be driven for a short period at rated speeds to insure that the generator, gearbox, and bearings are properly aligned, run smoothly and function properly. The price for these tests is expected to amount to $120.

Packaging

Finally, provision has been made for packaging the system for shipment. The two tower pipes would be bound together and the cables, turnbuckles, thimbles, and clamps made up and tied to the pipe sections. Any other miscellaneous hardware also would be strapped to the pipes. The rotor head would be shipped on a special pallet, assembled, and ready for installation on the top of the tower. Nuts, bolts, and similar hardware would be attached in a separate package. The flexbeam hub and pendulum would be shipped in its own protective container with bolts, nuts, and bushings for the blade retention joint made up hand tight. The blades also would be delivered in a protective container all prepared for final assembly. The packaging and containers add $400 to the system price.

The selling price for each of the subsystems mentioned above can be summarized quite easily. But the result can be made much more meaningful if it is presented with comparable figures relating distinct points in the program development. Shown tabulated below is the total system price presented at the Critical Design Review (CDR) at Rocky Flats, Colorado on March 31, 1978. At that time, undefined price reductions totaling $7,500 were considered a very reasonable possibility. Later the system price breakdown was updated to reflect major design changes and was presented at the Final Design Review on July 25 and 26, 1978. The results of these analyses are shown below:

TABLE 36

PRODUCTION COST ESTIMATES

	Critical Design Review	Final Design Review	Phase I Production Price Analysis
Blades	$ 5,496	$ 440	$ 733
Flexbeam & Hub	949	1,135	1,135
Rotor Head Assy.	8,013	3,965	5,405
Tower	2,433	2,614	2,614
Functional Test	120	120	120
Packaging	400	400	400
Total	$17,411	$8,674	$10,407

This tabulation clearly shows the variation in estimated selling price as the system design evolved. At the time of the CDR, the estimated FOB factory price of $17,411 was substantially higher than the target and the concept was re-examined to determine what changes could be made to improve the situation. At that time, it was estimated that a $7500 reduction could be achieved during the design phase and approval to proceed was received. Within a few months, the basic blade construction technique was changed, resulting in a projected savings of $5000. In the same period, changes in the operating speed and type of generating equipment allowed major reductions in the price of the generator and gearbox. With the visibility of these reductions in hand, the estimated production cost of $8,674 was reported at the Final Design Review. However, the circumstances which existed at that time gave no opportunity for this report to be reviewed or examined by Hamilton Standard cost analysts. Consequently, growth in the definition of the rotor head system amounting to approximately $1400 was not recognized or reported. The present system price of $10,407 reflects this growth in the rotor head assembly and a moderate increase in blade finishing operations. A more detailed breakdown of the system price of $10,407 is presented in Table 37.

The FOB factory cost estimate of $10,407 represents a reduction of $7,000 or 93% of the $7,500 cost reduction predicted at the CDR. In the course of arriving at the current estimated price, discussions of further modifications and cost reduction changes indicate that a final configuration with a price of approximately $8,500 is entirely reasonable. This 20% reduction would be achieved by a careful review and tailoring of the hardware for production. This effort would be accomplished by manufacturing/industrial engineers working with structural designers and could be accomplished with no basic changes to the machine configuration. To demonstrate the reality of the potential for savings, several suggestions are listed in Table 38 with their corresponding estimated savings.

The cost per kW at 9-m/s wind speed at the current estimated cost is $1155/kW, assuming 9 kW output using the 1:17 gearbox. This drops to $929/kW assuming 11.2 kW output using the 1:14 gearbox, and with the projected reduction in price this drops to $759/kW which is close to the target price for this size machine.

While these suggested savings may not all be realized fully in the production model, they indicate that the target reduction of $2000 is realistic and provide examples of the variety in effective cost saving alternatives. A thorough cost reduction program, as recommended above, would yield a long list of less substantial savings as well. When added together the total cost savings should easily exceed the conservative 20% cost reduction target.

A final cost estimate will be made following the fabrication and testing of the full-scale system. It is expected that many areas of the design will

TABLE 37

BREAKDOWN OF PRODUCTION PRICE ANALYSIS

Blades	Material	Labor	Detail Total	Subsystem Total
Shells	$117		$117	
Finishing		$173	$173	
Joint	$115	$130	$245	
Details	$137	$ 61	$198	
				$733
Flexbeam & Hub				
Flexbeam	$400	$194	$594	
Hub	$363	$178	$541	
				$1135
Tower				
Pipe	$660	$ 57	$717	
Wire	$658	$ 23	$681	
Hardware	$1175	$ 41	$1216	
				$2614
Rotor Head Assy.				
Generator	$531	-	$531	
Gearbox & Coupling	$1338	-	$1338	
Frame	$423	$582	$1005	
Details (Shafts, Bearings, F/G Cover, etc.)	$2201	$330	$2531	
				$5405
Functional Test				
Test		$120	$120	
				$120
Packaging				
Containers & Packing	$340	$ 60	$400	
				$400
			TOTAL	$10,407

be found to be unnecessarily conservative and will represent areas for cost reductions. The details of the final cost estimate will be included in the final contract report which will follow the field evaluation tests at Rocky Flats.

TABLE 38

SUGGESTED COST SAVINGS

	Suggestion	Savings
1.	Use a casting for the main frame instead of a weldment.	$ 300
2.	Delete tapered adapters under all main bearings.	120
3.	Incorporate a less expensive speed switch.	100
4.	Make blade reinforcing pads of cast aluminum rather than fiberglass lay-up.	75
5.	Use cast bearing plates with integral tapered washers for blade joint.	10
6.	Use steel rods in place of the wire ropes if flexibility of guy supports is found unnecessary.	300
7.	Fiberglass tower using pultrusion process in place of steel tower.	400
	TOTAL	$1305

Increment Due to Temperature Extremes

The temperature extremes specified in the work statement were -50°C to +60°C. The impact on cost in satisfying this requirement has been discussed with suppliers of off-the-shelf items as well as raw material suppliers. It has been concluded that the upper temperature would not influence costs with the exception of the generator it it were not properly ventilated. If high temperature protection were required the insulation for the windings would be increased, and the cost increase would be nominal, about $25. The increment for low temperature, -50°C, is determined using the general rule of thumb for raw material costs, suggested by suppliers, which is 1¢/lb per °C below -30°C. This amounts to $415 for the tower components and $258 for the remaining components for a total increase in cost of $673.

CONCLUDING REMARKS

The Phase I results have demonstrated that the UTRC wind turbine design satisfies the basic performance and structural requirements set forth in the contract work statement. It is felt that the prototype system will be somewhat more conservative in (structural) load carrying capacity than a final production design would or should be. Since the basic UTRC concept is untried in full-scale sizes, it is believed that the demonstration of its fundamental operating characteristics should be of highest priority, and that a highly efficient structure should be of secondary importance.

The estimated production costs of the system are encouraging, however they are greater than the contract goal by about 20%. Many cost saving suggestions have been identified, however, and following the acquisition of data from the field testing conducted in Connecticut and Rocky Flats, it is projected that design modifications could lead to a more efficient structure.

Specific results and conclusions which evolved during the course of the Phase I design are listed below.

1. The pendulum/flexbeam control system provides blade pitch control to achieve start-up, high performance efficiency, and blade stall for high speed survivability.

2. Analyses and wind tunnel results show that the design selected operates freely in yaw without instabilities or degrading performance.

3. The use of free yaw and a passive control system eliminates the need for all wind speed and direction sensors.

4. A 9.4-m-diameter rotor is calculated to provide power output of at least 8 kW at 9 m/s (20 mph) and an annual output of 23,000 kWh for a mean wind speed of 5.4 m/s (12 mph).

5. A simple transmission substitution, to provide a lower step-up ratio, results in a system with improved performance at high wind sites.

6. The induction generator is more cost effective than an alternator or synchronous generator due to its lower initial cost and the fact that an inverter is not required.

7. Fiberglass blades are best suited for the UTRC design due to their low weight and potentially low cost. Extruded aluminum blades are not practical due to their high weight and the resulting adverse effect on edgewise frequency.

8. A guyed column is favored over other tower configurations due to its low aerodynamic shadow and the ease with which it can be manually erected.

9. Wind turbine costs (F.O.B. factory) below $10,000 (1977 dollars) are feasible for high quantity production.

REFERENCES

1. Cheney, M. C., and P. A. M. Spierings: Self-Regulating Composite Bearingless Wind Turbine. ERDA Report COO-2614-76/1, September 1976.

2. Cheney, M. C., and P. A. M. Spierings: Self-Regulating Composite Bearingless Wind Turbine. Solar Energy, Vol. 20, 1978.

3. Spierings, P. A. M., and M. C. Cheney: Design of a Self-Regulating Composite Bearingless Wind Turbine. Final Report, ERDA COO-4150 77/8 UC-60, January 1978.

4. Bielawa, R. L., M. C. Cheney, and R. C. Novak: Investigation of a Bearingless Helicopter Rotor Concept Having a Composite Primary Structure. NASA CR-2636, March 1976.

5. Novak, R. C.: Torsion Fatigue Testing of Unidirectional Graphite/Epoxy Composites. UTRC Report M411894-2, April 1973.

6. Holmes, R. D., and D. W. Wright: Creep and Fatigue Characteristics of Graphite/Epoxy Composites. ASME Paper 70-DE-32, 1970.

7. Landgrebe, A. J.: An Analytical and Experimental Investigation of Helicopter Rotor Hover Performance and Wake Geometry Characteristics. USAAMRDL Technical Report 71-24, June 1971.

8. Paterson, R. W., and R. K. Amiet: Noise and Surface Pressure Responses of an Airfoil to Incident Turbulence. J. of Aircraft, Vol. 14, 1977, pp. 729-736.

9. Amiet, R. K.: Noise Produced by Turbulent Flow into a Propeller or Helicopter Rotor. AIAA Journal, Vol. 15, 1977, pp. 307-308.

10. Work Statement. Development of an 8 kW Wind Turbine Generator for Residential Type Application. UTRC Contract PF68186-F Under Rockwell International. October 5, 1977.

11. Rohrbach, C.: Experimental and Analytical Research on the Aerodynamics of Wind Turbines. ERDA Report C0012615-76-T-1, February 1976.

12. Jacobs, E. N., and R. M. Pinkerton: Tests in the Variable-Density Wind Tunnel of Related Airfoils Having the Maximum Camber Unusually Far Forward. NACA-TR-537.

REFERENCES (Cont'd)

13. Bellinger, E. D.: Experimental Investigation of Effects of Blade Section Camber and Planform Taper on Rotor Hover Performance. USAAMRDL Technical Report 72-4, March 1972.

14. Flonc, N.: Characterization of Boron, Graphite, and Glass Filament/Organic Matrix Composite Materials. Sikorsky Engineering Report SER-50644, January 1970.

15. Bielawa, R. L.: Aeroelastic Analysis for Helicopter Rotor Blades with Time-Variable, Nonlinear Structural Twist and Multiple Structural Redundancy. Mathematical Derivation and Program User's Manual. NASA CR-2637, February 1976.

16. Roark, R. J., and W. C. Young: Formulas for Stress and Strain. 5th Edition, McGraw-Hill Book Co., New York, 1975.

17. Gessow, A., and G. C. Meyers: Aerodynamics of the Helicopter. Frederick Ungar Publishing Co., New York, 1967.

Nomenclature

A	rotor disk area
b	chord dimension of composite material test specimen or number of blades
c	distance from neutral axis to outer fiber of member under load
C_p	Rotor power coefficient
D	Rotor diameter
E	Young's Modulus or edgewise
F	flatwise
G	Shear Modulus
GR	gear ratio
h	thickness dimension of composite material test specimen
I	area moment of inertia
J	torsional area moment of inertia
l	flexbeam length
L	specimen length
M	moment or pendulum weight
N	rotor rotational speed, H_z
P	load or indicating per rev or power
R	rotor radius
t	thickness
T	Torsion
V	wind speed

Nomenclature (cont'd)

VR	velocity ratio $\Omega R/V$
W	power in watts
	pendulum angle
	efficiency
	blade collective pitch
	air density
	stress
	rotor rotational speed, rad/sec

Subscripts

g	generator
i	initial
p	pendulum
tip	pitch or velocity at blade tip
W	wind

APPENDIX A

Foam and Polyurethane Formulations for Initial Blade Design

Foam and Resin Developments for Airfoil Application

The objective of this phase of the program was to develop a self-skinning closed cell structural polyurethane foam with an airfoil configuration, supported by a graphite/epoxy spar located centrally in the airfoil structure. Several polyurethane formulations were investigated with this objective in mind.

The design schematic for the polyurethane airfoil shape is shown in Fig. A-1. The important concept in this design approach is:

(1) The use of a self-skinning closed cell structural polyurethane foam in the form as an airfoil having a secondary structural role.

(2) Utilization of a solid polyurethane material for the leading edge of the airfoil structure. Aerodynamic aeroelastic stability considerations require that this material have a density of approximately 2.76 g/cc (0.10 lb/in.^{3}). This was to be accomplished by addition of metal filler to the polyurethane resin or by use of a solid steel rod placed strategically in the body of the leading edge.

(3) Utilization of a graphite/epoxy spar as the primary structural beam extending from the flexbeam joint into the airfoil structure. The results of the materials development studies carried out in each area of the design concept are described in this section.

Foam and Resin Experiments

Foam Experiments

The more promising formulations are summarized in Table A-1. The properties of interest in this material are the compressive strength, the tensile properties and the bulk density of the foam specimens. The component properties of the self-skinning foam were also measured. Foam samples were cut into skin and core sections. The volume fraction, density, and tensile properties of the skin and core foam were determined. Compressive properties of the core foam were also determined.

The compressive strength as a function of density of several polyurethane samples are listed in Table A-2. Two points are of importance in this table. The first is that the first three specimens listed have the highest densities, but do not necessarily possess the highest compressive strengths. The second point is that there is a correlation between density and compressive strength as illustrated by the last four specimens listed. Sample 77-5-1, with a bulk density of 288 kg/m^3 (18.0 lb/ft^3) failed at 5.63 MPa (816 psi) in compression,

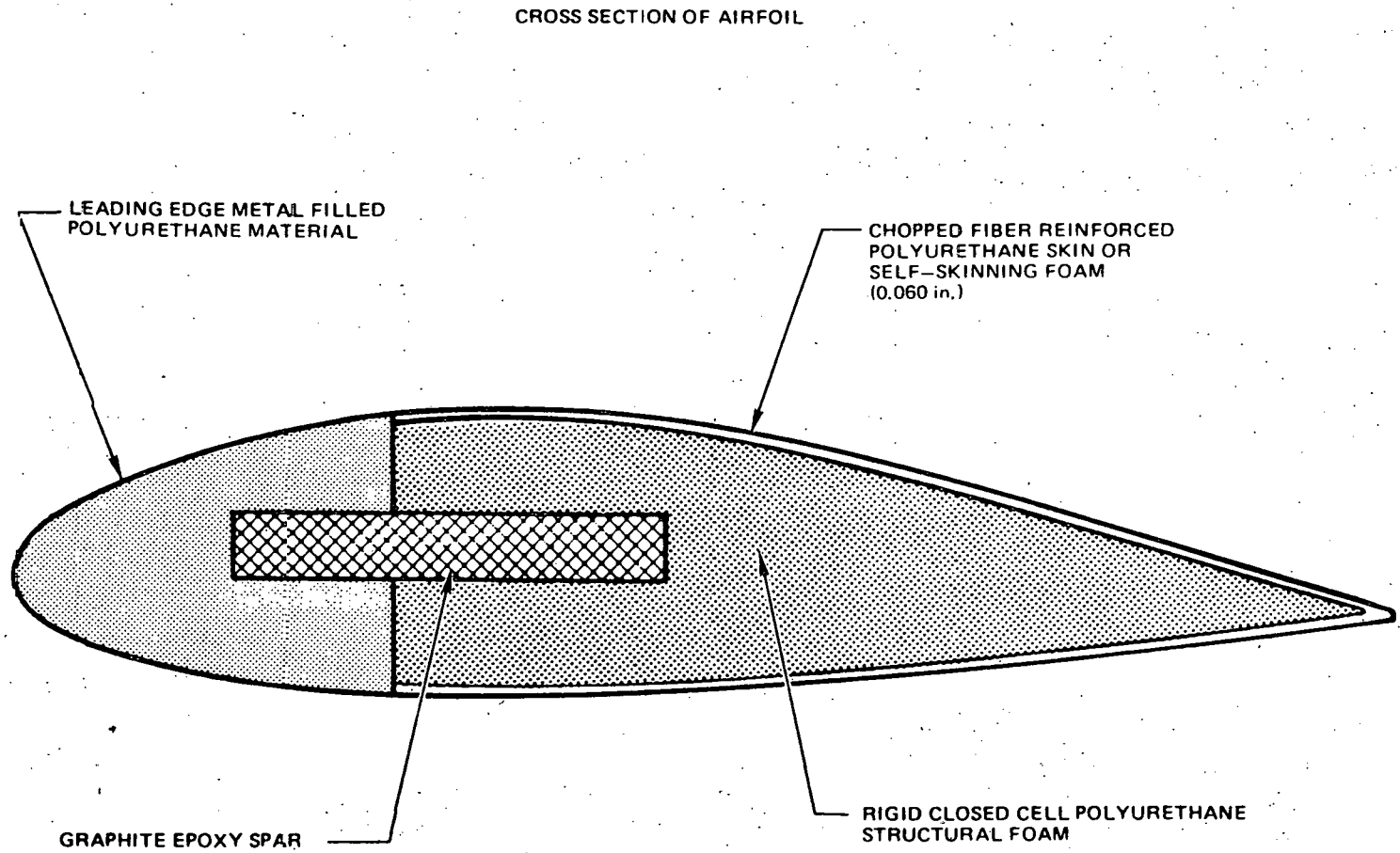

Fig. A1 Initial Blade Structural Concept

APPENDIX A

TABLE A-1

FOAM FORMULATIONS

78-0221, 78-0222	wt,g
Isonate 181	132.3
Polyol G 71-357	67.5
Poly G 70-600	13.5
DMEA	0.36
DC-193	1.8
Freon 11B	12.6

78-0504-1	wt,g
Isonate 181	44.3
Polyol LS490	27.5
Polyol 11-27	5.0
DMEA	0.12
Stannous octoate	0.10
DC-193	0.5
Freon 11B	5.0

78-0504-2	wt.g
Isonate 181	44.3
Polyol LS490	27.5
Polyol 11-27	5.0
DMEA	0.10
DBTL	0.12
DC-193	0.50
Freon 11B	5.0

78-0505-1	
Isonate 181	45.4
Polyol PCP-0301	25.0
Polyol 11-27	5.0
DMEA	0.10
DBTL	0.12
DC-193	0.50
Freon 11B	5.0

78-0505-2	
Isonate 181	45.4
Polyol PCP-0301	25.0
Polyol 11-27	5.0
TMBDA	0.10
Stannous octoate	0.12
DC-193	0.50
Freon 11B	5.0

78-0510-4	
Isonate 181	34.2
Polyol DAS361	28.7
Polyol 11-27	5.0
TMBDA	0.12
Stannous octoate	0.10
DC-193	0.50
Freon 11B	5.0

78-0512-1	
Isonate 181	34.2
Polyol DAS361	28.7
Polyol 11-27	5.0
DMEA	0.12
DBTL	0.10
DC-193	0.50
Freon 11B	5.0

78-0512-2	
Isonate 181	34.2
Polyol DAS 361	28.7
Polyol 11-27	5.0
TMBDA	0.12
DBTL	0.10
DC-193	0.50
Freon 11B	5.0

78-0512-3	
Isonate 181	46.0
Polyol BET530	26.2
Polyol 11-34	5.0
DMEA	0.12
Stannous octoate	0.10
DC-193	0.50
Freon 11B	5.0

78-0512-4	
Isonate 181	46.0
Polyol BET530	26.2
Polyol 11-34	5.0
TMBDA	0.12
Stannous octoate	0.10
DC-193	0.50
Freon 11B	5.0

78-0515-1	
Isonate 181	46.0
Polyol BET530	26.2
Polyol 11-34	5.0
TMBDA	0.12
DBTL	0.10
DC-193	0.50
Freon 11B	5.0

78-0515-3	
Isonate 181	46.0
Polyol LHT-240	50.0
Polyol 11-34	5.0
A-1 Catalyst	0.12
Stannous octoate	0.10
DC-193	0.50
Freon 11B	5.0

TABLE A-1 (Cont'd)

FOAM FORMULATIONS

-0516-2	wt,g	78-0516-4	wt,g	78-0404-5	wt,g
Isonate 181	46.0	Isonate 181	46.0	Isonate 181	45.4
Polyol BE375	38.0	Polyol BE375	38.0	Polyol PCP-0301	25.0
Polyol 11-34	5.0	Polyol 11-34	5.0	Polyol 11-27	5.0
A-1 Catalyst	0.12	DMEA	0.12	DMEA	0.12
Stannous octoate	0.10	DBTL	0.10	Stannous octoate	0.10
DC-193	0.50	DC-193	0.50	DC-193	0.50
Freon 11B	5.0	Freon 11B	5.0	Freon 11B	5.0

Key to Abbreviations:

DMEA = Dimethylaminoethanol
DC-193 = Surfactant
DBTL = Dibutyltindilaurate
TMBDA = Tetramethylbutane diamine
A-1 catalyst = Union Carbide amine catalyst, bis (2-dimethylaminoethyl) ether

TABLE A-2

COMPRESSIVE STRENGTH OF POLYURETHANE FOAMS[1]

Specimen No.	Density g/cc (lb/ft^3)		Compressive Strength MPa	Psi
78-0221-1	0.343	(21.4)	2.38	346
78-0222-1	0.362	(22.6)	1.13	165
78-0222-2	0.338	(21.1)	1.79	260
77-5-1	0.288	(18.0)	5.62	816
77-10-1	0.160	(10.0)	3.19	464
77-15-1	0.112	(7.0)	1.07	156
77-14-1	0.080	(5.0)	0.50	73

[1] Mixed at room temperature, poured into a preheated mold at 60°C, cured at 121°C for 30 minutes.

while samples 77-10-1, -15-1, and -14-1 with densities of 160, 112, and 80 kg/m^3 (10, 7 and 5 lb/ft^3) failed at 3.19, 1.07, and 0.50 MPa, respectively. Clearly for a given series as the bulk density increases, the compressive strength also increases. However, as shown above, a high bulk density does not necessarily yield high compressive strengths.

A self-skinning foam sample was dissected into skin and foam sections and these component sections were subjected to tensile tests. The results of these tests are listed in Table A-3. The differences in skin and foam tensile properties are clearly noted for the two foam samples.

The tensile strength and modulus of foam with skin (sample 78-0222-1a) is 3.57 MPa and 0.172 GPa, respectively while the tensile strength and modulus of the skin only (sample 78-0222-1eb) is 22.81 MPa and 1.19 GPa, respectively. The other foam sample 78-0222-2 showed similar differences. It should also be noted that the tensile strengths of skin samples 78-0222-1as, -1bs, -1cs dissected from the side are much lower than skin samples 78-0222-1eb and -1fb dissected from the bottom of the foam sample. In preparing samples, the mixed polyurethane formulation is quickly transferred to the mold. The material hits the bottom of the mold surface first, the cover of the mold is positioned in place quickly, and the foaming process occurs within seconds. The bottom skin formed in this process is thicker and appears to be harder than the side and top skins. Similar strength differences are noted for skin sample 78-0222-2bs dissected from the side, 13.5 MPa and skin sample 78-0222-2db and 78-0222-2eb dissected from the bottom, 23.91 MPa. Finally, core foam samples 78-0222-1b, 78-0222-2a, and 78-0221-1a show tensile strengths of approximately 1.5 MPa and moduli of 0.069 GPa, properties much lower than the skin sections.

Closely related to the strength distribution in a self-skinning closed cell polyurethane pour is the density and gradient vol % distribution of various sections of the foam sample. Density and vol % data are listed in Table A-4. The density gradient for skin samples of thicknesses 1.02, 0.76, 0.38 mm varies from 0.62 to 0.61 to 1.31 g/cc corresponding to volume percents of 20, 15 and 7.5. The largest volume fraction of the sample, the core, accounting for 85 vol %, has the lowest density 0.30 g/cc, as expected. It is clear from the tensile strength distribution and density distribution that the high density skin sections are the strongest, while the low density foam sections are the weakest.

A series of polyurethane formulations were screened for compressive strengths to determine materials variables required for optimum compressive properties. The results of these tests are listed in Table A-5. Although the strength differences between the various formulations are not significant, the data do suggest trends. The first is that dibutyltindilaurate (DBTL) accelerator in formulation 78-0504-2 (0.95 MPa compressive strength) generates

TABLE A-3

TENSILE PROPERTIES OF CUT SECTIONS OF SELF-SKINNING CLOSED CELL POLYURETHANE FOAM MATERIALS[1]

Self-Skinning Foam Sample	Section of Sample	Tensile Properties: Strength MPa	Strength Psi	Modulus GPa	Modulus 10^6 psi	Elongation %
78-0222-1b	foam no skin	1.46	217	0.082	0.012	4.52
1g	foam no skin	2.64	392	0.096	0.014	8.36
1a	foam with skin	3.57	530	0.172	0.025	2.24
1as	skin section	11.17	1660	0.709	0.103	2.64
1bs	skin section	11.91	1770	0.785	0.114	2.36
1cs	skin section	13.23	1920	0.751	0.109	4.12
1db	skin section	15.92	2310	0.951	0.138	3.60
1eb	skin section	22.81	3310	1.190	0.174	3.52
1fb	skin section	18.91	2750	0.882	0.128	4.40
78-0222-2a	foam no skin	1.55	226	0.599	0.087	5.76
2c	foam no skin	1.51	220	0.062	0.009	6.00
2d	foam no skin	1.55	226	0.069	0.010	7.64
2bsk	foam with skin	4.36	633	0.578	0.084	3.36
2bs	skin section	13.50	1960	0.951	0.138	1.80
2cb	skin section	20.39	2960	0.923	0.134	5.90
2db	skin section	21.91	3180	0.986	0.143	6.76
2eb	skin section	23.91	3470	1.070	0.156	5.52
78-0221-1a	foam no skin	1.80	261	0.068	0.010	12.00
1bsk	foam with skin	4.17	606	0.289	0.042	1.52
1a	skin section	14.47	2100	0.876	0.127	2.68
1b	skin section	13.64	1980	0.827	0.120	2.76

[1] Mixed at room temperature, poured into preheated mold at 60°C, cured at 121°C for 30 minutes.

TABLE A-4

DENSITY DISTRIBUTION THROUGHOUT SELF-SKINNING POLYURETHANE FOAM [1]

Portion of Specimen, mm	Density g/cc	Vol %
Total specimen 10.20	0.41	100
1.02 skin	0.62	20
0.76 skin	0.61	15
0.38 skin	1.31	7.5
5.08 core	0.30	85

[1] Same cure cycle as in Table 2.

TABLE A-5

COMPRESSIVE PROPERTIES OF SEVERAL FOAM FORMULATIONS[1]

Formulation No.	Material Variable Studied	Density		Compressive Properties			
				Strength		Modulus	
		g/cc	lb/ft^3	MPa	psi	GPa	10^6psi
78-0504-1	catalyst	0.082	5.12	0.50	72.5	0.020	.0025
78-0504-2	catalyst	0.127	7.92	0.95	138.0	0.040	.0056
78-0504-5	polyol	0.090	5.64	0.60	86.5	0.014	.0021
7840505-1	polyol	0.096	5.98	0.45	65.3	0.013	.0019
78-0505-2	polyol, catalyst	0.091	5.65	0.58	84.7	0.014	.0021
78-0510-4	polyol	0.071	4.43	0.47	67.9	0.012	.0017
78-0512-1	polyol	0.098	6.15	0.42	61.2	0.014	.0020
78-0512-2	polyol	0.123	7.70	0.72	105.0	0.021	.0030
78-0512-3	polyol	0.093	5.82	0.88	128.0	0.037	.0053
78-0512-4	polyol	0.111	6.95	0.89	129.0	0.033	.0047
78-0515-1	polyol	0.121	7.53	0.75	109.0	0.022	.0032
78-0515-3	polyol	0.225	14.04	0.38	55.6	0.011	.0017
78-0516-2	polyol, catalyst	0.108	6.74	0.72	105.0	0.023	.0034
78-0516-4	polycl, catalyst	0.144	8.99	1.20	174.0	0.042	.0061

[1] Mixed at room temperature, poured into a preheated mold at 60°C, cured at 121°C for 30 minutes.

a stronger foam than stannous octoate in formulation 78-0504-1 (0.50 MPa compressive strength). A similar conclusion can be drawn by comparing formulations 78-0512-2 with 78-0510-4, having compressive strengths of 0.72 Mpa and 0.47 MPa, respectively. Secondly, compressive strengths of about 0.8 MPa for systems 78-0512-3, -4, and 78-0515-1 suggest that polyols BET-530 and 11-34 are excellent materials for structural foams and can be optimized for increased compressive properties. The same conclusion can be deduced for polyol BE-375 in formulation 78-0516-4, which yielded a compressive strength of 1.20 MPa. Based on the data in Table A-4, formulations 78-0504-2, 78-0515-1, 78-0512-2,-3, or -4, and 78-0516-4 are considered strong candidates for optimization studies, i.e. cure, temperature, blowing agent concentration, sulfactant concentration, and catalyst concentration.

Fiber Reinforced Skin Formulations

A few formulations were evaluated to determine the effect of chopped S-glass fiber on the strength properties of polyurethane, intended for skin applications. The concept is to coat the fiber reinforced polyurethane resin on the mold surface as a gel-coat, and then introduce polyurethane foaming resin to fill the cavity and bond directly to the glass fiber-filled gel-coat. Only a limited number of specimens were prepared to test the concept. The results of the tensile properties of these skin specimens are shown in Table A-6. The formulations are listed in Table A-7. The tensile strength of the best specimen (78-0426-2) is not encouraging compared to a tensile strength of 3470 psi for skin material (sample 78-0222-2eb) removed from the self-skinning foam sample 78-0222, Table A-3. These results are unexpected. Therefore, additional experiments must be performed for a full assessment of this approach, since reinforced skin samples should be considerably stronger than unreinforced samples.

Resin for Leading Edge Application

A thorough study of the materials required to produce a tough elastomeric leading edge material was made. This study first considered literature and commercial sources for the required materials. Then, based on data from these sources, certain commercial materials were selected for study in various formulations. The formulations investigated are summarized in Tables A-8 and A-9. The tensile properties of several elastomeric polyurethane materials and metal-filled polyurethane materials are listed in Tables A-10 and A-11, respectively. As noted in Table A-10, there is a wide range in tensile strengths, and even broader range in moduli for the formulations listed. Tensile strengths range from 1.24 to 8.27 MPa, while moduli range from 0.055 to 0.345 GPa. From the point of view of strength and toughness, formulations 78-0403-4, and 78-0330-3, with strengths 8.27 MPa and 6.54 MPa and moduli of 0.345 and 0.289 respectively,

TABLE A-6

TENSILE PROPERTIES OF CHOPPED GLASS FIBER REINFORCED POLYURETHANE [1]

Specimen No.	Chopped Glass Fiber Content, wt%	Tensile Properties				Elongation %
		Strength		Modulus		
		MPa	psi	GPa	10^6 psi	
78-0426-1	14.4	4.47	650	0.186	0.027	3.0
78-0426-2	15.7	7.58	1100	0.690	0.100	6.0
78-0426-3	14.1	6.48	940	0.276	0.040	8.0

[1] Cured at 121°C for two hours.

TABLE A-7

FIBER REINFORCED POLYURETHANE
SKIN FORMULATIONS

78-0426-1	wt,g
Isonate 181	12.6
Poly G 55-28	16.8
Ethyleneglycol	1.32
Polyol RF-70	0.30
Chopped glass fiber	5.20

78-0426-2	wt,g
Isonate 181	13.1
Poly G 85-36	12.5
Ethyleneglycol	2.0
Polyol RF-70	0.30
Chopped glass fiber	5.2

78-0426-3	
Isonate 181	13.4
Poly G 85-36	15.0
1,4-butanediol	2.80
Polyol RF-70	0.30
Chopped glass fiber	5.20

TABLE A-8

POLYURETHANE FORMULATIONS
INVESTIGATED FOR LEADING EDGE APPLICATIONS

78-0330-2,-3	wt, g
Isonate 181	126.0
Poly G 55-28	80.0
Ethyleneglycol	20.0
Polyol RF-70	3.0
Dabco 33LV	0.35
Dibutyltindilaurate	0.10

78-0331-2	wt, g
Isonate 181	126.0
Poly G 55-28	100.0
Ethyleneglycol	19.7
Polyol RF-70	3.0
Dabco 33LV	0.35
Dibutyltindilaurate	0.10

78-0331-3	
Isonate 181	92.7
Poly G 55-28	168.6
Ethyleneglycol	13.2
Polyol RF-70	3.0
Dabco 33LV	0.35
Dibutyltindilaurate	0.10

78-0403-4	
Isonate 181	127.00
Poly G 85-36	85.00
Ethyleneglycol	20.00
Polyol RF-70	3.00
Dabco 33LV	0.35
Dibutyltindilaurate	0.10

78-0403-5	
Isonate 181	131.0
Poly G 85-36	125.0
Ethyleneglycol	20.0
Polyol RF-70	3.0
Dabco 33LV	0.35
Dibutyltindilaurate	0.10

78-0404-1	
Isonate 181	134.0
Poly G 85-36	150.0
Ethyleneglycol	20.0
Polyol RF-70	3.0
Dabco 33LV	0.35
Dibutyltindilaurate	0.10

78-0404-2	
Isonate 181	55.0
Poly G 85-36	85.0
1,4-butanediol	11.0
Polyol RF-70	3.0
Dabco 33LV	0.35
Dibutyltindilaurate	0.10

78-0404-4	
Isonate 181	63.1
Poly G 85-36	85.0
1,4-butanediol	13.0
Polyol RF-70	3.0
Dabco 33LV	0.35
Dibutyltindilaurate	0.10

TABLE A-8 (Cont'd)

POLYURETHANE FORMULATIONS
INVESTIGATED FOR LEADING EDGE APPLICATIONS

78-0303-2	wt,g
Isonate 181	61.0
Poly G 85-36	42.1
Ethyleneglycol	10.0
Dabco 33LV	0.175
Dibutyltindilaurate	0.05

78-0307-2	wt,g
Isonate 181	122.0
Poly G 85-36	84.3
Ethyleneglycol	20.0
Dabco 33LV	0.35
Dibutyltindilaurate	0.10

78-0307-3	
Isonate 181	122.0
Poly G 85-36	100.0
Ethyleneglycol	19.6
Dabco 33LV	0.35
Dibutyltindilaurate	0.10

TABLE A-9

METAL-FILLED POLYURETHANE FORMULATIONS INVESTIGATED FOR LEADING EDGE APPLICATIONS

78-0224-1	wt,g
Isonate 181	103.3
Poly G 85-36	78.0
1,4-Butanediol	22.0
Dabco 33LV	0.4
DBTL	0.5
Titanium powder	40.0

78-0301-1	wt,g
Isonate 181	103.3
Poly G 85-36	78.0
1,4-Butanediol	22.0
Dabco 33LV	0,4
DBTL	0.5
Titanium powder	166.0

78-0308-4	wt,g
Isonate 181	63.0
Poly G 85-36	42.0
Ethyleneglycol	10.0
Dabco 33LV	0.175
DBTL	0.05
Cab-o-sil	1.50
Titanium powder	93.5

78-0313-2	
Isonate 181	122.0
Poly G 85-36	84.3
Ethyleneglycol	20.0
Dabco 33LV	0.35
DBTL	0.10
Tungsten powder	21.3

78-0314-1	
Isonate 181	122.0
Poly G 85-36	84.3
Ethyleneglycol	20.0
Dabco 33LV	0.175
DBTL	0.05
Tungsten powder	63.9

78-0314-2	
Isonate 181	122.0
Poly G 85-36	84.3
Ethyleneglycol	20.0
Dabco 33LV	0.175
DBTL	0.05
Tungsten powder	85.2

78-0320-2	
Epon 828	50.0
Epon 871	50.0
Sonite 41	14.9
Cab-o-sil	3.0
Tungsten powder	165.8

78-0321-2	
Epon 828	50.0
Epon 871	50.0
Sonite 41	14.9
Cab-o-sil	3.0
Tungsten powder	165.8

78-0322-1	
Isonate 181	122.0
Poly G 85-36	84.3
Ethyleneglycol	20.0
Dabco 33LV	0.175
DBTL	0.10
Tungsten powder	300.0

78-0428-1	
Isonate 181	63.5
Poly G 55-36	42.5
Ethyleneglycol	10.2
Polyol RF-70	1.5
Dabco 33LV	0.10
DBTL	0.05
Stainless steel powder	300.0

78-0428-2	
Isonate 181	65.5
Poly G 55-36	62.5
Ethyleneglycol	10.2
Polyol RF-70	1.5
Dabco 33LV	0.10
DBTL	0.05
Stainless steel powder	300.0

78-0501-1	
Isonate 181	67.0
Poly G 85-36	75.0
Ethyleneglycol	10.2
Polyol RF-70	1.5
Dabco 33LV	0.10
DBTL	0.05
Stainless steel powder	

TABLE A-9 (Cont'd)

METAL-FILLED POLYURETHANE FORMULATIONS INVESTIGATED FOR LEADING EDGE APPLICATIONS

78-0501-2	wt,g	78-0501-3	wt,g	78-0501-4	wt,g
Isonate 181	63.0	Isonate 181	63.0	Isonate 181	46.3
Poly G 55-28	40.0	Poly G 55-28	50.0	Poly G 55-28	64.3
Ethyleneglycol	10.0	Ethyleneglycol	9.8	Ethyleneglycol	6.6
Polyol RF-70	1.5	Polyol RF-70	1.5	Polyol RF-70	1.5
Dabco 33LV	0.10	Dabco 33LV	0.10	Dabco 33LV	0.10
DBTL	0.05	DBTL	0.05	DBTL	0.05
Stainless Steel powder	300.0	Stainless steel powder	300.0	Stainless steel powder	290.0

*Key abbreviations:

DBTL - dibutyltindilaurate

are considered excellent materials for leading edge application. Tensile properties of metal-filled polyurethane elastomeric materials are listed in Table A-11. Two formulations with an epoxy resin are shown for comparison. Formulation 78-0301-1, with 45 wt% titanium exhibited the best properties of the titanium samples with a tensile strength of 9.1 MPa, modulus of 0.42 GPa and percent elongation of 11.0%. Formulation 78-0313-2, the best of the tungsten-filled polyurethane samples, exhibited a tensile strength of 12 MPa, modulus of 0.469 GPA, and elongation of 63%. However, this sample is considerably lower in density (0.88 g/cc compared to 1.44 g/cc) than the titanium-filled polyurethane material. The desired density is 2.74 g/cc. The 58 wt% tungsten-filled epoxy systems exhibited strengths equivalent to the titanium-filled polyurethane system but considerably higher moduli, 0.62 to 0.69 GPa, compared to 0.42 GPa and much lower percent elongation, 1.1% compared to 11%, than the polyurethane system. From the point of view of toughness, titanium formulation 78-0301-1 demonstrates the desired properties for the polyurethane leading edge application.

Tensile properties of stainless steel polyurethane samples are listed in Table A-12. As shown in Table A-12, the use of stainless steel powder resulted in the formation of filled polyurethane samples with close to theoretical densities. All powdered metal samples required heat treatment at 150°C in vacuum for 1 h to remove absorbed moisture. Failure to remove absorbed moisture results in a porous sample. This porosity is caused by reaction of the moisture with urethane to form carbon dioxide gas, which foams the sample. The tensile properties listed in Table A-12 are adequate for consideration of these materials for this application.

Bonding of Polyurethane Foam and Leading Edge Materials to Graphite/Epoxy Structural Beam

In order to determine if the bond formed betwen the graphite/epoxy spar and in-situ formation of the self-skinning polyurethane foam and polyurethane leading edge material would be adequate to sustain the shear loads imposed on this interfacial bond while in service, three specimens were prepared for tensile shear tests. Figure A-2 is a photograph of the test specimen. The graphite/epoxy specimen was fixed in a mold, urethane resin mixture was added to the mold, and allowed to foam around the graphite/epoxy specimen. In the case of leading edge material a nonfoaming formulation was used. The specimens were then cured at 121°C for 20 minutes. The specimens were tested in tension to obtain the tensile shear strength of this bond. The results are shown in Table A-13. Included in the table is the design shear strength which the system must sustain. It is clear that the bond strengths between the graphite/epoxy spar specimen and the polyurethane leading edge material are more than adequate for the intended application, and in fact, have a safety factor of about 16.

TABLE A-10

TENSILE PROPERTIES OF
ELASTOMERIC POLYURETHANE LEADING EDGE
MATERIALS[1]

Specimen No.	Observations	Tensile Properties				% Elongation
		Strength		Modulus		
		MPa	psi	GPa	10^6 psi	
78-0330-2	brittle	5.09	740	0.186	0.027	3.2
78-0330-3	tough hard, excellent sample	6.54	950	0.289	0.042	8.0
78-0331-2	tough, rubbery excellent sample	6.34	920	0.206	0.030	28.0
78-0331-3	tough, very rubbery	1.24	180	0.055	0.008	20.0
78-0403-4	tough, rubbery excellent sample	8.27	1200	0.345	0.050	9.0
78-0403-5	tough, rubbery excellent sample	5.51	800	0.096	0.014	11.0
78-0404-1	tough, rubbery, hard, excellent sample	4.47	650	0.055	0.008	8.0
78-0404-2	very rubbery, excellent sample	4.47	650	0.017	0.0025	7.5
78-0404-4	tough, very rubbery, hard	2.76	400	0.021	0.003	10.8

[1] Mixed at room temperature, poured into a mold, cured at 121°C for 10 minutes.

TABLE A-11

TENSILE PROPERTIES OF METAL-FILLED POLYURETHANE ELASTOMERIC LEADING EDGE MATERIALS [1]

Formulation No.	Weight % Metal Powder	Density g/cc	Tensile Properties				Elongation %
			Strength		Modulus		
			MPa	psi	GPa	10^6 psi	
78-0224-1	16.4 titanium	1.18	7.0	1040	0.241	0.035	18.2
78-0301-1	45 titanium	1.44	9.1	1330	0.420	0.061	11.0
78-0308-4	45 titanium	1.45	5.2	750	0.351	0.051	8.0
78-0310-1	52 titanium	0.43	1.47	212	0.0081	0.0011	-
78-0316-2	8.5 titanium	1.15	7.61	1100	0.101	0.0147	-
78-0313-2	8.5 tungsten	0.88	12.0	1750	0.469	0.068	63.0
78-0314-1	22 tungsten	1.08	6.3	900	0.248	0.036	20.0
78-0314-2	27 tungsten	1.15	4.5	500	0.138	0.020	11.5
78-0322-1	57 tungsten	2.34	2.06	300	0.138	0.030	1.8
78-0329-1	49 tungsten	1.84	3.39	492	0.095	0.0139	-
78-0405-1	60 tungsten	2.26	1.75	250	0.137	0.019	-
78-0406-1	58 tungsten	1.62	2.95	427	0.026	0.0037	-
78-0406-3	60 tungsten	0.57	3.80	550	0.063	0.0092	-
78-0320-2	58 tungsten/epoxy	2.03	6.06	880	0.620	0.090	1.1
78-0321-2	58 tungsten/epoxy	2.39	7.71	1120	0.690	0.100	1.3

[1] Mixed at room temperature, poured into a mold, cured at 121°C for 10 minutes.

TABLE A-12

STAINLESS STEEL–FILLED POLYURETHANE ELASTOMERIC LEADING EDGE MATERIALS[1]

Formulation No.	wt% Stainless Steel	Density g/cc	Composition Varied	Tensile Properties Strength MPa	Strength Psi	Modulus GPa	Modulus 10^6 psi
78-0405-2	62.9	2.14	polyglycol	6.67	878	0.172	0.0249
78-0406-2	58.8	2.17	polyglycol	5.82	843	0.076	0.011
78-0501-1	66.1	2.34	ethyleneglycol	5.36	778	0.057	0.0083
78-0501-2	72.3	2.53	ethyleneglycol	5.68	856	0.273	0.0396
78-0501-3	70.7	2.53	ethyleneglycol	6.61	957	0.262	0.038
78-0501-4	73.4	2.49	ethyleneglycol	2.89	420	0.0384	0.0055

[1]Mixed at room temperature, poured into a mold, cured at 121°C for 10 min.

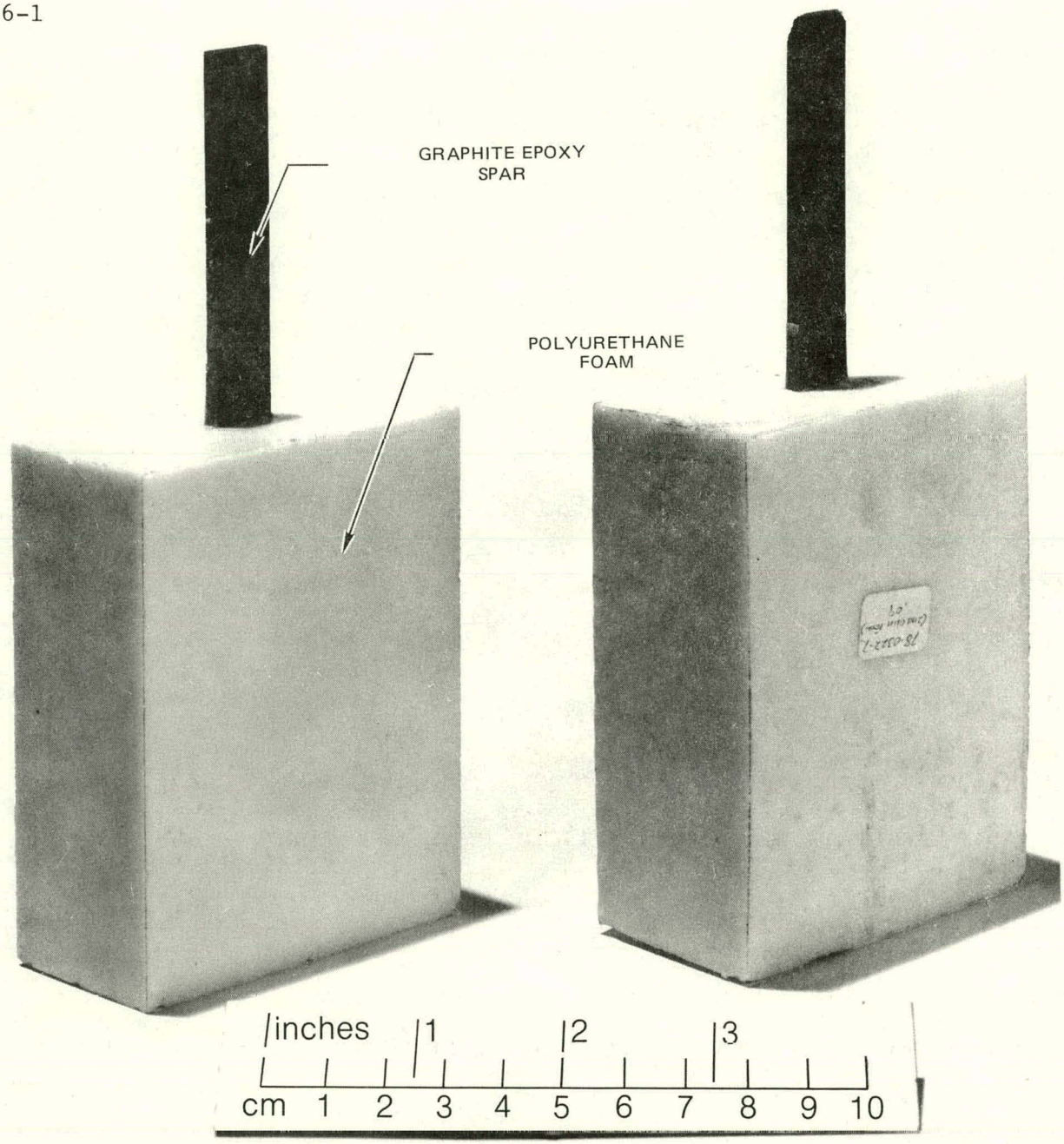

Fig. A2 Graphite/Epoxy-Polyurethane Foam Tensile Specimens for Shear Tests

78–128–A

78–10–171

TABLE A-13

TENSILE SHEAR STRENGTHS OF
GRAPHITE/EPOXY-POLYURETHANE SPECIMENS [1]

Specimen No.	Specimen Type	Tensile Shear Strength MPa	Tensile Shear Strength psi
78-0323-1	G/E - Polyurethane foam	2.42	352
-2	Bond	2.21	322
78-0323-3	G/E Polyurethane Leading	1.73	252
-4	Edge Bond	2.66	386
Calculated design loads	---	0.138	20

[1] Mixed at room temperature, poured into the mold containing the leading edge graphite/epoxy composite, cured at 121°C for 30 min.

Fabrication of Leading Edge/Graphite Epoxy/Polyurethane Foam Specimen

In order to determine the extent to which a self-skinning foam would fill in areas between the graphite/epoxy spar and the polyurethane leading edge, a composite comprised of these components was fabricated. Figure A-3 is a photograph of the cross section of the fabricated specimen. Several points are worthy of mention; (1) material contact between spar and polyurethane leading edge and polyurethane foam is excellent; (2) the foam material fills in all the corners near the spar and the highlighted leading edge portions; (3) the foam density appears higher near the surface than in the core; (4) close contact between the surfaces of the three materials suggests that adhesion could be adequate and that this concept (interfacing three materials) of fabricating an airfoil configuration is worthy of larger scale tests.

Conclusions

The materials study undertaken for this aspect of the program was directed toward developing materials for this concept of an airfoil construction as shown in Fig. A-1. It could be concluded from the results of this investigation that materials developed and tested possess the desired properties for this airfoil concept, and moreover, can be adapted to scaled-up production prototype and a full scale airfoil wind turbine blade.

The results show that a self skinning polyurethane foam with properties adequate for the intended application, an airfoil structure for a wind-turbine 8 kW electric power generator is feasible. The foam material has a compressive strength of 5.62 MPa and a density of 0.29 g/cc, with the skin section having a tensile strength of about 20.7 MPa and core foam strength of about 4.1 MPa. The modulus of the skin varied from 0.71 to 1.20 GPa, while the foam modulus varied from 0.07 to 0.28 GPa.

The studies further show that several other foam formulations have potential application in this concept, but require optimization studies to improve strength properties.

The polyurethane material filled with stainless steel powder, formulation 78-0501-3, exhibited excellent tensile properties for the leading edge application. In addition, adhesion between the graphite/epoxy spar and the leading edge material and self-skinning foam is more than adequate for this application.

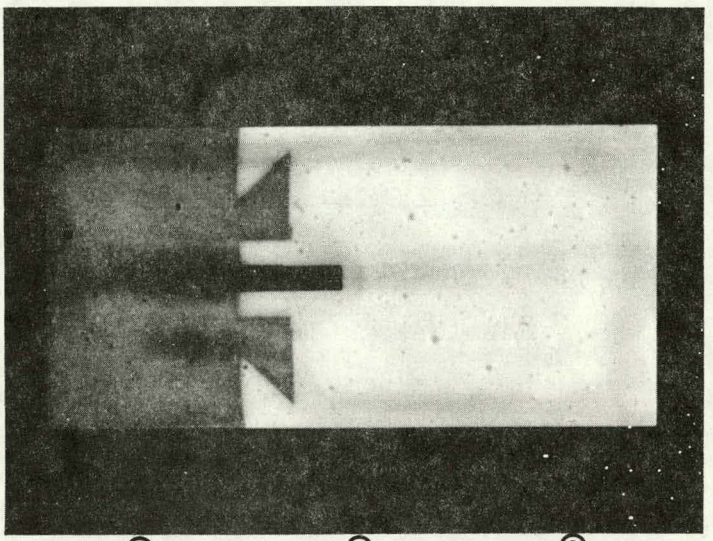

Fig. A3 Polyurethane Leading Edge/Graphite Epoxy Spar/Polyurethane Foam Composite Specimen

78-10-171-2

APPENDIX B

Computer Plots of Rotor Response Characteristics and Blade Stress Time Histories

(See Table 29 for Nomenclature)

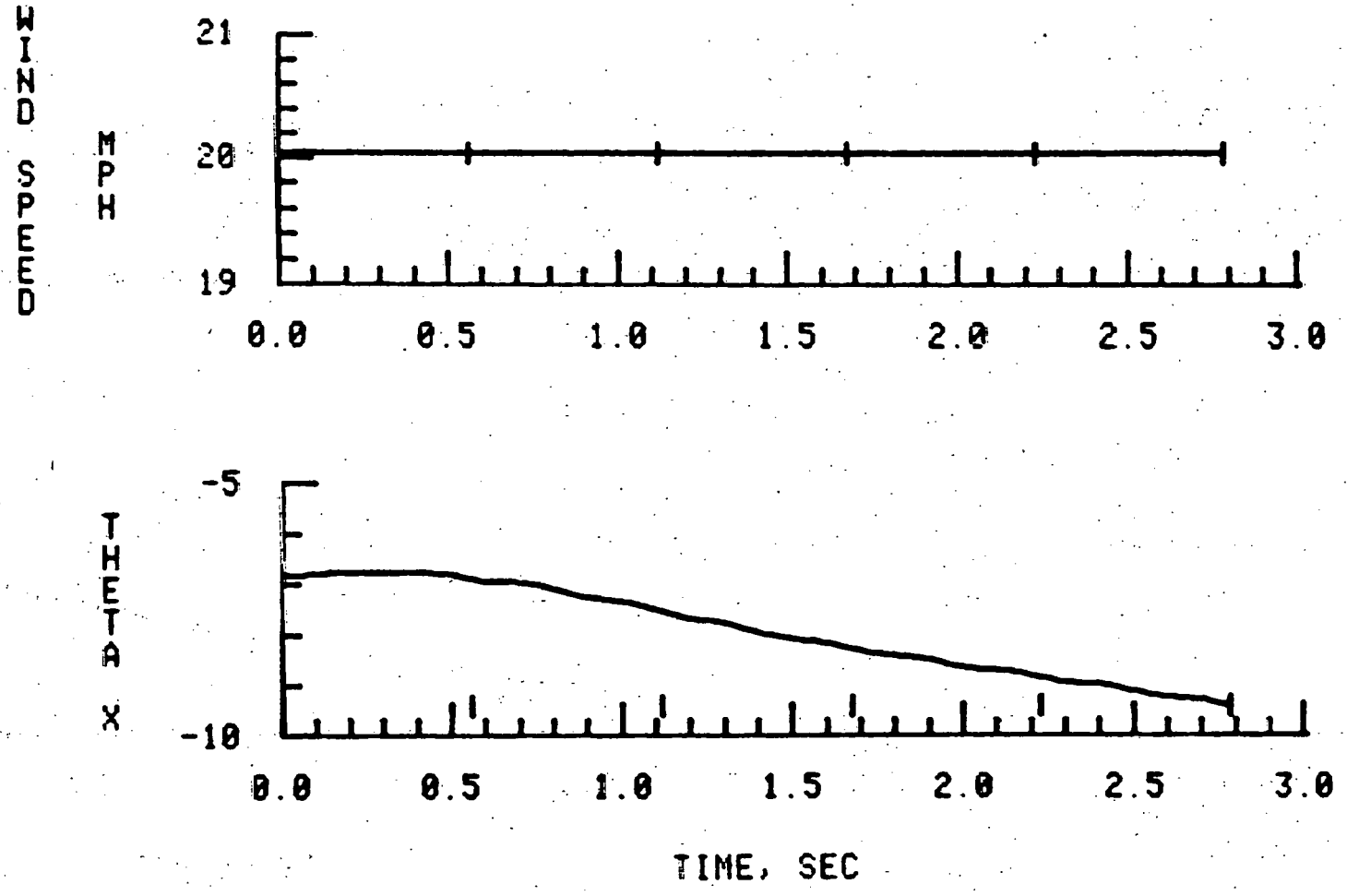

Fig. B-1 Rotor Response Characteristics, V=9 m/s, ΩR = 53.3 m/s

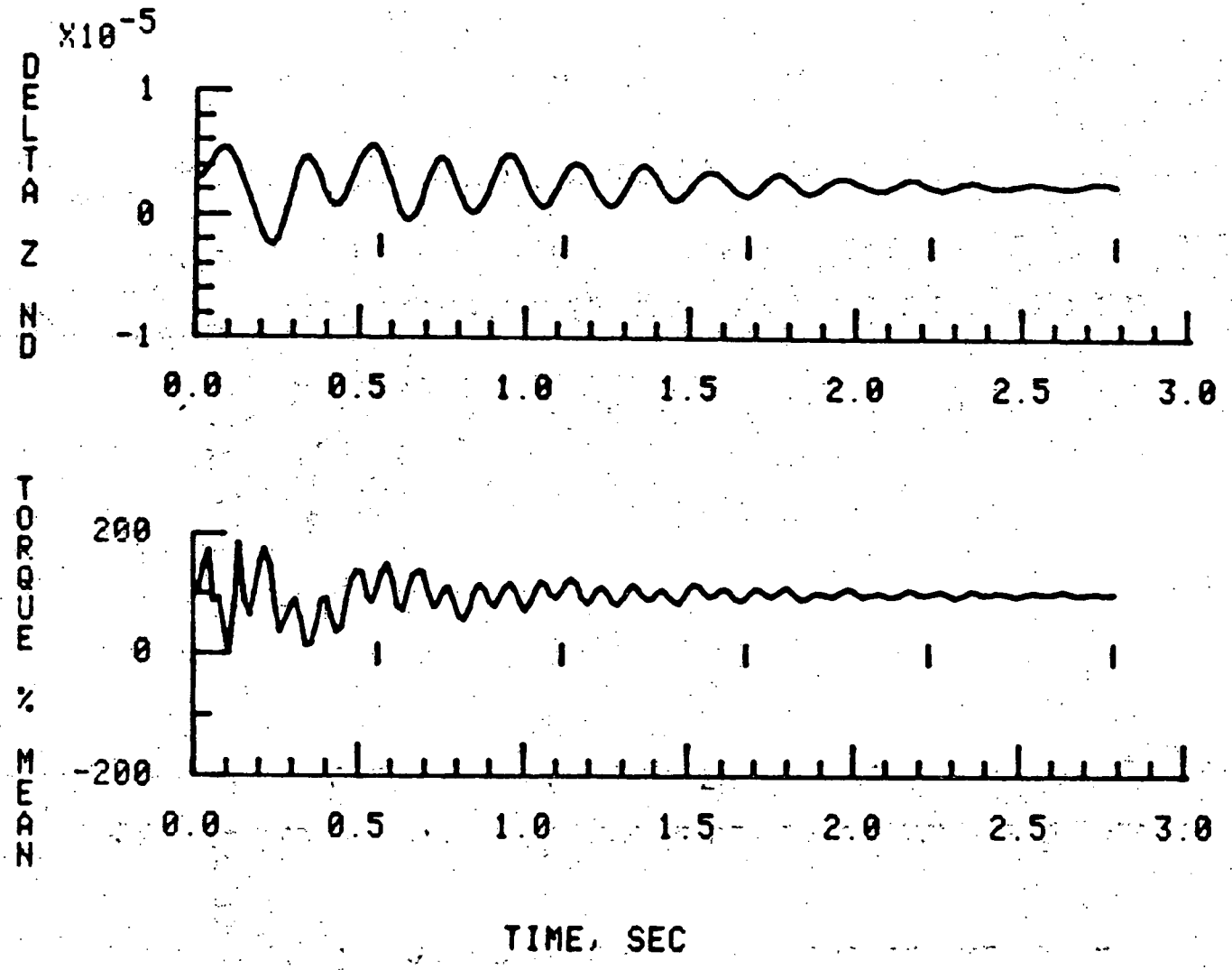

Fig. B-1 Continued

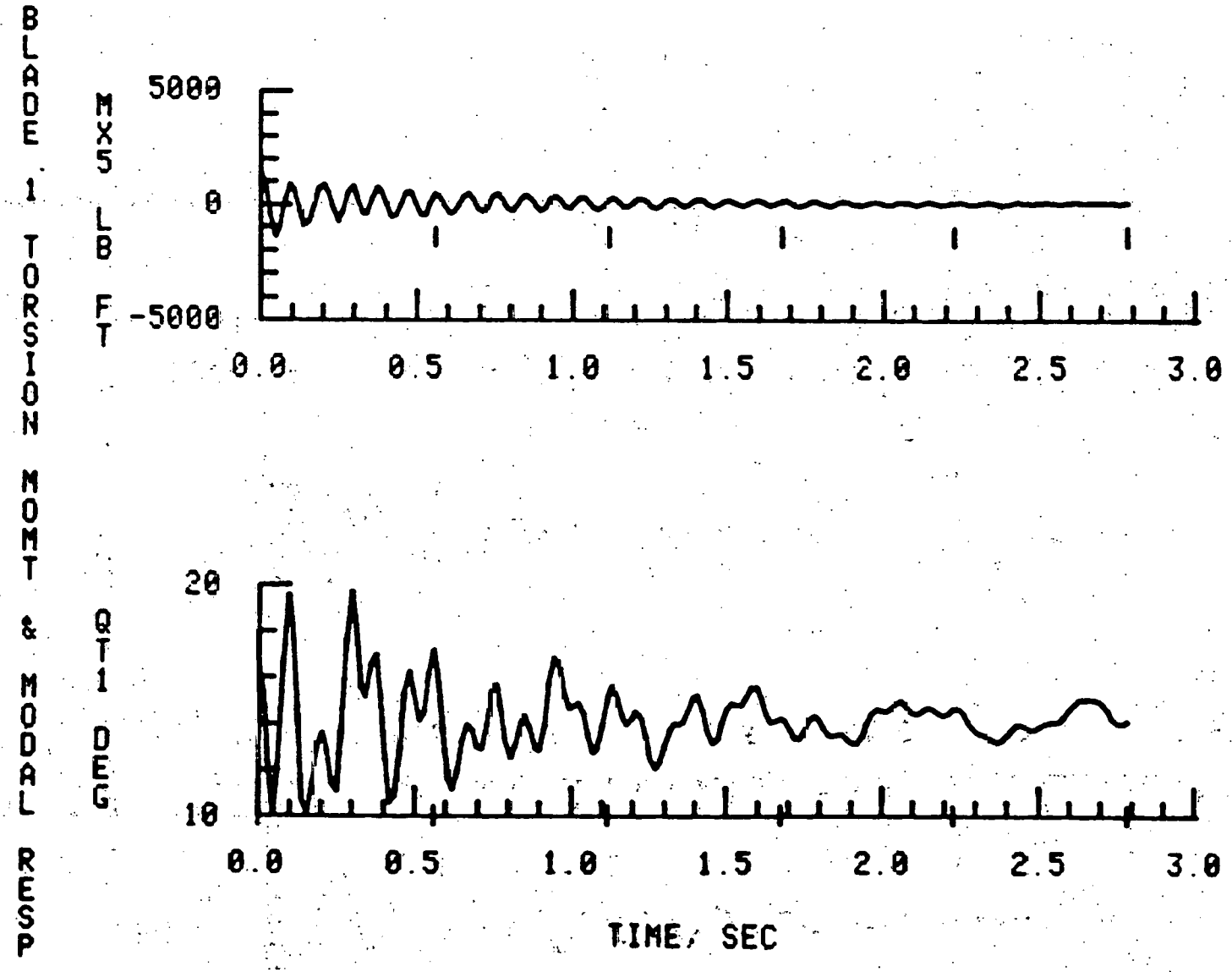

Fig. B-1 Continued

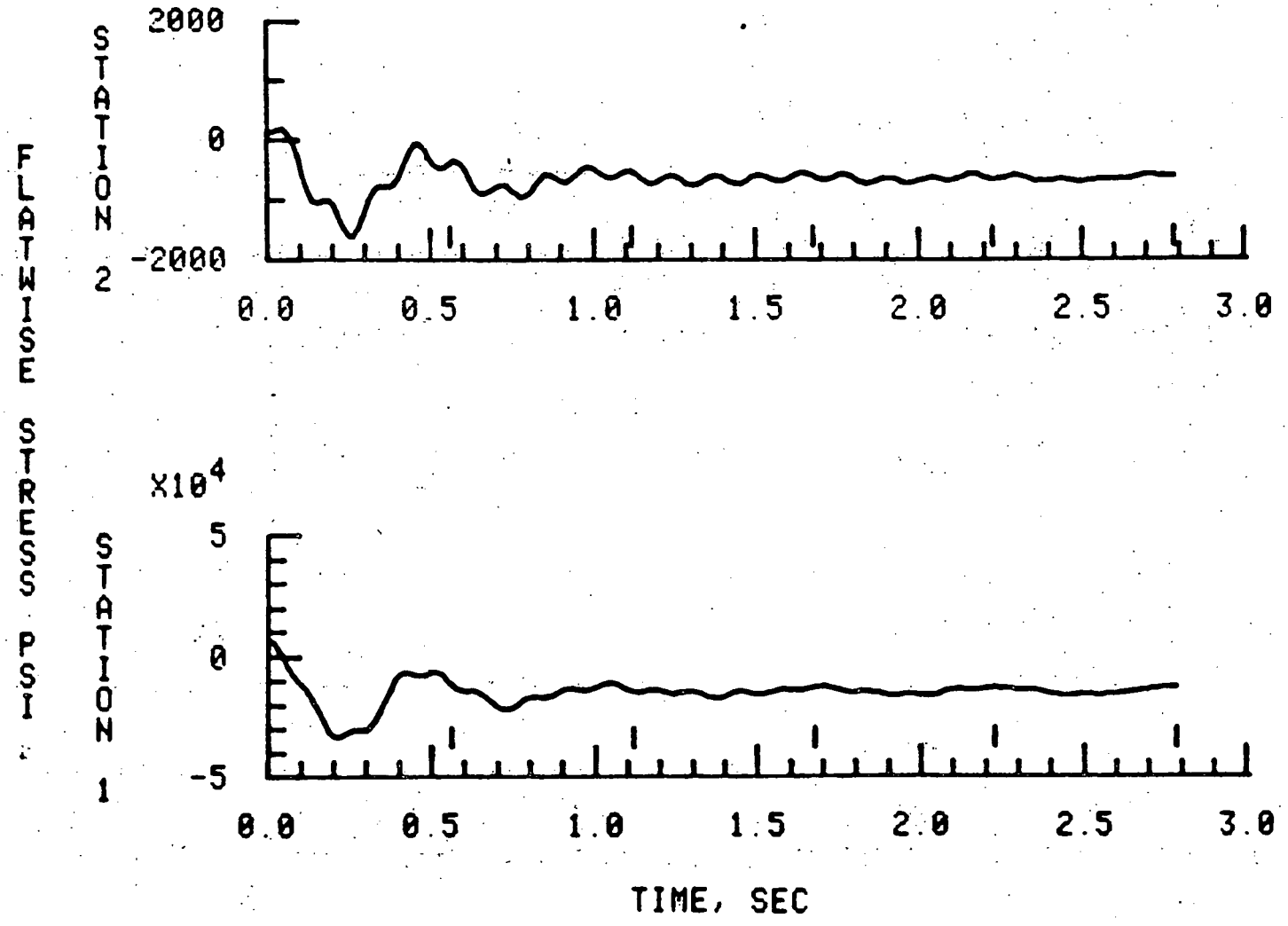

Fig. B-1 Continued

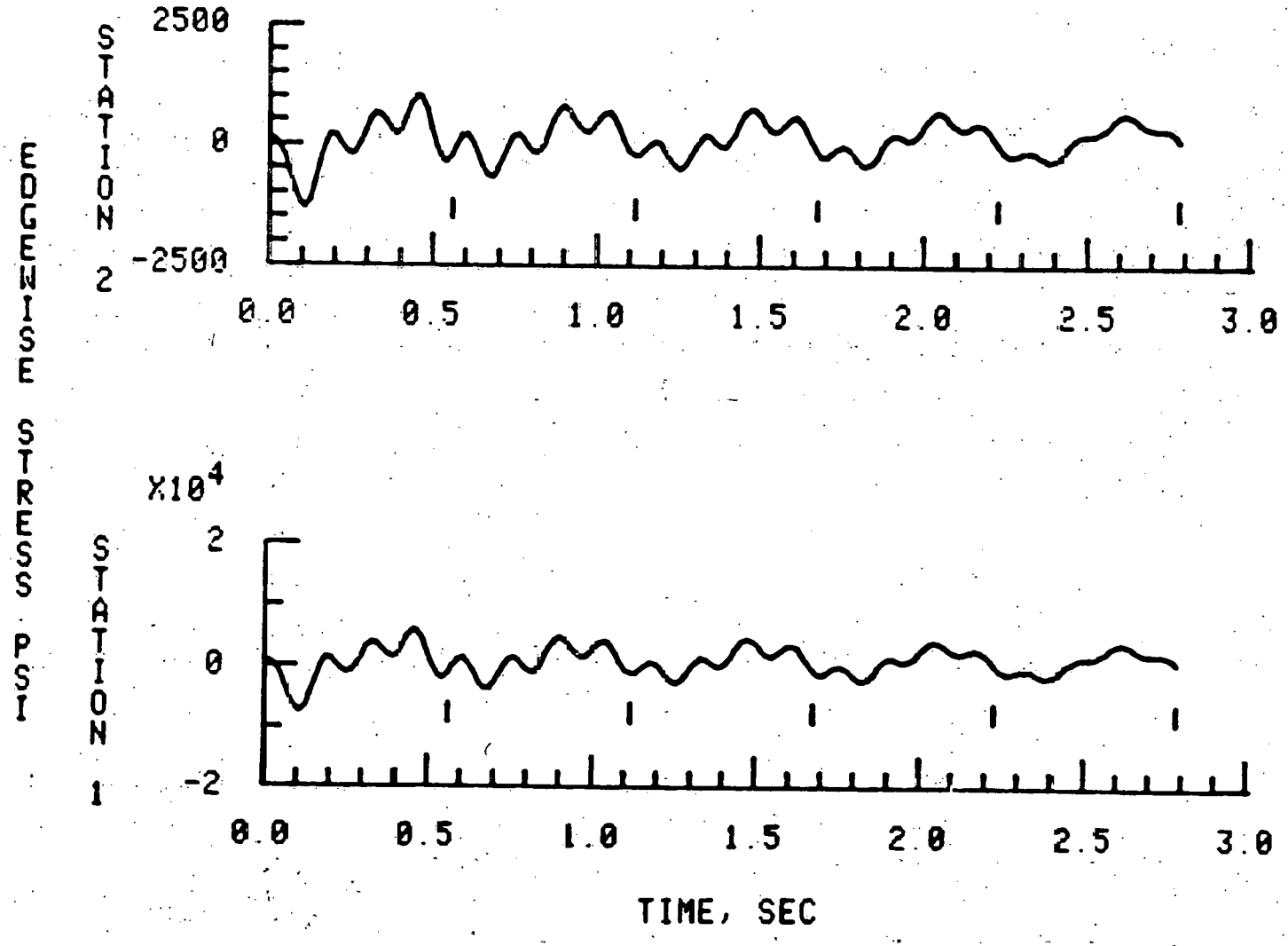

Fig. B-1 Continued

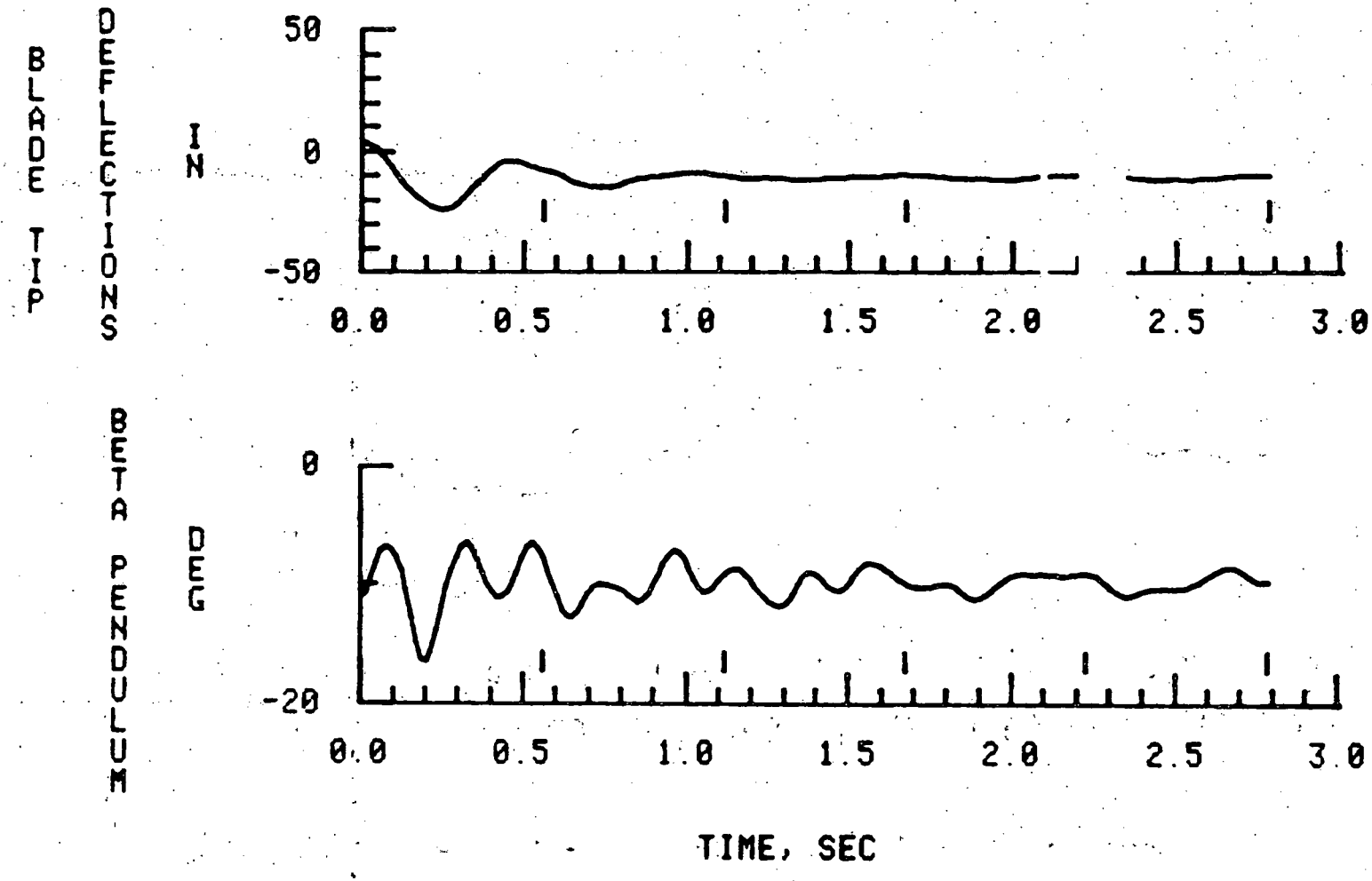

Fig. B-1 Concluded

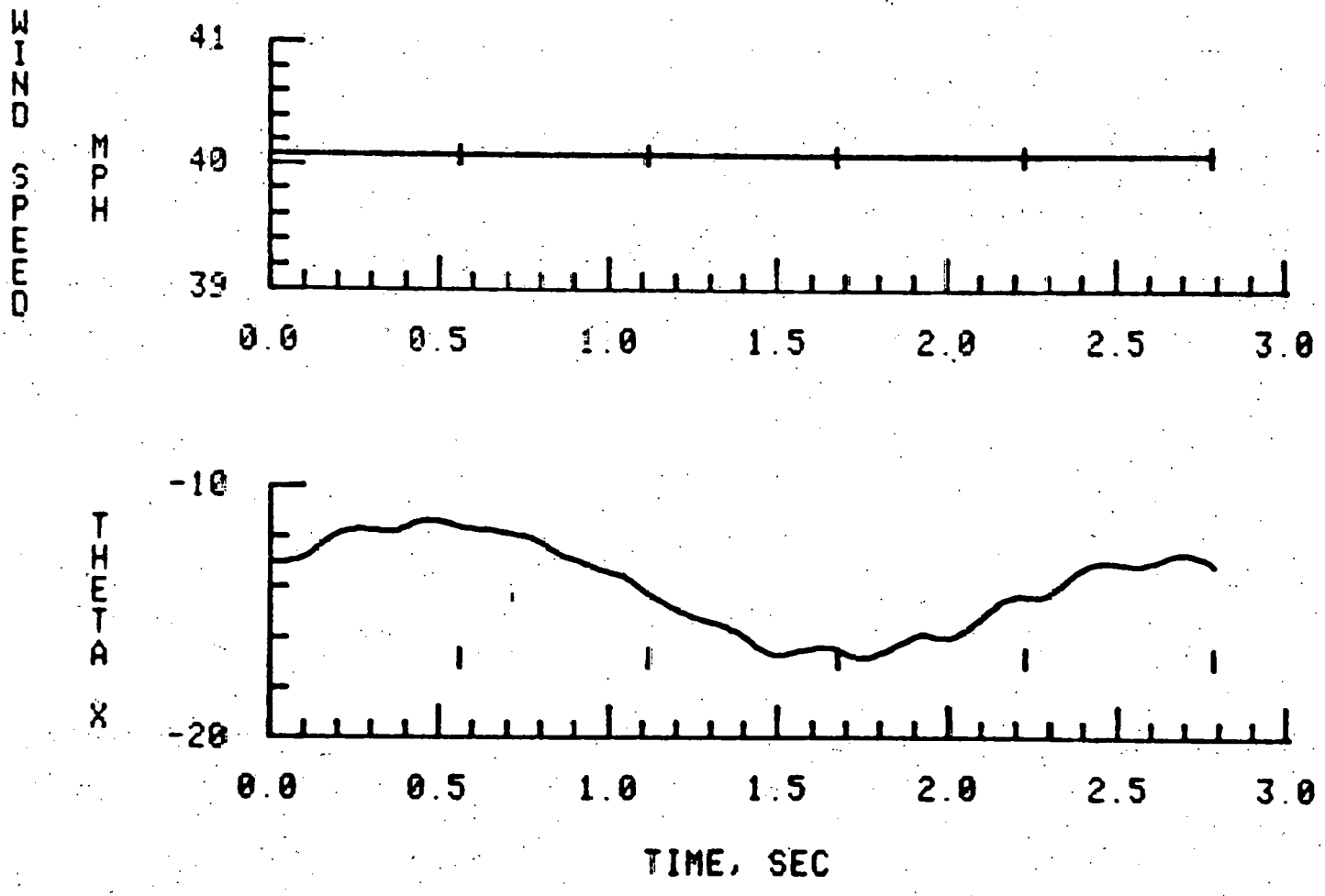

Fig. B-2 Rotor Response Characteristics, V=19 m/s ΩR = 53.3 m/s

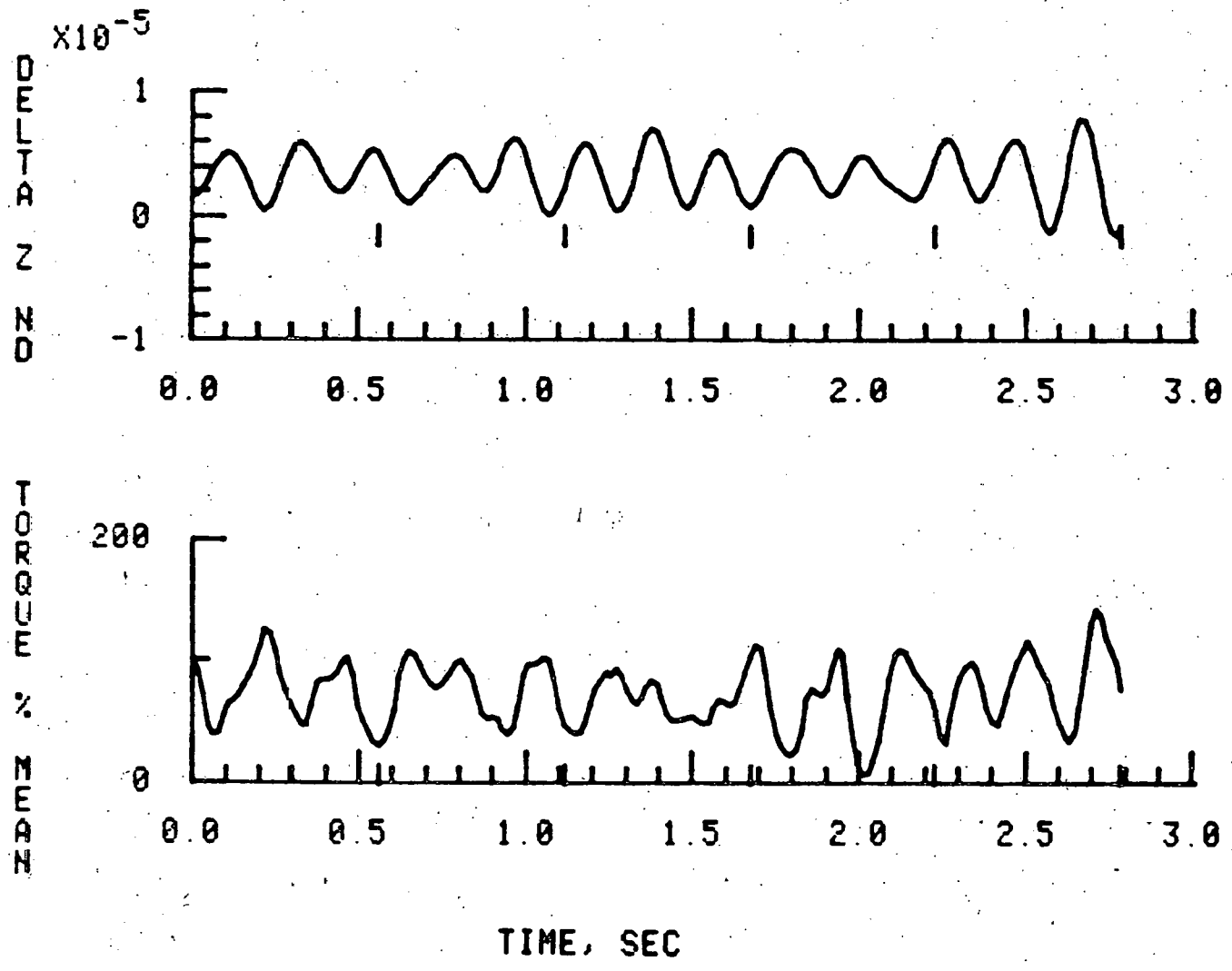

Fig. B-2 Continued

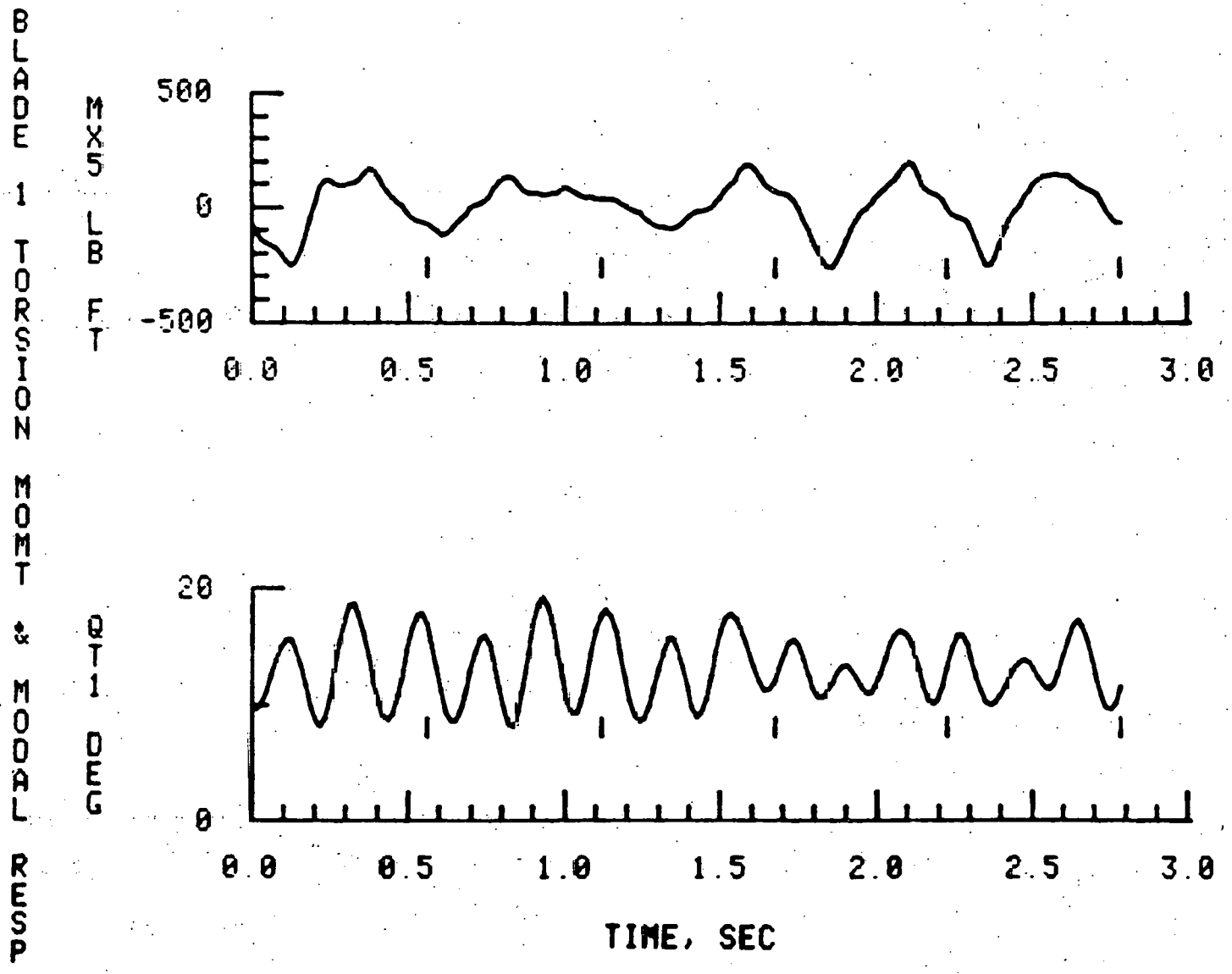

Fig. B-2 Continued

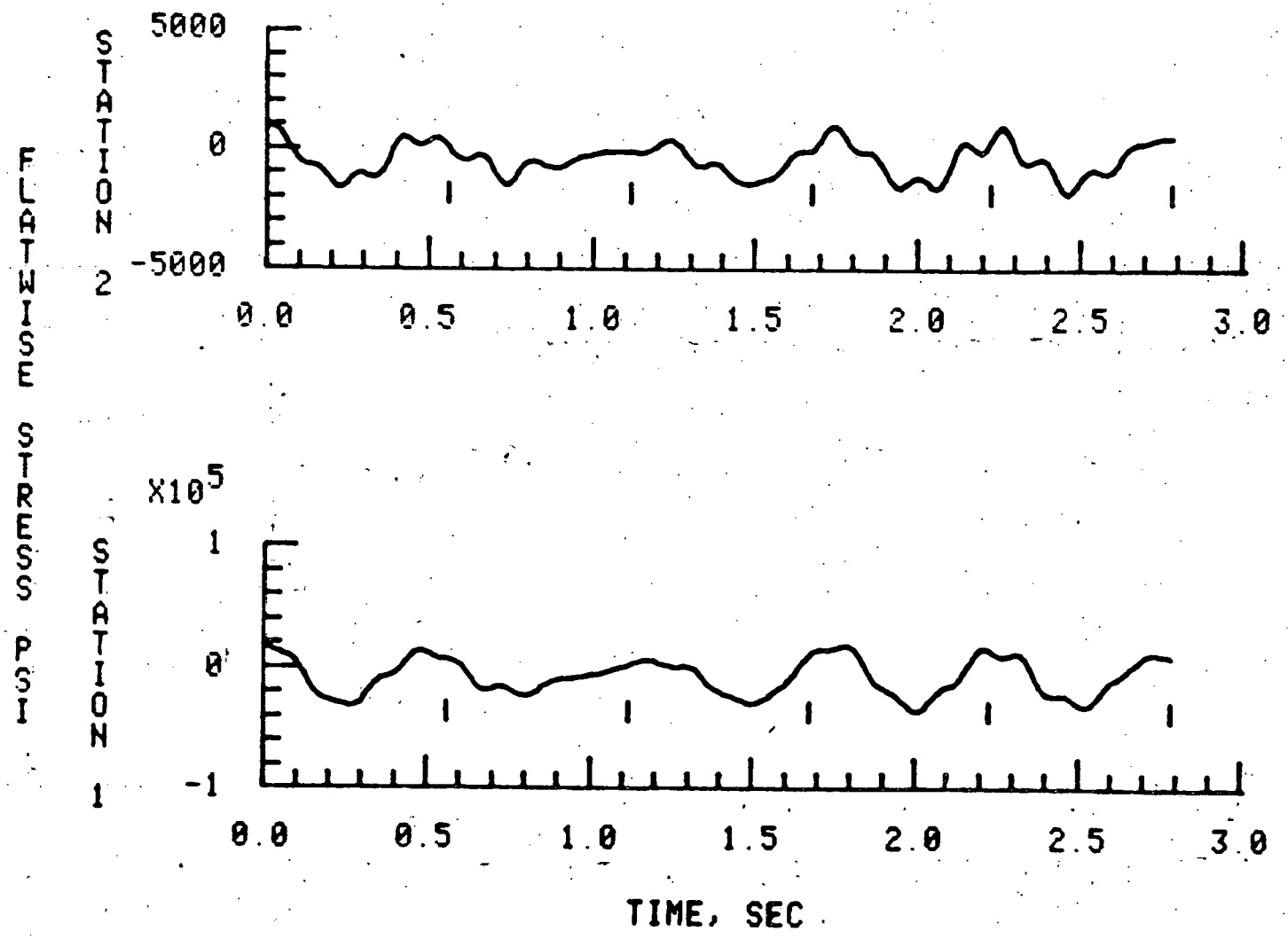

Fig. B-2 Continued

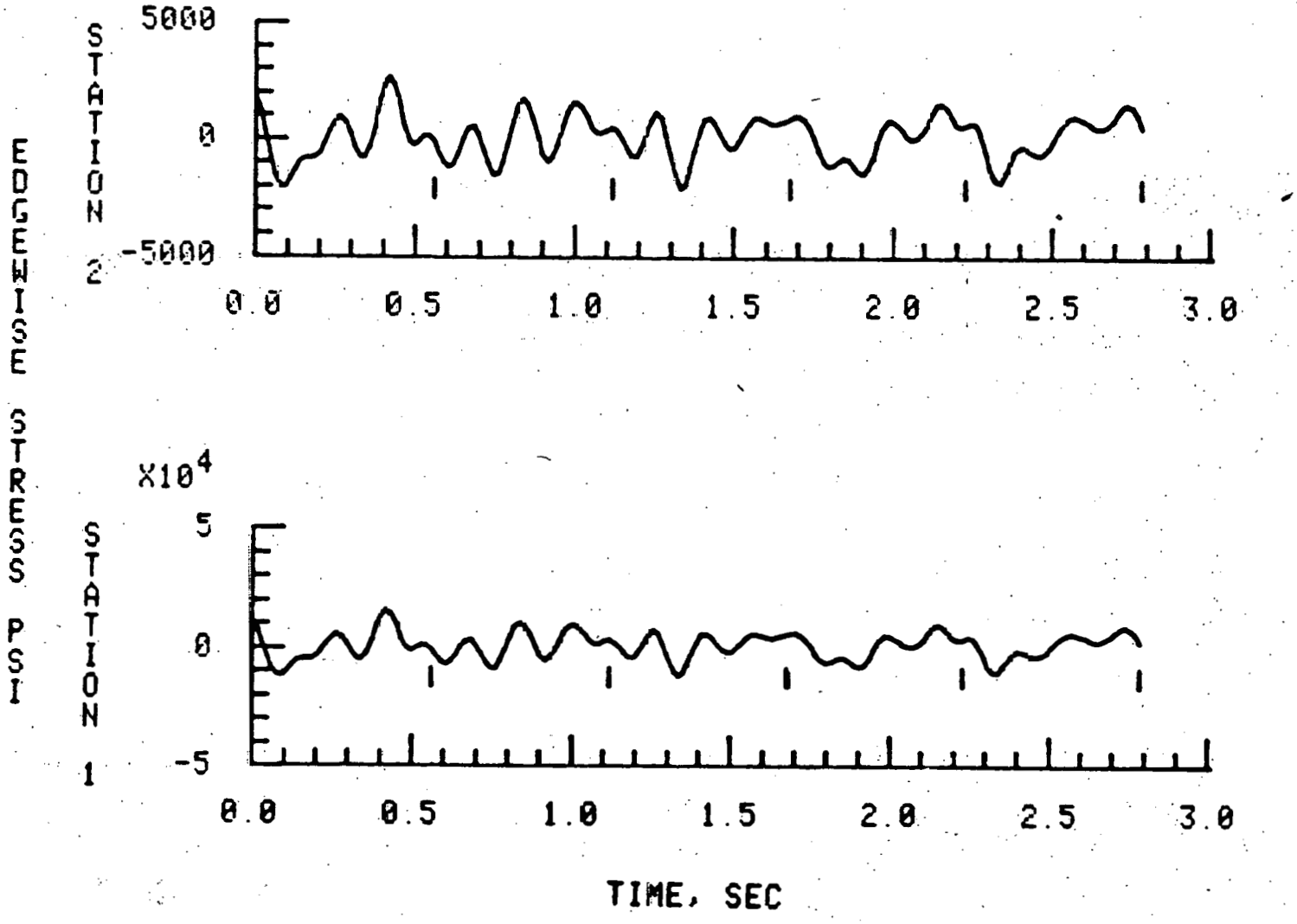

Fig. B-2 Continued

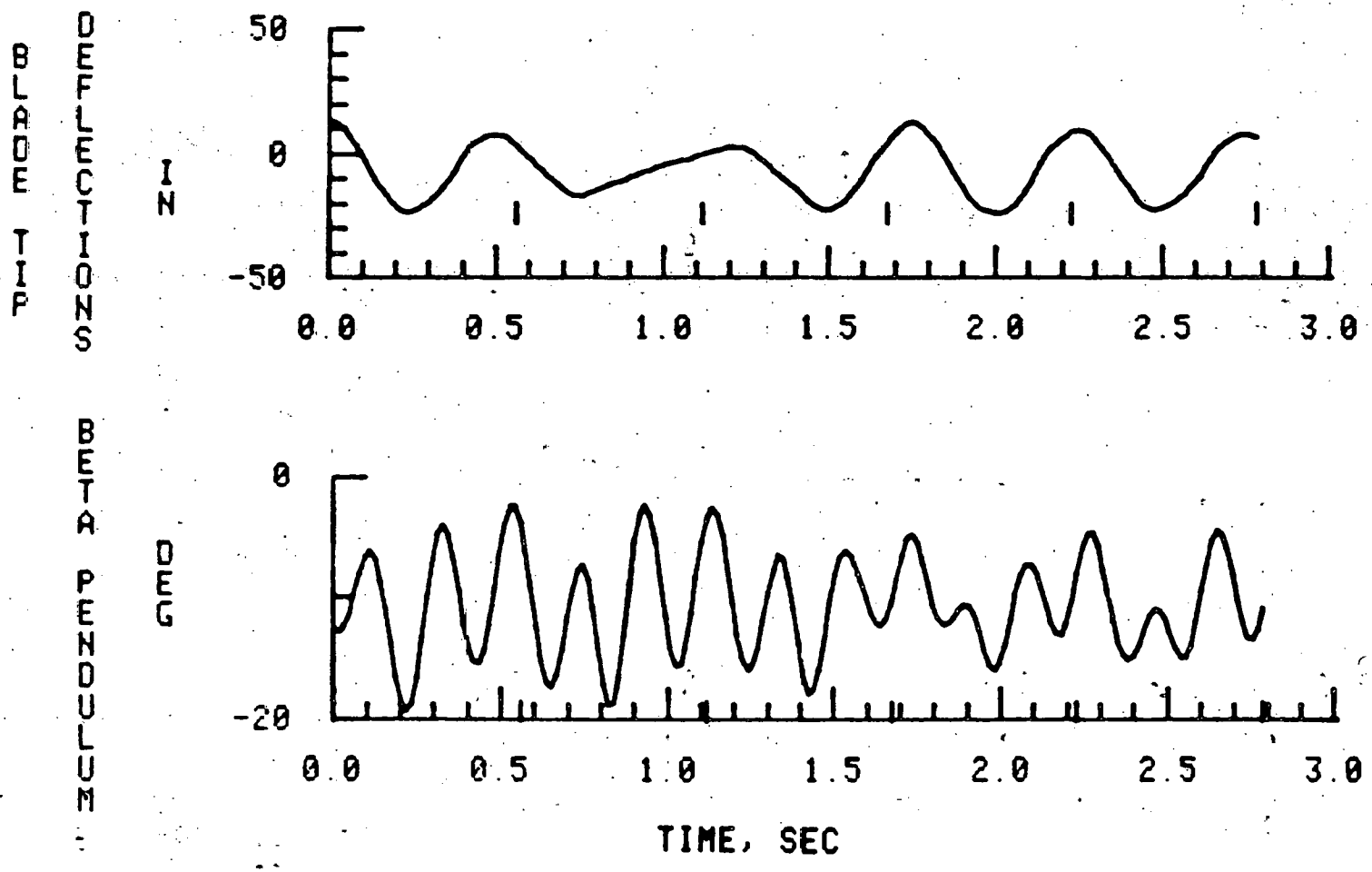

Fig. B-2 Concluded

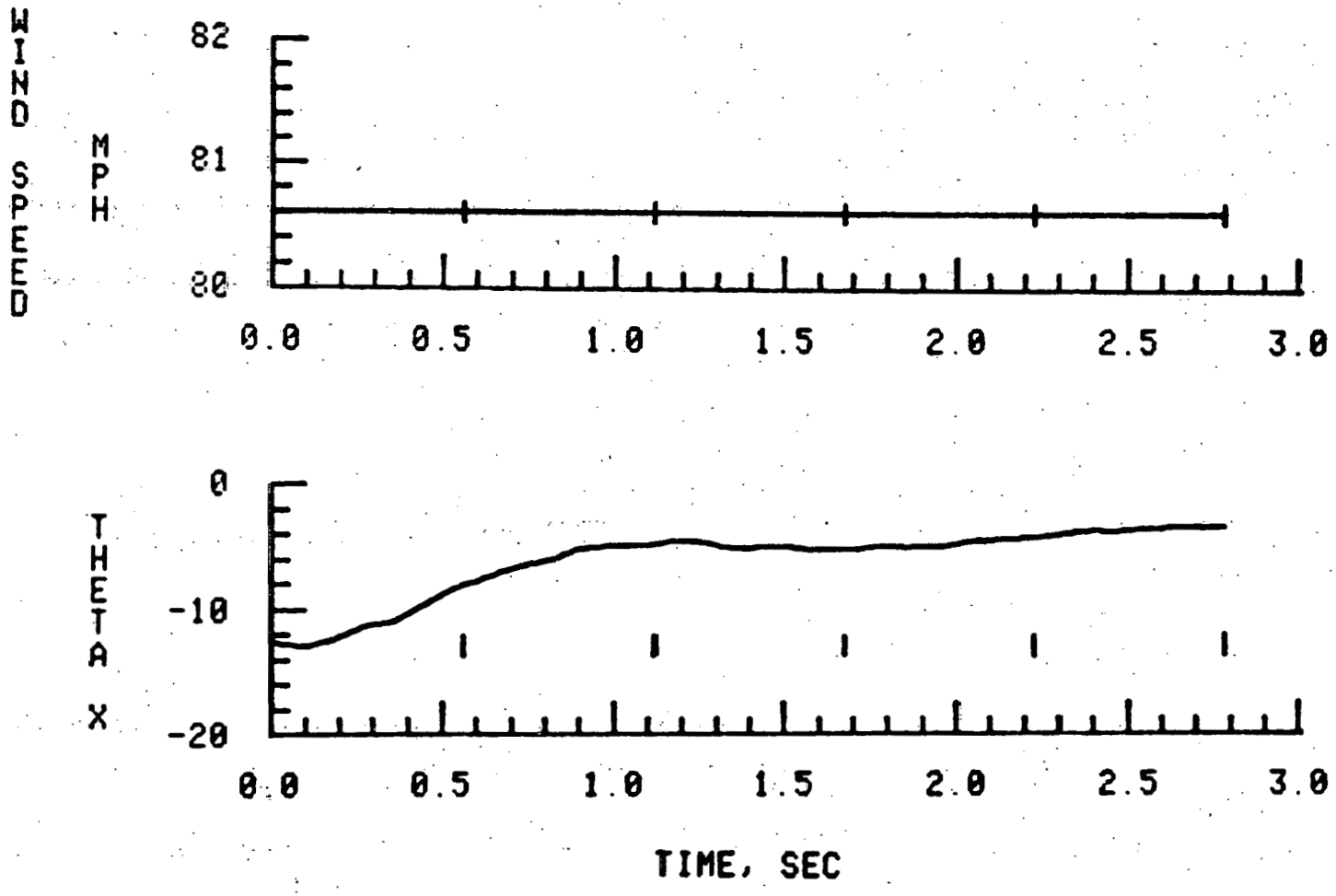

Fig. B-3 Rotor Response Characteristics, V_w = 36 m/s, ΩR = 53.3 m/s

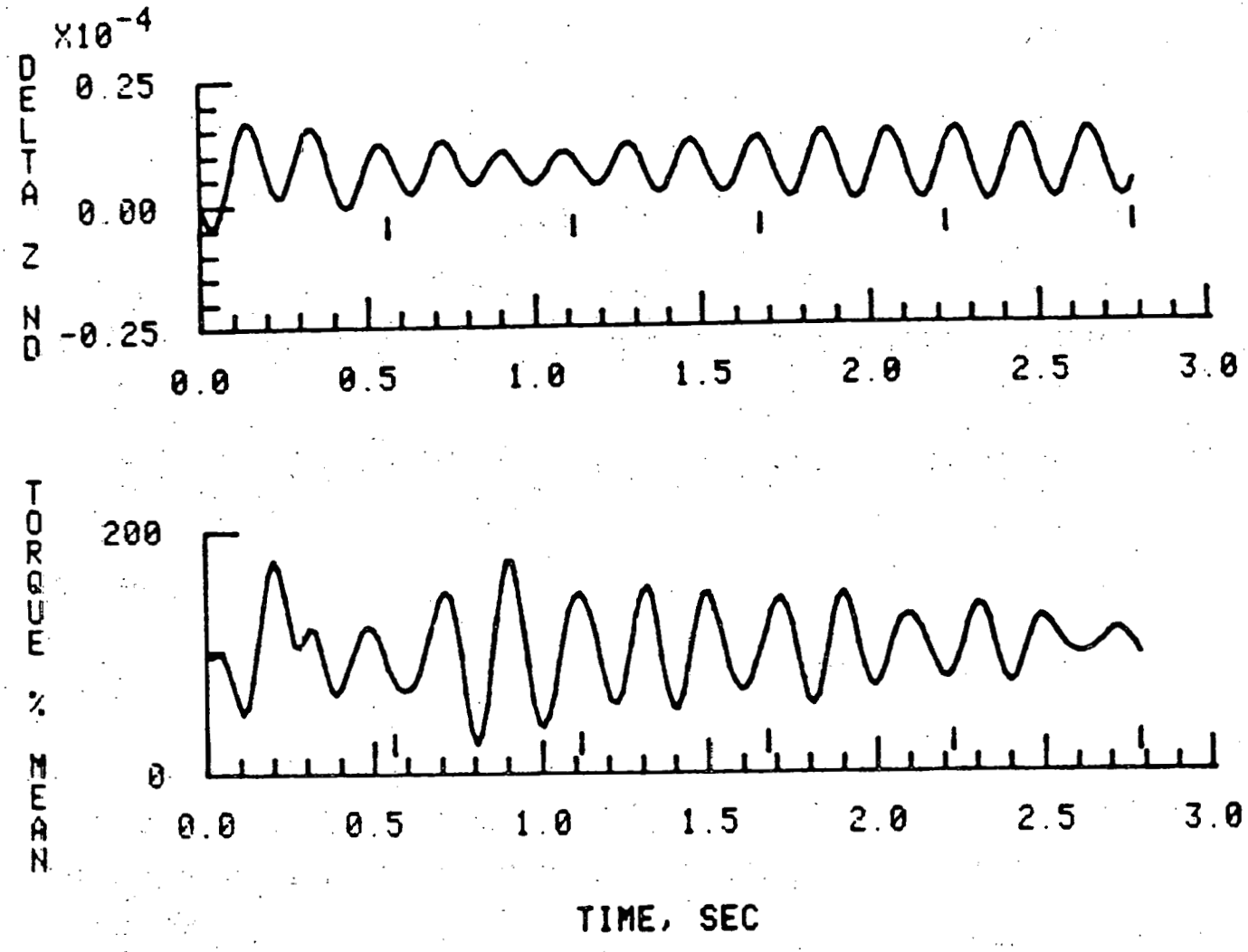

Fig. B-3 Continued

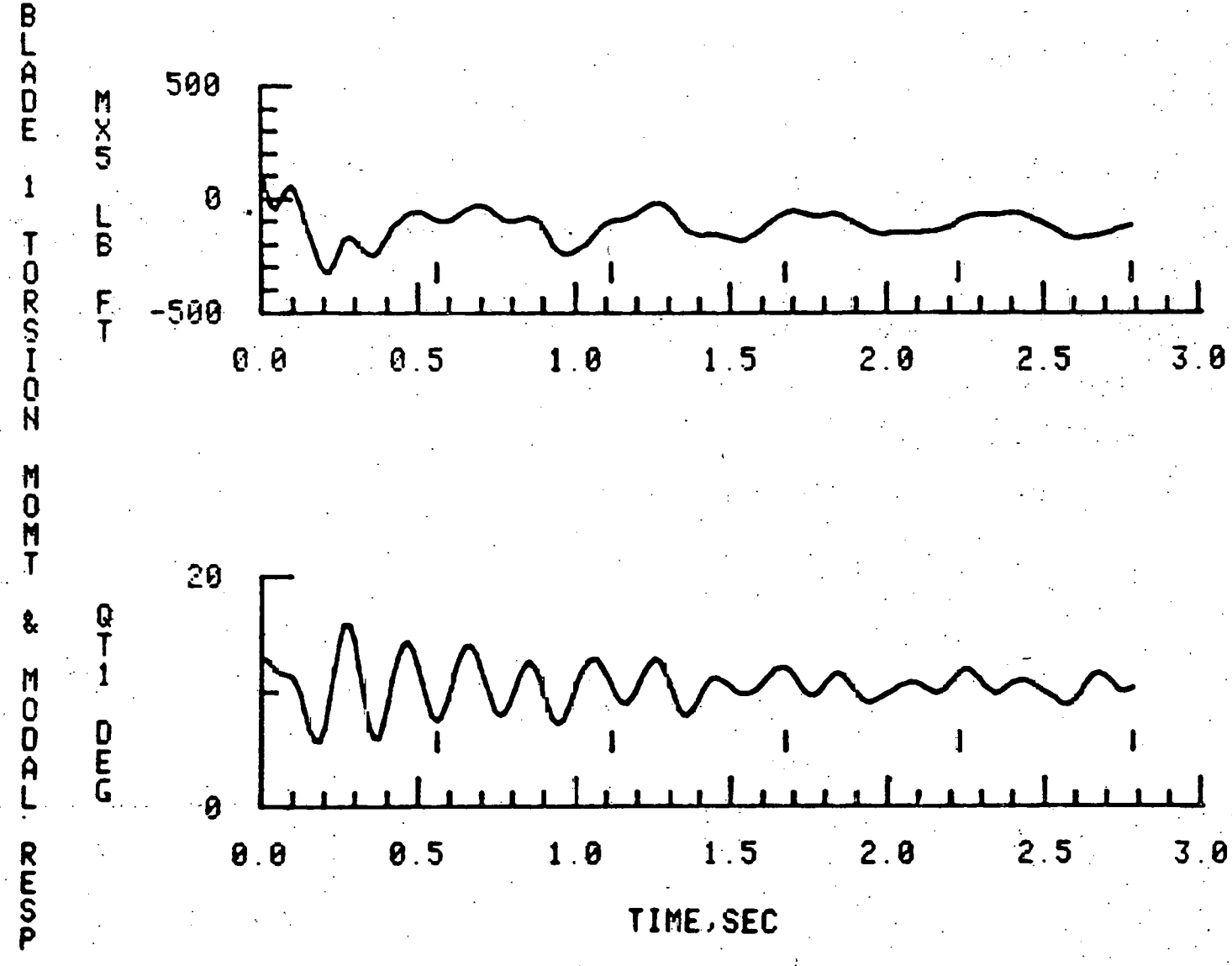

Fig. B-3 Continued

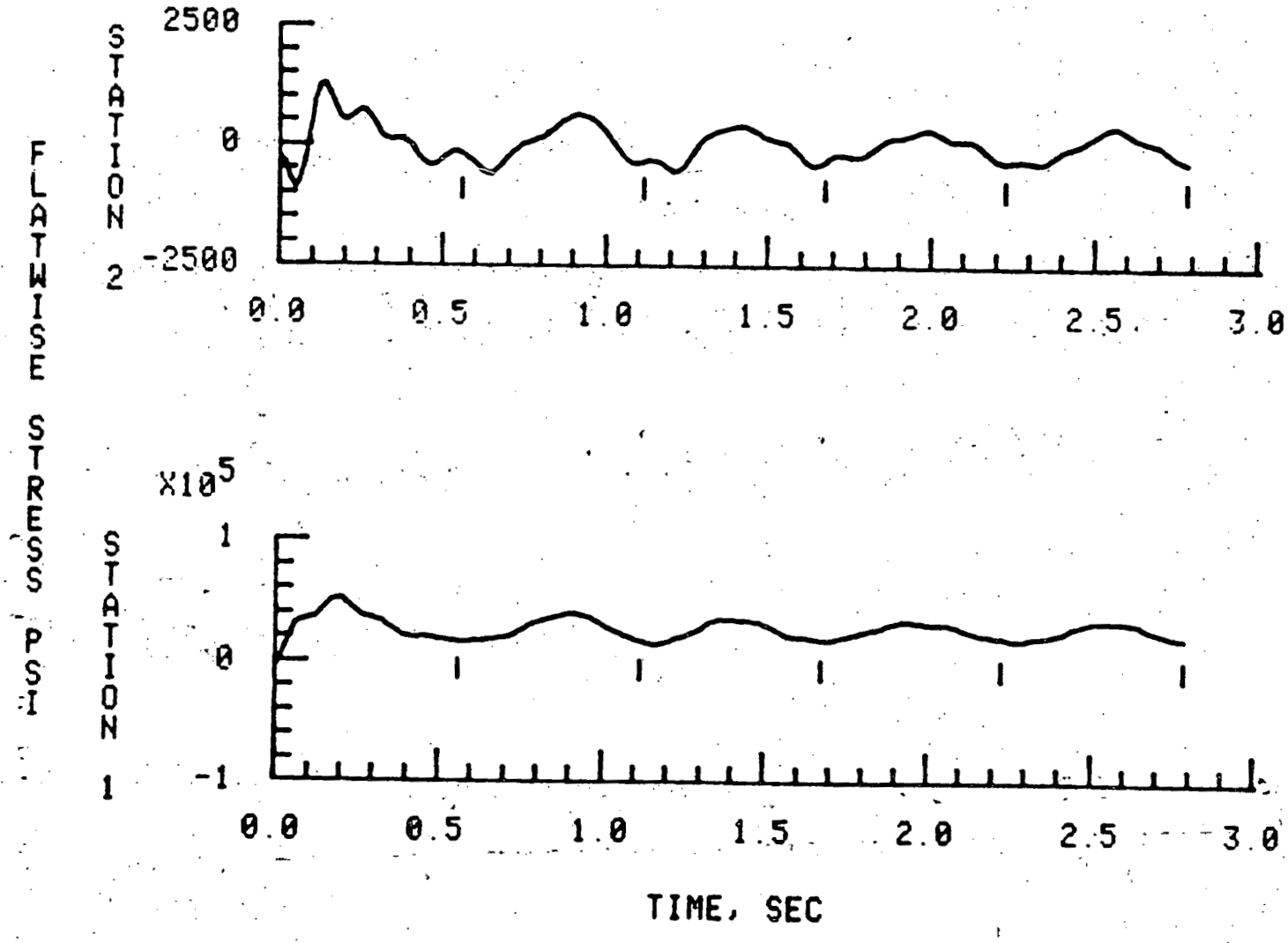

Fig. B-3 Continued

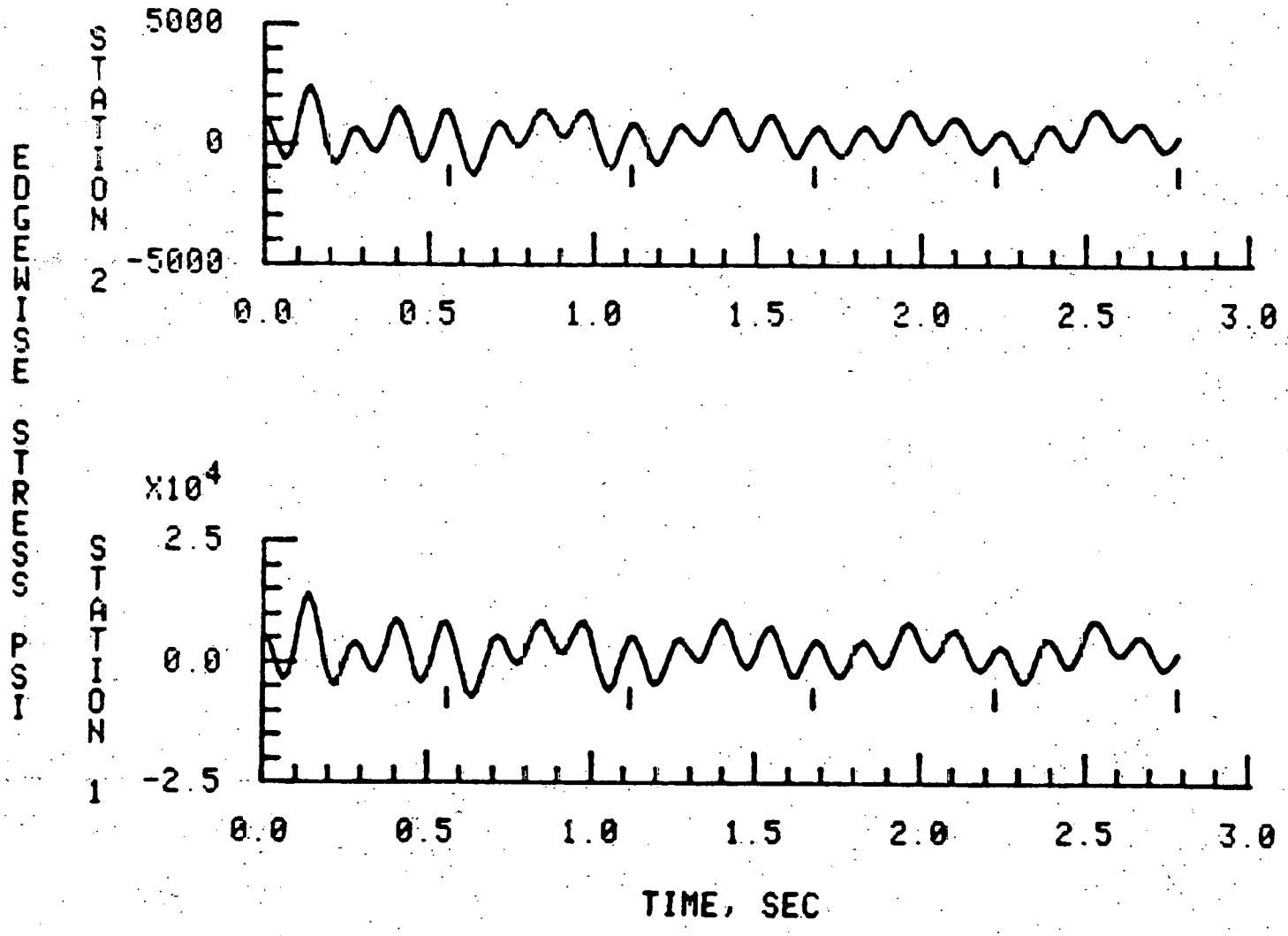

Fig. B-3 Continued

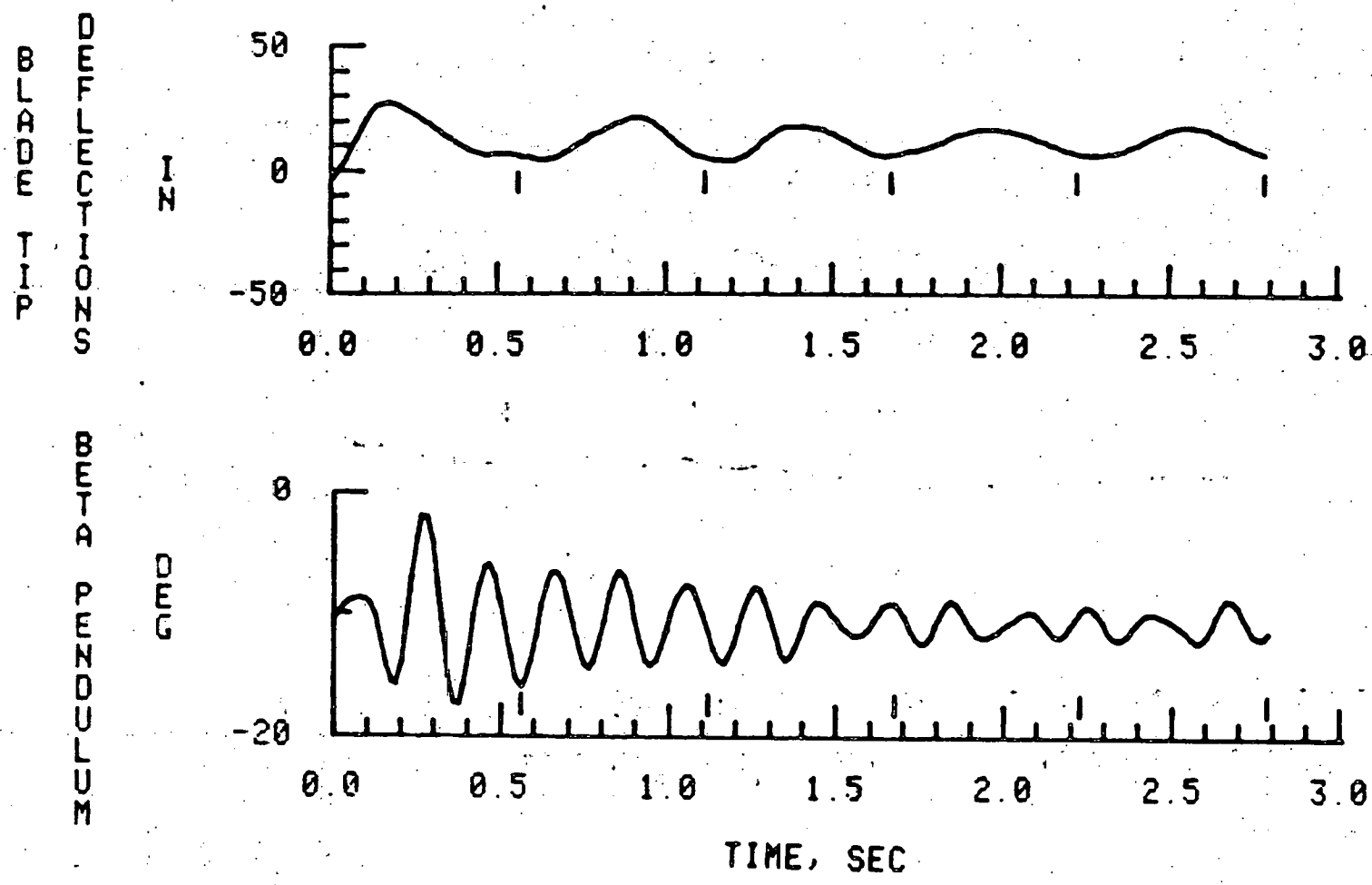

Fig. B-3 Concluded

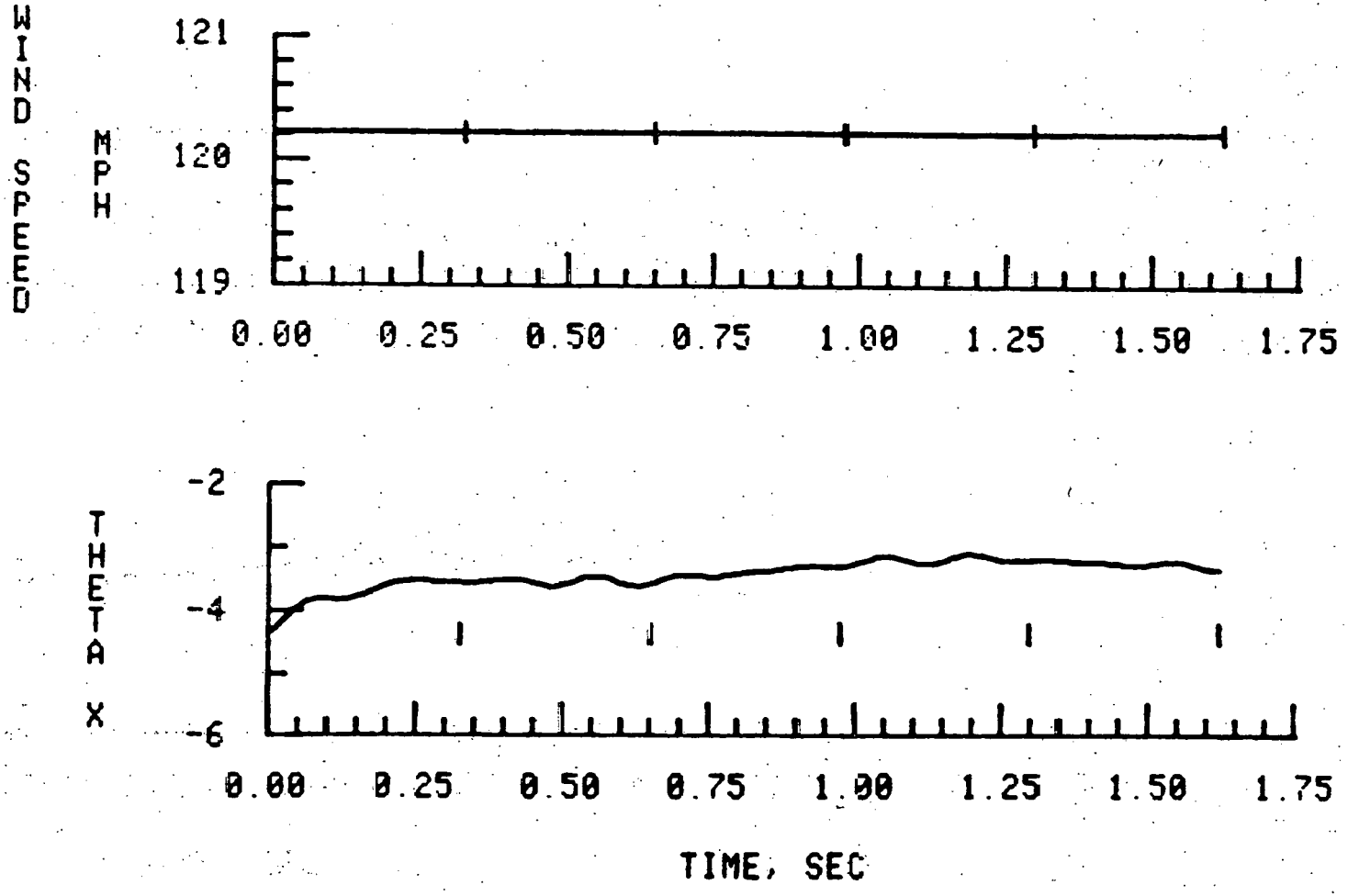

Fig. B-4 Rotor Response Characteristics, V_w = 54 m/s, ΩR = 91 m/s

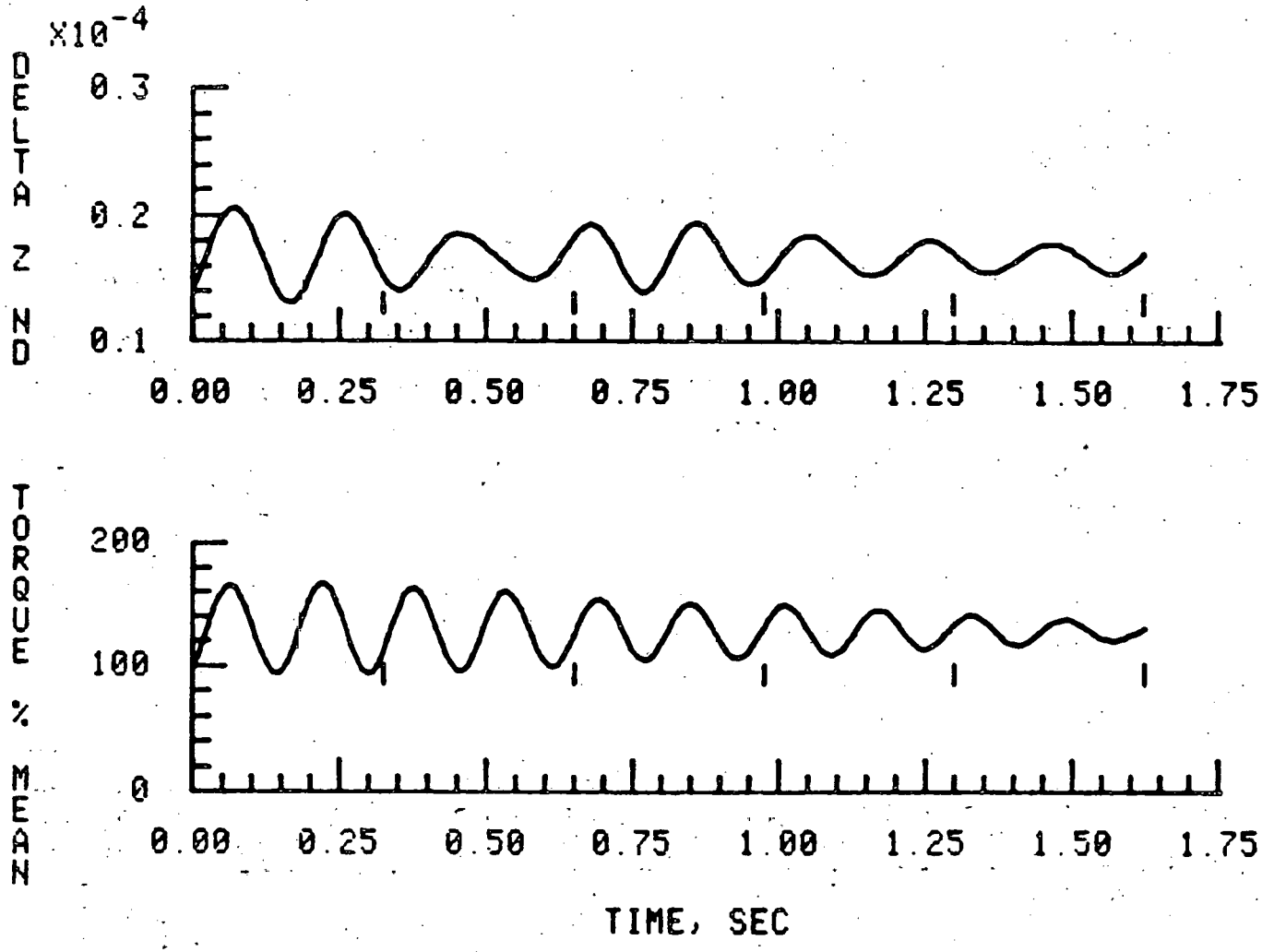

Fig. B-4 Continued

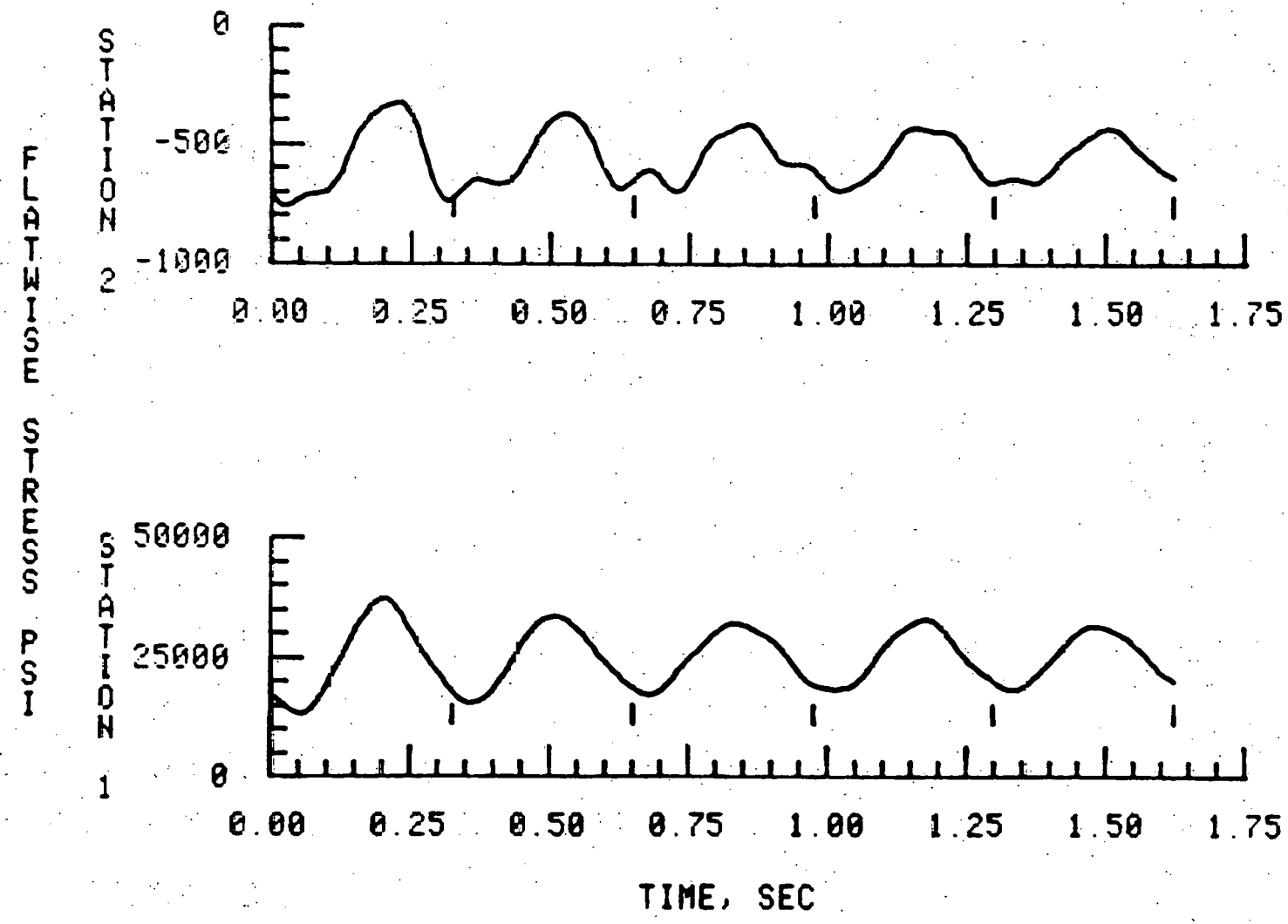

Fig. B-4 Continued

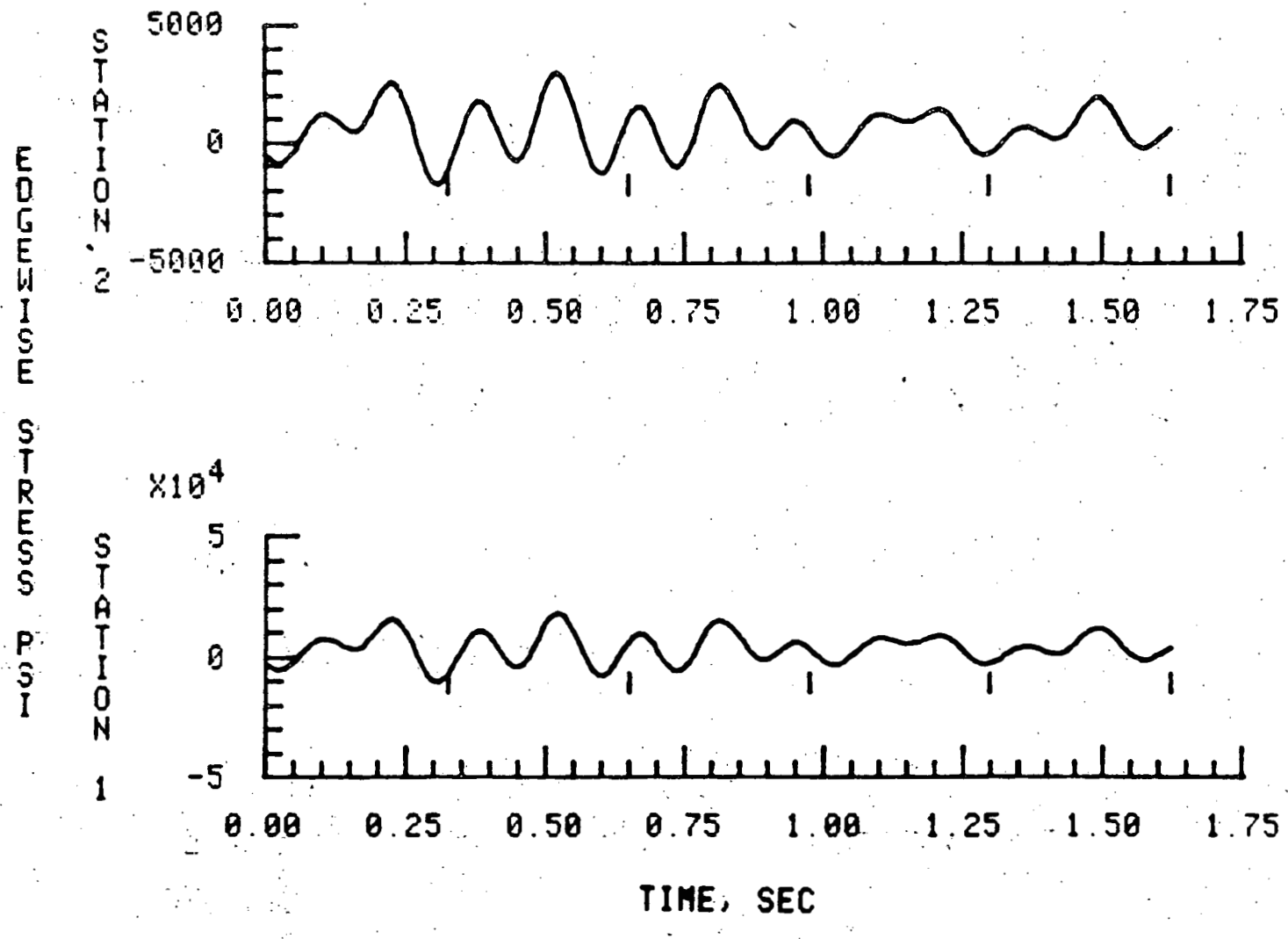

Fig. B-4 Continued

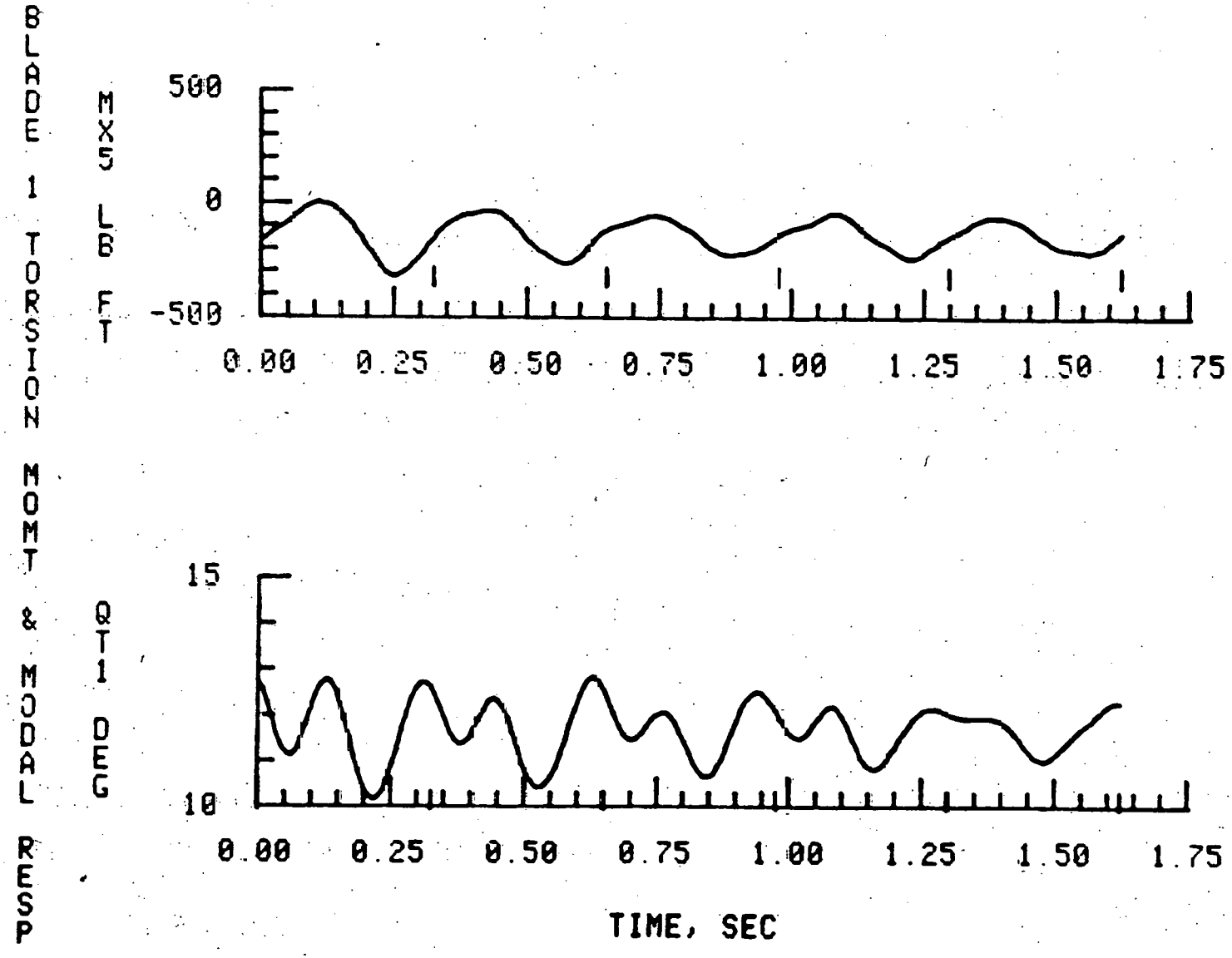

Fig. B-4 Continued

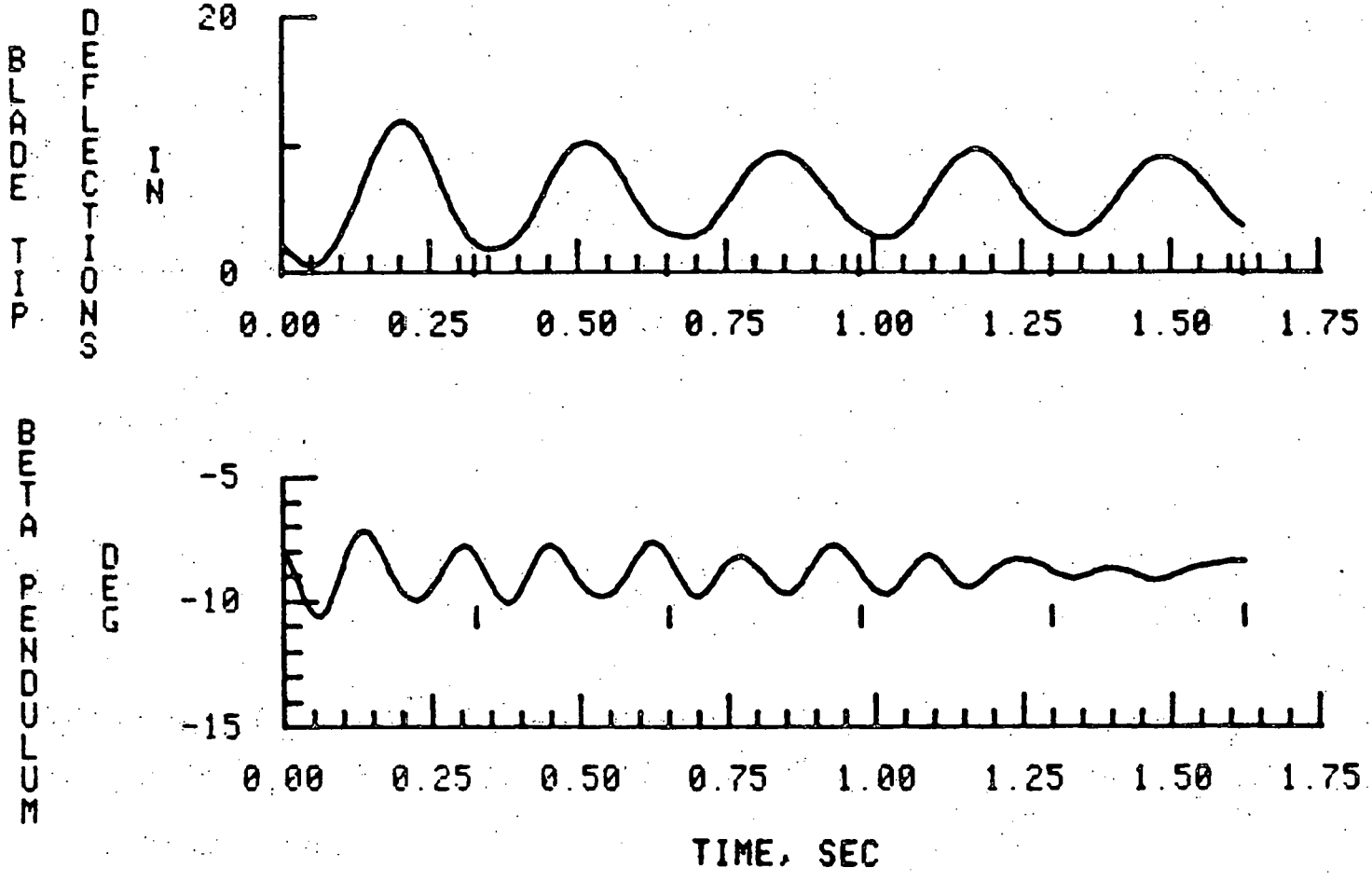

Fig. B-4 Concluded

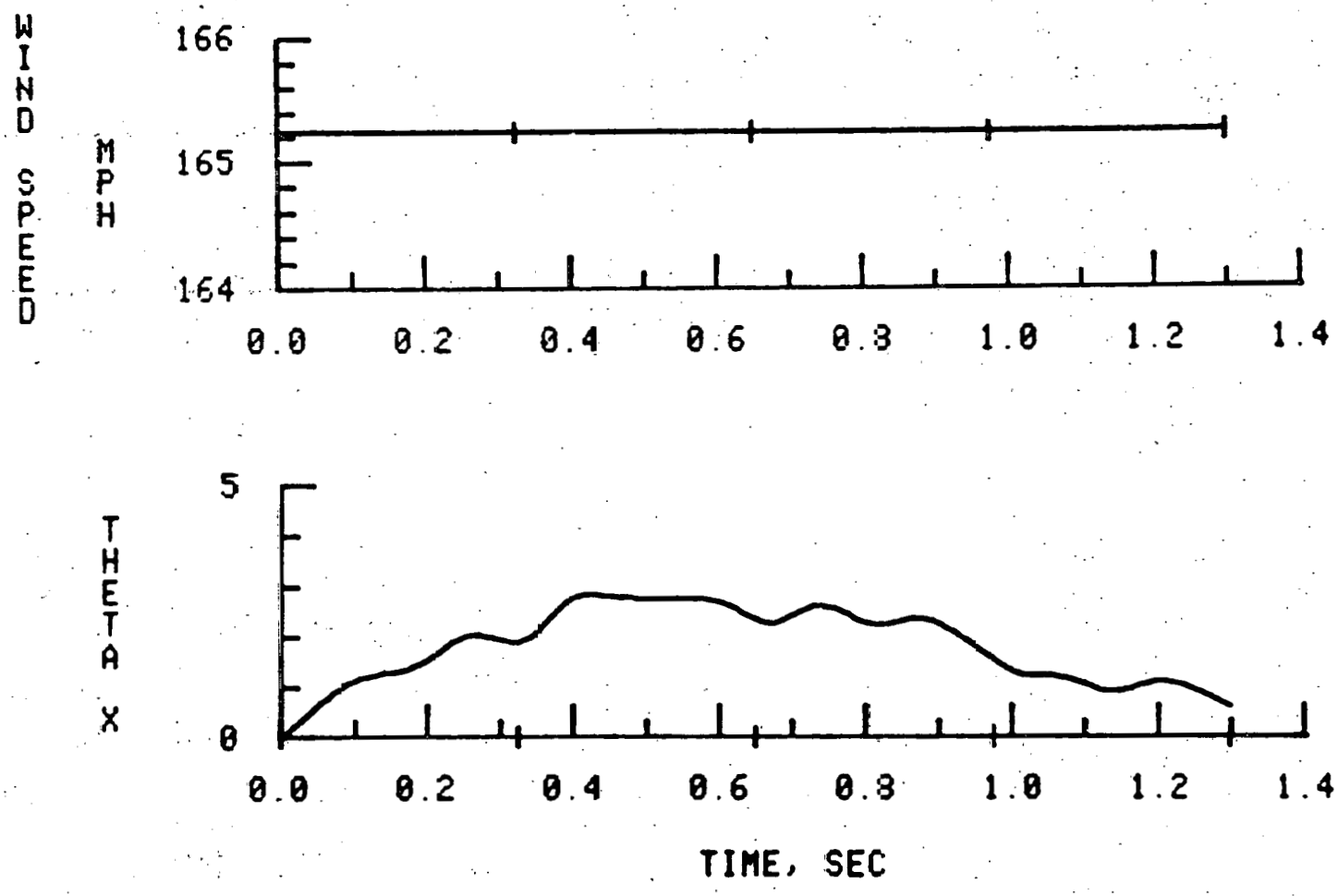

Fig. B-5 Rotor Response Characteristics, V_w = 75 m/s ΩR = 91 m/s

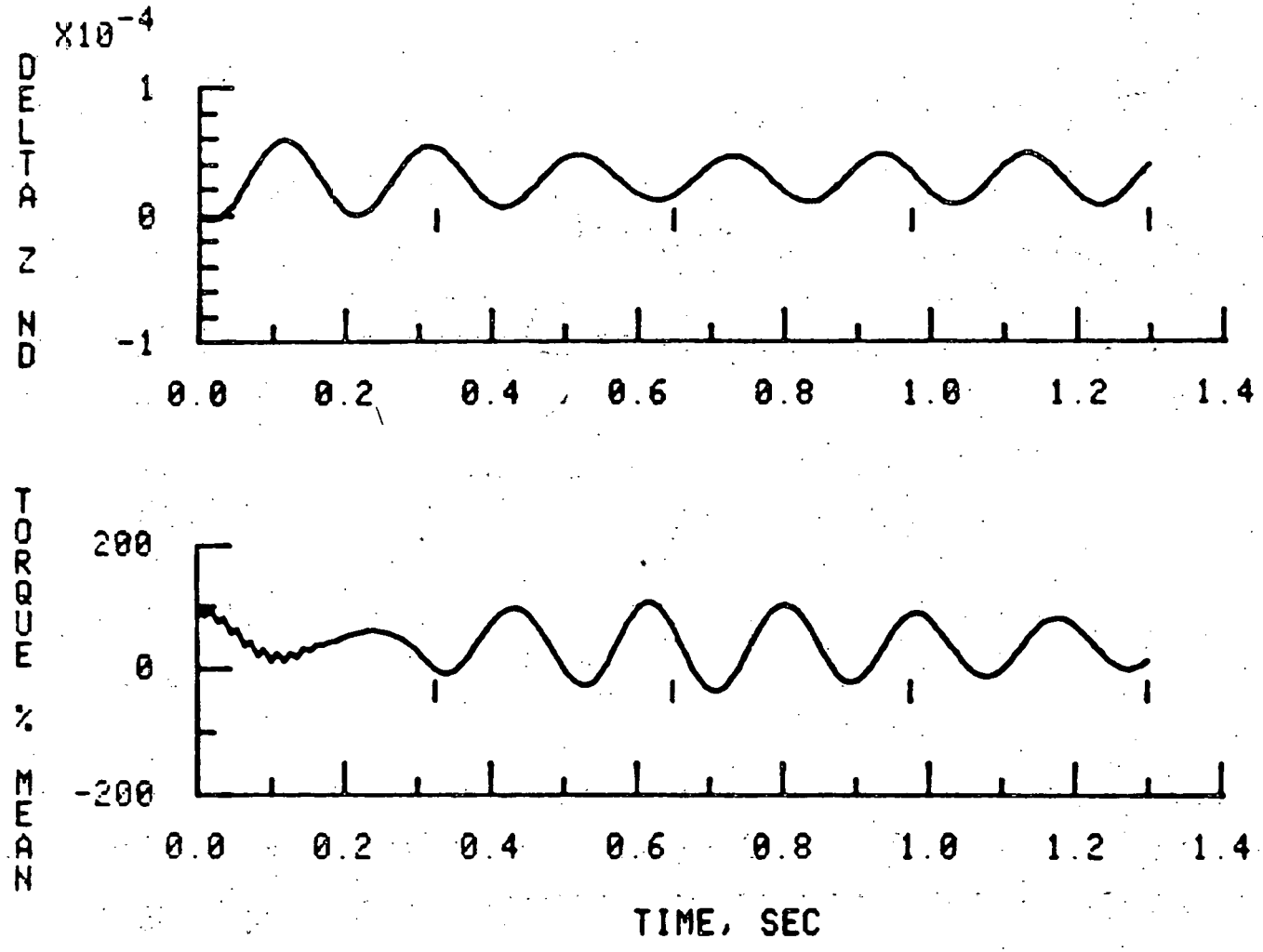

Fig. B-5 Continued

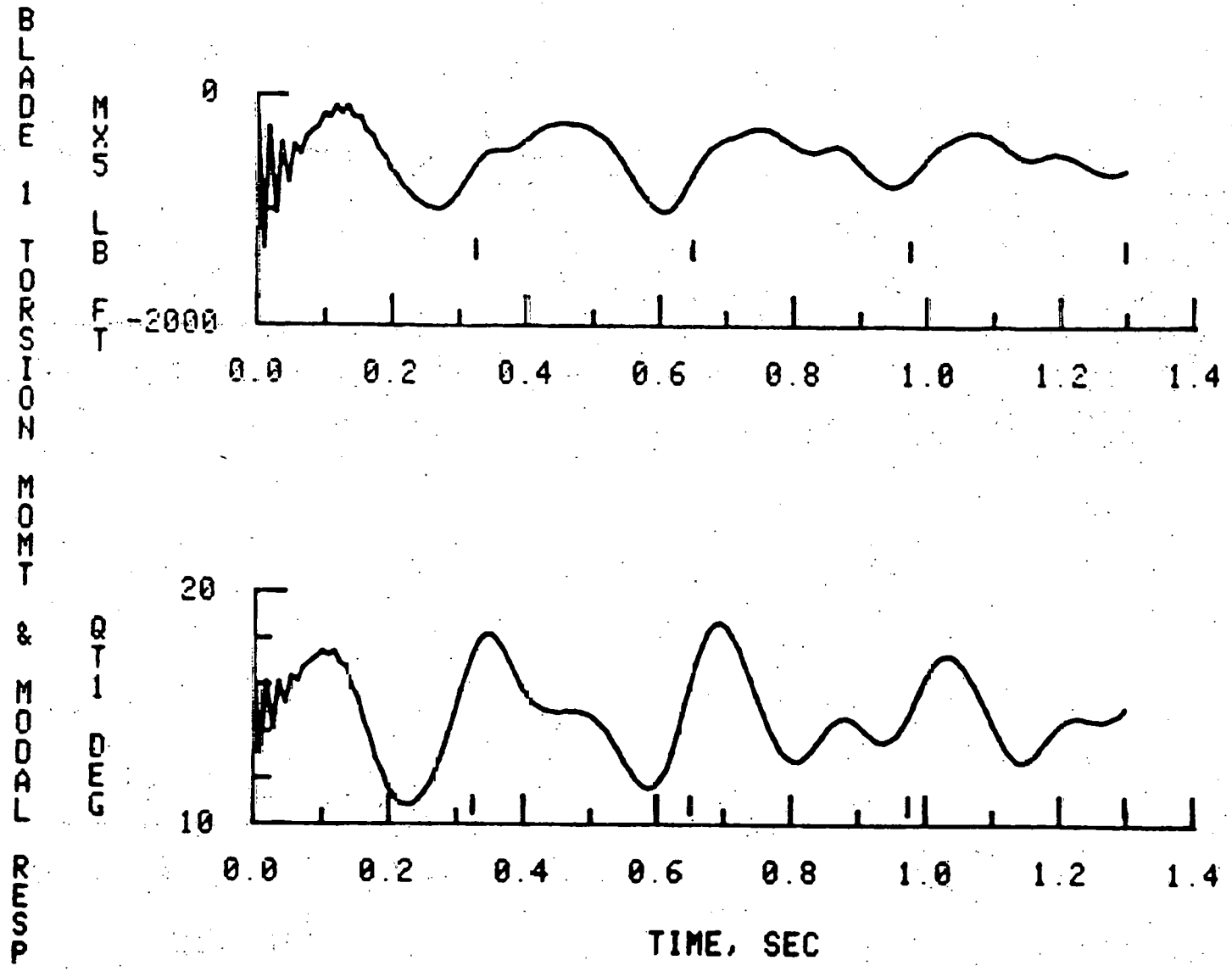

Fig. B-5 Continued

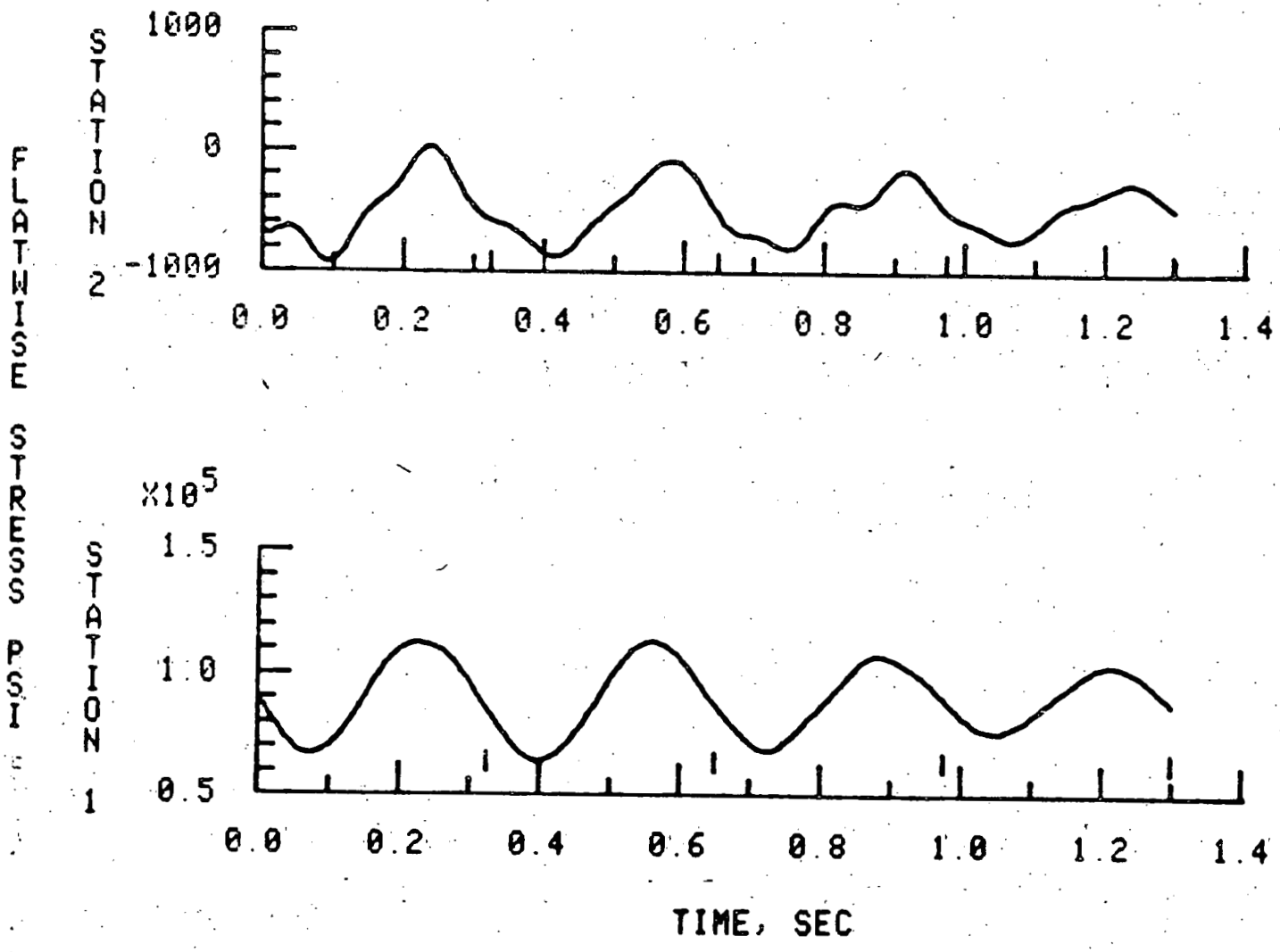

Fig. B-5 Continued

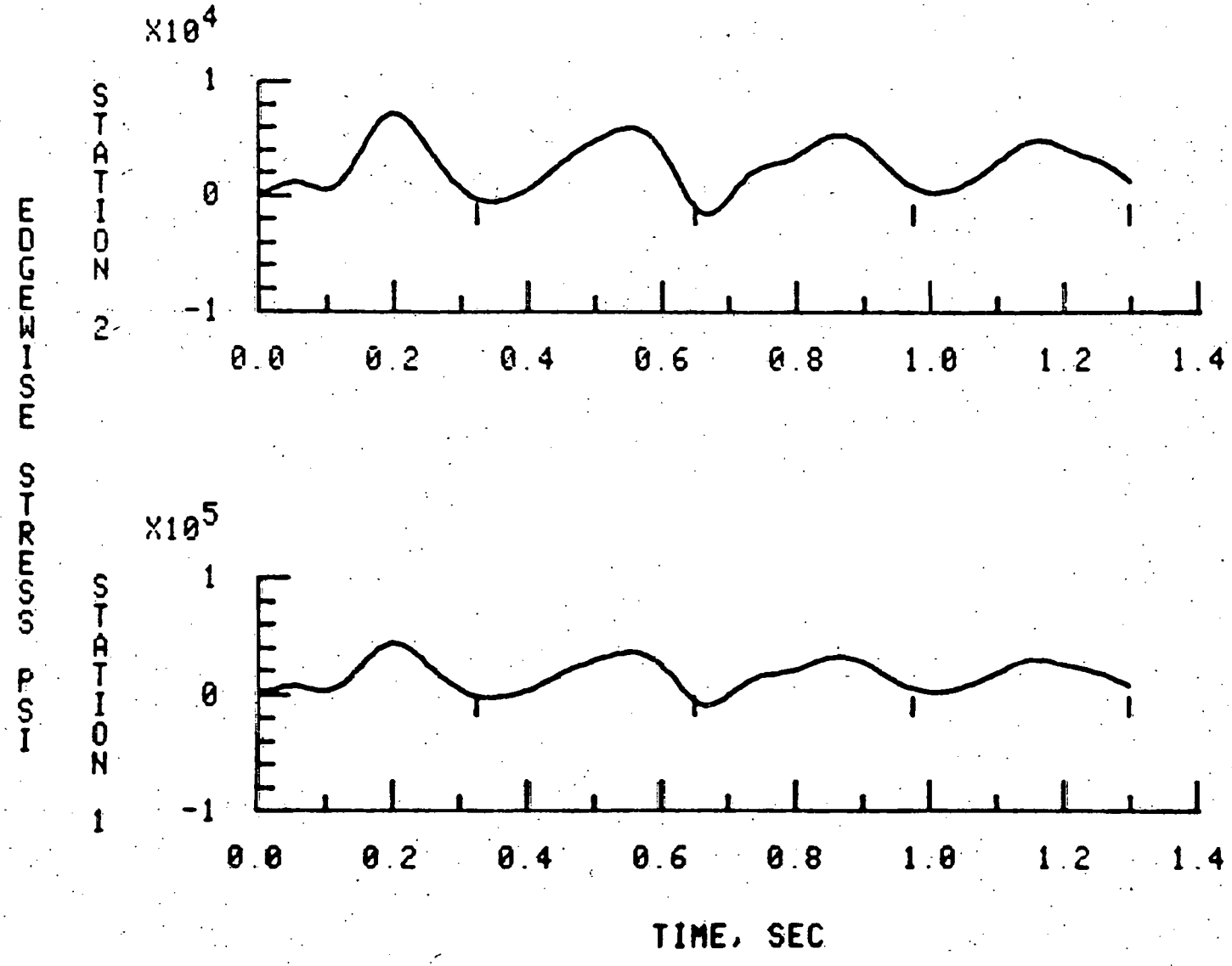

Fig. E-5 Continued

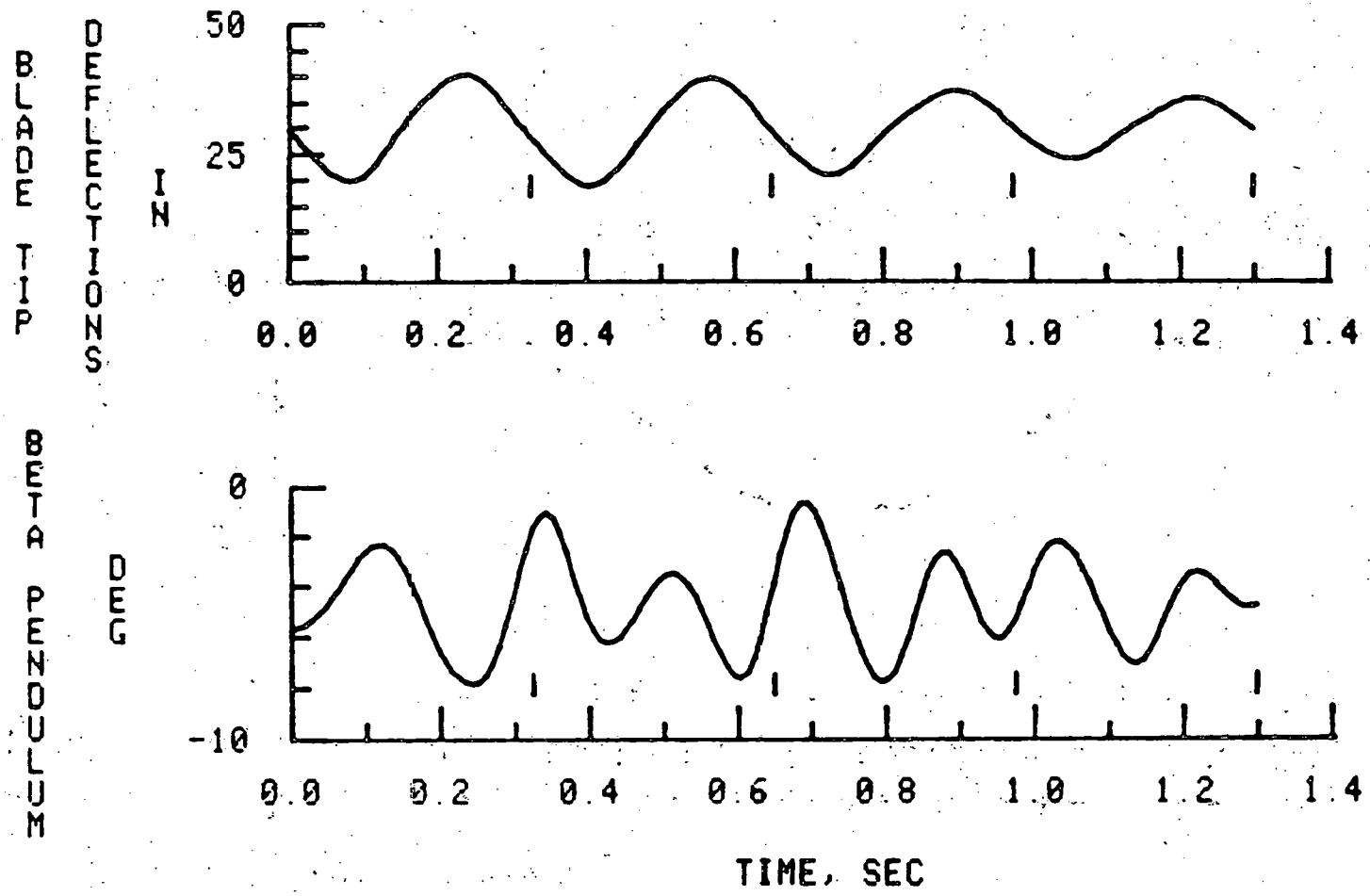

Fig. B-5 Concluded

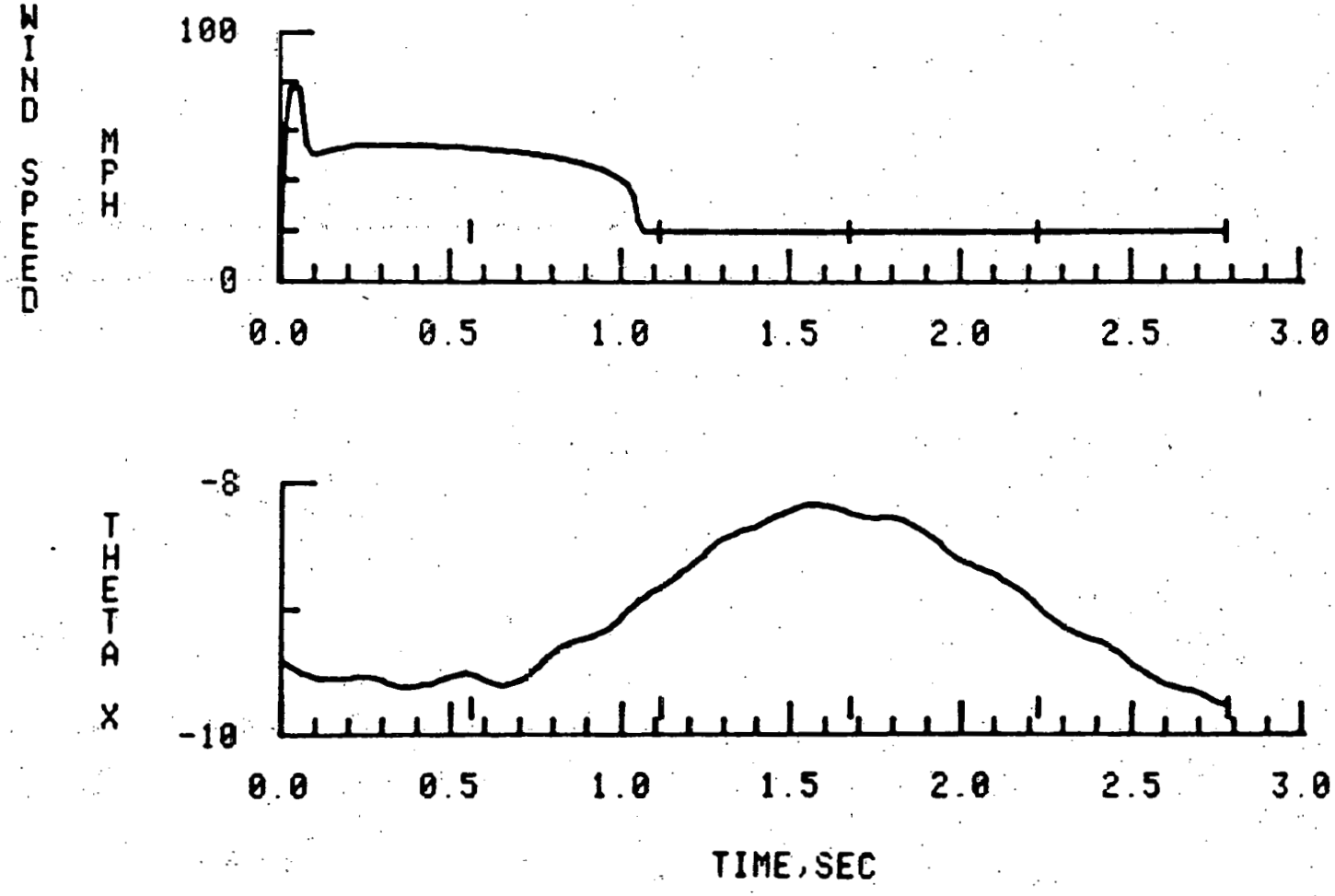

Fig. B-6 Rotor Response Characteristics, V_w = 9 m/s with Gust I, ΩR = 53.3 m/s

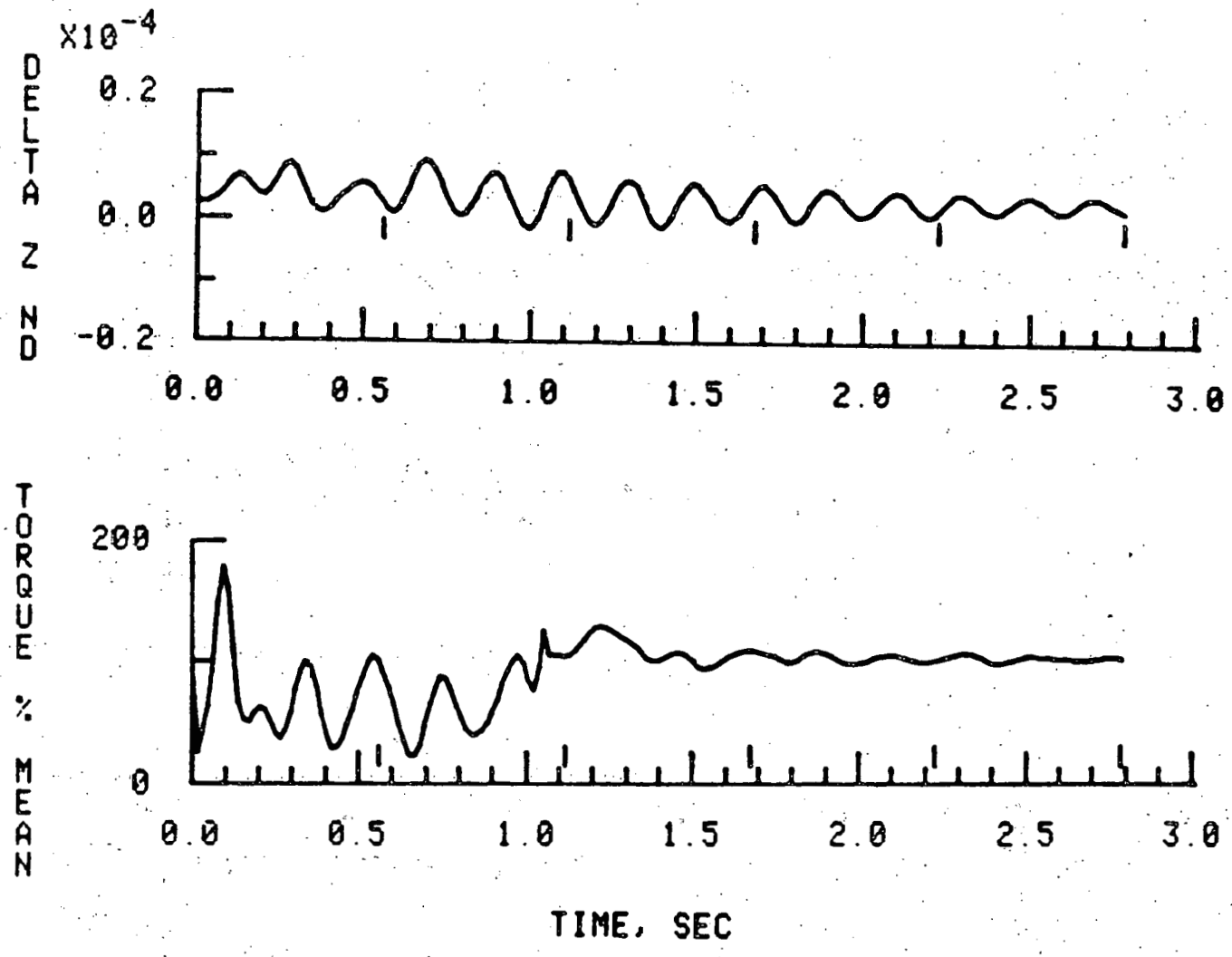

Fig. B-6 Continued

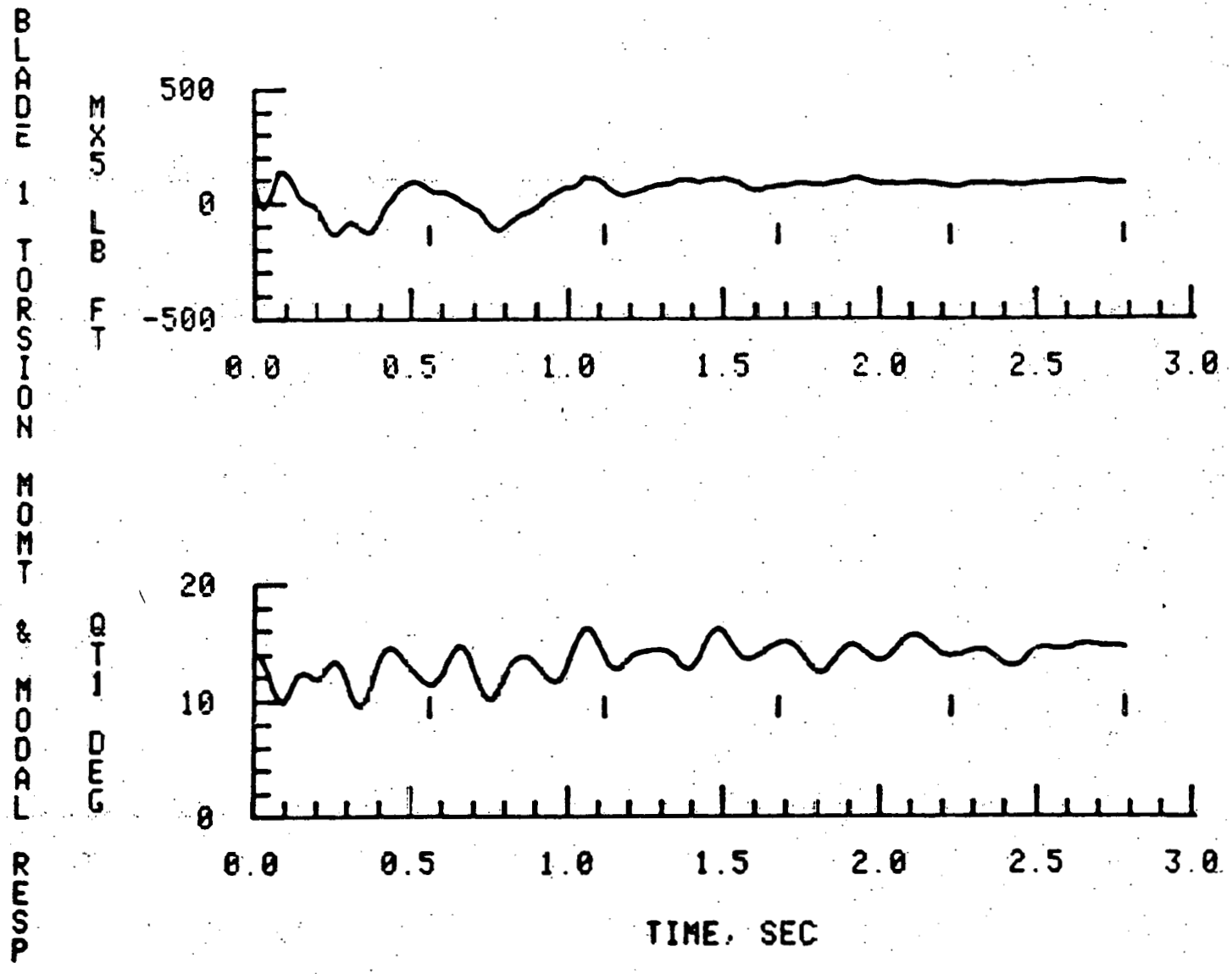

Fig. B-6 Continued

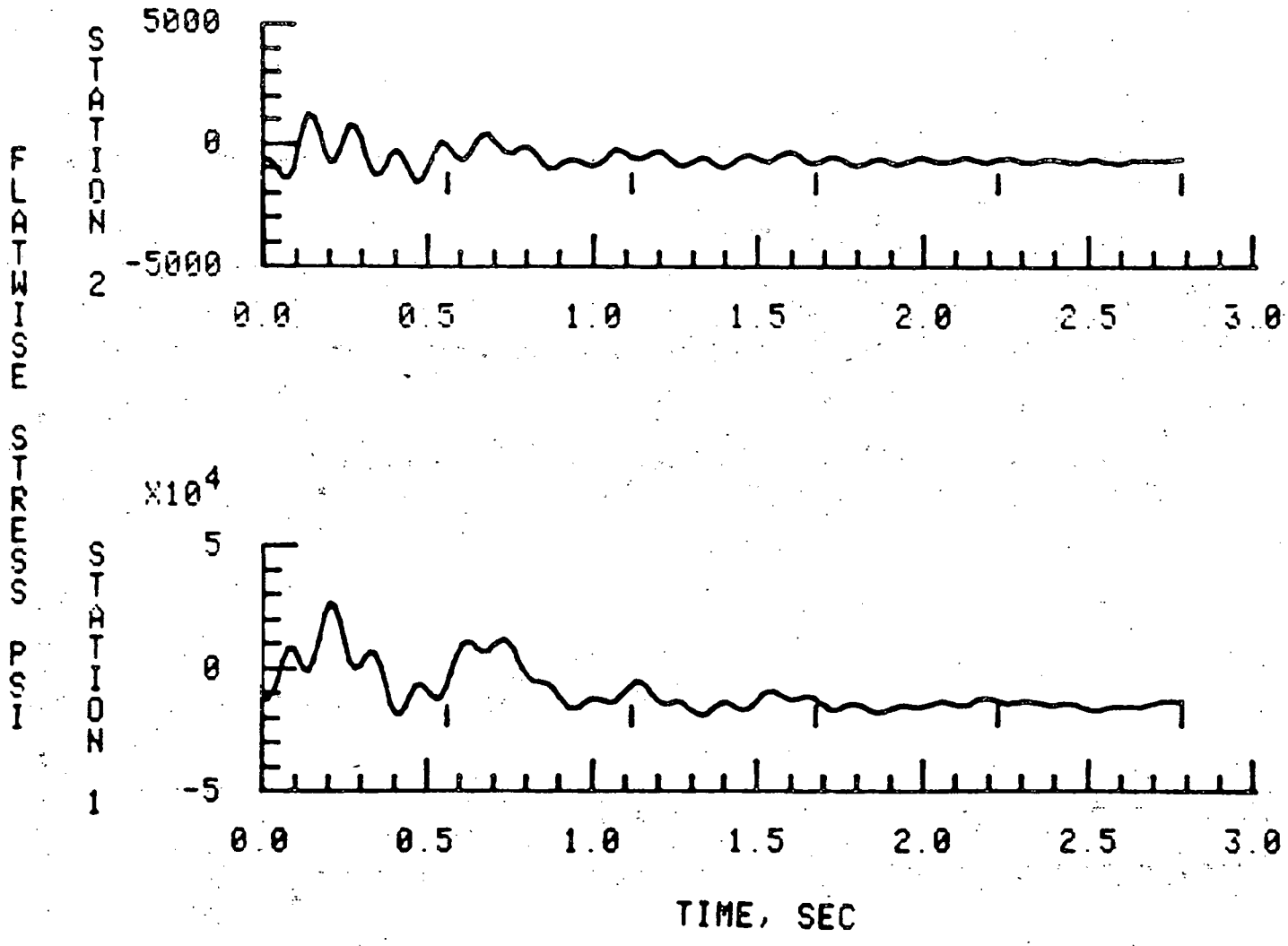

Fig. B-6 Continued

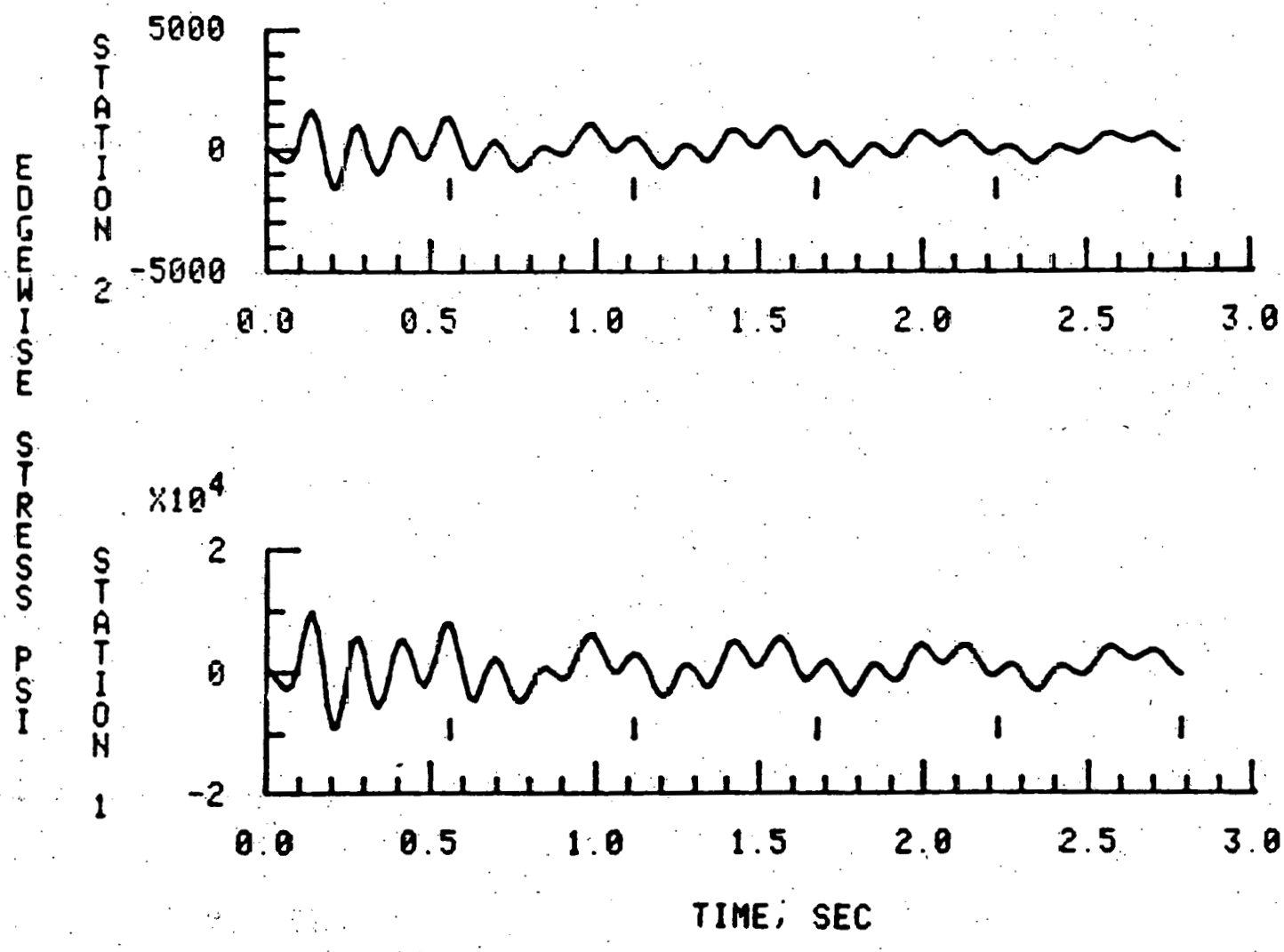

Fig. B-6 Continued

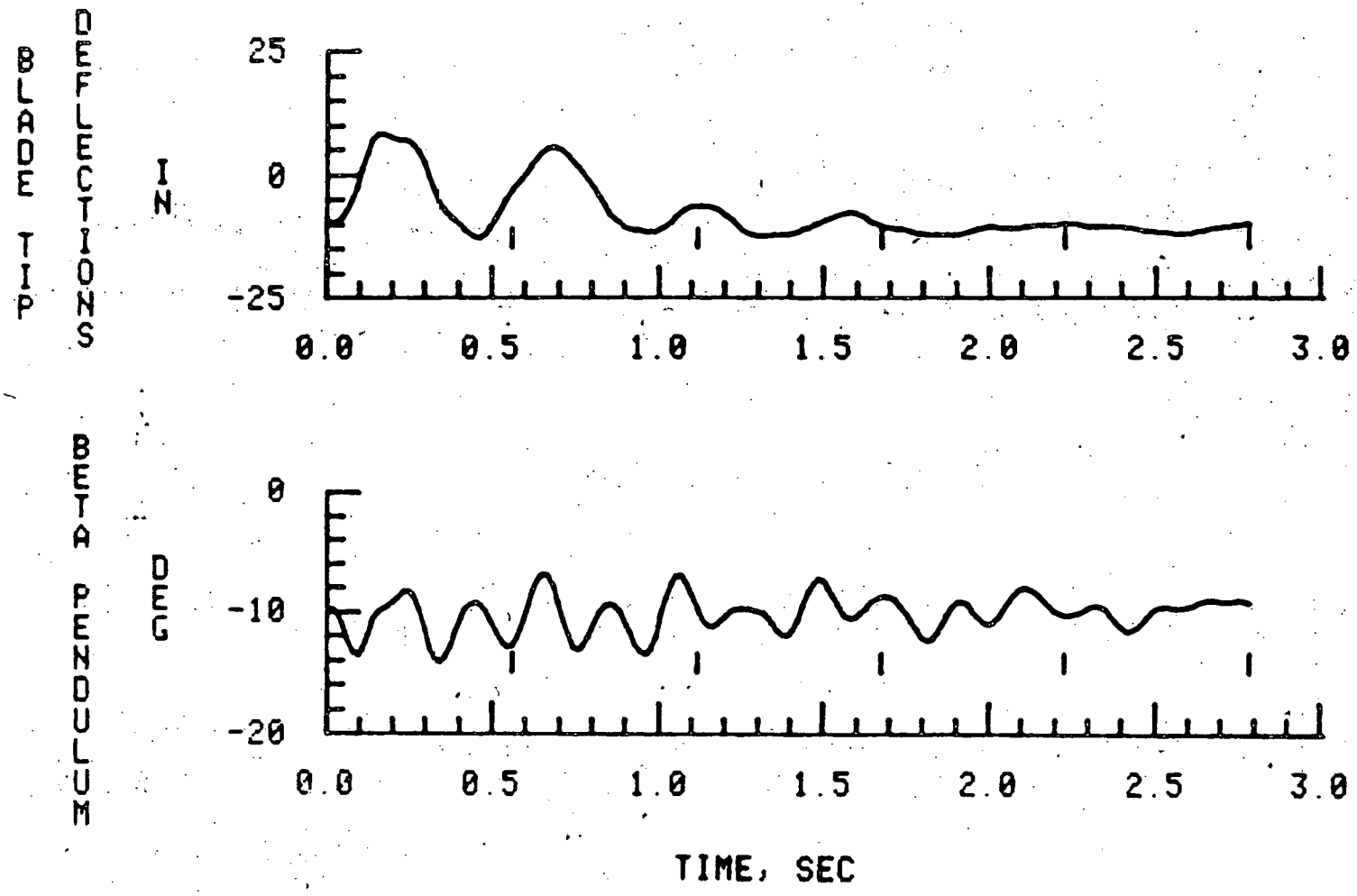

Fig. B-6 Concluded

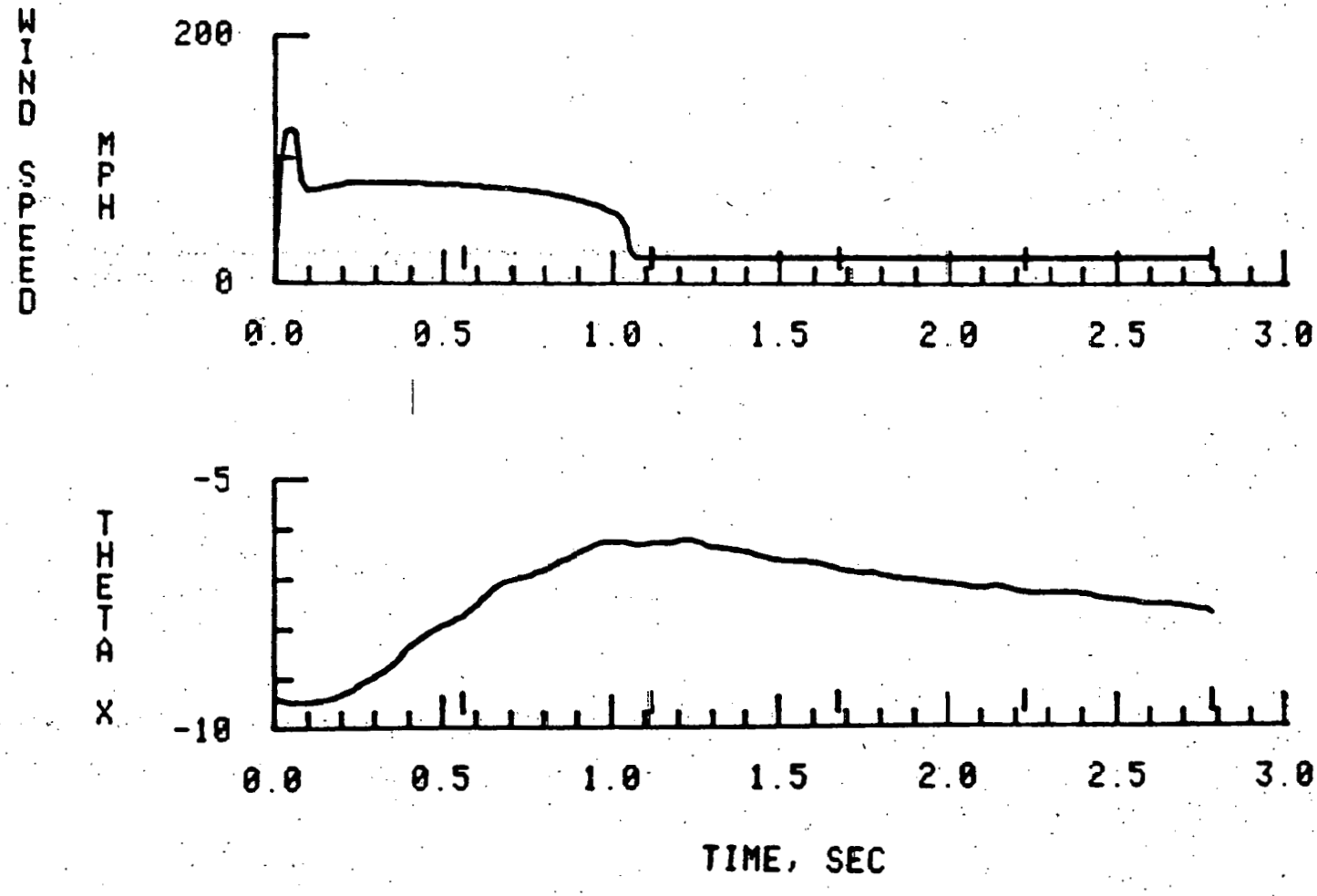

Fig. B-7 Rotor Response Characteristics, V_w = 9 m/s with Gust II, ΩR = 53.3 m/s

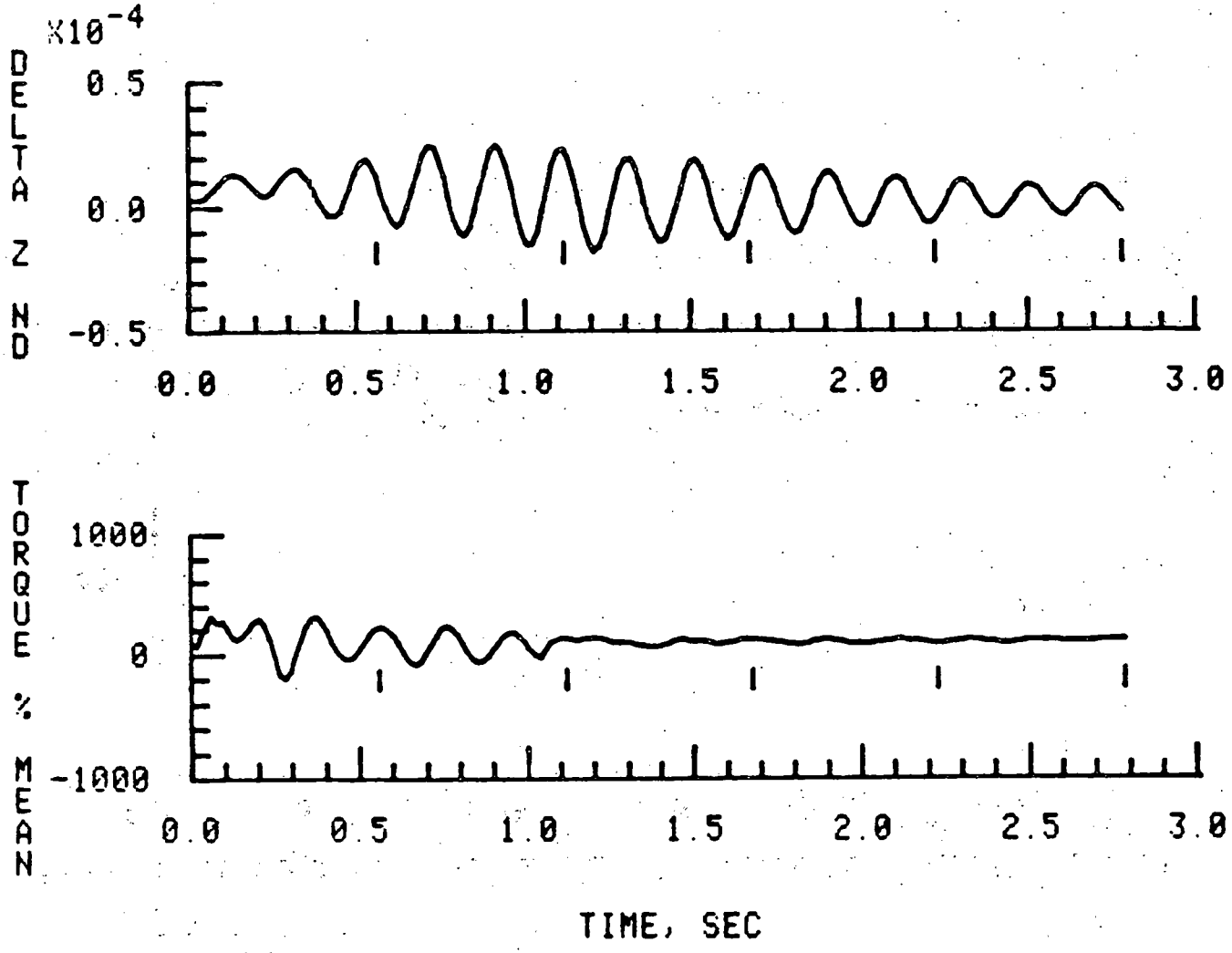

Fig. B-7 Continued

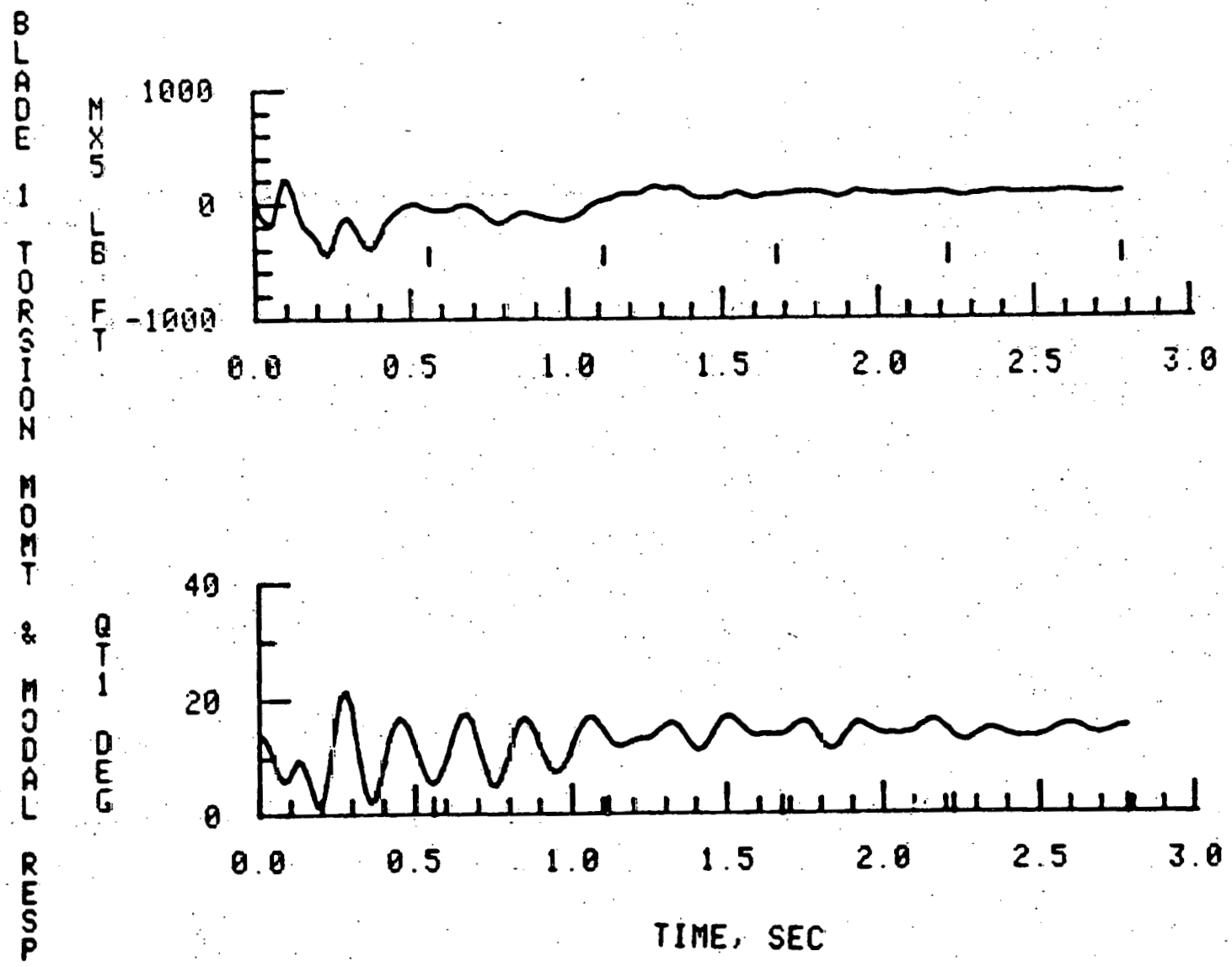

Fig. B-7 Continued

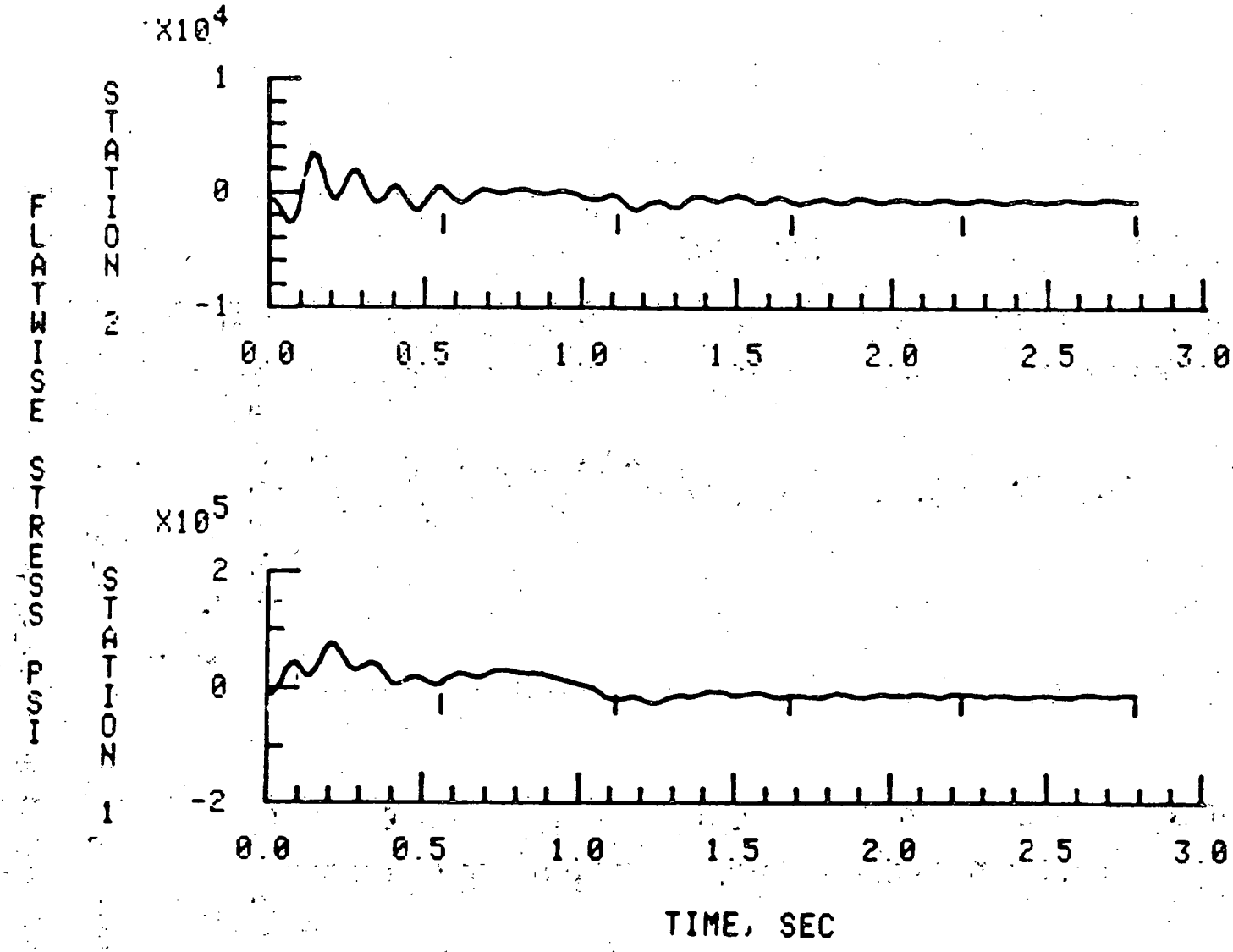

Fig. B-7 Continued

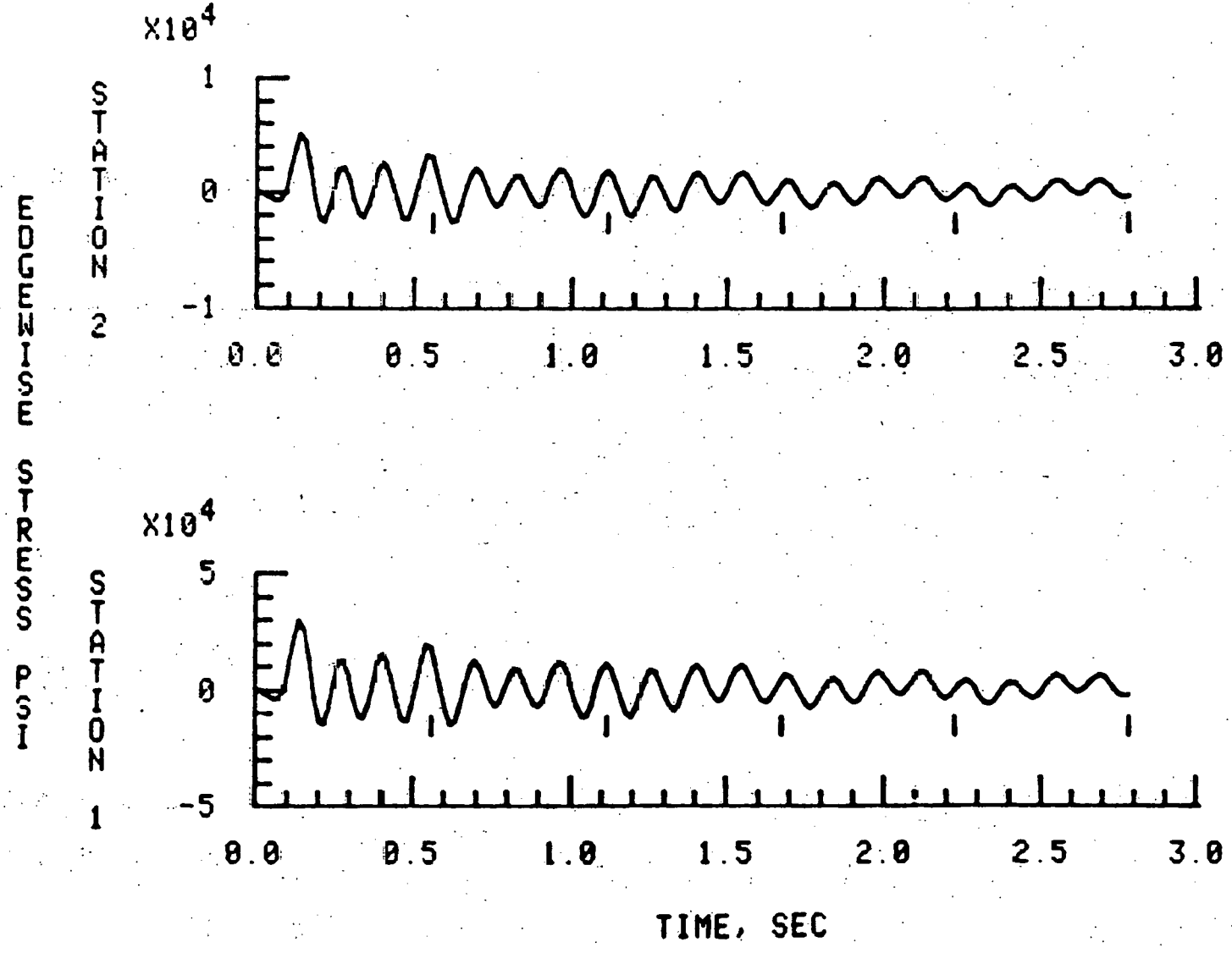

Fig. B-7 Continued

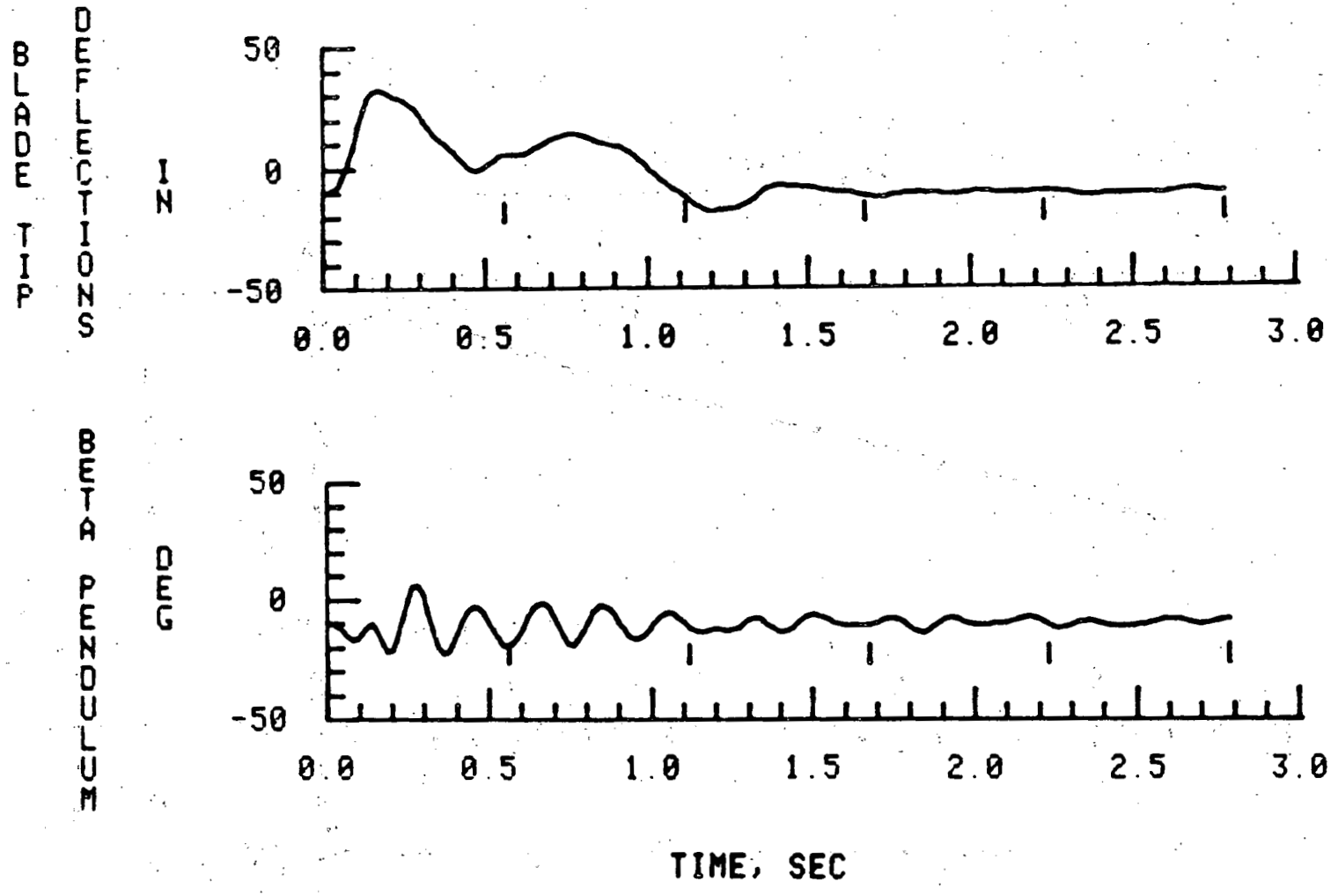

Fig. B-7 Concluded

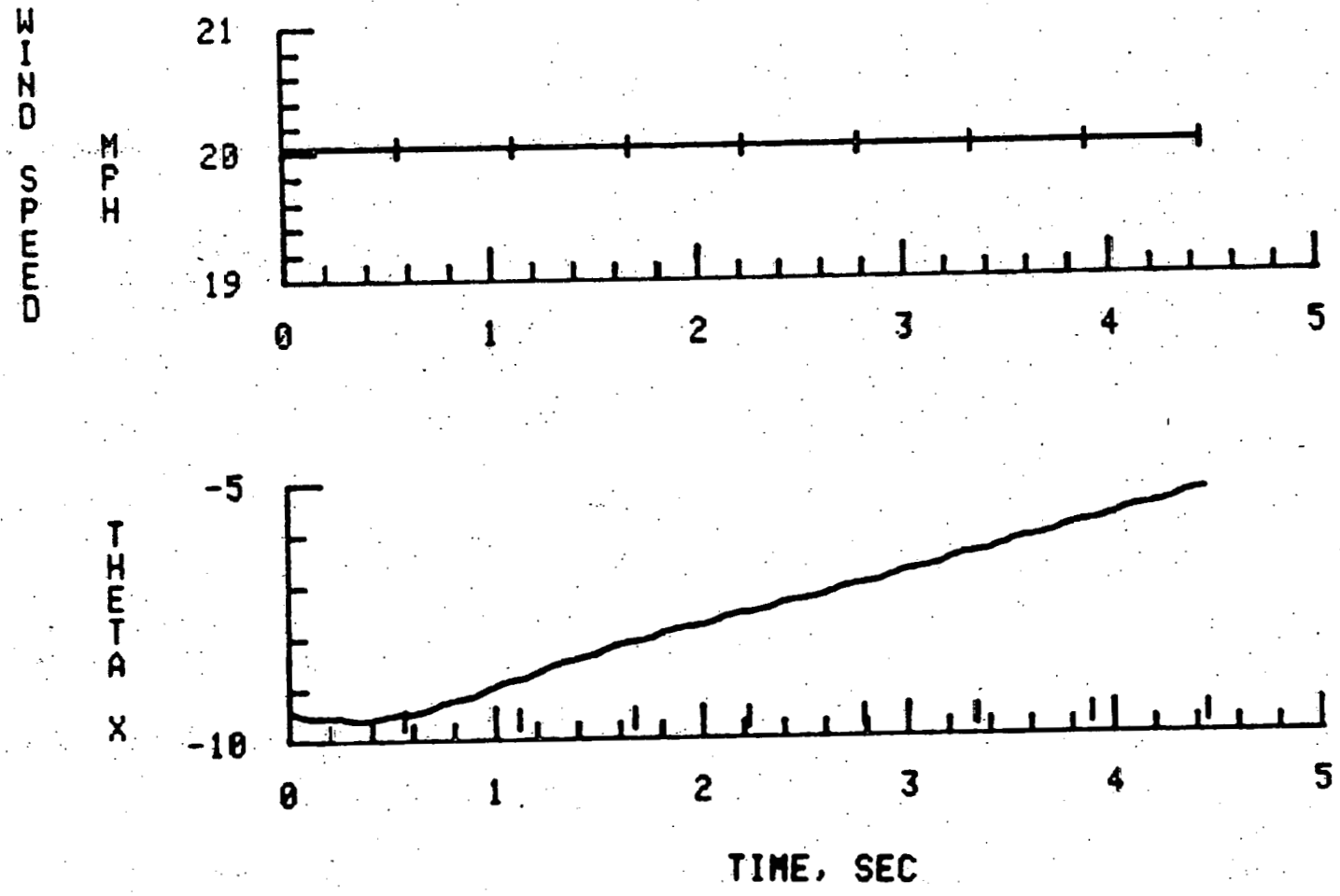

Fig. B-8 Rotor Response Characteristics, V_w = 9 m/s with lateral gust = +40 deg.

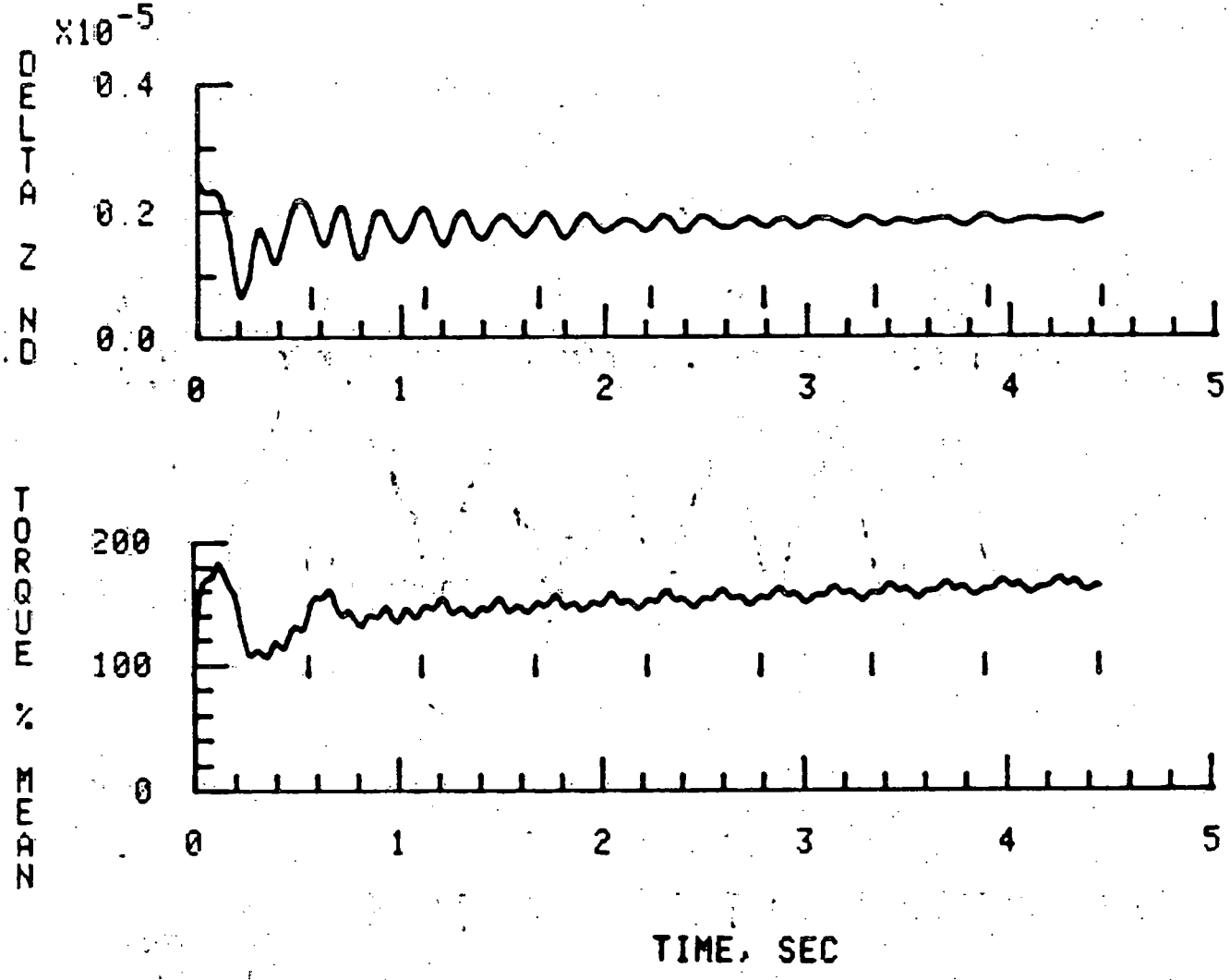

Fig. B-8 Continued

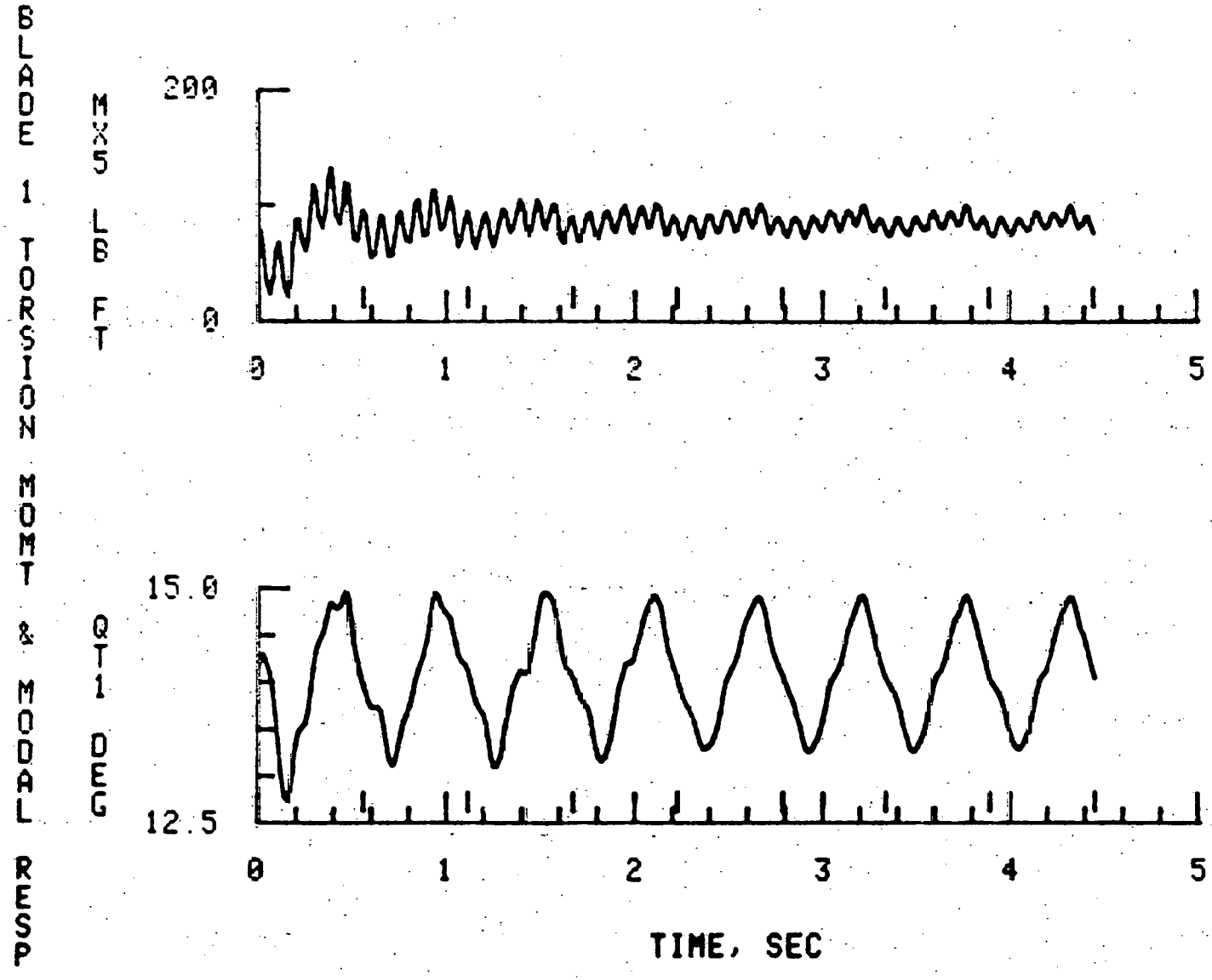

Fig. B-8 Continued

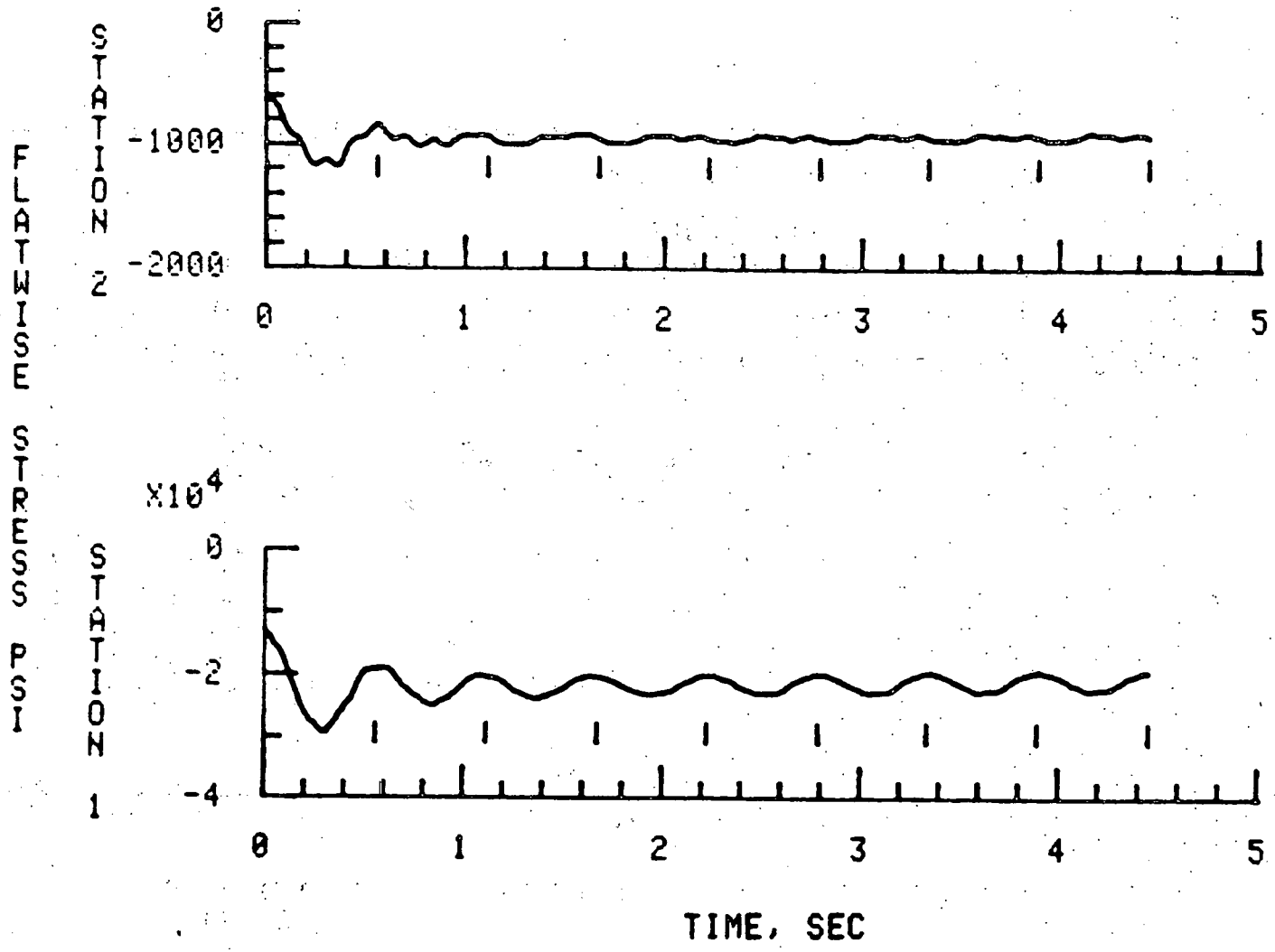

Fig. B-8 Continued

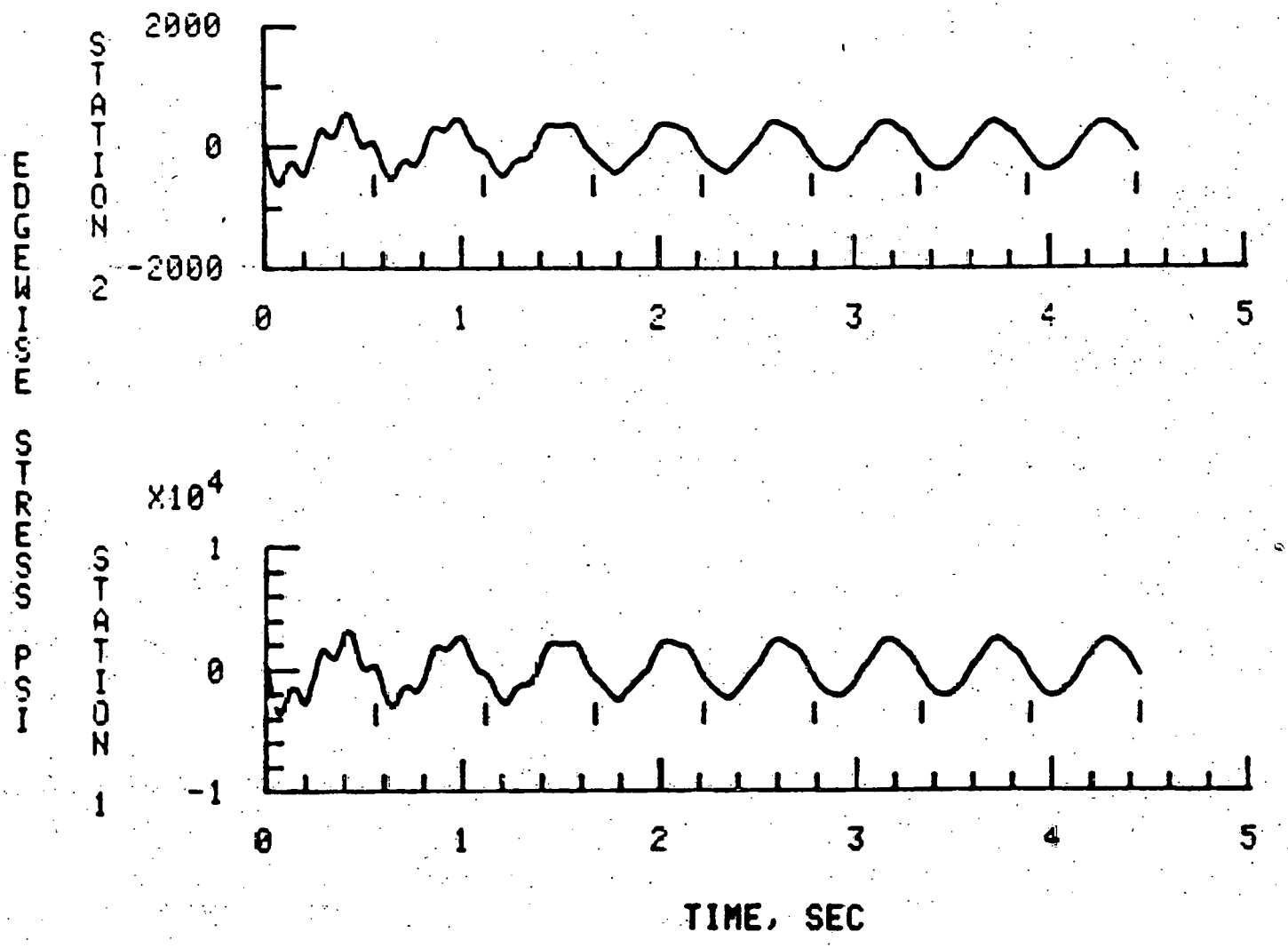

Fig. B-8 Continued

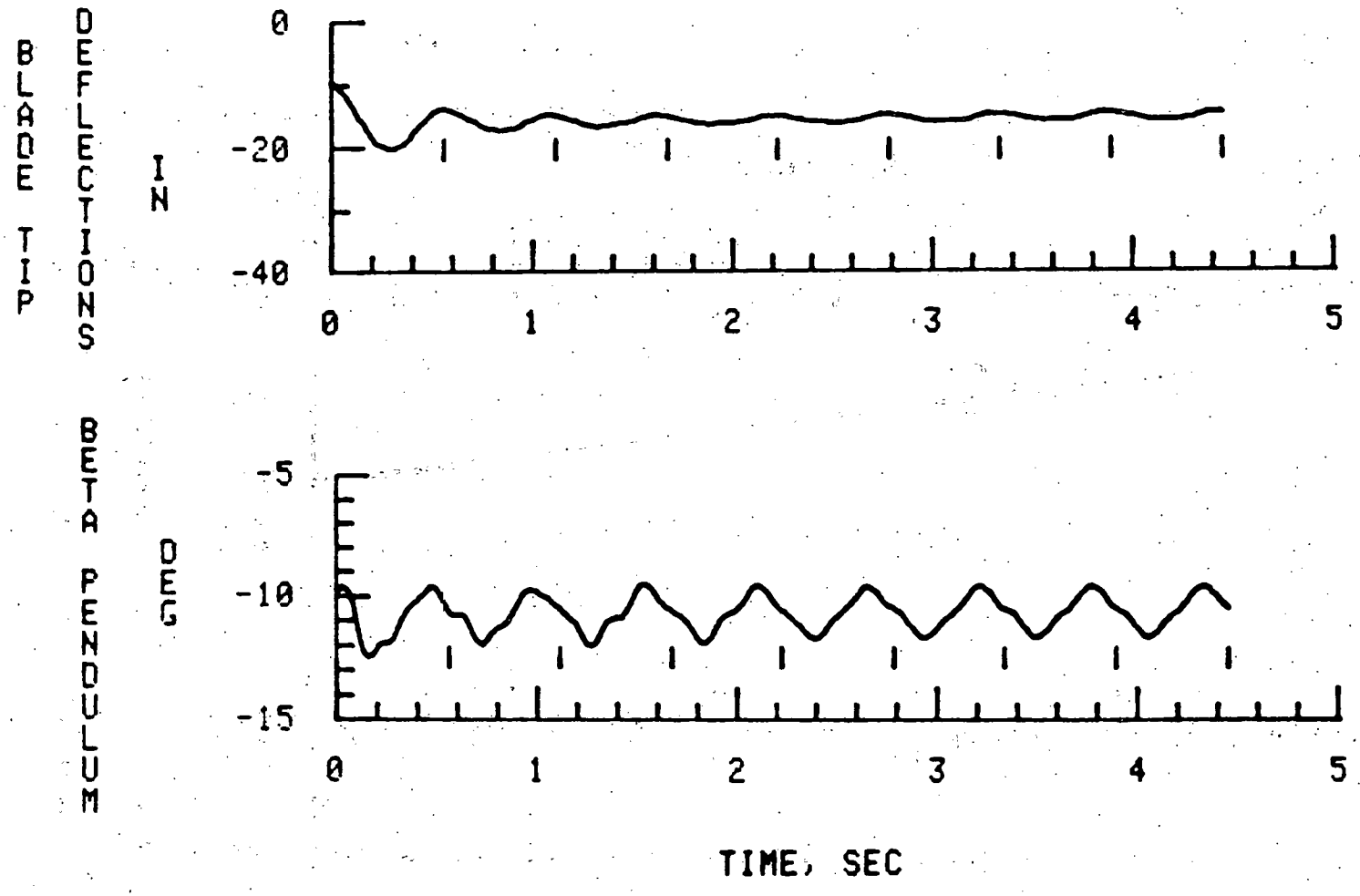

Fig. B-8 Concluded

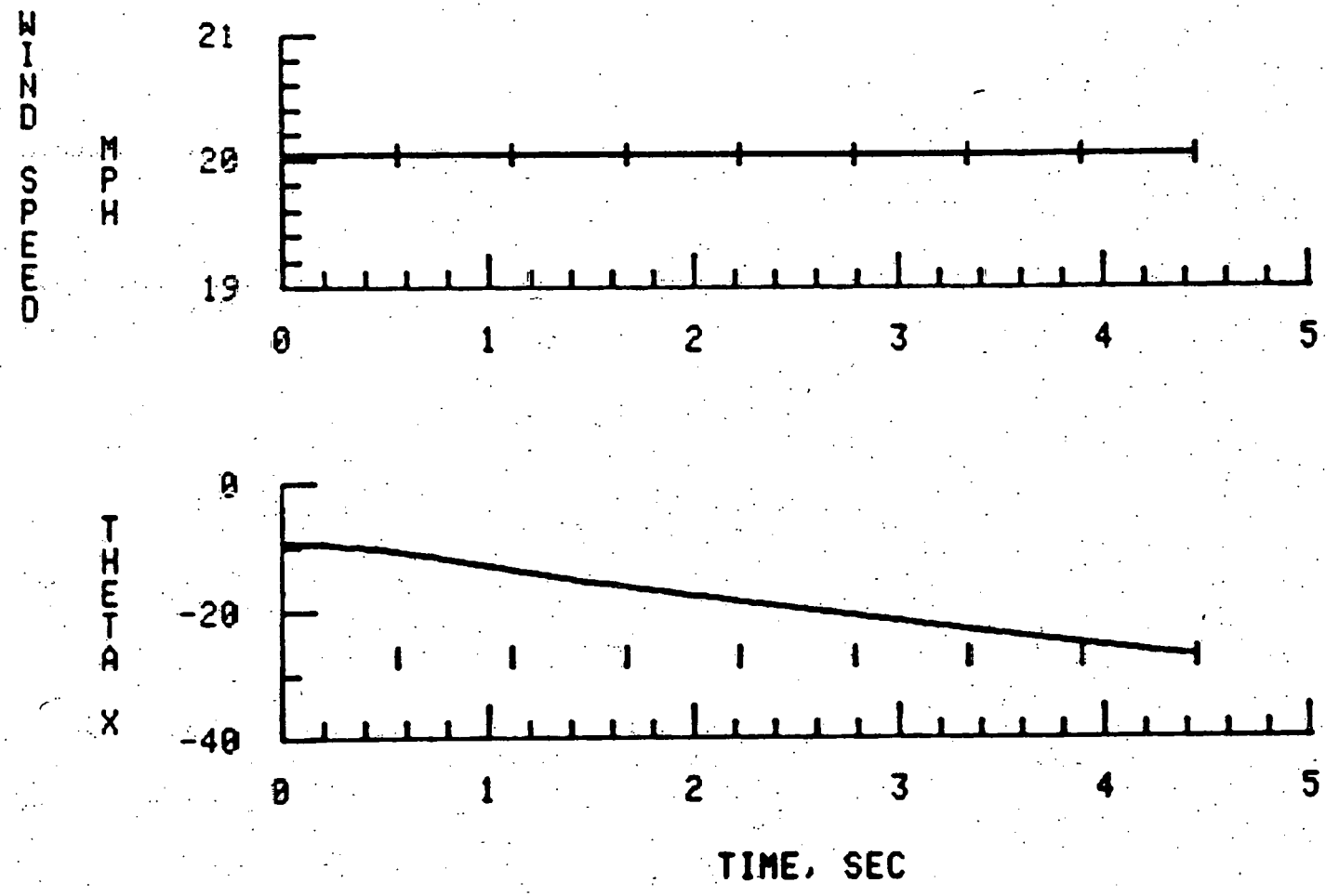

Fig. B-9 Rotor Response Characteristics, V_w = 9 m/s with lateral gust = -40 deg.

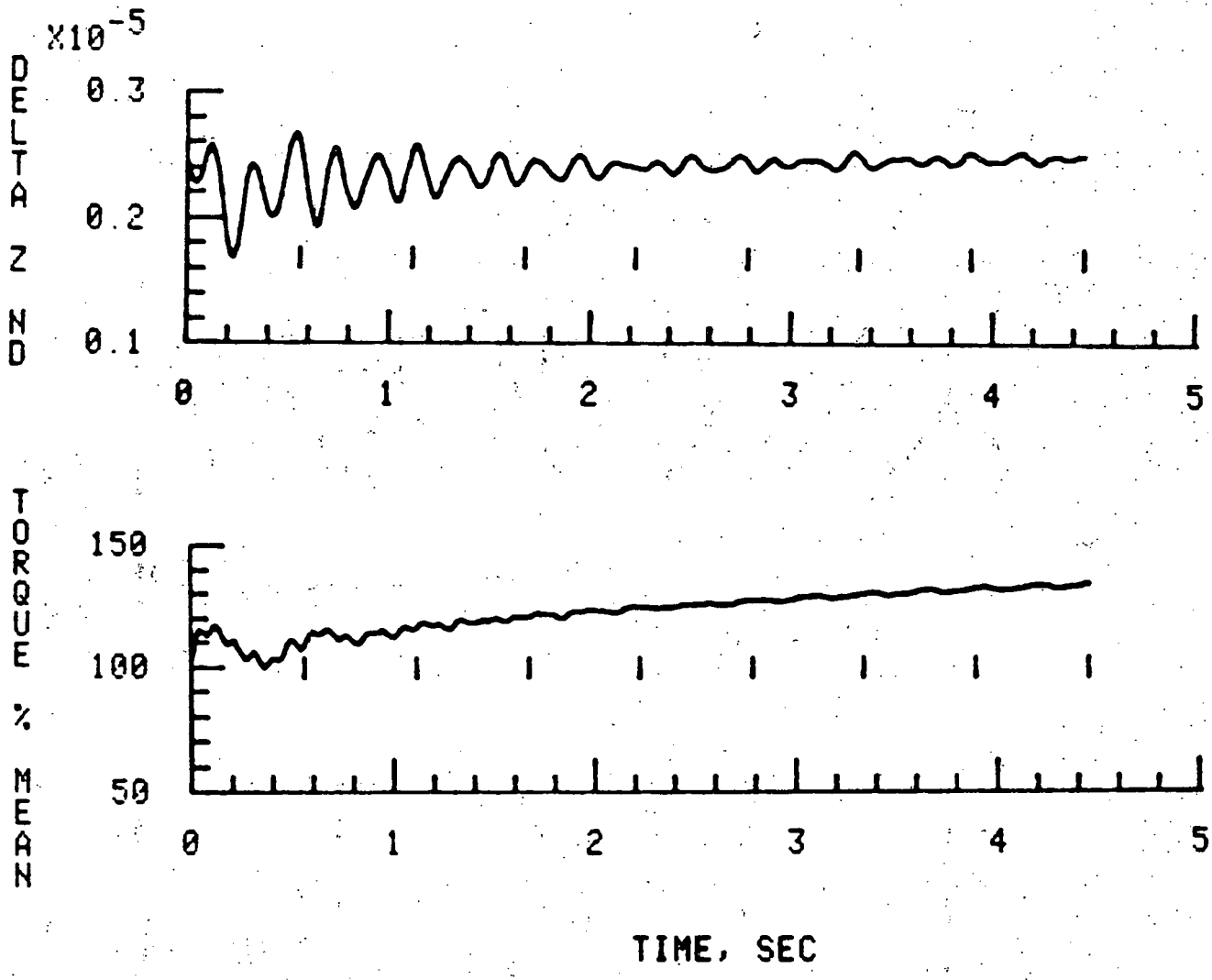

Fig. B-9 Continued

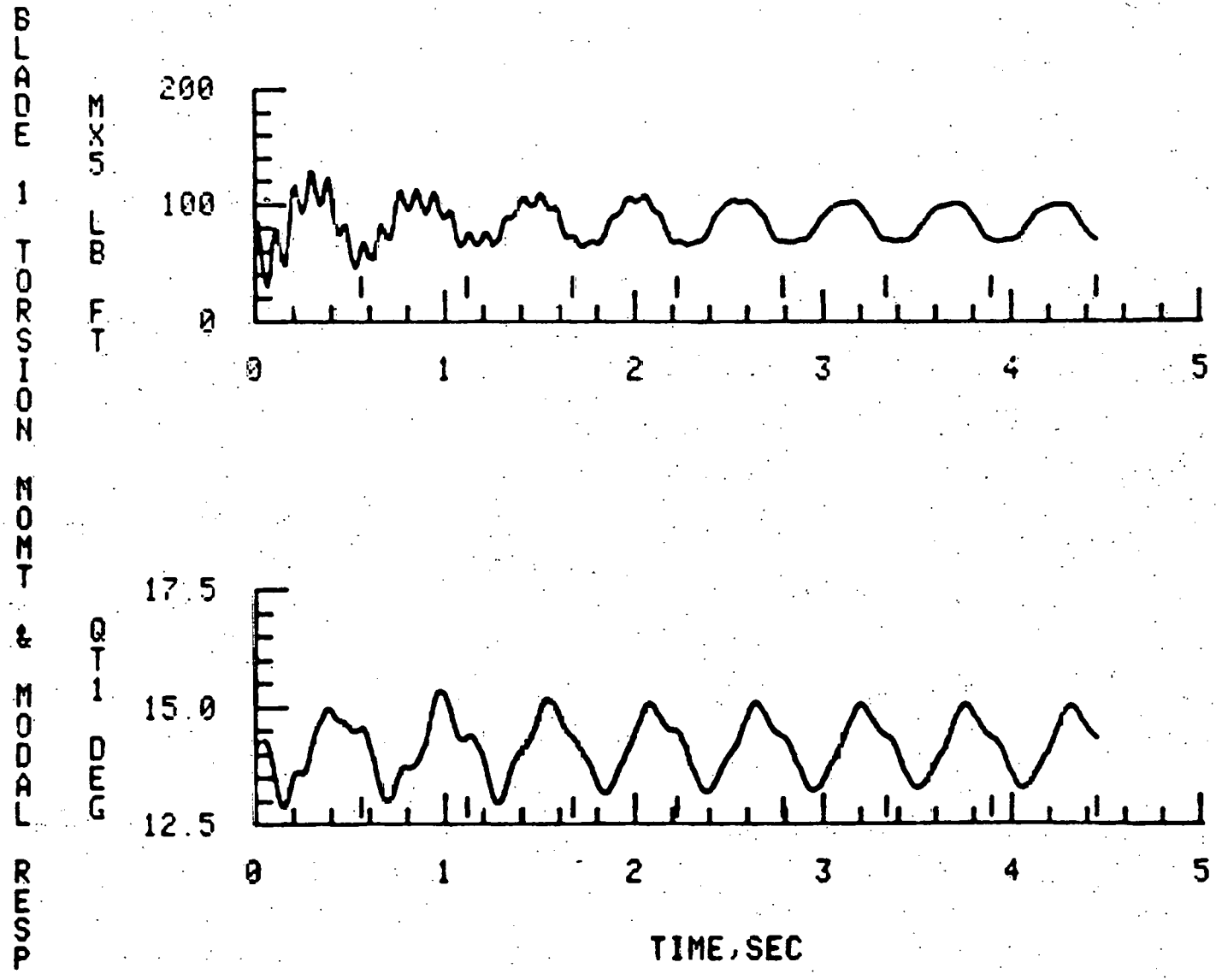

Fig. B-9 Continued

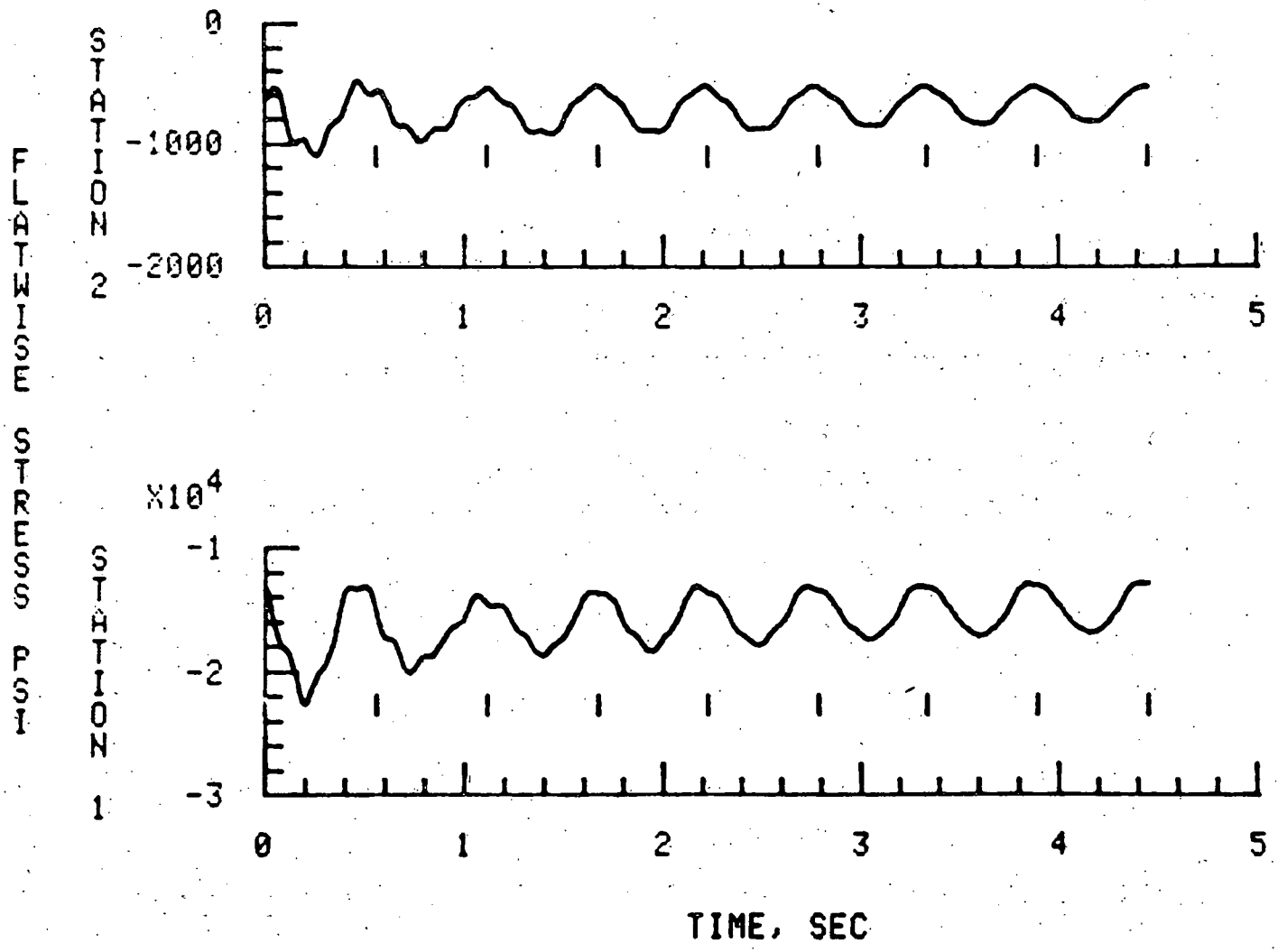

Fig. B-9 Continued

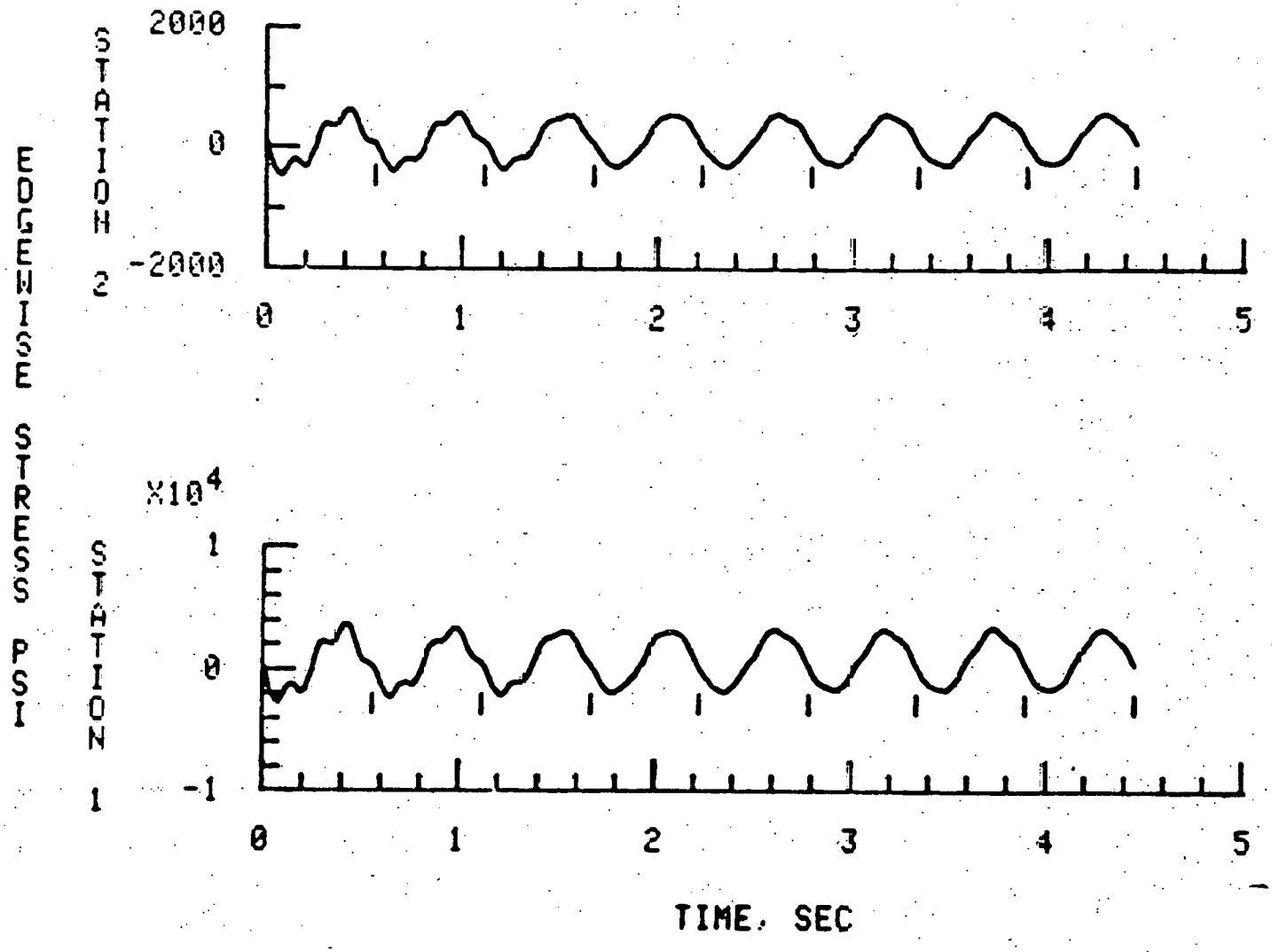

Fig. B-9 Continued

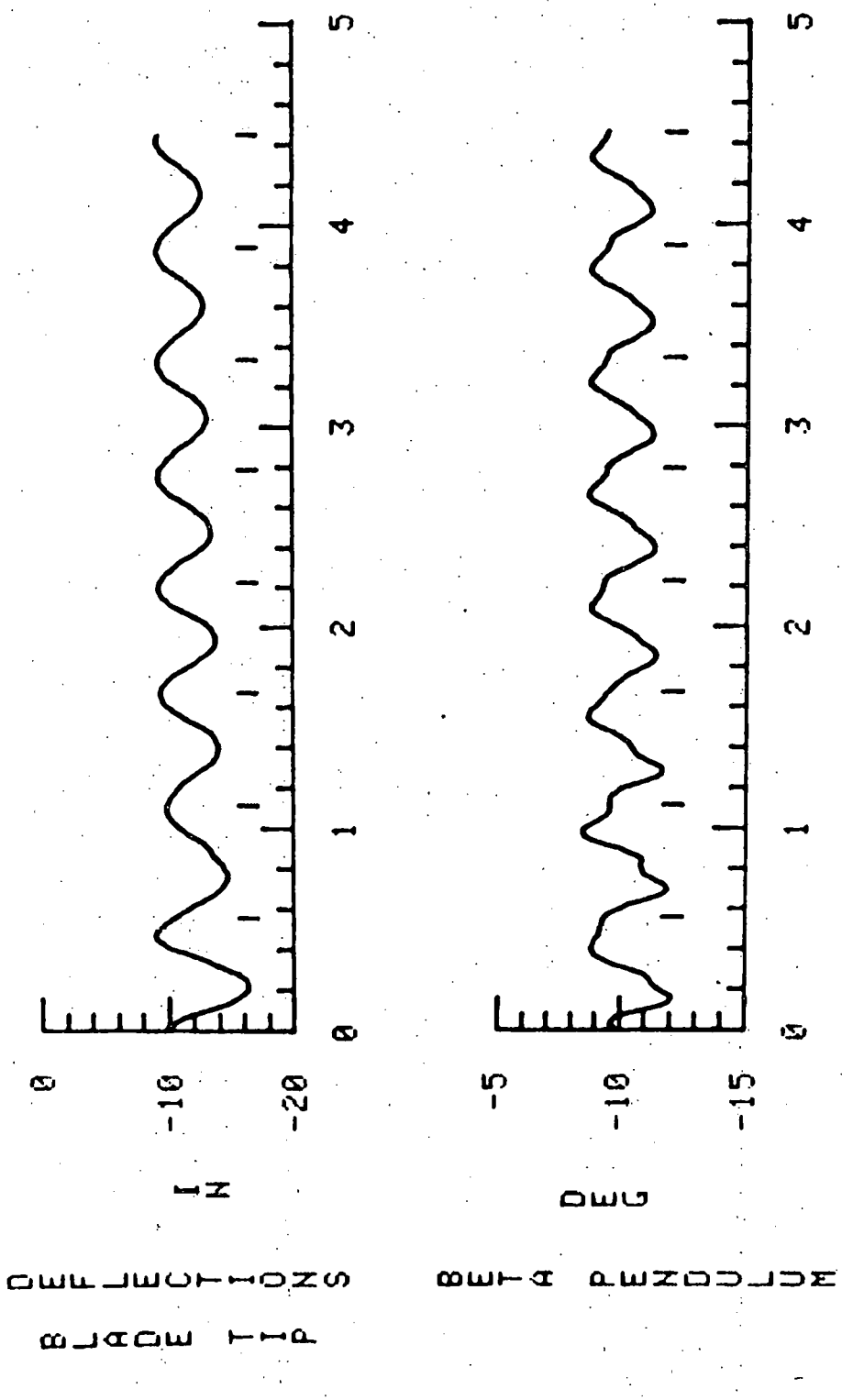

Fig. B-9 Concluded

GPO: 1980--677-262/508